Spray drying of food and herbal products

Article · January 2010

CITATIONS
18

READS
4,785

4 authors, including:

Wanderley Pereira Oliveira
University of São Paulo
146 PUBLICATIONS **3,786** CITATIONS
SEE PROFILE

Cláudia R. F. Souza
University of São Paulo
78 PUBLICATIONS **2,094** CITATIONS
SEE PROFILE

Louise Kurozawa
University of Campinas
109 PUBLICATIONS **2,353** CITATIONS
SEE PROFILE

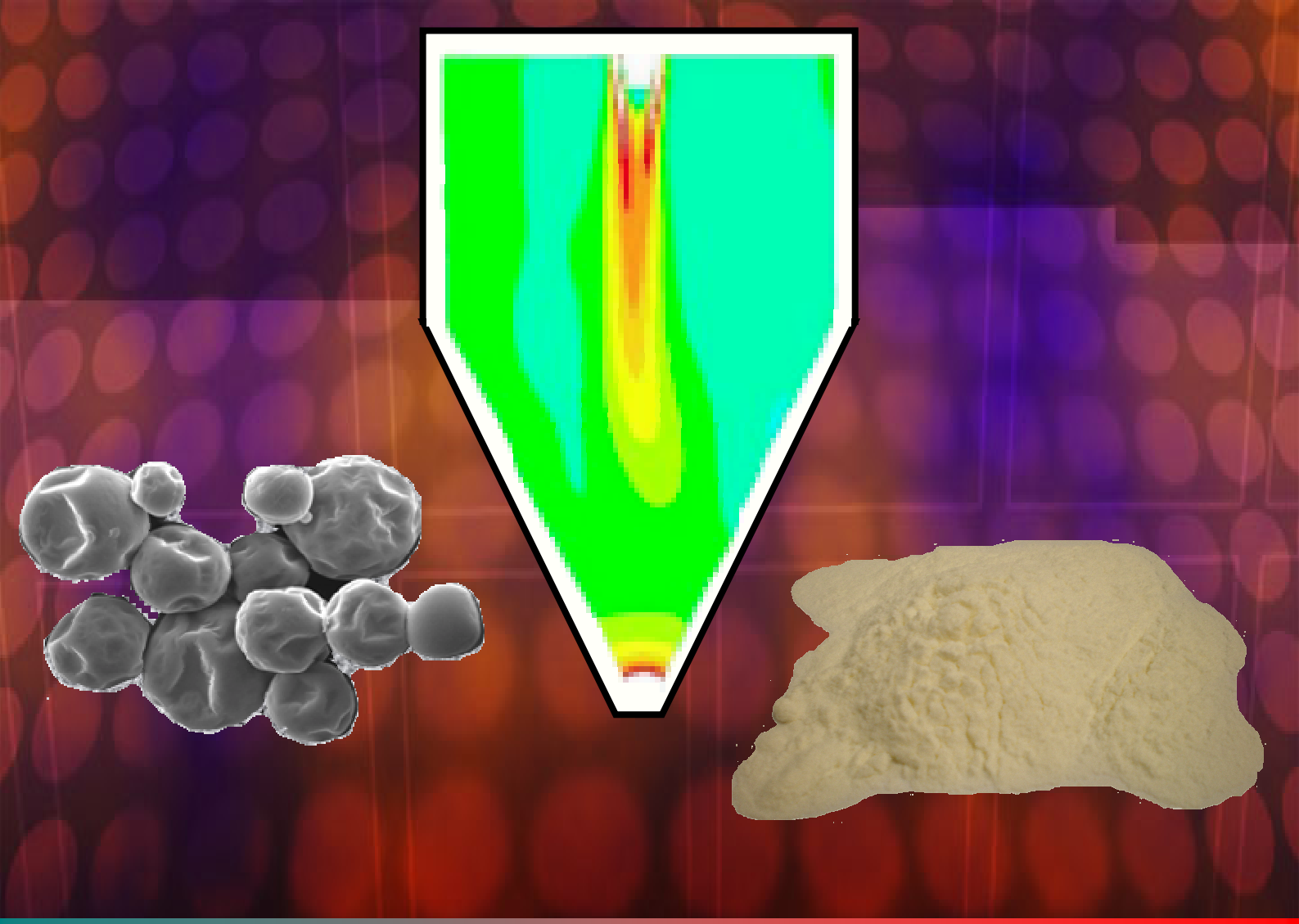

Spray Drying Technology

Volume One

Editors

M.W.Woo, A.S. Mujumdar, W.R.W. Daud

Preface

Spray drying is a ubiquitous industrial operation found in numerous industrial sectors. It is employed to produce engineered powders from liquid feedstocks in a single step. Extensive research and development efforts in understanding the fundamentals and applications of spray drying in recent years has prompted us to edit this book enlisting the assistance of experts in the field. Recent research has seen developments in many aspects of spray drying technology. One end of the R&D spectrum concerns large scale design of such equipment, in certain cases incorporating very detailed flow and heat and mass transfer analysis, while the other end of the spectrum focuses on the functionality of the single particle.

This book aims to provide in a concise form of some of the latest research in these diverse areas of spray drying. However, the philosophy of this book does not end there. Keeping in mind that knowledge is useful only if it is able to reach a wider technical and research community, we have decided to publish this book in the form of an e-book that is freely downloadable. Thus, it is accessible without charge even in parts of the world where resources are not available to purchase high cost books and journals. It is hoped that this endeavour will allow the latest developments in this field to reach the global audience, particularly those who need access to the latest information but cannot afford it.

Each chapter in this book was contributed by experts active in one particular area of spray drying. Each chapter has been prepared in a way that is self-contained to extent possible. Two chapters are devoted to computational fluid flow and particle trajectory analysis in spray dryers. Three chapters focus on the functionality of particles by manipulating powder physical properties, crystallinity and in the production of herbal extracts. Extension of the spray drying process to incorporate the freezing phenomenon is also included. A unique feature of this book is in its electronic form of publication which allows this book to be updated as required in order to keep abreast with the latest development in the area. Therefore, as a service to our reader, we will endeavour to invite continuous feedback from our authors and readers to further improve this book. Lastly we would like to thank all the authors for their contribution in making this book project possible. It is through their selfless effort, we hope this book will be useful to the spray drying community.

Contributions to our e-book series are made by editors as well as authors entirely as a volunteer effort. The copyrights rest with the authors of individual contributors. They have agreed to allow free access to their work for the benefit of free and fast global access to the knowledge they have created. Although freely available,readers should note that all contribtors are peer-reviewed and accepted only if they meet our quality requirements. We do plan to update and produce revised/enhanced editions of the e-books or produce additional volumes as a series.

Meng Wai Woo
Arun Sadashiv Mujumdar
Wan Ramli Wan Daud

List of Authors

Arun Sadashiv Mujumdar	Mechanical Engineering Department & M3TC National University of Singapore, Singapore
Wan Ramli Wan Daud	Chemical Engineering Department National University of Malaysia, Malaysia
Meng Wai Woo	Chemical Engineering Department Monash University, Australia
Li Xin Huang	Research Institute of Chemical Industry and Forest Products, Nanjing, China
Maria Laura Passos	Chemical Engineering Department, Federal University of Sao Carlos, Brazil
Viviane S. Birchal	Chemical Engineering Department, Federal University of Sao Carlos, Brazil
Timothy Langrish	Department of Chemical and Biomolecular Engineering, University of Sydney, Australia
Sam Sukgoo Yoon	School of Mechanical Engineering Korea University, Korea
Wanderley Pereira Oliveira	University of São Paulo/FCFRP, Ribeirão Preto, SP, Brazil
Claudia R.F. Souza	University of São Paulo/FCFRP, Ribeirão Preto, SP, Brazil
Louise E. Kurozawa	University of São Paulo/FCFRP, Ribeirão Preto, SP, Brazil
Kil J. Park	University of São Paulo/FCFRP, Ribeirão Preto, SP, Brazil

Hasan Sadikoglu — Department of Chemical Engineering, Gebze Institute of Technology, Turkey

Xiao Dong Chen — Chemical Engineering Department
Monash University, Australia (Department of Chemical and Biomechanical Engineering, College of Chemistry and Chemical Engineering, Xiamen University, China)

Sean Xu Qi Lin — Chemical Engineering Department
Monash University, Australia

Kamlesh Patel — Chemical Engineering Department
Monash University, Australia

M.J. Perea-Flores — Departamento de Ingeniería Bioquímica, Sección de Graduados e Investigación. Escuela Nacional de Ciencias Biológicas del Instituto Politécnico Nacional

J.J. Chanona-Perez — Departamento de Ingeniería Bioquímica, Sección de Graduados e Investigación. Escuela Nacional de Ciencias Biológicas del Instituto Politécnico Nacional

E. Terres-Rojas — Departamento de Ingeniería Bioquímica, Sección de Graduados e Investigación. Escuela Nacional de Ciencias Biológicas del Instituto Politécnico Nacional

G. Calderon-Domingues — Departamento de Ingeniería Bioquímica, Sección de Graduados e Investigación. Escuela Nacional de Ciencias Biológicas del Instituto Politécnico Nacional

G.F. Gutierrez-Lopez — Departamento de Ingeniería Bioquímica, Sección de Graduados e Investigación. Escuela Nacional de Ciencias Biológicas del Instituto Politécnico Nacional

L. Alamilla-Beltran — Departamento de Ingeniería Bioquímica, Sección de Graduados e Investigación. Escuela Nacional de Ciencias Biológicas del Instituto Politécnico Nacional

V. Garibey-Febles — Laboratorio de Microscopia Electrónica de Ultra-Alta Resolución del Instituto Mexicano de Petróleo

Content

Woo, M.W., Huang, L.X., Mujumdar, A.S., Daud, W.R.W. CFD simulation of spray dryers - Volume 1, Ed. Woo, M.W., Mujumdar, A.S. and Daud, W.R.W., **2010**, ISBN - 978-981-08-6270-1, Published in Singapore, pp. 1-36.

CFD simulation of spray dryers

Chapter 1

Woo M.W.[1], Huang L.X.[2], Mujumdar A.S.[3], Daud W.R.W.[4]

[1] Department of Chemical Engineering, Monash University
[2] Research Institute of Chemical Industry and Forest Products, Nanjing, China
[3] Mechanical Engineering Department & M3TC National University of Singapore, Singapore
[4] Department of Chemical and Process Engineering, National University of Malaysia

Contents **Page**

1.0 Introduction

The CFD technique has emerged as a useful tool to provide very detailed visualization of the internal phenomenon in the chamber. In the design of spray dryers, this can be used to complement existing design practice and as an economical scale up tool from pilot or lab scale experiments. However, it is pertinent that a CFD model of a spray dryer is properly set up and most importantly is interpreted correctly by the user. Therefore, this chapter aims to introduce the important aspects and numerical practice in using the CFD technique to model spray drying.

For the fresh reader, this chapter will be useful in introducing the components important when setting up their own spray drying CFD models. On the other hand, for the experienced modeller, this chapter will be useful in providing the different perspective in applying the CFD technique to spray dryer modelling. This is important to allow the reader to effectively understand the current limitations of the CFD technique in spray drying when interpreting their own models. On top of that, validation of the spray dryer CFD model is another challenge in this area. Some useful validation method is provided in the second part of the chapter.

2.0 Components of a spray dryer CFD

A CFD simulation of a spray dryer encompasses many different sub-models or modelling areas combined. Five main areas are highlighted in this section and they are all inter-related to cover the diverse physics involved in spray drying. Figure 1 schematically shows the major components of a CFD simulation with the airflow simulation forming the main model. It is important to note that the submodels involved is not limited to those in Figure 1 and certainly depends on the complexity (or details) required from the simulation. While capturing the actual physics, this also forms a big challenge in the development of each sub-model as it is difficult to independently isolate each process. Different research as well as commercial groups has attempted to look at the different components of a CFD simulation. We will now look into each component in detail and in the course look at some numerical practice in such CFD modelling effort. For in-depth review of CFD techniques as applied to a wide assorted of dryers, the reader may refer to an extensive review of relevant literature carried out by Tarek and Ray[1]. Mujumdar and Wu[2] have proposed use of mathematical models for intensification of innovation since a validated model allows designers to test novel designs and unorthodox operating conditions without the risk and cost involved in physical testing.

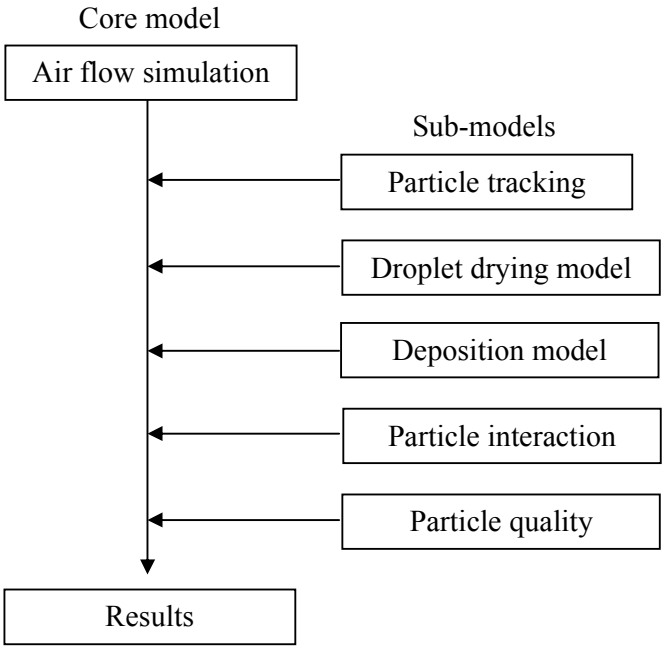

Figure 1 Schematic layout of a CFD simulation of spray drying

2.1 Airflow simulation

The core of a spray dryer CFD model from which other components are based on is the airflow simulation. Airflow pattern in the chamber mainly determines the movement of the particles which subsequently affects the residence time of the particles and whether the particles get deposited or escape from the chamber. In the computational sense, getting this right is the prerequisite for subsequent modelling effort.

Most spray dryer CDF simulations reported are currently undertaken using commercial codes such as FLUENT, CFX, STAT3D e.g. as well as in-house codes[3-6]. The basic CFD techniques are relatively established and will not be repeated here. It is expected that the reader is familiar in the technique and references can be found elsewhere[7]. However, we will only focus on some specific important general considerations when modelling the internal airflow within the chamber of a spray dryer:

1. Transient or steady simulation
2. Two-dimensional versus three-dimensional
3. Turbulence modelling approach

Transient or steady simulation

The steady state approach has been the work horse of many early reports on CFD simulation of spray dryers[8-12]. To be more specific, it implies that there are no long time scale changes in the flow, although there can still be turbulence fluctuations present. Under the assumption that the airflow within the chamber is steady, these simulations managed to capture engineering data of interest. In particular, the third report by Kieviet *et al.* [10] illustrated relatively good comparison between the simulated and the measured velocity profiles although some unsteady pattern can be observed in their experimental work. This work has further become a relatively 'standard' test case in some recent studies[13][14]. Relying on the ability of the steady state approach, a European Union (EU) project was funded, EDECAD, to implement the CFD technique to large industrial scale dryers[6], further illustrates the application of the steady state approach.

On the other hand, recent experimental work suggests that the internal airflow pattern can exhibit significant transient behaviour. Observations in a co-current pilot scale unit indicated that the central core flow tend to fluctuate sidewards with transient eddies being formed near the wall[15][16]. Not to be confused with rapid turbulence fluctuation, this transient behaviour refers to relatively long time scale self-sustained fluctuations. Figure 2 gives a simplified illustration of such transient behaviour in the airflow. There will be tendency for the central jet to deflect to the sides. The transient behaviour is also called self-sustained fluctuations as the transient behaviour is sustained due to pressure imbalances around the central jet. Additional experiments using a scaled down experimental unit provided more evidence of the transient behaviour particularly in the central core flow[17] . In order to obtain more insights into the transient behaviour, extensive simulations were further undertaken by making analogy to sudden pipe expansion flows. Depending on the inlet conditions, in general, it was found that a larger expansion ratio promotes more instability[18-20]. Some workers in the field have also recently switched to the transient approach [21][22].

However, based on a jet feed-back mechanism, it was recently numerically shown that the internal flow pattern in a spray dryer can exhibit steady-like behaviour, depending on the diameter of the chamber and the inlet velocity [23]. In a separate simulation for a unit with a rotating disk, Ullum (2006) also noted that their CFD predicted flow field resembles that of steady state; even when the simulation was switched to the transient solution framework. Harvie *et al.*[8] and Langrish *et al.* [5] further provide illustration of the contrasting effect of swirls in stabilizing or de-stabilizing the flow field. On more fundamental grounds analogous to the spray dryer, studies on sudden pipe expansion and cavity expansion systems showed that steady or transient behaviour in the flow is strongly dependent on the expansion ratio and operating conditions [19][24]. Coupled with the ability of the steady approach in the earlier work, these are strong evidence in the possible existence of a transient-steady stability map in spray dryers. However, this point is still expected to be under discussion in the near future and mapping out of the entire stability map might not be possible due to the myriad possible designs of spray dryers. The key objective in illustrating these different cases and in making the comparison is so that the readers are aware of the possible

scenarios on both sides of the fence when setting up and interpreting their own simulations.

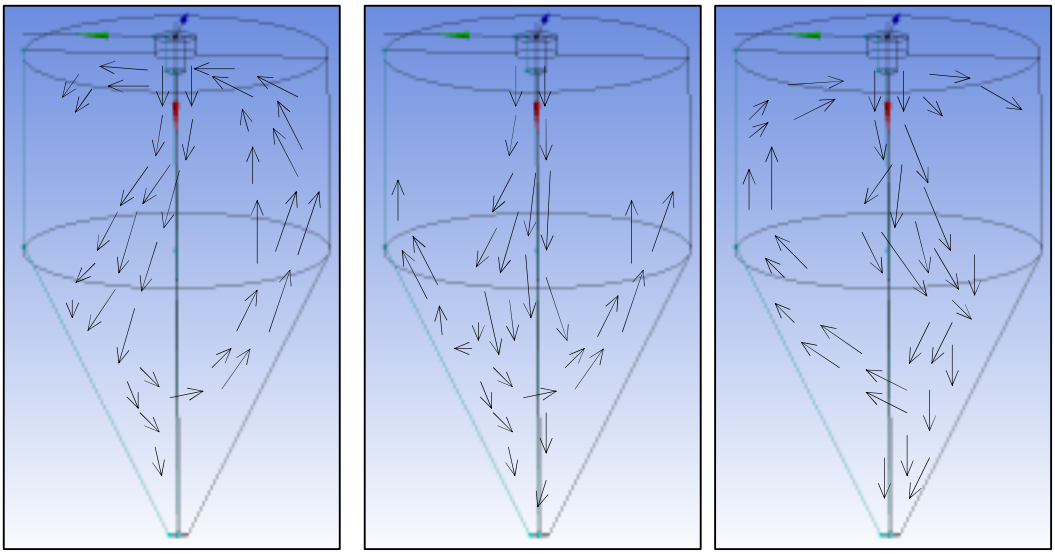

Figure 2 *Simplified illustration of the long time scale fluctuation (focusing on the deflection of the central jet). This illustration also highlights the jet feedback mechanism (Woo et al. 2009)*

At this juncture, as a guide for future workers, it is pertinent to venture briefly into the numerical aspect of such possibly self-sustained fluctuating flow. One main question is, in the absence of experimental data, on how do we know if the transient or steady treatment should be used? It will be useful to use a step-by-step solution to the CFD model (Figure 3). The model is initially solved with a steady state solution in the first step. The results or the developed flow field from the steady state solution will then be used as the initial condition for the second transient solution. Such a practice is also commonly recommended by commercial code developers (eg. FLUENT, CFX).

In the first steady solution step, two possible scenarios are possible. If the flow field is inherently steady, the numerical residuals will reduce to a low level and in certain cases form a horizontal pattern giving a good convergence indication. In order to further check, the converged flow field should not significantly change at further iterations. However, if the flow is inherently transient, the residuals will tend to oscillate at a relative high level without giving convergence. In such a case, very aberrant flow contours will be produced. The flow pattern will also most likely be asymmetric and changes at each subsequent iterations. Figure 4 illustrates and compares typical residual plots of such possible scenarios. It is noteworthy that the residual pattern might differ depending on the solver and model parameters.

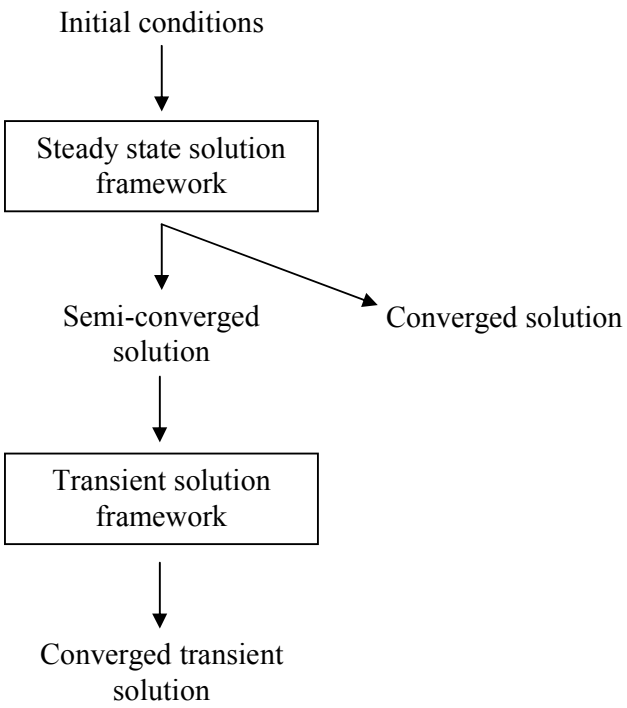

Figure 3 Numerical solution practice for spray dryer simulation

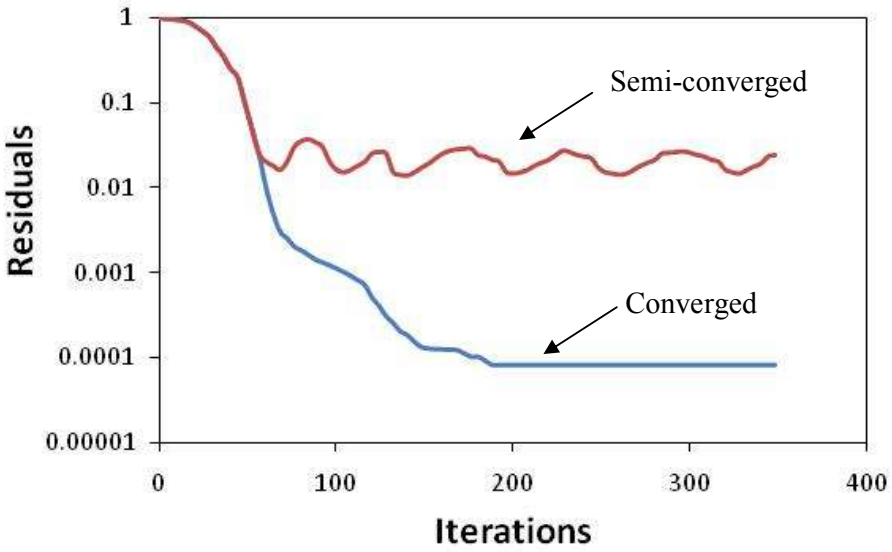

Figure 4 Typical residual patterns for the initial steady state solution

If the former case is encountered, it is then a good indication that the less computationally expensive steady state solution is suitable for the model; flow is inherently steady. However, although a converged solution might be achieved in the steady state, it is important to check if the solution is physically 'logical'. Although not reported, it was found that certain numerically converged solutions produce aberrant flow patterns. Such aberrant behaviour was alleviated when the solution was changed to the transient framework. On the other hand, the oscillating residual pattern as mentioned above is definitely a good indication to switch to the transient solution framework, using the semi-converged solution from the steady state. Both of these numerical aspects were reported by Woo *et al.* (2009) and Ullum (2006). In addition, one should also check if the flow field significantly changes at subsequent iterations after 'convergence'. If the flow field changes significantly or even produces aberrant flow contours, then it is most likely an indication of inherently transient behaviour.

Another key numerical aspect is in the refinement of the mesh used. It is common CFD practice to perform mesh independence tests particularly for regions of high gradients. This is normally undertaken by systematically and progressively using smaller mesh sizes until the solution is independent of the mesh size. However, for such possibly self sustained fluctuation flow, on top of providing mesh independence to the solution, the mesh size also determines whether or not the possibly transient flow structures are captured. This was firstly reported by Oakley *et al.*[25], where their steady axisymmetric solution becomes progressively unsteady when the mesh size was reduced to a certain high refinement. Although not specifically shown, Langrish *et al.* [5] also observed such numerical behaviour in their Very Large Eddy Simulations (VLES) of a pilot unit. Such a numerical behaviour is attributed to the ability to capture smaller flow structures as too coarse a mesh will make the solution too diffusive, thus damping out any transient behaviour. Woo *et al.* (2009) further reported on this behaviour by using an extensive combination of mesh sizes and chamber diameter[23]. In their three-dimensional simulation work on a short-form co-current spray dryer, a total of 946071 mesh elements are warranted for a transient solution whereas a mesh of only 288511 produces a steady state flow solution without any self-sustained fluctuations.

Two dimensional versus three-dimensional

Consideration in using a two-dimensional (including axisymmetric models) or three-dimensional simulation will greatly affect the computational time and resources (Figure 4). Such requirements are further amplified in transient simulations as the flow field needs to be developed and statistical averaging might be required in the transient framework [21][26]. Most early work typically utilizes the axisymmetric [25][27]and two-dimensional models [10-11]. In recent reports, workers have shifted to three-dimensional simulations[23][26][28]. Apart from the computational requirements, another important consideration between the two approaches concerns the ability to capture any possible transient behaviour in the flow. Guo *et al.* [20] have shown that transient fluctuation, particularly of the central jet, is three-dimensional. To be more precise, the jet tends to flap about a moving axis precessing around the chamber. Further illustration of such fluctuation is illustrated by Woo *et al.* using the jet feedback mechanism[23]. Using a two-dimensional model for such flows will prohibit the precision of the model in capturing such important

flow structures; limiting any possible transient behaviour to a two-dimensional plane. In certain cases, such restriction might even make the flow behave in a steady like behaviour. This was observed in simulations of a rotary atomizer fitted pilot unit using both the three-dimensional and the axisymmetric approach[23][27]. Such numerical implications could be due to the inability of axisymmetric simulations to capture possible cross-flows as well as flow rotation (or swirls) which might not be uniform along the circumference of the chamber. Therefore, these factors should be kept in mind when interpreting an axisymmtric simulation of a spray dryer. However, it is important to note that an axisymmetric approach drastically reduces the computational resources and time in a compromise with accuracy.

Turbulence modelling approach

All the CFD simulations undertaken so far are confined to the Reynolds Averaged Navier-Stokes (RANS) approach in which the large scale turbulent eddies are modelled. Under this family, different closures were reported in the literature. However, it would not be useful to specifically pinpoint any particularly useful model as myriad flow patterns can be observed in a chamber: e.g. non-swirling, vane induced swirls, rotating disc induced swirls. Rather, it will be useful to identify how different turbulence models work for different situations. Most of the simulations reported in the literature uses the conventional work horse for the CFD technique, k-e closures [26][29][30]. For highly swirling flow induced by a rotating atomizer, a very useful comparison can be found in the report by Huang *et al.* [12] in which the different variant of k-e closures were tested against the anisotropic Reynolds Stress Model (RSM). Taking the RSM as a basis, Huang *et al.* concluded that the RNG variant of the k-e closure can be a suitable and computationally economical approach. In terms of transient simulations, Langrish and his associates[5][28] have shown that the k-e closure as well as the Shear Stress Transport (SST) method, which is a hybrid between the k-e and k-w closure, has the ability to capture the fluctuation frequencies relatively well.

In these conventional RANS based turbulence closures, the resolution of the turbulence scale in the simulation is limited by the size of the mesh used. It might be important, although yet to be illustrated, that the capturing of these small scale turbulences might significantly affect subsequent transport of the particles or droplets in the chamber. Recently, Fletcher and Langrish [31] evaluated the use of the Scale-Adaptive-Approach (SAS) technique applied to the SST closure to capture the smaller turbulence scales without the need to use a relatively much finer mesh. It was found that the SAS-SST technique was able to capture some of the transient eddies previously observed in the pilot scale experiments [16].

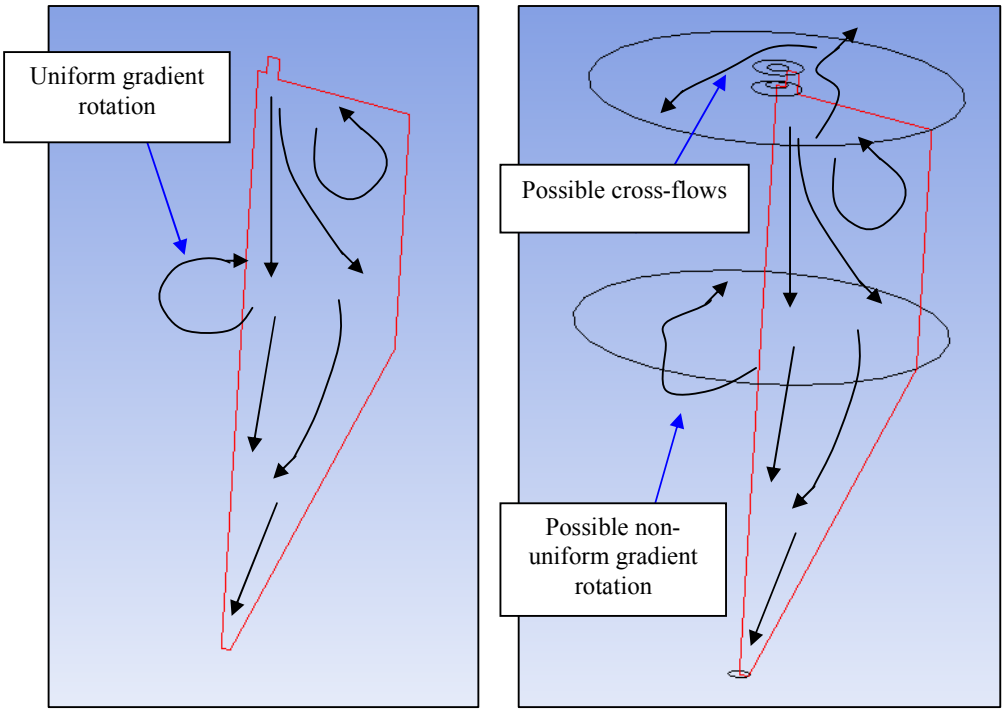

Figure 5 Axisymmetric and three-dimensional considerations

2.2 Particle tracking and atomization

Particle loading in a spray dryer is relatively dilute. On top of that, unlike other multiphase particle-air processes such as the fluidized bed or pneumatic powder conveying, the particles in a spray dryer are not in constant contact with each other. In fact, contact between the particles can be viewed as 'instantaneous'. It is for these reasons, the Euler-Lagrange method is preferred in all the work reported hitherto. Apart from that, stemming from the development of the Particle-Source-In-Cell method developed by Crowe *et al.* [32], it is also more realistic to incorporate the droplet drying phenomenon through the Euler-Lagrange method. Nevertheless, there are also reports where the Eulerian-Eulerian method is employed treating both the droplet/particle and the gas phase as interpenetrating continuum liquid. This treatment of particle tracking will not be covered in here and an illustration in the application of this approach can be found in the work of Li *et al.* [33]. It is noteworthy that the pure evaporative model used in the work of Li *et al.* has to be modified in the application of spray drying in order to account for the solid formation of the droplets.

In the Euler-Langrange method, a spray or a steam of atomized liquid is represented by a distribution of parcels. Each parcel represents a group of particles with the same size and mass (Figure 6). It is then assumed that particles of the same size and mass follow the same path. Such an approach does not necessitate the need to track a huge number of particles. The parcels are then individually tracked throughout the flow field following Newton's drag law of motion assuming that all the particles in a parcel follows the same path due to the similarity in mass and diameter,

$$\frac{du_P}{dt} = F_D(u - u_P) + \frac{g_X(\rho_P - \rho)}{\rho_P} + F_X p \quad (1)$$

where F_D, drag force, is normally expressed in the following form assuming spherical particles,

$$F_D = \frac{18\mu}{\rho_P d_P^2} \frac{C_D \,\mathrm{Re}}{24} \quad (2)$$

with the Re given by,

$$\mathrm{Re} = \frac{\rho d_P \left| u_P - u \right|}{\mu} \quad (3)$$

Another advantage from this method is that additional forces can be easily incorporated into the model. This feature has found applications in other fields such as spray coating which utilizes electrostatics to manipulate the spray trajectories. Some reports can be found in experimentally charging particles during spray drying in an attempt to reduce the deposition problem [34]. However, there is yet to be incorporation of additional forces in the modelling effort so far. Additional forces such as the Basset or Magnus forces are normally not incorporated due to the relatively big difference in density between air and a typical particle found in spray drying. Turbulence dispersion of the particles is normally modelled by the Random Walk type of model which is based on the principle that a parcel successively enters and leaves random eddies distributed throughout the domain. Mathematical details for such stochastic treatment of particle dispersion can be found in the chapter on Lagrangian particle tracking in this book (Sukgoo *et al.* – Chapter 10). Figure 7 shows the random stochastic obtained for a same particle injected into a simulated flow field.

Although the Lagrangian tracking method has been widely used and is the accepted method in modelling particle movements in the chamber, there is virtually no development done in this area with application to spray drying. Only some validation work was undertaken to validate such Lagragian particle tracking by measuring particle concentration and sizes in different regions of the chamber [35-36].

Important consideration when applying the Lagrangian technique is in coupling with the flow field. As a particle is tracked from its injection, it generates momentum, energy and species source terms in the CFD domain in which it passes. While the effect of species and energy source terms on the flow field is apparent, there can be debate in the significance of the momentum coupling due to the aforementioned low particle loading; particularly for 'cold flow' research applications in which heat and mass transfer from the droplet is not considered [28]. In the region near the atomizer, where the particles are yet to be dispersed, particle loading can be quite high going beyond the recommended threshold for one-way coupling [32].

Depending on the case, such high loading can significantly affect the flow field near the atomizer which subsequently affects the flow field in the other downstream regions [4]. Recently, in a full transient simulation, the effect of particles on the flow field was further illustrated by Jin and Chen [26].

In the wake of recent developments in transient CFD simulations of spray dryers, usage of the steady or transient particle tracking has also emerged as an important consideration. Figure 8 shows the difference in numerical procedures when implementing full coupled steady or transient particle tracking. In the steady approach, particles are injected and tracked until it reaches the boundary of the simulation domain [11][23][28]. On the other hand, in the transient approach, particles are typically tracked and penetrate the flow field following the simulation time step and duration [21][22]. This has three major implications: (1) relatively large simulation time is required for all the injected parcels to initially penetrate the simulation domain, (2) once the particles have penetrated the flow field, further transient duration is required for any statistical analysis of the particle simulations, (3) particles have to be injected at each time step drastically increasing memory requirements (increasing total number of particle in simulation). It is also clear that the coupling iterations are required for each time step in the transient tracking making it computationally expensive. Therefore, full transient air-particle simulation is a very computationally expensive undertaking. In terms of coupling with the continuous phase as alluded to earlier, for steady state particle tracking, it is important to incorporate these source terms in developing the flow field by repeatedly injecting the particles and reiterating flow field until insignificant change occurs in the computed flow field.

Many different atomizers can be found in spray drying. For example: eg. pressure nozzle, ultrasonic nozzle, two fluid nozzle and rotary disk. In a CFD simulation, these different atomizers are characterized by the particle size distribution, mass flow rate and the initial particles velocity components. As noted by Kieviet *et al.* [10], getting these initial parameters can be a big challenge by itself. While the mass flow rate can be easily known as an overall simulated operation capacity, the latter two parameters are less apparent. Most commercial nozzles and rotary disks come with specifications of the droplet size distribution; the former includes the cone angle.

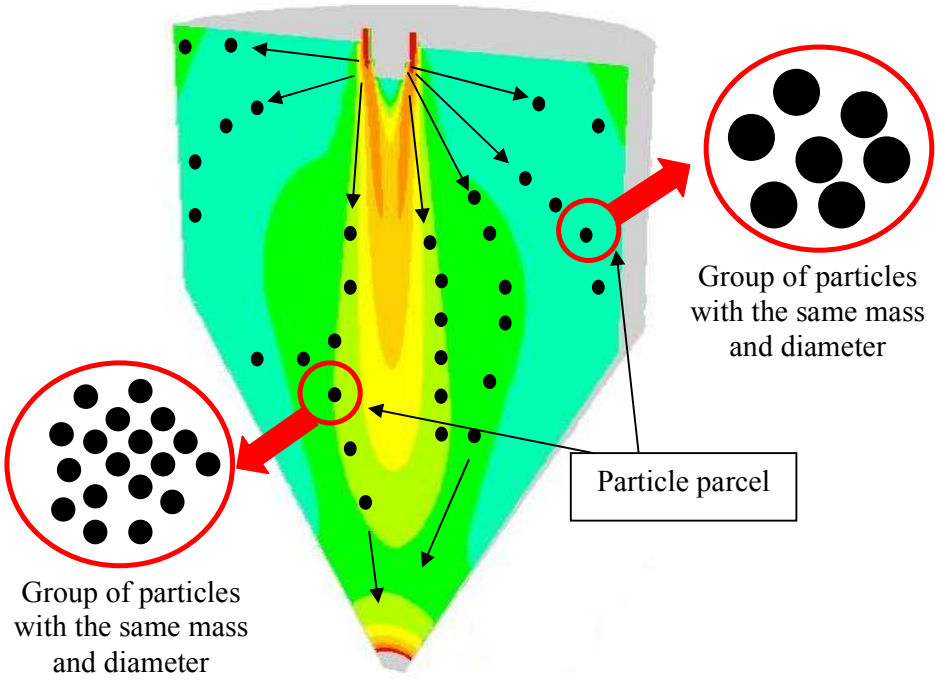

Figure 6 Tracking of a parcel of particles

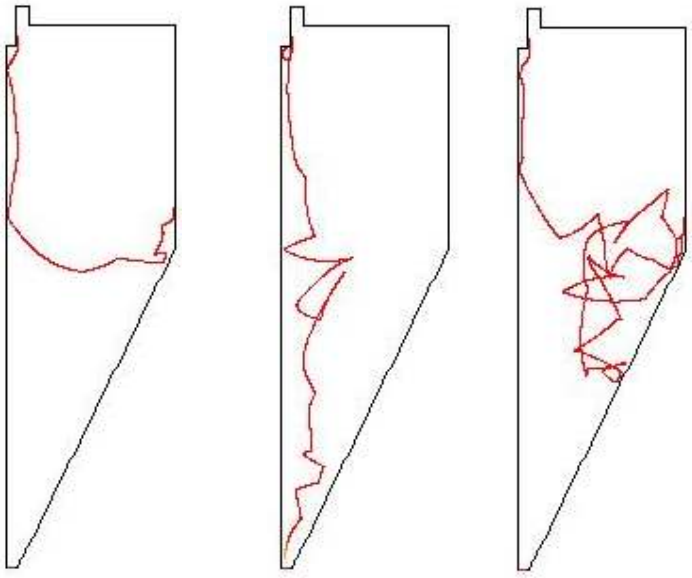

Figure 7 Stochastic tracks of a particle incorporating turbulence dispersion

However, it is important to note that the resultant droplet size distribution or cone angle is strongly dependent on the feed material and the operation of the atomizer such pressure and feed rate. For their simulations, Kieviet *et al.*[10] characterized their atomizer by collecting and measuring maltodextrin droplets in silicone oil. Huang *et al.* [35]and Nijdam *et al.* [37] used laser diffraction technique to obtain particle size distribution of their atomizers. Al-Hakim *et al.* [38] further used PDA to obtain the initial droplet velocity from their nozzle. In the absence of experimental data, correlations for the initial droplet

size distribution and the initial velocity for both rotating and nozzle atomizers can be found in Masters' Handbook [39] . However, in view of the myriad designs of an atomizer, it is important to assess the applicability of these correlations. Huang *et al.* [37] recently re-evaluated its applicability and noted that the effect of viscosity has to be further incorporated into one of the correlations available for a rotary atomizer.

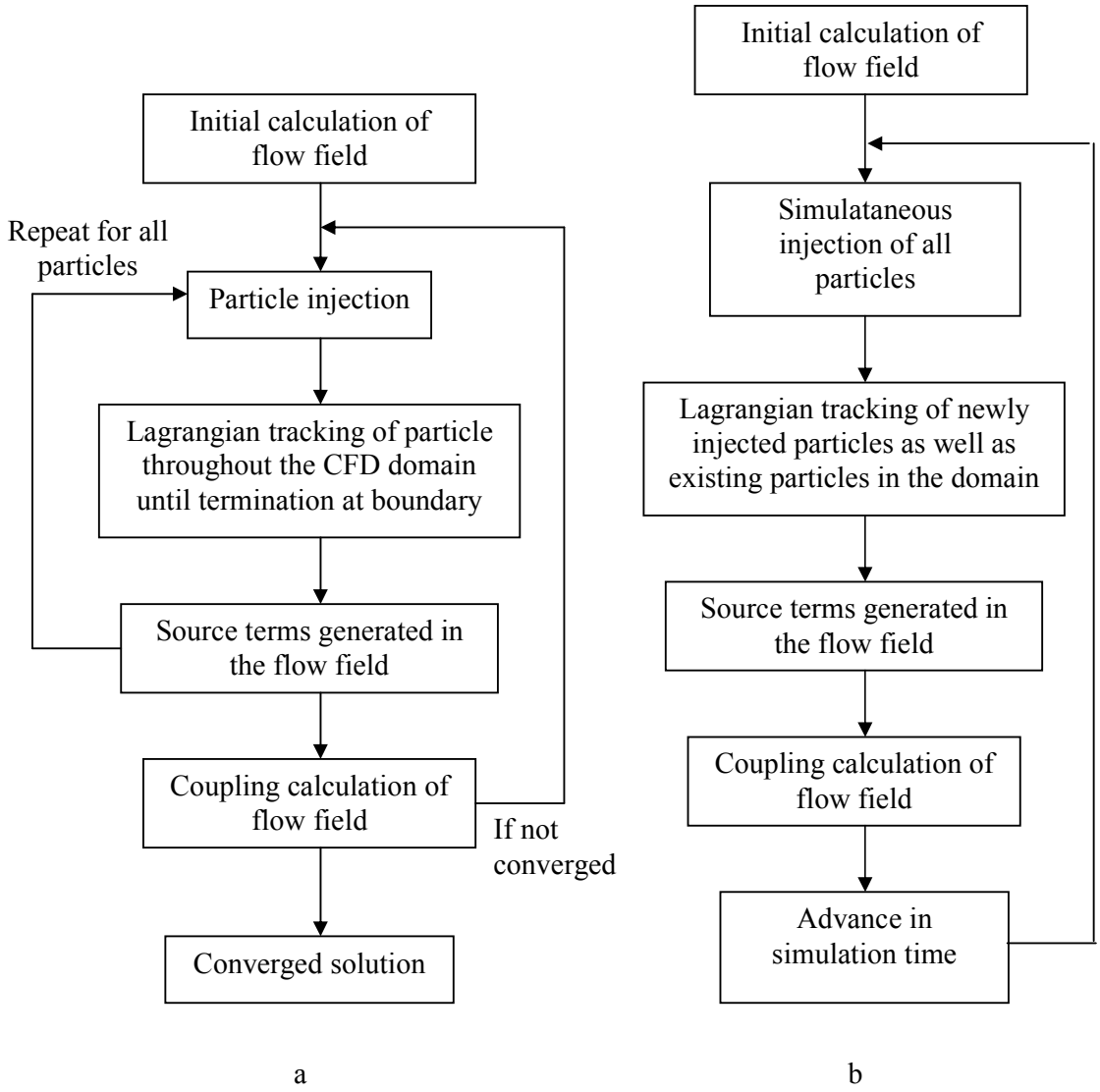

Figure 8 Typical numerical procedure for coupled Lagrangian particle tracking: (a) steady state and (b) transient simulation

Typically, nozzle atomization is implemented by injecting particle into the domain at a point corresponding to the location of the nozzle. For the rotating disk atomization, Huang *et al.* [40] devised a novel method by evenly putting multiple particle injection points around the peripheral of the side wall of the disk. An important note when modelling the rotating disk is to set the disk walls (boundary conditions) to give a rotational momentum source term to the flow field. This modelling effort is crucial as the rotation of the disk will impart significant swirls to the chamber, stabilizing as well as resulting in recirculation

vortex in the region below the disk [16]. Building up from the method by Huang *et al.* [40], some recent work has also incorporated the pumping effect caused by the construction of the rotating disk [4]. Explanation and experimental observation of this pumping effect can be found in the papers provided here [41].

2.3 Droplet drying in CFD simulations

There is a lot of development in the area of droplet drying which includes comprehensive diffusion models [42-44] and other semi-empirical models [45][46]. Description of these models and the fundamental phenomenon in droplet drying will be covered in another chapter in this e-book. The focus of this section is only on the modelling approach applicable to CFD modelling.

In general, as noted by Kieviet *et al.* [47], it is not practical to implement the diffusion type model in a CFD simulation due to the high numerical demand and complexity in the solution of these models. One way is to use a simplified version of the diffusion model [47]. Utilizing this model, their CFD simulation produced humidity and temperature profiles which followed very well to the measured field in their pilot scale unit. In contrary, Lo [48] and Verdumen *et al.* [6] adopted the full diffusion model for their CFD simulations of industrial scale spray dryers.

For simplicity, another approach adopted by some authors is to treat the mixture droplets as pure water[12][13]. In essence, it is assumed that drying of a droplet continues in a saturated manner without any falling rate period. In the event that the particle reaches the boiling point, it is further assumed that the moisture is 'boiled off' from the particle or droplet. Huang *et al.* [14] showed that this approach managed to reproduce the experimental measurements of Kieviet *et al.* [10].

Recent developments have moved to the use of semi-empirical models. Two such semi-empirical models are the: (1) Characteristic Drying Curve (CDC) and (2) Reaction Engineering Approach (REA). The CDC approach assumes that the falling rate period follows a fixed pattern. Langrish and Kockel [46] developed the CDC approach for spray drying with application of milk and proposed a linear falling rate. Such linear falling rate was also used by Zbicinski *et al.* [49] for maltodextrin solutions. However, there can also be many falling rate pattern such as a convex or concave shape. Huang *et al.* [12] evaluated the effect of different falling rate pattern in their CFD simulations. Building up form their work, Woo *et al.* [50] further noted that suitable shape of the falling rate period is strongly dependent on the droplet material by making comparison with single droplet experimental data of carbohydrates. In general, following the suggestion of Langrish and Kockel [46], the CDC mathematically takes the form,

$$\frac{dX}{dt} = f\frac{Ah}{m_S \Delta H_{evap}}\left(T_a - T_{wb}\right) \tag{4}$$

$$f = \left[\frac{\left(X - X_{eq}\right)}{\left(X_{cr} - X_{eq}\right)} \right]^{n} \quad , \quad X \le X_{cr}$$

$$f = 1 \quad , \quad X > X_{cr}$$

On the other hand, the REA visualizes the drying process as an activation process in which an 'energy' barrier has to be overcome for moisture removal to occur [51]. The drying rate then takes the following form,

$$\frac{dm}{dt} = -\frac{h_m A}{m_s}\left(k P_{v,sat}\left(T_d\right) - P_{v,\infty}\right) \tag{5}$$

The core of this model lies in modelling the fracitonality term, k, which should progressively reduce as moisture is being removed. This fractionality is expected to be a function of moisture and temperature, which can be approximated by,

$$k = \exp\left(-\frac{\Delta E_V}{RT}\right) \tag{6}$$

where ΔE_v is the apparent activation energy, which is likely to be dependent on the 'mean' or 'average' moisture. The original authors proposed the following function to be taken as the fingerprint of a material applicable to all drying conditions,

$$\frac{\Delta E_v}{\Delta E_{v,\infty}} = a\, e^{-b\left(X - X_\infty\right)^c} \tag{7}$$

At high moisture content

$$\frac{\Delta E_V}{\Delta E_{V,\infty}} \to 0 \ , \ k \to 1 \tag{8}$$

At low moisture content

$$\frac{\Delta E_V}{\Delta E_{V,\infty}} \to 1 \ , \ 0 < \text{min}imal\ K\ value < 1 \tag{9}$$

Application of the REA model in CFD simulations can be found [21][26][27]. Good comparison was obtained with experimental data. A general comparison between the two approaches, CDC and REA, can be found in the review by Chen [52]. With application to CFD simulations, Woo *et al.* [27] further showed that both approaches response differently to the initial droplet moisture. It is important for the reader to assess these differences and behaviour of the models when applying them in their CFD simulations.

Another development is in the use of the droplet drying model in predicting particle quality. Harvie *et al.* [29] used the predicted particle moisture to further compute and determine the stickiness of the particles in their CFD simulation. This concept was extended by Woo *et al.* [27][50] to determine particle surface rigidity exploiting the ability of the Reaction Engineering Approach to compute surface moisture. Such surface computation might have implications in deposition or any surface quality predictions using the CFD technique. As noted in a few reports[21][27], usage of such surface moisture computation will have big implication particularly in modelling preservation of surface active materials, such as proteins or bioactive substance, within the droplets.

Coming in from the industrial perspective, the CFD team in Niro has adopted an alternative semi-empirical approach in modelling droplet drying. The approach is based on the development of an acoustic levitation dryer in which a droplet can be levitated and evaporated while its drying rate can be continuously monitored [53]. From the acoustic levitator, extensive sets of drying rates data, specific to the material, can be determined at different drying conditions and inserted into the CFD simulation corresponding to the condition of the Lagrangian parcel in the domain. Recent reports from Ullum [54] indicate that this approach corresponds well with pilot scale data. This useful predictive tool, under the tradename Drynetics, is already commercially used in their design and optimization work (www.foodproductiondaily.com).

2.4 Wall deposition modelling

Sticking criterion

The wall deposition model determines the fate of the particles when they are tracked and reaches the simulation boundary (wall). Choosing a suitable wall deposition model will affect the prediction of yield and final product moisture prediction. Most of the simulations reported in the literature utilize the stick-upon-contact approach [12][30][55]. In essence, it is assumed that once a parcel touches the simulation boundaries (wall), it will be adhered and removed form the simulation.

This approach is a simplifying assumption which does not capture the important effect of particle rigidity on the collision outcome. It has been a common practice and as illustrated by Bhandari and his co-workers, that increasing the rigidity of the particles increases the yield from the spray drying process [56][57]. Such an effect was also fundamentally investigated by Zuo *et al.*[58] using a particle gun experimental setup in which powders are pneumatically impinged onto a substrate wall material. Along this line, Ozmen and Langrish [59] investigated this effect in a pilot scale spray dryer unit and arrived at a deposition model based on the Glass Transition – Sticky Point concept. Figure 8 shows the typical glass transition curve of lactose as predicted by the Gordon-Taylor correlation. From Figure 9, the glass transition temperature (and the corresponding sticky point temperature) is a strong function of the particle moisture. At higher moisture contents, the sticky point becomes lower and vice versa. If the particle temperature is

above the sticky point, the particle is then deemed sticky and will adhere to the walls of the processing equipment.

Following this concept, the sticky point of material is taken as the cut-off point in determining whether or not a particle sticks to the wall. With application to amorphous carbohydrates, it is common to take the sticky point as 20-25 degrees higher than the glass transition point [27][29][42].

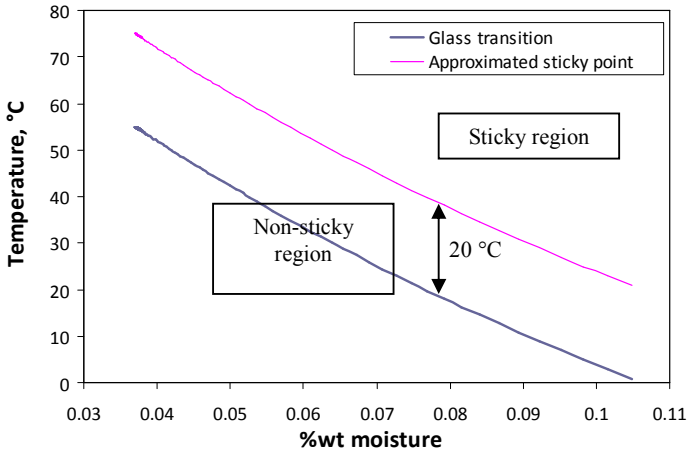

Figure 9 Typical glass transition and approximated sticky point curve for lactose

However, it is noteworthy that this concept in using the glass transition as the cut off point does not account for the effect of impacting velocity and angle on the collision outcome. Murti *et al.* [60] utilizing particle gun experiments have shown that the impact velocity and angle do affect the deposition of skim milk powders. A higher impact velocity causes a higher critical T-Tg value, which translates to a lower propensity for the particle to get adhered. Apart from that, it was also found that beyond the critical T-Tg value, a smaller impact angle reduces the dependency of particle stickiness on temperature. Therefore, the particle impacting momentum does affect the deposition outcome.

In order to address these aspects of deposition modelling, a recent work involved the development of a rheology based deposition model [61]. The premise of this model is based on the viscoelastic property of amorphous particles often encountered in spray drying [62]. Starting from and assuming a Kelvin-Voigt element, the elastic and dissipation forces experienced by a particle can then take the form,

$$F_{approach} = -\frac{A}{2R}\left(E\,x + \eta\,v\right) \tag{10}$$

Adopting the superposition technique, which is a commonly accepted technique in polymer sciences, master curves for the elastic and loss modulus in the equation above can be determined from DMTA experiments [63]. From the master curves coupled with the superposition technique, the rigidity of the particle at different temperatures, which is delineated by the elastic and loss

modulus, can be obtained to be used in the collision modelling. From Equation xx, it can be seen that the effect of impacting velocity is also incorporated into the model. It is noteworthy that this approach is still at its infancy and full validation of this approach is currently in progress.

Particle build-up and near wall particle transport

These physical aspects in deposition modelling have not been attempted before in any CFD modelling of spray dryers. This section is aimed at giving some perspectives in this area and also to touch on some possible significance (or lack thereof) in capturing such phenomena. Another aim of this section is to let the reader become aware of the limitations in current CFD modelling effort when interpreting their own results.

When particles get deposited onto the walls of the chamber, they tend to retain or continuously release moisture while in the deposited state. When the layers get sufficiently built-up, the released or trapped moisture can affect the overall humidity and temperature predictions in the chamber. This was observed in industrial operations (Dr. Huang – personal plant experience). To further complicate things, in certain materials such as dairy products, the deposition rate will tend to decrease overtime to reach a relatively constant deposit thickness in which the entrainment rate balances out the deposition rate. On top of that, there might also be tendency for the deposits to get dislodged and slide down as an 'avalanche' once it reaches a certain deposited weight [64]. Such deposit build-up phenomenon has been extensively modelled in CFD simulations of boilers [65]. In the CFD boiler simulation of Kaer *et al.* [65], the combination of transient-steady approach was formulated which does not necessitate tracking the particles following the transient fluid flow time. It will be interesting if such technique is implemented or evaluated in the spray dryer framework. This can be an area to look at in future simulation development work.

Another area in which methods can be adopted from CFD simulation of boilers is in the near wall particle transport modelling. All the CFD simulations for spray dryers reported so far rely solely on Lagrangian tracking. This assumes that sufficient particle parcels are used to represent the dispersion of the particle cloud near the wall (as well as in the central region of the chamber). Recently, Kaer *et al.* (2006) argued that although parcels are considered not depositing when they are tracked in the Lagrangian manner to move in parallel closely above a wall, in reality, part of the particles in the parcel might actually disperse away from the mean parcel flow to reach the wall [65]. Kaer *et al.* introduced a turbulent-pipe-deposition based dispersion model in the CFD simulation of a straw boiler on top of the typical lagrangian tracking dispersion model. Figure 13 illustrates in a simplified manner the difference between the current Lagrangian deposition tracking method and the deposition pipe based deposition model as proposed by Kaer *et al.* (2006) for boiler simulation. Attempt to use such a turbulent-pipe-deposition based deposition model was also made by Kota and Langrish [66] in their analysis by considering the spray dryer as a 'large pipe'. However, this approach produced limited success in their analysis based on the experimental deposition fluxes obtained from a pilot scale unit. It will be interesting to see how such turbulent-pipe-deposition based model can be further developed for application in CFD simulation of spray dryers.

2.5 Particle interaction modelling

Most work reported in the literature does not consider particle interactions in their simulation. This is partly justified by the dilute loading of the particles resulting in the particle being effectively separated form each other. However, recent interest to use CFD in predicting the final particle size due to agglomeration and coalescence has led to extensive developments in the interaction models under the EDECAD project [6]. Under this project, particle interactions were discriminated in the form of: droplet-droplet, droplet-particle and particle-particle interactions. The first interaction simply implies that droplets coalescence and form a larger droplet composed of the volume of the two coalescing droplets. For the latter two interactions, a Newtonian-based viscous penetration model was assumed to capture how particles will penetrate each other during collision to form agglomerates. On top of collision criteria, part of the effort in modelling such particle interactions is also focused on a stochastic approach in determining collision partners for each particle in the simulation domain. Instead of relying on the 'physical' collision as predicted by the Lagrangian tracking, the developed approach determines the collision partner of a particle based on the distribution of the neighbouring particles within the computational cell [6]. Along the same line, Guo *et al.* [20] evaluated the applicability of the Lagrangian approach in modelling such stochastic particle collisions due to turbulent flow. A latter evaluation further confirms the advantage of the Lagrangian approach in modelling such turbulent dispersion of droplets [35]. From the EDECAD project, Relatively reasonable results were obtained from their approach in comparing with pilot scale experimental data [6].

Looking at a different aspect, on top of the coalescence phenomenon, Mezhericher *et al.* [55] recently showed that incorporation of particle-particle interaction (bouncing) does affect the dispersion of the particles in the chamber. Therefore, this lends further weight on the significance of particle interactions within the chamber. However, further experimental validation is required in this area.

3.0 Simulation validation

The flip side of any CFD simulation is model validation, which is a big challenge in spray drying due to the harsh conditions within the chamber which make local measurements extremely difficult- even impossible. The task is further complicated with the presence of droplets or particles which might foul measurement equipments inserted into the chamber. This section aims to introduce the current validation method available and also some of the experimental data available for comparison.

3.1 Quantitative and qualitative airflow visualization

One option for partial validation is to measure the velocity profiles within the chamber. As mentioned earlier, presence of droplets or particles and the harsh conditions in the chamber tend to hamper such measurements. Therefore, most measurements and experimental velocity profile data available were done in 'cold-flow' conditions and without atomization of feed.

Kieviet *et al.* [10] provided very useful air velocity profile measurements from their pilot scale unit using a hotwire anemometer. This set of experimental work has somehow recently emerged as a standard test case for many reports [14]. For the benefit of future experimenters, it is noteworthy that strong turbulent fluctuations might exist within the chamber depending on the location of measurement. Measurements near the central jet might exhibit relative high fluctuation whereas in the recirculation region near the wall region, fluctuations might be relatively lower. It is useful, as done by Kieviet *et al.* [10], to report the average velocity as the mode of the velocity distribution and also to take note of the fluctuation range in measurements. This will ensure a more useful comparison with the CFD prediction. In a recent work, such a method was also adopted by Woo *et al.* [23] in their measurements in a pilot scale dryer.

Apart from obtaining the average velocity profiles, another possible output in the usage of hotwire measurements is to produce data of the transient behaviour in the chamber. Such measurements can be found in the published work of Langrish and his co-workers to measure the long time-scale behaviour of the flow [16][67]. In analyzing these transient data, the Fast Fourier Transform (FFT) is a useful tool to analyze the transient data by transforming the time-series data into the frequency spectrum so that dominant or secondary frequencies in the flow can be identified [15]. Important criteria when choosing a hotwire measuring system for such transient analysis is to have sufficiently high sampling frequency and sampling intervals.

Recently more advanced methods such as the Laser Doppler Anemometry (LDA) and PIV are used to provide more detailed measurements of the air flow [36][68]. Some special notes on these methods is that significant modifications has to be to allow such optical based measurements to penetrate into the chamber and high cost is involved in such methods. In order to use the LDA method, Bayly *et al.* [68] had to make measurements from a scale down spray tower made of transparent perspex. In the spray tower of Zbicinski *et al.* [68], transparent observation panel were installed at different elevations to allow PIV measurement access. As to date, these methods were only used to provide average velocity contours but yet to be explored to provide transient data. Besides, flow in the presence of particles is bound to be different from the particle-free flowfield.

In qualitative manner, flow visualization experiments had been carried out on pilot scale units using flexible turfs and smoke [16]. Turfs can be positioned at different regions in the chamber to provide a rough indication of the flow direction in the chamber. However, usage of tufts will not be able to capture small length scale or low velocity structures. These small scale

structures can then be visualized using smoke. There can be many options to introduce smoke into the chamber. When analyzing the atomization region, Langrish *et al.* [42] introduced smoke from the air inlet pipe to flow across their rotary atomizer. Smoke can also be introduced into the chamber via tubes or 'tube racks' to be positioned at different regions of interest within the chamber [16]. Using smoke visualization, they managed to observe small eddy formations in the recirculation region when swirl was imparted to the flow by atomizer disk rotation. A key issue in using such visualization method particularly smoke visualization; is the illumination required to make the smoke contrastingly visible for analysis. The concentration of smoke in the region of interest is also another factor which makes this method useful.

3.2 Humidity and temperature measurements

A huge difficulty in measuring the humidity and temperature field is because of the presence of droplets and particles. A seminal advancement in this area was contributed by Kieviet *et al.* [47] in the development of a micro-separator. This device allows particles or droplets in the air to be separated before reaching humidity and temperature probes which can be inserted into different regions in the chamber. Separation is achieved by enforcing a tight flow curvature of the particle-laden air, causing the particles to traverse the air flow and thus prevents any particle in reaching the measurement sensors. Incidentally, the development of the micro-separator by Kieviet *et al.* [47] also involved use of the CFD technique.

3.3 Final product and deposition flux comparison

For full CFD simulations incorporating particles injections, it is typical to make comparison of the predicted particle moisture with that of experiments. So far, there is limited comparison reported in the literature. Quantitative deposition flux data, *hitherto*, can be found in numerous reports [59][69][70]. Deposition fluxes were mainly determined by inserting plates into the chamber and allowing the particles to deposit over a relatively short period of operation time. Based on the pilot scale experimental deposition fluxes, Kota and Langrish [28] noted that their simulations produced realistic deposition trends. However, the CFD prediction only produce reasonable quantitative match to the experimental data. Qualitative data particularly on regions of high deposition in industrial scale dryers was also reported by a few workers[71][72]. Such observations can certainly complement CFD simulations although only limited comparisons can be made due to the confidentiality of such commercial operations.

3.4 Residence time measurements

There has been attempt to characterize the residence time in the chamber utilizing the nuclear tracing approach[73]. Kieviet *et al.*[64] attempted to measure the residence time their pilot unit using pulsed injection of coloured feed material. However, their experimental findings did not compare very well with correpsondign CFD simulations. Accurate prediction and validation of the residence time in spray drying will have big implication in the usage of the CFD technique to predict in-process crystallization[74] or preservation of biological material within the chamber [75].

4.0 A sample CFD simulation

This section presents two samples of the prediction results for a co-current spray dryer fitted with a pressure nozzle. The CFD results for a steady state spray drying are compared with the published data of Kieviet et al. [10][47].

4.1 Steady state

Problem description

Figure 10 shows the tested spray dryer geometry used in this work which is the same as that studied by Kieviet[10]. The chamber is a cylinder-on-cone vessel, 2.215m in diameter and with a cylinder top section, height of 2.0m and the bottom cone with 1.725m height. The angle of the cone is 60^0. Hot air is blown from the ceiling of the drying chamber through an annular tube which has an outer diameter of 495.6mm and an inner diameter of 411.6mm. The pressure nozzle is located at the center of drying chamber, 229mm away from the flat ceiling of chamber. There is an exit tube for the exhaust air conveying the dried particles at the center of the cone. The outlet diameter is 172mm.

Mesh independence test

The simulations are performed for steady state operations. The 2D axi-symmetrical model which is same as the model used by Kieviet[10] was selected for simulation. Square grids (size 0.03m) were used for the drying chamber. The results for airflow patterns and temperature fields were similar when different mesh sizes were used. Hence, the results are considered to be grid-independent. The number of grid point used for the geometry tested is 3765.

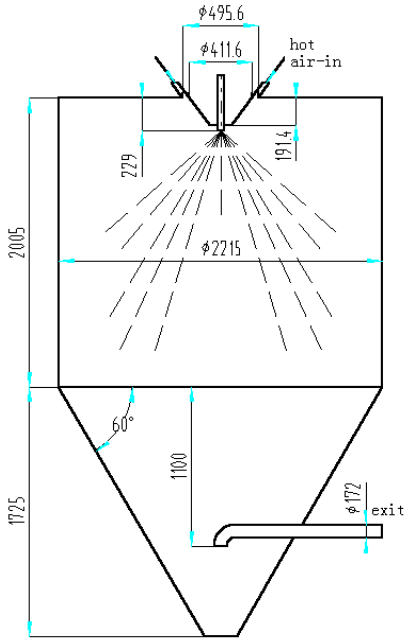

Figure 10 Tested geometry with dimensions in mm

Boundary conditions

Cases A and B are defined as spray dryer without spray and with spray, respectively. Inlet air: The velocity of drying air is 7.36m/s for the case without spray and 9.078m/s with spray. Temperature of the air at inlet is set at 468K and its relative humidity is 75% at 25°C. Outlet conditions: The outlet pressure is set at –150Pa, i.e., a fan is assumed to draw air out from the drying chamber. Chamber wall conditions: According to the options that could be selected for the present work in the FLUENT code, when a droplet/particle hits the wall of the drying chamber, it can be assumed to be "trapped" or "escaped" or "reflected" by the wall. Under the "trap" condition, all non-volatile material is "lost" from the calculation at the point of impact with the wall. The volatile material present in the trapped particle/droplet is assumed to be released to the gas phase at this point. However, under the "escape" condition, the particles are removed from the calculation at the point of impact with the wall. According to the "reflect" condition, the particles rebound off the wall with a change in its momentum as defined by the coefficient of restitution. In this validation case, the "escape" boundary condition is used.

The overall heat transfer coefficient from the wall to the outside of the drying chamber is estimated to be 3.5W/m^2.K and the chamber wall is assumed to be made of 2mm thick stainless steel. This coefficient value is obtained by fitting published measurement results [10] with a simulation carried out with spray. Spray from nozzle: An "injection" condition is defined here to specify the spray with a given droplet size distribution. The droplet diameters and mass flow rates used are shown in Table 1. The spray mass flow rate is 50kg/h (0.013889kg/s) with 42.5% solids content. The feed temperature is set at 300K. The spray angle is assumed to be 76^0. The droplet size distribution is such that $10.0\mu m$ is the minimum droplet diameter and $138.0\mu m$ is the maximum droplet diameter with an average droplet diameter D_m of $70.5\mu m$. The droplet diameter distribution is modeled using a Rosin-Rammler curve with these parameters and the spread parameter equal to 2.05. The droplet

velocities at nozzle exit are fixed to be 59m/s (46.49m/s in the x-axis and 36.32m/s in the y axis). In order to simplify the calculation, the feed physical properties are assumed to be those of water, except that the volatile content is allowed to change as drying proceeds.

Table 1 Diameters and mass rate of droplets injected by the atomizer

Droplet No.	*0*	*1*	*2*	*3*	*4*	*5*	*6*	*7*	*8*	*9*
Diameter (10^{-5}m)	1	1.67	2.35	3.02	3.69	4.37	5.04	5.72	6.39	7.06
Mass rate (10^{-4}kg/s)	3.31	5.62	7.71	9.47	10.8	11.6	11.9	11.8	11.3	10.4

Droplet No.	*10*	*11*	*12*	*13*	*14*	*15*	*16*	*17*	*18*	*19*
Diameter (10^{-5}m)	7.74	8.41	9.08	9.76	10.4	11.1	11.8	12.5	13.1	13.8
Mass rate (10^{-4}kg/s)	9.3	8.09	6.83	5.62	4.50	3.51	2.67	1.98	1.43	1.01

Turbulence model: For the 2D-axisymmetric model, the standard k-ε turbulence model was used. Because there is no swirling flow in the drying chamber, the standard k-ε model is expected to be an appropriate choice for simulating such a flow [Oakley, 1994]. The turbulent kinetic energy at the inlet was set at $0.027m^2/s^2$ and the energy dissipation rate at the inlet to be $0.37m^2/s^3$ which are the same values as those used by Kieviet [10]. For tracking the droplets, the turbulent stochastic model (TSM) option was used. Turbulent stochastic tracking of droplets allows for the effect of random velocity fluctuations of turbulence on particle dispersion to be accounted for in the prediction of particle trajectories.

Predicted results

The predicted velocity profiles for Case A and measured results by Kieviet at different levels in the drying chamber are shown in Figure 11. Figure 11 shows that the predicted velocities agree well with the measured results. It is seen that there is a non-uniform velocity distribution in the core region of the chamber. The highest velocity magnitude is about 7.0m/s at the 0.30m level. The velocity magnitude is reduced as the air goes into the chamber further due to the expanding area.

Figure 12 shows the predicted temperature profile for Case B and the measured data by Kieviet at different levels in the drying chamber. It is found that the predicted results agree well with the measured results. The simulation results provide details of the temperature field at different levels and anywhere inside the chamber. The measurement results however do not give such detail because of the limited number of measurement points.

From the predicted temperature profiles (Figure 12), it is observed that the temperatures in the central core up to a radius of 0.1m are quite different at different levels, which is expected as a direct result of drying. There is only a minor radial variation in the gas temperature. The largest temperature changes usually occur at the first level. It is the result of very high heat and mass transfer rates in the nozzle zone due to high relative velocities between the gas and the droplets coupled with large temperature driven forces.

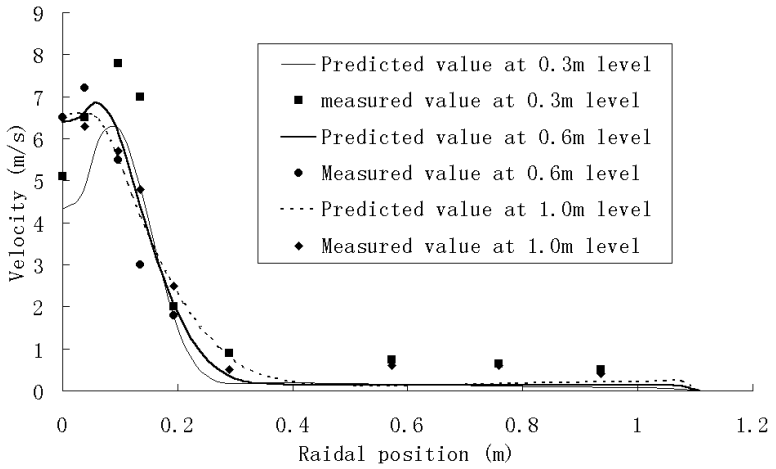

Figure 11 Comparison of velocity profiles between present prediction and Kieviet's measurement at no spray condition

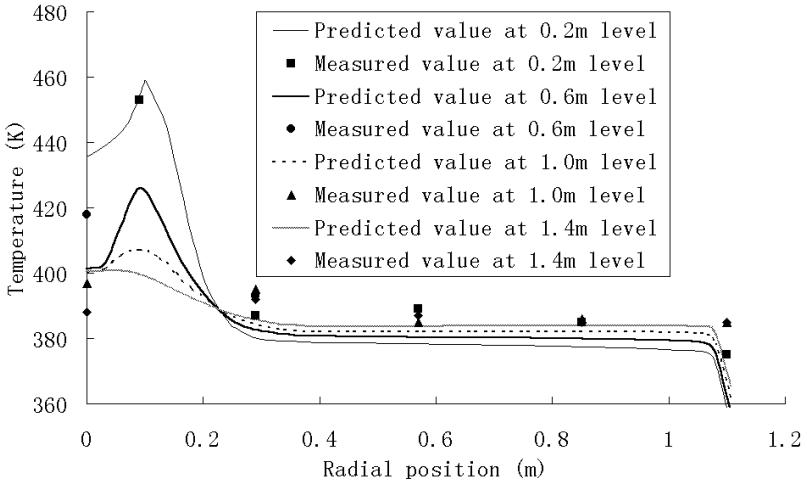

Figure 12 Comparison of temperature profiles between prediction and Kieviet's measurement at spray condition

4.2 Transient state

The example below aims to illustrate the intricacy and certain numerical aspects of undertaking a transient spray dryer CFD simulation. A pilot scale cylinder on cone dryer (1.7m high with 1m diameter) is simulated (Figure 13 a). The unit is equipped with a rotating atomizer at the top which imparts rotation to the flow field when the atomizer is operated (Figure 13b).

a b

Figure 13 Spray dryer considered for the transient simulation (fitted with a rotating atomizer – National University of Malaysia)

Southwell and Langrish [16] previously observed that such rotating flow, particularly the central core, is transient in behaviour. Figure 14 illustrates the flow pattern generated when a steady state or a transient is used in the simulation. It can be seen that a steady state simulation resulted in a very aberrant flow field. When the simulation was switched to the transient approach, the appropriate flow field was achieved. This illustrates the importance for future worker to firstly indentify the nature of the flow in the spray chamber when interpreting their own results.

It was further found later on from the numerical work that the flow field is transient in terms of the rotating recirculation region. Figure 15 further compares the effect of incorporating swirls in a simulation; if swirls are physically present in the actually dryer operation such as those induced by inlet swirls or atomizer rotation. It is noteworthy that non-inclusion of these phenomenons, if it arises in the physical system, can result in completely different flow fields which will subsequently affect particle trajectory predictions.

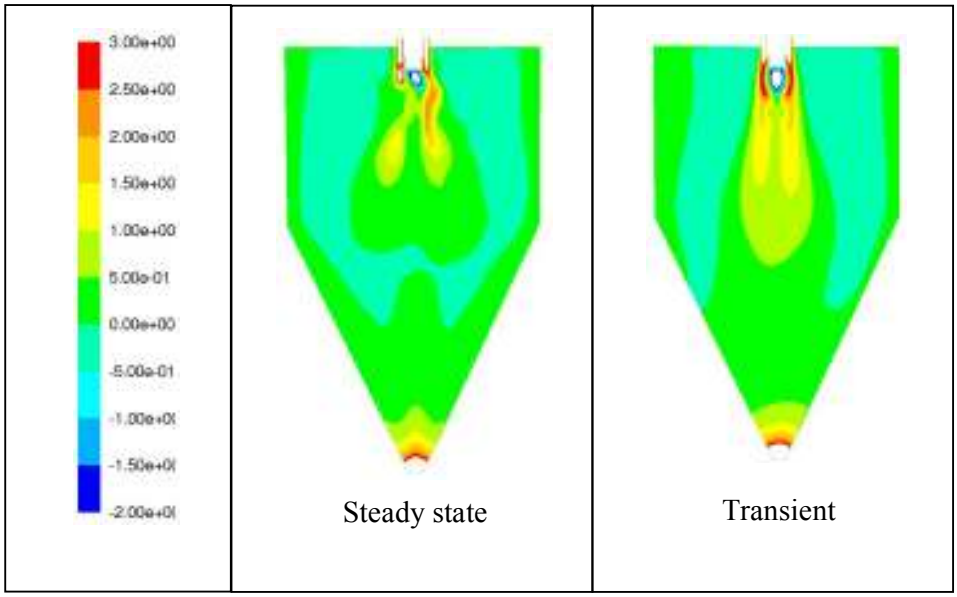

Figure 14 Comparison between flow fields generated using the steady and transient simulation approach for a predominantly transient flow

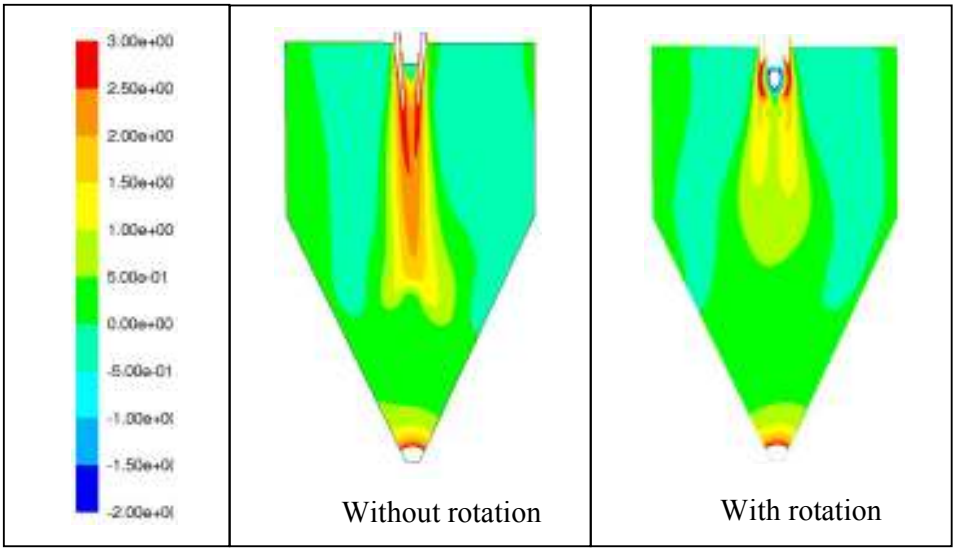

Figure 15 Comparison between flow fields generated with and without atomizer rotation

In comparison to the preceding example, transient particle tracking is used in this work. This means that the particles are tracked following the flow field simulation time. The implication of this, as can be alluded from Figure (16), is that it takes quite s significant amount of time for the particle to penetrate into the chamber. Therefore, interpretation and post-processing of any transient results should only be undertaken discarding the initial portion of the simulation so that the actual operating condition of the chamber can be analyzed and not only the initial 'flow developing' period. On the contrary, in the steady state particle tracking, each particle is tracked throughout the flow field one at a time, until it leaves or terminates at the boundary. These are important considerations in future transient simulation of a spray dryer.

5.0 Typical applications

This section aims to highlight the possible applications and usage of modelling the spray drying process using the CFD technique. Applications can be found in troubleshooting the process or arriving at optimal operation and design of the unit.

5.1 Operation and design optimization

In terms of process troubleshooting, Straatsma *et al.* [11] illustrated the use of the CFD technique using an in-house NIZO-DrySim CFD code to troubleshoot a problem occurring in an industrial scale spray dryer fitted with a rotating atomizer. In their dryer, operation problem occurred when the rotary

atomizer was operated at a higher capacity (faster rotation), giving strange behaviour. Although the operators suspected that this could be due to air by-pass from the central air inlet to the outlets located at the side on the ceiling, they could not provide the evidence to facilitate modifications to the unit. From CFD simulations, they managed to show that the relatively higher atomizer rotation caused the air flow to by-pass to the air outlets without effectively penetrating the chamber.

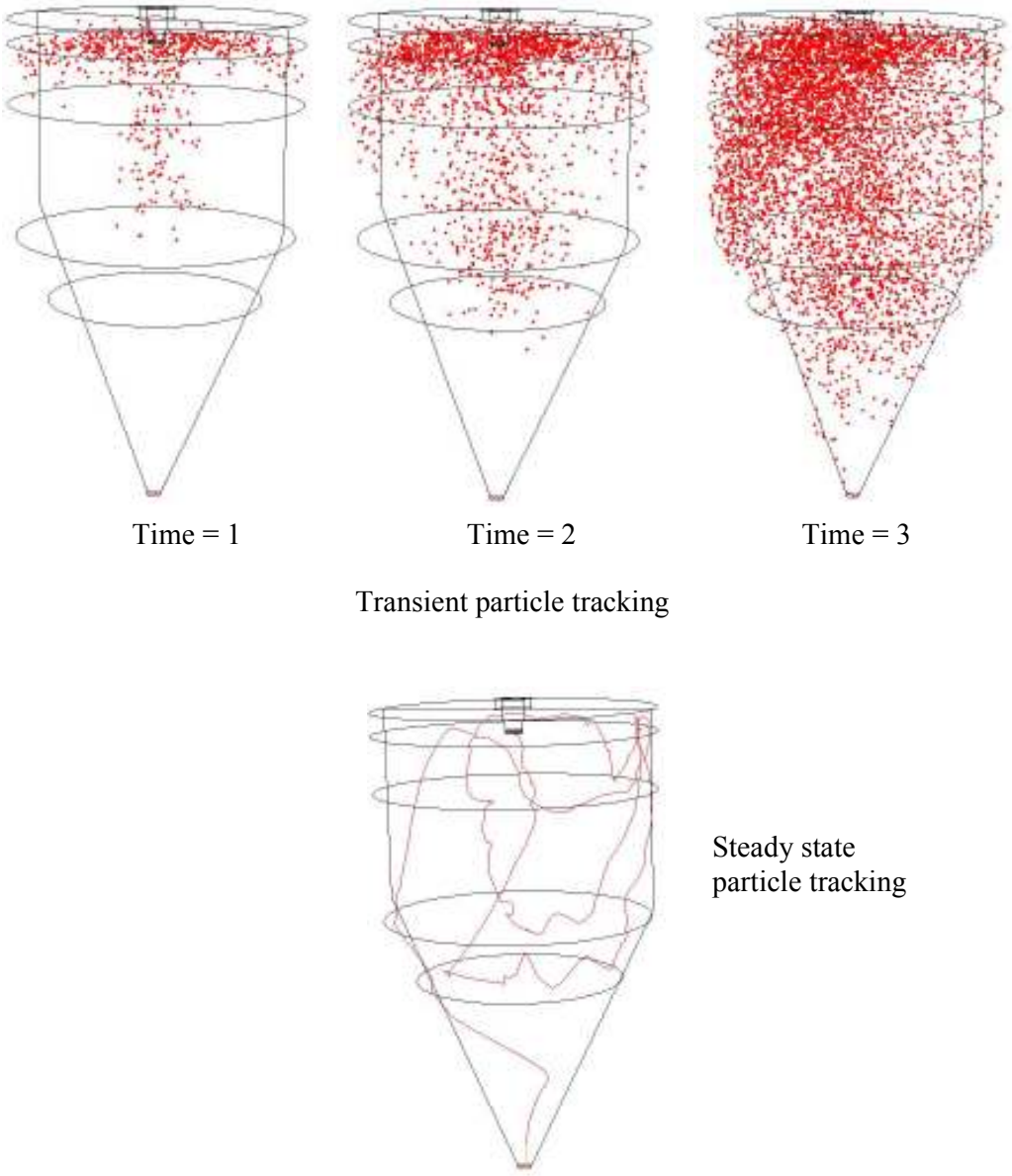

Figure 16 Illustration for a transient and a steady state particle tracking approach

In a process analogous to spray drying, spray cooler, Poh *et al.*[76] showed how the CFD technique can be used to assist in the modification of an existing unit. In the industrial spray cooler investigated, collision between the hot molten fatty acid particle with the wall causes the production capacity to decrease. CFD simulations were then used to modifications to the inlet geometry to provide more swirl in the chamber which minimized the particle accumulation on the chamber wall. Other illustrations on the application of the CFD technique to better understand and manipulate the airflow patterns includes studying the effect of chamber size and air inlet turbulence or design [5][23][29].

Operating parameters such as atomization can also be evaluated using CFD simulations. Straatsma *et al.* [11] and Langrish and Zbicinski [30] also used CFD simulations to assess the effect of cone spray angle on the deposition problem. Although it is relatively established that a wider spray angle results into more propensity for the particles to reach the wall, visualization from the CFD simulations allows clearer evidence for decision making.

The CFD technique can also be used as an overall optimization tool for the process. Lo [48] used the CFD technique to determine the optimal operating condition of their spray tower to use minimal air flow rate in achieving the desired product quality in dairy products. Optimization was undertaken by looking at the yield, particle outlet moisture and particle outlet temperature as predicted by the CFD model.

5.2 Exploring new ideas

Using the advantage of CFD which enables the non-linearity of the process to be captured, Huang *et al.* [77] assessed and visualized the efficiency different chamber configurations. Some of the different configurations are the lantern type chamber and the inverted type spray dryer, in which standard design correlations might not be applicable. Along that line, Huang *et al.* [78] also evaluated the horizontal spray drying process, incorporating a bottom fluidized bed, using the CFD visualization technique. In a recent paper, Huang and Mujumdar [79] also proposed and evaluated a method of using low humidity conditions in a spray dryer to cater for drying of heat sensitive materials. It was found that such operation conditions are advantageous for heat sensitive materials. Therefore, the CFD can be a cost effective method to explore and design new spray drying chambers. New ideas can be evaluated without the need for expensive pilot scale construction in the preliminary stage, particularly as a scale up tool as noted by Oakley [80]. As mentioned earlier, Niro has already reported the use of CFD in their commercial design of spray dryers. CFD could also be used in future for on-line control of spray dryers.

6.0 Concluding remarks

This chapter discusses the various important aspects of setting up a CFD model of a spray dryer. These different aspects are important as they cover the different physical phenomenon occurring simultaneously in the chamber during spray drying. Knowing the current developments as well the limitations in the modelling effort of each aspect is important to allow better interpretation of the CFD model. On the flip side of a CFD simulation is validation of the model, which is a big challenge in spray drying due to the harsh internal conditions of the chamber. A few common validation approaches are discussed and experimental data available in the literature was laid out. In the final part of this chapter, important applications of the CFD modelling effort in spray drying were discussed. The applications highlighted here is not exhaustive and illustration on other applications, particularly for industrial operations, are certainly welcome.

7.0 References

1. Tarek, J.; Ray, M. Application of computational fluid dynamics for simulation of drying processes: A review. Drying Technology **2010**, *28*, 120-154.
2. Mujumdar, A.S.; Wu, Z.H. Thermal drying technologies – cost effective innovation aided by mathematical modelling approach. Drying Technology, **2008**, *26(1)*, 145-153.
3. Woo, M.W.; Daud, W.R.W.; Mujumdar, A.S.; Wu, Z.H.; Talib, M.Z.M.; Tasirin, S.M. Steady and transient flow simulations in short-form spray dryers. Chemical Product and Process Modelling **2009**, *4(1)*, Article 20.
4. Ullum, T. Simulation of a spray dryer with rotary atomizer: The appearance of vortex breakdown. Proceedings of the 15th International Drying Symposium **2006**, pg. 251-257.
5. Langrish, T.A.G.; Williams, J.; Fletcher, D.F. Simulation of the effects of inlet swirl on gas flow patterns in a pilot-scale spray dryer. Chemical Engineering Research and Design **2004**, *82*, 821-833.
6. Verdumen, R.E.M.; Menn, P.; Ritzert, J.; Blei, S.; Nhumaio, G.C.S.; Sorenson, T.S.; Gunsing, M.; Straatsma, J.; Verschueren, M.; Sibeijn, M.; Schulte, G.; Fritsching, U.; Bauckhage, K.; Tropea, C.; Sommerfeld, M.; Watkins, A.P.; Yule, A.J.; Schonfeldt, H. Simulation of Agglomeration in Spray Drying Installations: The EDECAD Project. Drying Technology **2004**, *22(6)*, 1403-146.
7. Versteeg, H.K; Malalsekera, W. An introduction to Computational Fluid Dynamics: The Finite Volume Method. **2007**. Pearson Education, New York.

8. Harvie, D.J.E.; Langrish, T.A.G.; Fletcher, D.F. A Computational Fluid Dynamics Study of A Tall-Form Spray Dryer. TRANS. IChemE **2002**, *80(C)*, 163-175.
9. Sano, Y. Gas flow behaviour in spray dryer. Drying Technology **1993**, *11(4)*, 697-718.
10. Kieviet, F.G.; Van Raaij, J.; De Moor, P.P.E.A.; Kerkhof, P.J.A.M. Measurement and modelling of the air flow pattern in a pilot-scale spray dryer. Chemical Engineering Research and Design **1997**, *75(3)*, 321-328.
11. Straatsma, J.; Van Houwelingen, G.; Steenbergen, A.E.; De Jong, P. Spray Drying of Food Products: Simulation Model. Journal of Food Engineering **1999**, *42*, 67-72.
12. Huang, L.X.; Kumar, K.; Mujumdar, A.S. Computational Fluid Dynamic Simulation of Droplet Drying in a Spray Dryer. Proceedings of the 14th International Drying Symposium **2004**, pg. 326 – 333.
13. Anandharamakrishnan, C.; Gimbun, J.; Stapley, A.G.F.; Rielly, C.D. Application of computational fluid dynamic simulations to spray-freezing operations. In: 16th International Drying Symposium IDS 2008, 9-12th November **2008**, Hyderabad, India. Vol A pp. 537-545
14. Huang, L. X.; Kumar, K.; Mujumdar, A.S. A comparative study of a spray dryer with rotary disc atomizer and pressure nozzle using computational fluid dynamic simulations. Chemical Engineering and Processing **2006**, *45*, 461-470.
15. Southwell, D.B.; Langrish, T.A.G. The effect of swirl on flow stability in spray dryers. Chemical Engineering Research and Design **2001**, *79*, 222-234.
16. Southwell, D.B.; Langrish, T.A.G. Observations of flow patterns in a spray dryer. Drying Technology **2000**, *18(3)*, 661-685.
17. Lebarbier, C.; Kockel, T.K.; Fletcher, D.F.; Langrish, T. A.G. Experimental measurement and numerical simulation of the effect of swirl on flow stability in spray dryers. Chemical Engineering Research and Design **2001**, *79*, 260-268.
18. Guo, B.; Langrish, T.A.G.; Fletcher, D.F. Simulation of turbulent swirl flow in an axisymetric sudden expansion, AIAA Journal **2001a**, *39(1)*, 96-102.
19. Guo, B.; Langrish, T.A.G.; Fletcher, D.F. Numerical simulation of unsteady turbulent flow in axisymmetric sudden expansions. Journal of Fluids Engineering **2001b**, *123*, 574-587.
20. Guo, B.; Langrish, T.A.G.; Fletcher, D.F. Simulation of gas flow instability in a spray dryer. Chemical Engineering Research and Design **2003**, *81*, 631-638.
21. Jin, Y.; Chen, X.D. Numerical Study of the Drying Process of Different Sized Particles in an Industrial-Scale Spray Dryer. Drying Technology **2009**, *27(3)*, 371-381.
22. Mezhericher, M.; Levy, A.; Borde, I. Modeling of droplet drying in spray chambers using 2D and 3D computational fluid dynamics. Drying Technology **2009**, *27*, 359-370.
23. Woo, M.W.; Daud, W.R.W.; Mujumdar, A.S.; Talib, Wu, Z.H.; M.Z.M., Tasirin, S.M. Steady and transient flow simulations in short-form spray

dryers. Chemical Product and Process Modelling **2009**, *4(1)*, Article 20.

24. Maurel, A.; Ern, P.; Zielinska, B.J.A.; Wesfreid, J.E. Experimental study of self-sustained oscillations in a confined jet. Physical Review E **1996**, *54(4)*, 3643-3651.
25. Oakley, D.E.; Bahu, R.E. Spray/Gas mixing behaviour within spray dryers. Proceedings of the 6th International Drying Symposium **1991**, pg. 303-313.
26. Jin, Y.; Chen, X.D. A Three-Dimensional Numerical Study of the Gas/Particle Interactions in an Industrial-Scale Spray Dryer for Milk Powder Production. Drying Technology **2009**, *27(10)*, 1018-1027.
27. Woo, M.W.; Daud, W.R.W.; Mujumdar, A.S.; Wu, Z.H.; Talib, M.Z.M.; Tasirin, S.M. Evaluation of droplet drying models in a CFD spray drying environment. Drying Technology **2008**, *26(10)*, 1180-1198.
28. Kota, K.; Langrish, T.A.G. Prediction of Deposition Patterns in a Pilot-Scale Spray Dryer Using Computational Fluid Dynamics (CFD) Simulations. Chemical Product and Process Modeling **2007**, *2(3)*, Article 26.
29. Harvie, D.J.E.; Langrish, T.A.G.; Fletcher, D.F. Numerical simulations of gas flow patterns within a tall-form spray dryer. Chemical Engineering Research and Design **2001**, *79*, 235-248.
30. Langrish, T.A.G.; Zbicinski, I. The Effects of Air Inlet Geometry and Spray Cone Angle on the Wall Deposition Rate in Spray Dryers. Transaction of IChemE **1994**, *72(A)*, 420-430.
31. Fletcher, D.F.; Langrish, T.A.G. Scale-adaptive simulation (SAS) modelling of a pilot-scale spray dryer. Chemical Engineering Research and Design **2009**, *10*, 1371-1378.
32. Crowe, C.T.; Sharma, M.P.; Stock, D.E. The particle-source-in-cell (PSI-Cell) model for gas-droplet flows. Journal of Fluid Engineering **1977**, *99*,325-332.
33. Li, T..; Pougatch, K.; Salcudean; Grecov, D. Numerical simulation of an evaporative spray in a gas-solid crossflow. International Journal of Chemical Reactor Engineering **2010**, *8*, A43.
34. Johnson, R.K.; Anantheswaran R.C.; Law, S.E. Electrostatic-Enhanced Atomization for Spray Drying of Milk. Lebensm.-Wiss. U.-Technology **1996**, *29*, 71-81.
35. Nijdam, J.J.; Guo, B.; Fletcher, D.F.; Langrish, T.A.G. Validation of the lagrangian approach for predicting turbulent dispersion and evaporation of droplets within a spray. Drying Technology **2006**, *24(11)*, 1373-1379.
36. Zbicinski, I.; Piatkowski, M. Spray drying tower experiments. Drying Technology **2004**, *22(6)*, 1325-1349
37. Huang, L.X.; Wang, C.P.; Zhou, R.J.; Mujumdar, A.S. Spray droplet size distribution using a spinning disk atomizer. In Proceedings of the 6th Asia Pacific Drying Symposium **2009**, pg 589-594.
38. Al-Hakim, K.; Wigley, G.; Stapley, A.G.F. Phase doppler anemometry studies of spray freezing. Chemical Engineering Research and Design **2006**, 84(A12),1142-1151.
39. Masters, K. **1979**. *Spray Drying Handbook*. London: George Godwin Limited.

40. Huang, L.X.; Kumar, K.; Mujumdar, A.S. Simulation of a Spray Dryer Fitted with a Rotary Disk Atomizer Using a Three-Dimensional Computational Fluid Dynamic Model. Drying Technology **2004**, *22(6)*, 1489-1515.
41. Langrish, T.A.G.; Keey, R.B.; Hutchinson, C.A. Flow visualization in a spray dryer fitted with a vane-wheel atomizer: photography and prediction. Chemical Engineering Research and Design **1992**, *70*, 385-394.
42. Adhikari, B.; Howes, T.; Bhandari, B.R.; Truong, V. Effect of addition of maltodextrin on drying kinetics and stickiness of sugar and acid-rich foods during convective drying: experiments and modelling. Journal of food Engineering **2004**, *62,* 53-68.
43. Handscomb, C.S.; Kraft, M.; Bayly, A.E. A new model for the drying of droplets containing suspended solids after shell formation. Chemical Engineering Science **2009**, *64*, 228-246.
44. Mezhericher, M.; Levy, A.; Borde, I. Heat and mass transfer of single droplet/wet particle drying. Chemical Engineering Science **2008a**, *63(1)*, 12-23.
45. Chen, X.D.; Lin, S.X.Q. Air Drying of Milk Droplet under Constant and Time-Dependent Conditions. AIChe Journal **2005**, *51(6)*, 1790-1799.
46. Langrish, T.A.G.; Kockel, T.K. The assessment of a characteristic drying curve for milk powder for use in computational fluid dynamics modeling. Chemical Engineering Journal **2001**, *84*, 69-74.
47. Kieviet, F.G., Van Raaij, J., Kerkhof, P.J.A.M. A device for measuring temperature and humidity in a spray dryer chamber. Chemical Engineering Research and Design **1997**, 75, 329-333.
48. Lo, S. Application of computational fluid dynamics to spray drying. Lait **2005**, *85*, 353-359.
49. Zbicinki, I.; Piatkowski, M.; Prajs, W. Determination of spray drying kinetics in a small scale. Drying Technology **2005**, *23(8)*, 1751-1759.
50. Woo, M.W.; Daud, W.R.W.; Mujumdar, A.S.; Talib, M.Z.M.; Wu, Z.H.; Tasirin, S.M. Comparative Study of Drying Models for CFD Simulations of Spray Dryers. Chemical Engineering Research and Design **2008**, *86(9)*, 1038-1048.
51. Chen, X.D.; Xie, G.Z. Fingerprints of the drying behaviour of particulate or thin layer food materials established using a reaction engineering model. Trans. IChemE **1997**, *75(C)*, 213-222.
52. Chen, X.D. The basics of a reaction engineering approach to modelling air-drying of small droplets or thin layer materials. Drying Technology **2008**, *26*, 627-639.
53. Brask, A.; Ullum, T.; Thybo, P.; Wahlberg, M. High-temperature ultrasonic levitatorfor investigating drying kinetics of single droplets. Niro A/S **2007** – ADB Test and Development.
54. Ullum, T. CFD simulation of a spray dryer using an empirical drying model. Proceedings of the 16th International Drying Symposium **2008**, pg. 301-308.
55. Mezhericher, M.; Levy, A.; Borde, I. Droplet-droplet interactions in spray drying using 2D computational fluid dynamics. Drying Technology **2008**, *26(3)*, 265-282.

56. Adhikari, B.; Howes, T.; Lecomte, D.; Bhandari, B.R. A glass transition temperature approach for the prediction of the surface stickiness of a drying droplet during spray drying. Powder Technology **2005**, *149*, 168-179.
57. Bhandari, B.R.; Datta, N.; Crooks, R.; Howes, T.; Rigby, S. A Semi-Empirical Approach to Optimise the Quantity of Drying Aids Required to Spray Dry Sugar-Rich Food. Drying Technology **1997**, *15(10)*, 2509-2525.
58. Zuo, J.Y.; Paterson, A.H.; Bronlund, J.E.; Chatterjee, R. Using a particle-gun to measure initiation of stickiness of dairy powders. International Dairy Journal **2007**, *17*, 268-273.
59. Ozmen, L.; Langrish, T.A.G. An Experimental Investigation of the Wall Deposition of Milk Powder in a Pilot-Scale Spray Dryer. Drying Technology **2003**, *21(7)*, 1253-1272.
60. Murthi, R.A.; Paterson, A.H.J.; Pearce, D.; Bronlund, J.E. Controlling SMP stickiness by changing the wall material: feasible or not? Proceedings Of Chemeca **2006**, paper 209 (CD-ROM).
61. Woo, M.W.; Daud, W.R.W.; Mujumdar, A.S.; Tasirin, S.M.; Talib, M.Z.M. The role of rheology characteristics in amorphous food particle-wall collisions in spray drying. Powder Technology **2009**, *198*, 433-443.
62. Palzer, S. The effect of glass transition on the desired and undesired agglomeration of amorphous food powders. Chemical Engineering Science **2005**, *60*, 3959-3968.
63. Ferry, J.D. **1970**. Viscoelastic properties of polymers. 2nd Edition. New York: John Wiley & Sons.
64. Kieviet, F.G.; Kerkhof, P.J.A.M. Measurements of particle residence time distributions in a co-current spray dryer. Drying Technology **1995**, *13*, 1241-1248.
65. Kaer, S.K.; Rosendahl, L.A.; Baxter, L.L. Towards a CFD-based mechanistic deposit formation model for straw-fired boilers. Fuel **2006**, *85*, 833-848.
66. Kota, K.; Langrish, T.A.G. Prediction of wall deposition behaviour in a pilot- scale dryer using deposition correlations for pipe flows. Journal of Zhejiang University SCIENCE A **2007**, *8(2)*, 301-312.
67. Langrish, T.A.G.; Oakley, D.E.; Keey, R.B.; Bahu, R.E.; Hutchinson, C.A. Time-dependent flow patterns in spray dryers. Chemical Engineering Research and Design **1993**, *71*, 355-360.
68. Bayly, A.E.; Jukes, P.; Groombridge, M.; McNally, C. Airflow patterns in a counter-current spray drying tower – simulation and measurement. Proceedings of the 14th International Drying Symposium, **2004**, Sao Paulo, 22-25 August, vol.B, 775-781.
69. Kota, K.; Langrish, T.A.G. Fluxes and patterns of wall deposits for skim milk in a pilot-scale spray dryer. Drying Technology **2006**, *24(8)*, 993-1001.
70. Woo, M.W.; Daud, W.R.W.; Talib, M.Z.M.; Tasirin, S.M. Controlling Food Powder Deposition in Spray Dryers at Quasi-Steady Wall Thermal Condition: Wall Surface Energy Manipulation as an Alternative. Journal of Food Engineering **2009**, *94*, 192-198.

71. Huang, L.X.; Mujumdar, A.S. Simulation of an industrial spray dryer and prediction of off-design performance. Drying Technology **2007**, *25(4)*, 703-714.
72. Chen, X.D.; Lake, R.; Jebson, S. Study of Milk Powder Deposition on a Large Industrial Dryer. Trans. IChemE **1993**, *71(c)*, 180-186.
73. Mazza, M.G.G.; Brandao, L.E.B.; Wildhagen, G.S. Characterization of the residence time distribution in spray dryers. Drying Technology **2003**, *21(3)*, 525-538.
74. Chiou, D.; Langrish, T.A.G.; Braham, R. Partial crystallization behaviour during spray drying: Simulations and experiments. Drying Technology **2008**, *26(1)*, 27-38.
75. Anandharamakrishnan, C.; Rielly, C.D.; Stapley, A.G.F. Effect of process variable on the denaturation of whey proteins during spray drying. Drying Technology **2007**, *25(5)*, 799-807.
76. Poh, H.J.; Turangan, C.K.; Lou, J. Improvement of an industrial co-current spray cooler operation for a fatty acid product using tangential side-entry design – A modelling study. Proceedings of the 5th Asia-Pacific Drying Symposium **2007**, pg. 215-220.
77. Huang, L.X.; Kumar, K.; Mujumdar, A.S. Use of computational fluid dynamics to evaluate alternative spray dryer chamber configurations. Drying Technology **2003**, *21(3)*, 385-412.
78. Huang, L.X.; Mujumdar, A.S. Numerical study of two-stage horizontal spray dryers using computational fluid dynamics. Drying Technology **2006**, *24(6)*, 727-733.
79. Huang, L.X.; Mujumdar, A.S. A computational fluid dynamic study of a low-humidity co-current spray dryer. Asia-Pacific Journal of Chemical Engineering **2007**, *2(1)*, 12-19.
80. Oakley, D.E. Scale-up of spray dryers with the aid of computational fluid dynamics. Drying Technology **1994**, *12(1)*, 217-233.

Passos, M.L., Birchal, V.S. Manipulating physical properties of powder - Volume 1, Ed. Woo, M.W., Mujumdar, A.S. and Daud, W.R.W., **2010**, ISBN - 978-981-08-6270-1, Published in Singapore, pp. 37-60.

Manipulating physical properties of powder

Chapter 2

Passos M.L.[1], Birchal V.S.[2]

[1] Drying Center - Chemical Engineering Department, Federal University of Sao Carlos, Brazil
[2] Chemical Engineering Department, Federal University of Minas Gerais, Brazil

Contents **Page**

1.0 Introduction

Spray drying is the most common industrial powder manufacturing technology. It consists on atomizing a liquid, solution, emulsion or suspension into a hot gas medium to dry and transform it into particles in a one step operation. Having been used by the dairy industry since the late 1850s, this technology attends now different sectors, extending from the food industry to the agrochemical, biotechnology, heavy and fine chemicals, mining and metallurgical, dying, pharmaceutical sectors among others. The statistics indicate that over 25000 spray dryers are commercially in use nowadays, with their evaporation capacity ranging from few kg/h to over 50 ton/h [1].

Since the current market requires from any manufacture sector a high powder product quality associated to low costs and reduced environment impacts, efforts to identify powder formation mechanisms are increasing toward the powder process production optimization. Note that the spray drying is the unique technique to produce almost spherical and usually hollow particles with a relatively narrow size distribution. Besides, as a friendly powder manufacture technique, spray drying allows modifying the process-operation parameters to manipulate powder properties toward desirable characteristics with improvement of the final product quality.

This chapter presents and analyzes a methodology for describing the main physical properties of spray-dried powders as function of the process-operation parameters in order to manipulate these properties toward maximizing the powder product quality. To attain this objective, it is necessary first to identify briefly the main mechanisms to dry and produce a spray-dried powder. This allows anyone discriminating, not only, the operational variables that can control the powder characteristics, but also, the main physical properties that can be manipulated and controlled. In sequence, definitions and methods to measure these specific physical properties during drying operation are succinctly reviewed. Based on actual cases, it is shown how to obtain empirical equations to express the dependence of these specific powder properties on process-operation spray-dryer variables. Finally, a discussion is presented focussing on the use of these empirical equations for optimizing the spray-dryer operation in relation to the best quality of the final powder.

2.0 Powder formation mechanism

As well known, spray drying is a continuous process-operation, which comprises several steps, mainly atomizing of the liquid feed into droplets, mixing of these droplets with the hot drying gas, evaporating of solvent (commonly water) and separating of powder product from exhaust gas. Specific products, such as instant powdered foods, require two or three stages of drying since particle agglomeration is desirable to improve their quality. As shown in Figure 1a, in a single-stage drying, composed of a spray dryer with a pneumatic conveying system, the final product is fine non-agglomerated particles that are difficult to disperse in water. The two-stage drying process-operation, shown in Figure 1b, uses the spray dryer followed by a vibrofluidized bed dryer system, which not only dries the powder to the final moisture content generating new agglomerates by particle sliding, but also, cools gently the product improving the agglomerate stability. In the three-stage drying, besides the vibrofluidized bed system a static fluid bed, inserted into the conical base of the spray dryer, works as a dryer-agglomerator [2].

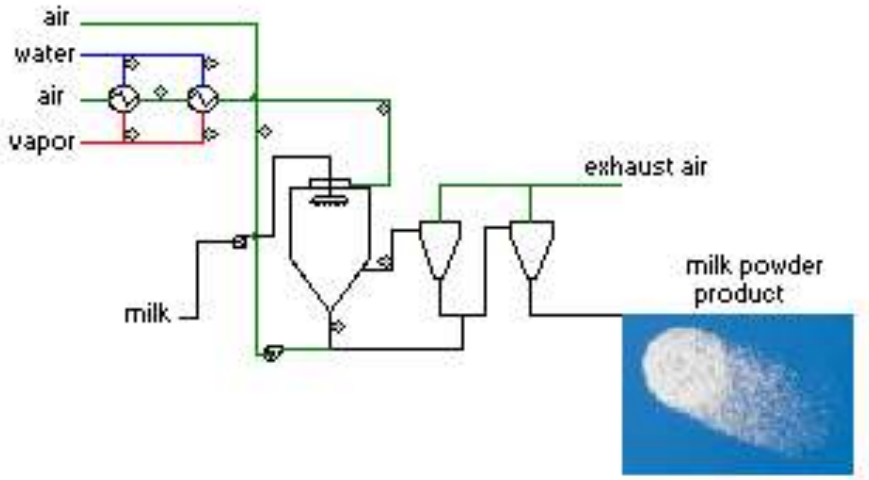

Figure 1a Single-stage drying for milk powder production

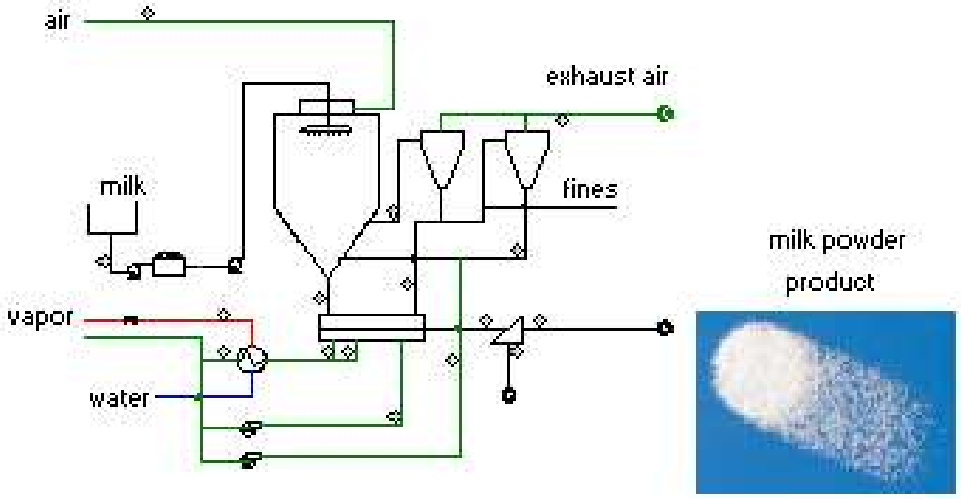

Figure 1b Two-stage drying for milk powder production

Independently on the number of stages used for drying the solution or suspension, particle formation occurs always in the spray dryer, as soon as the atomized droplets fall into the chamber in direct contact with the hot gas (usually air). Figure 2 schematizes the drying history of a droplet containing insoluble or dissolved solids, in a spray dryer [3, 4]. At the beginning of the first drying period, the droplet temperature changes until reaching the wet bulb temperature, determining by the operation conditions. During this first period, water (solvent) evaporates as a pure liquid, with the surrounding saturated vapor film being the only resistance to heat and mass transfer between gas and droplet. Moreover, the droplet shrinks, decreasing its size and concentrating solids at its surface due to the inward movement of its boundary. Once the droplet moisture content becomes too low to keep this saturated condition, dissolved solids from solution start being deposited at the droplet surface, forming a partial porous crust around the liquid droplet. As drying proceeds, the droplet transforms into a particle with a wet core completely surrounded by the porous crust. Note that any change in the spray

dryer operation conditions to those, under which the droplet shrinks slowly at a rate that assure a uniform distribution of the solid concentration, can lead to development of a full particle without a crust.

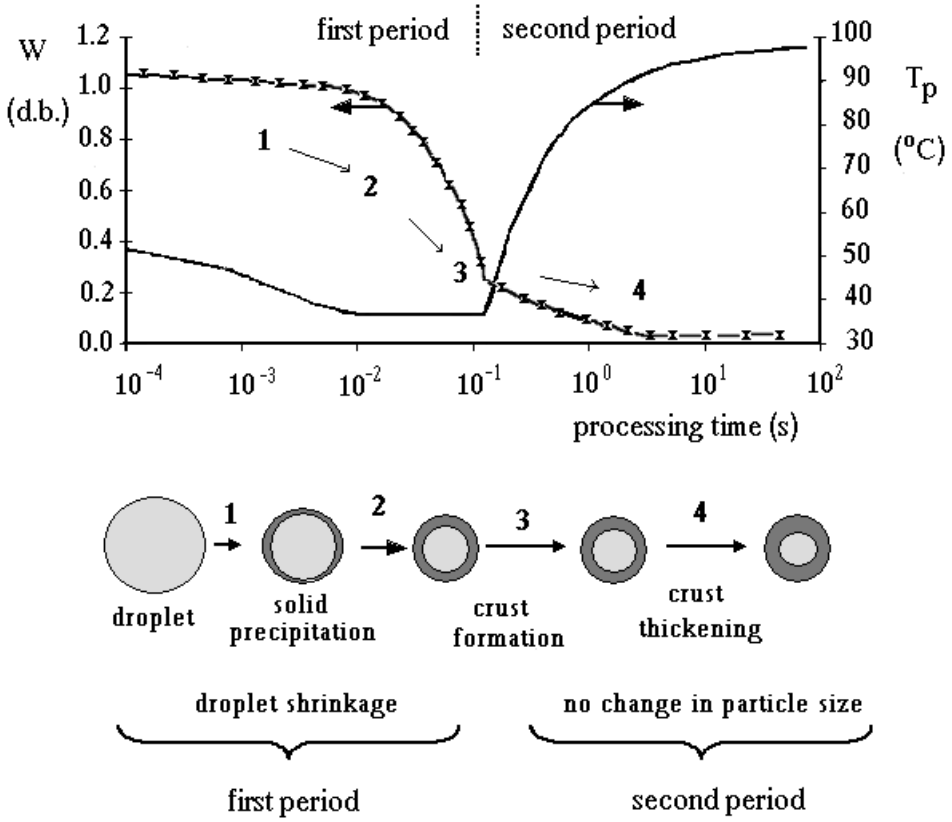

Figure 2 Drying history of a droplet containing solids in a spray dryer

For the case illustrated in Figure 2, the second drying period starts when the porous crust covering the entire droplet surface. At this point, there is no more a droplet, but a particle constituted by a wet core and a porous crust. This period is characterized by thickening the crust towards the interior of particle, as well as, by reducing the drying rate, since the porous crust constricts the vapor mass transfer from the inner core surface to the surrounding gas. Therefore, the particle temperature increases, supplants the wet bulb temperature, and tends to reach the thermal equilibrium with the gas. For cases, in which the gas operation temperature exceeds the solution boiling temperature, a bubble can be generated inside the particle when its temperature equals to this boiling point. Under this condition, vapor is intensively generated inside the particle, raising its internal pressure. Therefore, the particle inflates, or bursts, or cracks, depending on the permeability and mechanical characteristics of the crust. Consequently, by varying either the spray dryer operation parameters or the feed solution properties, many different particle morphologies can be obtained [4 -8].

In order to evaluate the crust properties, it is important to emphasize that, in some cases mainly in the food process, the crust composition differs from the droplet solid composition due to the segregation of these

components during drying. Based on drying kinetics and mass transfer fundamentals, solids with smallest mass-diffusion coefficients must be concentrated at the particle surface. This segregation also explains the high concentration of free fat on the whole milk powder crust surface [5]. Simultaneously to drying and particle formation mechanisms, in many applications, the powder is subjected to agglomeration, for the purposes of improving appearance and/or dispersability. Particle agglomeration can be enhanced in spray dryer systems for processes, in which it is required, as the instant powder production. Therefore, primary, secondary and tertiary agglomerations between droplets and/or particles should be intensified by respectively:

(a) Using an atomizer device to generate a wider droplet size distribution. This promotes, at the atomizing zone, effective collisions between smaller and larger droplets due to their different falling velocity;
(b) Recycling fines (separated from the exhausted gas) to the upper wet region of the drying chamber, where droplets are descended, as shown in Figures 1b. These fine particles are incorporated into droplets producing secondary agglomerates. Different agglomerate structures can be achieved depending on the design and location of the fine return system [9];
(c) Inserting a fluid bed into the conical region of the spray dryer to improve or create agglomerates by rolling down wet particles.

This brief description of drying and particle formation corroborates the concept of manipulating the spray dryer operation variables to achieve the desirable powder properties in order to optimize the product quality. Additionally, it leads to choose the most general powder properties that can be manipulated and controlled by the spray dryer operation. These properties can be integrated into four groups, as: (i) moisture content, including the water activity and sorption isotherms; (ii) particle size distribution incorporating the mean particle size and dispersion index, as well as, the particle shape and its superficial area; (iii) density, concerning the solid, particle and in bulk; (iv) stickiness, including the degree of particle cohesion and adhesion. Other properties, specific of the desirable product, should be added to these general ones to complete the powder quality requirements.

3.0 Main powder properties

The four groups of properties identified and analyzed in this chapter are the basic ones to control powder morphology. Therefore, they need to be measured and quantify as a function of the solution or suspension properties and of the spray drying operational variables (mainly the atomizer device characteristics, the solution feed flowrate and concentration, the inlet gas temperature and flowrate). Figure 3 schematizes the cause-effect relationships influencing powder quality parameters in spray drying.

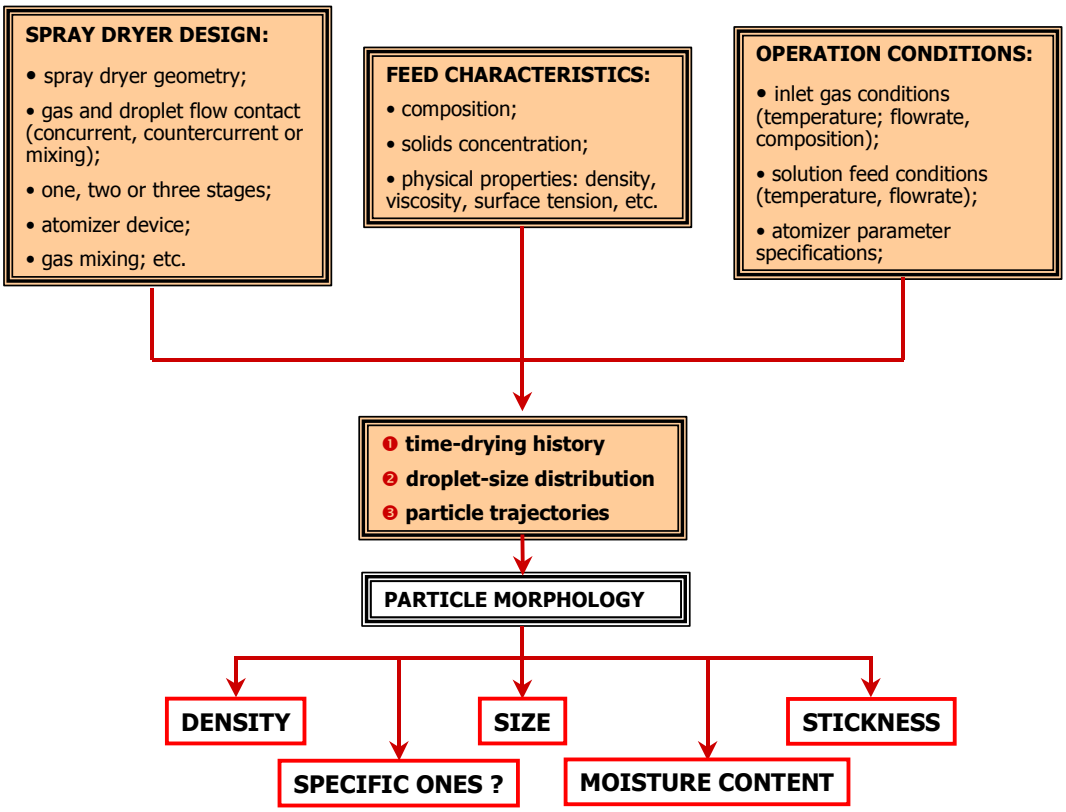

Figure 3 Cause-effect relationships influencing powder quality parameters in spray drying. (Modified from [10]).

3.1 Moisture content

The residual moisture content of spray dried powder is of great important to define the product quality, since this quantifies the amount of water presented in the material. This parameter is straightly related to drying conditions and to droplet formation mechanisms. Consequently, it must vary with changes in the spray dryer operation variables (mainly the inlet air temperature), as well as, the solution or suspension feed composition and concentration. Depending on the methods used for measuring the moisture content, the different forms of water, available in the powder, can be identified, such as water weakly bounded (free or retained water), water strongly bound (hydrate water), water with weaker bonds and water imbibed in proteins. The drying oven method at a controlled temperature until constant mass of the sample is the most widely method used. Generally for food or pharmaceutical powders, this method is normalized concerning the drying temperature, sample exposure and oven type [11]. Moreover, for these powders, both, the residual moisture content and the water activity, are required in order to develop a procedure to control adequately the product shelf life, taste and texture, agglomeration, contaminant growth and microbial proliferation [12]. Water activity, expressed by the air relative humidity in

equilibrium with the powder at ambient conditions or at specified conditions, can be measured by a faster reading electrical or electronic hygrometer.

Water sorption isotherms (equilibrium curves between the moisture content and the water activity of a powder at different temperatures) provide a more complete moisture analysis. These curves are complex but unique for each material due to different interactions (colligative, capillary, and surface interactions) between water and solid components at different moisture contents. Measurements of these sorption curves can be divided into static and dynamic procedures. The further consists on placing a powder sample, dried (adsorption), hydrated (desorption) or raw (working), into controlled air humidity chambers at constant temperature and measuring the sample mass sequentially until establishing the equilibrium (constant mass). Although the dynamic procedure seems similar to the static one regarding the sample mass measurements, rather than using a confined controlled atmosphere, air at constant and controlled temperature and humidity flows continuously over the powder sample, enhancing the time to reach the equilibrium. Based on this dynamic procedure, complete equipment is commercially available for faster measuring water sorption isotherms of common materials [13]. Moisture sorption isotherms are the required data for modeling the droplet drying and powder formation in any one type of spray dryers.

3.2 Particle size distribution

Particle size distribution supplies information not only the mean size, but also, the size dispersion, the particle agglomeration and, depending on the method used for measurement, the particle shape and its superficial area. Spray-dried powder size and distribution are straightly related to the droplet size and distribution and, consequentially, depend mainly on the atomizer device and suspension feed properties [1][10][14]. Pneumatic atomizers can produce very small uniform size droplets, even with very viscous suspensions; pressure nozzles generate droplets whose sizes depend on the nozzle pressure, but with a narrow size range. Rotary atomizers are very versatile with the droplet size being controlled either by wheel revolutions or by the feed rates. Although in development, sonic atomizers, in which the ultrasonic energy is used by passing the liquid over a surface vibrated at ultrasonic frequencies, can produce very fine droplets at low flowrates. To obtain the desired powder size, the atomizer selection must be made carefully considering, as a general rule, that an increase in the energy available for atomization (i.e. air-liquid ratio in a pneumatic atomizer, nozzle pressure, or rotary atomizer speed) reduce the particle size [1][15][16].

To determine the mean particle diameter, the powder size distribution curve must be obtained experimentally. This curve represents the frequency or cumulative frequency (expressed as fraction or percentage) of occurrence of each particle size in the powder sample, as exemplified in Figure 4 [17]. As shown by the fitted curve in this figure, the lognormal distribution is the most common model for characterizing the particle size distribution of uniform

spray-dried powders. This lognormal distribution curve leads to define the dispersion index of particle size distribution, i_d, as [18, 19]:

$$i_d = \frac{D_{84,1\%} - D_{15,9\%}}{2D_{50\%}} \quad (1)$$

with $D_{x\%}$ representing the size that corresponds to the X% (or 0.X) value on the curve of cumulative percentage undersize versus size (see Figure 3.4 for determination of $D_{50\%}$).

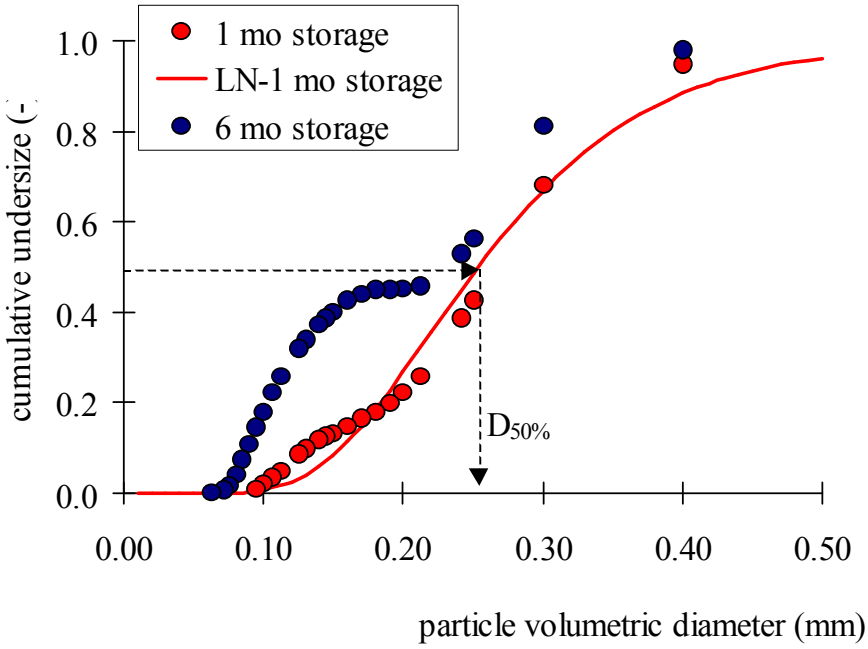

Figure 4 Size distribution curve for goat milk powder as a function of the storage time. Data obtained using the laser diffraction method. (LN – lognormal distribution curve). (Modified from [17])

Depending on the method selected for measurement, different types of particle size distribution curve can be obtained (i.e. by number, by surface, or by mass or volume), and, consequently, several mean particle diameters can also be defined and determined. Although there are many methods for measuring particle size distribution (see, for example, reference [18]), those ones most useful in the powder measurements comprise two classes, the sieve analysis and the laser diffraction. Both performed in a dry or wet medium lead to the particle size distribution by mass (sieving) or volume (laser diffraction). The sieve analysis (standardized by ASTM D6913) consists of a simple shaking of the powder sample in sieves until the mass retained in each sieve becomes quasi-constant. This method is the most widely used method for larger particles (generally, from 37 μm to 4000 μm) and requires a relatively long time for measurement (5 to 30 min), as well as, a special procedure for cohesive and agglomerated powder [20, 21]. In the second class method, the diffracted light is produced when a laser beam passes through a dispersion of particles in a gas or in a liquid, thus, measuring the scattered

energy versus the diffraction angle allows generating the volume size distribution curve of the powder sample [18]. This laser diffraction method (standardized by ASTM B822) is the fastest (10 s) and most precise method of analysis, is non-destructive and non-intrusive and actually used by industries. This method is applied to the particle size range from 0.1 μm to 2000 μm and particularly precise for measuring sizes below 1 μm, since the light diffraction angle increases as particle size decreases.

Returning to Figure 4, one can see that particle size distribution data concerning goat milk powder with 6 months of storage must not be well fitted to the lognormal distribution model, either other distribution model developed for homogeneous powders. The 6-month storage milk powder has an unusual size distribution with two peaks in the curve. This bimodal (or even multi-modal) size distribution usually results from two different phenomena that occur simultaneously or subsequently during powder formation. In the case of Figure 4, after 6 months of storage, the lactose crystallization seems to be occurred subsequently the drying and powder formation, since the goat milk powder sample has not been hermetically storage [17].
Although there are several ways to define the mean particle size that characterizes the whole powder distribution, the so-called Sauter mean diameter is one of the most useful mean values [18-20]. This corresponds to the particle diameter with the same volume-to-surface ratio as the entire powder, i.e.:

$$D_{3,2} = \frac{\sum D_i^3 f_i}{\sum D_i^2 f_i} = \left(\sum \frac{x_i}{D_i} \right)^{-1} \tag{2}$$

with f_i representing to the number frequency of D_i particle size, and x_i the volume or weight fraction of D_i particle.

As discussed earlier, basically, the water evaporation rate and the suspension composition should affect mainly the particle shape and morphology. The parameter mostly used to quantify the particle shape is the sphericity factor, which is the ratio of the surface area of equivalent volume sphere to the surface area of the particle [19]. Only image analysis provides true powder shape information, being, nowadays, scanning electron microscope (SEM) and transmission electron microscope (TEM) the most used methods to qualify powder particle shape or particle shape distribution in powders. However, when the determination of the powder surface area is of interest, SEM and TEM supply only a qualitative picture based on measurements of average pore and ligament sizes and on the assumption of a structural isotropy of the substrate of interest. Brunauer Emmett Teller (BET) method represents the best quantitative alternative to measure the particle surface area, since it is based on the physical monolayer adsorption of gas molecules (nitrogen or krypton) on the particle surface. The BET methodology is well described in the standard DIN 66131 and applicable to nonporous solids or macro and mesoporous solids with pore widths higher than 2 nm. In addition, BET also features some limitations and shortcomings related to its efficiency for powder characterization, associated manly with pre-treatment procedures at elevated temperature and large quantity of the analyzed samples [20]. Another alternative method is based on the gas

permeability, as the ESA (envelope surface area analyzer) available commercially that uses compressed air.

3.3 Density

Powder density (ρ) is one of its basic properties, defined as the ratio of mass to volume. It has economical, commercial and functional importance. A high density implies in a low volume, which favors the material transportation, handling and storage, on the other hand, a low density can sometimes be required either by operational conditions or by product quality criteria [19,22]. Since a powder is formed by individual particles, which can exhibit internal pores and/or can agglomerate to form greater particles, there are several ways to specify its density. To avoid misunderstanding concerning these definitions, the terminology adopted is followed, as well as, illustrated in Figure 5 [23]:

(a) grain – meaning individual or primary particles (not linked);
(b) agglomerate – referring to greater particles formed by linking one or more grains;
(c) particle – referring indistinctly to an agglomerate or to a free grain;
(d) internal pores or intraparticle porosity – meaning pores inside the grain or among grains, when they form agglomerates;
(e) external pores or interparticle porosity – corresponding to the empty space (not filled by particles and not included internal pores) in a defined volume.

Using this terminology, different powder densities can be identified, mainly the solid density, the particle density and the bulk density.

Solid density

The true or real solid density, ρ_s, represents the mass of solid content in the particle, m_s, divided by the volume actually occupied by this solid (excluding internal pores), V_s, i.e.:

$$\rho_s = \frac{m_s}{V_s} \tag{3}$$

Helium pycnometry is one method used to determine ρ_s, since helium can even penetrate the smallest pores or voids, measuring the unknown volume of a known powder mass. The final result is often referred to as skeletal density. The ρ_s value depends straightly on the powder solid composition and, when the chemical composition of powder is evaluated, the following correlation can used to estimate ρ_s [24]:

$$\rho_s = \left(\sum_{i=1}^{n} \frac{x_i}{\rho_i} \right)^{-1} \tag{4}$$

In this Equation (4), ρ_i represents the density of the *i*-solid component and x_i its mass concentration in dry-basis (mass of i-component/dry mass of total solids). Once changes in the powder composition must occur in order to change ρ_s value, meaning that ρ_s is unique for each powder product.

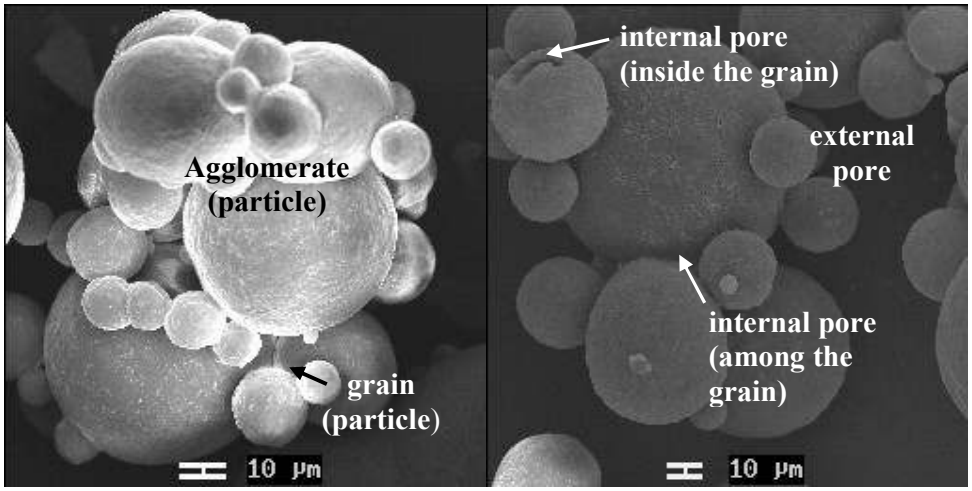

(a) (b)

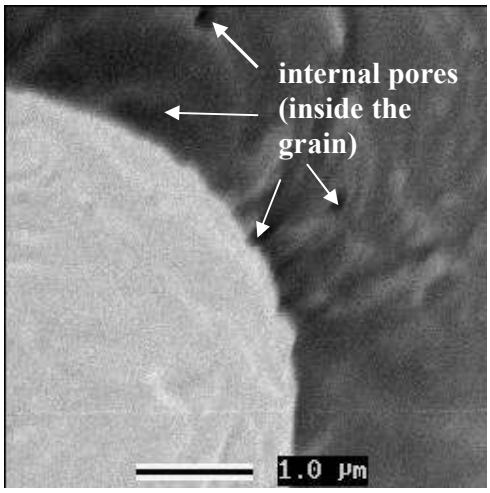

(c)

Figure 3.5 SEM micrographs of whole powder milk obtained in a spray dryer. (Modified from Birchal [23])

Particle density

The particle density, ρ_p, represents the ratio of the mass of solids present in the particle, m_s to its actual volume, V_p, including all internal pores, as:

$$\rho_p = \frac{m_s}{V_p} = \frac{m_s}{V_s + V_{ip}} = (1-\gamma)\frac{m_s}{V_s} = (1-\gamma)\,\rho_s \qquad (5)$$

with V_{ip} corresponding to the internal pore volume of the particle (grain or agglomerate) and being the volumetric concentration of these internal particle pores ($\gamma = V_{ip}/V_p$).

Therefore, the ρ_p determination demands measurements of γ, the volumetric concentration of the internal pores. Mercury porosimetry is one of applied methods for this, because it uses the non-wetting properties of mercury to gain information on the porous characteristics of powder (i.e. porosity, pore volume, pore size distribution and density). During a typical analysis in a mercury porosimetry analyzer, a higher pressure is necessary to force intrusion of mercury in smaller pores, whereas mercury is intruded into larger pores at low pressures. In this way a wide dynamic range of pore sizes can be measured and a pore size distribution can be obtained starting from 4 nm (pressure = 400 MPa) up to approximately 800 μm (vacuum). However, a low-pressure mercury porosimeter (pressure range from 0.01 to 140 kPa) seems to be suitable to spray-drier powder measurements (particle size range from 330 to 15 μm), as shown by Drusch and Schwarz [25]. Another alternative method to evaluate γ is the BET analysis using now the volumetric technique that provides a full adsorption-desorption isotherm with information on BET surface area, pore volume and pore size distribution. Although Hahne [20] has chosen this method to determine, her results showed the difficulty to apply this method to the whole milk powder, once there was a great tend to destroy or alter milk agglomerates during the sample preparation. Moreover, this author demonstrated that the volume of internal pores in an individual or primary milk particle is insignificant, comparing to the one of internal pores among grains in milk agglomerate. Even though tedious and time-consuming procedure, the γ value can also be determined basing on statistical analyses of particle images or micrographs, obtained by microscopy.

Bulk density

The bulk or apparent density, ρ_b, refers to the particle packing (particle arrangement) into a vessel to form a bed, and represents the mass of particles contained in a vessel, m_s, divided by the bed volume formed by this mass, V_{bed}, i.e.:

$$\rho_b = \frac{m_s}{V_{bed}} = (1-\varepsilon)\frac{m_s}{V_p} = (1-\varepsilon)\rho_p = (1-\varepsilon)(1-\gamma)\rho_s \tag{6}$$

in which ε is the bed porosity (or void fraction), defined as the total volume of pores formed among particles divide by the total bed volume. Once the values of ρ_b and ρ_p are determined, the bed porosity can be found:

$$\varepsilon = 1 - \left(\frac{\rho_b}{\rho_p}\right) \tag{7}$$

There are two important conditions, under which ρ_b must be identified and specified. The first one, corresponding to the determination of the loose bulk density, $\rho_{b\text{-}min}$, represents a loose packed bed condition. The second condition, relating to the determination of the tapped bulk density, $\rho_{b\text{-}max}$, represents the maximum packing density of a powder achieved under the influence of well-defined, externally applied forces. The bed porosity, at this second condition, achieves its minimum reproductive value.

The $\rho_{b\text{-}min}$ value can be measured by pouring, slowly and gradually, a known mass of powder into a graduated vessel. The ratio of the mass to the

volume occupied may correspond to $\rho_{b\text{-}min}$, if the vessel is larger enough to avoid the wall effect on the particle packing. Better procedure is pouring the powder through a vibrating sieve and allowing it to fall a fixed height (about 25 cm) into a graduated cylindrical vessel [19]. Although measuring of this density is far from standardized, another alternative procedure is to inject homogeneously a gas (basically air) through the packed bed of particles until fluidization and, then, shoot down the gas flow and, immediately, measure the loose bed volume [20].

Despite the fact that many industries measure $\rho_{b\text{-}max}$ by tapping the powder sample manually (dropping continuously the graduated vessel containing powder a specific height until no noticeable change in the bed volume [20]), the best procedure is to use a mechanical tapping device. With this device, the conditions of sample preparation are more reproducible. Instruments to achieve such reproducibility are available commercially with their tap density tests normalized by the American Society for Testing and Materials Standards (ASTM), International Organization for Standardization (ISO), International Dairy Federation (IDF), United States Pharmacopoeia (USP). These tests generate standardized and repeatable results of measuring tapped and even packed volumes of different powders.

3.4 Stickiness

Spray-dried powders can be hygroscopic that, under humid conditions, clump together becoming sticky and, consequently, no free flowing powders. Such powders require special attention during packaging and storage, as many food powders [10][20-23][26-27], and, sometimes, during spray drying operation because they not only stick to each other but, mainly, adhere to the equipment walls decreasing the drying efficiency and powder production. Typical examples are milk powders [21][27], sugar-rich powders as fruit-juice ones [10][26] among others.

To avoid the powder adherence to the walls, two different approaches have been used industrially. The first is to interfere in the suspension or emulsion composition, adding to it carrier agents (polymers and gums) that reduce the powder hygroscopicity and also protect the sensitive food components [26]. Another approach is to inject cool gas (generally air) into the dryer or to cool the walls of the spray dryer chamber for reaching wall-temperatures below the sticky-point temperature of the semi-dry product [28-30]. For processing, storage and packaging, the final powder stickiness needs to be measured and well controlled.

Flow of powders is governed mainly by physical properties rather than by chemical ones, and it depends on the size, shape and size distribution of particles, as well as moisture content and time-consolidation. Cohesive and adhesion forces include mechanical forces arising from interlocking surface asperities and irregularities, solid bridges formed from re-crystallization, capillary forces in an adsorbed liquid layer, molecular forces as Van der Waals and electrostatic forces [31]. Although several indexes exist in the literature to quantify the powder flowability (as Jenike flow index, Hausner ratio, repose and slide angles, among others), there is no single flow tester

that can be universally accepted as reliable and easy-to-use for determining this property. Therefore, two or more indexes must be measured, compared and analyzed in order to define the degree of powder stickiness.

Jenike flow index

Jenike shear tests, industrially used as standards for measuring powder flowability (ASTM Standard D6128-97), involve two basic steps: pre-shear and shear. After loading the powder sample into the shear cell, the pre-shear starts consisting in consolidating the sample at a specific normal stress (dependent on the initial powder bulk density) and, then, shearing it at the same normal stress. Subsequently, the shear step (also called shear to failure step) initiates with a reduction in the normal stress to a fraction of the pre-shear stress and, then, shearing starts. To determine the yield locus of the powder, several of these described tests must be performed, in which each sample must be first consolidated at identical normal stress (pre-shear) and then sheared (to failure) under different normal stresses. By pre-shearing at identical normal stress, each sample reaches the same state of consolidation. Therefore, each test yields the same pre-shear point, and one individual shear point in accordance with the different normal stresses applied at shear. Figure 6 shows a typical diagram obtained from these tests, as well as the definition of Jenike flow-index. This index decreases with increasing powder cohesion, and when it is lower than 1 the powder flowability tends to zero (not flowing). Although this technique has proven to be reproducible and valid for different powders, shear test results are complicated to be interpreted and to be validated, requiring technical knowledge in soil mechanics [31-33]. In addition to time-consuming, these shear tests are difficult to operate and expensive for high-value powder [31, 33]. Therefore, this technique tends to be replaced by a simple one.

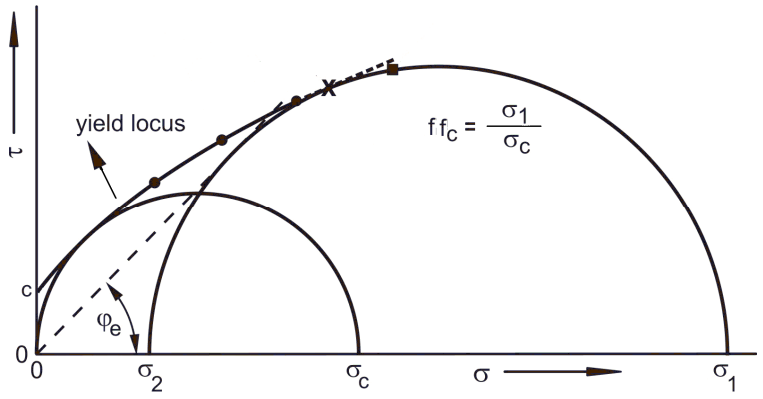

Figure 6 *Schematic representation of a cohesive powder yield locus curve obtained in direct shear tests and the Jenike flow index, ff_c.*

Hausner ratio

The Hausner ratio, H_R, defined as $H_R = \rho_{b\text{-}max} / \rho_{b\text{-}min}$, expresses the cohesion degree of powders. As discussed by Geldart [19], when powder with strong interparticle forces is poured into a vessel, an open powder structure is formed that prevents particles from rolling over each other. Conversely, this open structure can easily be disrupted by mechanical vibration, resulting in a closer matrix. This explains higher H_R values for cohesive powders (lower $\rho_{b\text{-}min}$ and higher $\rho_{b\text{-}max}$). Hayes [34] has proposed the following classification for evaluating the powder flowability using this H_R ratio: $1.0 < H_R < 1.1$ - free flowing powders; $1.1 < H_R < 1.25$ - medium flowing powders; $1.25 < H_R < 1.4$ - difficult flowing powders; $H_R < 1.4$ - very difficult flowing powders. As this parameter is directly related to bulk densities, it can be easily obtained, however caution is needed for evaluating the results obtained because H_R values may be sensitive to the procedure and/or the apparatus used [31][35].

Angle of repose and angle of slide

Another simple measurement of powder flowability is the static angle of repose, α_R, which represents the angle formed between the side of a stationary pile of powder and the horizontal. This pile must be made by a standard procedure, in which a fixed mass of powder is poured through a conical funnel mounted with its stem 6 cm from the horizontal surface [31]. This parameter may present poor reproducibility because it depends on the powder sample history; nevertheless it is one recommended as a quantitative measure of cohesiveness of any granular material (ISO Standard 3435-1977-E). Note that the greater is the angle of repose the more cohesive is the powder. The following scale can be used for quantify the powder flowability: $\alpha_R < 35°$ - free flowing powders; $35° \leq \alpha_R < 45°$ - medium flowing powders; $45° \leq \alpha_R \leq 55°$ - difficult flowing powders (cohesiveness); $\alpha_R > 55°$ very difficult flowing powders (tending to zero flow). The slide angle is measured by placing the powder sample on a fat smooth horizontal plate, which is inclined slowly until the powder starts moving. The angle at which the movement occurs is the slip or slide angle [17]. Other most useful parameter to quantify the powder stickiness is the glass transition temperature.

It is important to emphasize that other specific properties should be added to these four powder property groups to describe entirely the product quality. Tonon et al. [26] have introduced to the first two groups of properties, described in items 3.1 and 3.2, more one parameter that quantifies the anthocyanin retention in the powder product in order to analyze the antioxidant activity of this açai powder. Drusch and Schwarz [25] have used parameters of the first three groups of properties, described in items 3.1, 3.2 and 3.3, adding more two other specific parameters, the final powder content of non-encapsulated fat and the lipid oxidation rate. These parameters together supply information for selecting the best starch in the formulation of the wall material for microencapsulation of a fish oil rich in long-chain polyunsaturated fatty acids. Ståhl et al. [36] have set into the first two groups of properties, described in items 3.1 and 3.2, the amount of insulin degradation to analyze the spray-dried insulin powder quality to be used for inhalation as function of the drying operation conditions. Healy et al. [37], worked in the similar theme, have applied the particle engineering technique to produce the spray-dried nanoporous microparticles with the desirable product quality to attend processes of drug delivery to the respiratory human tract by oral

inhalation. For that, product quality parameters have been defined following particles properties presented in items 3.2 and 3.3, complemented by the identification and quantification of the powder structural forms (from amorphous to crystalline structure).

4.0 Empirical model to maximize product quality

A strategy to manipulate the spray-dryer operation variables in order to obtain the desirable powder product with the best quality is presented in Figure 7. The first step is to define precisely the quality for the desirable product. For example, if the desirable product is whole milk powder for selling in the market, then, the product quality must be focussed in powder instantizing (i.e. a quick powder reconstitution in water). Associated to the physical-chemical characteristics of milk powder agglomerates, this reconstitution phenomenon involves four basic mechanisms [38]:

- Immersibility, corresponding to the powder ability to break up water surface tension and submerge into the liquid;
- Wettability, meaning the susceptibility to the water penetration;
- Dispersibility, meaning the powder ability to disperse and mix in water, forming a homogeneous emulsion;
- Solubility, representing the ability to maintain, once it is formed, a stable emulsion in water.

The second step, after defining precisely the product quality, is to quantify this powder quality. Thus, it is necessary to select those powder properties that can describe this quality. Considering the example already presented, the four mechanisms, which characterize the milk instantizing, are closely related to the bulk density, the residual moisture, protein and fat contents, the powder size distribution and powder stickiness [23][38].

As shown in Figure 7, in the third step, values of the powder properties, which assure the best product quality, must be specified, as well as any operational restriction or limitation for these properties. Returning to the given example and considering the two-stage drying of milk emulsion, it is recommended that powder, which leaves the spray chamber, should present the following characteristics [23][38]:

- moisture content varying from 5.3 to 6.4% (dry base) for whole milk powder and from 6.4 to 7.5% for skim milk powder;
- tapped bulk density, $\rho_{b\text{-}max}$, varying from 450 to 550 kg/m^3;
- wide powder size distribution with particle diameter varying from 40 to 600 mm;
- cohesion between particles being high enough to build and rearrange agglomerates at the desirable narrow particle size distribution in the vibrofluidized bed system and low enough to minimize deposition of particles on dryer walls. According to Hahne [20], the recommended value of H_R is about 1.4 for processing whole milk powder in vibrofluidized beds (sufficient condition to fluidize whole milk agglomerates).

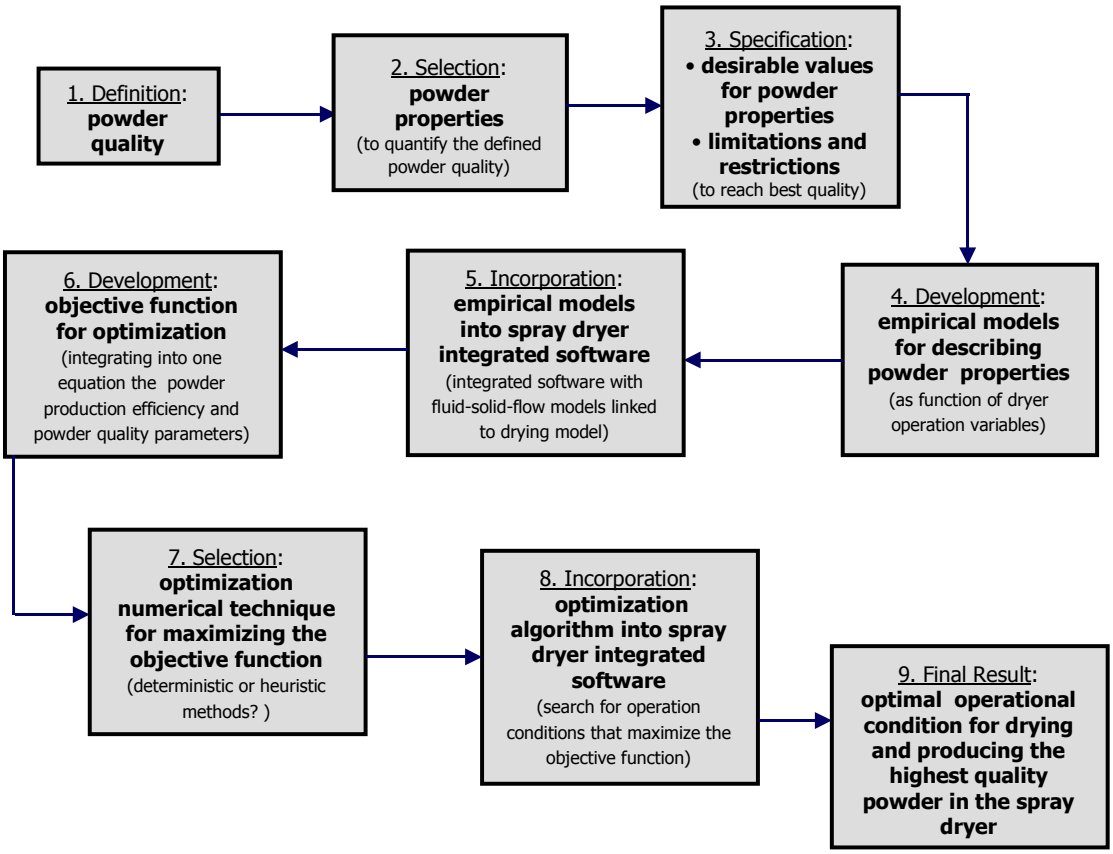

Figure 7 Schematic steps for optimizing the operation variables of the spray dryer concerning the drying-production efficiency and the product quality.

Since the powder property variation is directly dictated by the spray dryer operation conditions, the powder quality should be quantified by the relationship between the operational process variables that best describe these properties. Therefore, in the fourth step presented in Figure 7, empirical models are developed to express these powder properties as a function of the spray dryer operational variables. The procedure to develop these empirical models is discussed in the next sub-item 4.1.

These empirical models can be incorporated into a computational program, or even into CFD commercial software, developed to simulate simultaneously drying and powder formation in spray dryers. This incorporation represents the fourth step in the diagram in Figure 7. By defining the objective function (fifth step in Figure 7), combining the powder production efficiency and the powder product quality in such a way that they can be maximized simultaneously, the optimization of the spray-dryer operation should be performed, following the sixth, seventh and eighth steps shown in Figure 7.

4.1 Experimental design for empirical model

Concerning Figures 3 and 7, it is known that many other powder properties can be selected to best describe the product quality, depending on the required product. Due to this multiplicity of choices and to the complexity of the powder product, models for describing powder properties as a function of the spray dryer operational variables are invariably empirical. Therefore, experiments must be performed to correlate these properties with the operational variables, maximizing their levels and, consequently, increasing the product quality. This item presents briefly the most useful techniques to design these experiments in order to develop more accurate empirical models.

The powder properties, chosen to quantify the product quality, are, in this context, denominated *response variables* or *dependent variables*. The operational variables that should influence powder properties, called *predictor variables* or *independent variables*, are probably:

- temperature, feed rate and humidity of the inlet drying gas;
- concentration, feed rate and temperature of the feed emulsion or solution;
- type, pressure or rotation of atomizer (according to the type);
- type of air-fluid contact (concurrently, counter-currently and combined flow);
- pressure inside the spray dryer chamber.

After selecting the predictor variables, it is necessary to define the interesting range of study, i.e. how these variables should vary in the experiments, which are called *levels*. As shown in Figure 7 and discussed by Birchal et al. [38], the methodology to establish the relation of all these variables involves:

(1) identification and characterizations of the powder parameters that assure its high quality (response variables);
(2) selection of the spray-dryer operational parameters that most influence quality (predictor variables);
(3) design and development of experiments, choosing the most suitable technique; and
(4) statistical analysis of results and correlations, leading to the best range for operating the spray dryer to produce powder at higher quality..

The most recommended method of planning experiments is called *Factorial Design*, where predictor variables are also called *factors* of the experiments. The basic idea is to performance a set of experiments considering all possible variations of the factors, using a minimum number of them [39]. The advantages of using this method are: it is a simultaneous method; the variables of interest that, in fact, present significant influence on the response are evaluated as well as the interaction among them; and, it is more efficient than using a design that varies one factor at each time.

In factorial design, frequently it is used the 2^k factorial type (k factors at 2 levels), resulting in 2^k number of experiments. This scheme is particularly

useful at the beginning of study, when there are a large number of variables to be investigated [39]. The main tendencies can be observed and the variables and interactions that really influence the phenomena can be better explored in as many levels as necessary. The selected levels is codified as low (-) and high (+) ones. All the analyses assume that: the designs are completely randomized and the normality assumptions are satisfied. As there are only two levels, it is assumed that the response is approximately linear in the range of study. If only two factors (A and B) are involved, the statistical model is:

$$\hat{y} = \beta_0 + \beta_1 A + \beta_2 B + \beta_3 AB \quad (8)$$

with $\hat{y}$ representing the estimate for the response variable and β_0, β_1, β_2, β_3 are the model parameters: the interception, the influence of A and B in the response and the influence of A and B interaction, respectively. These parameters are called *effects* and are determined using the minimum square method. Performing replicates of experiments is strongly recommended, which allows the analyses of variance, including the F (Fisher distribution) t (student) and p-value. Consequently, the parameter significance can be evaluated. Also, response surface and counter plots can simplify the result interpretation.

If it is not possible to do replicates, the effects significance can be evaluated by: the effects magnitude; normal probability plot and Pareto chart of the effects; main and interactions plots; and the residues verify any normality violation. However, only descriptive statistics is acceptable. No inference can be established because of the lack of degree of freedom. It only describes the data in the range of study [40].

Adding experiments replicated in the central points, provides n_c-1 degrees of freedom (n_c = number of replicates), making it possible to determine the residue and, hence, some inference. This kind of addition can be done only when there are only numerical variables involved, which frequently occurs when studying spray drying.

Frequently, there is interest in determining first and second order coefficients. In this case, it is necessary to add some points to the design. An interesting strategy is to include axial points what is called *Central Composite Design*. One possibility of determining the axial point levels is to choose ± α, with $\alpha = (2^k)^{1/4}$. Hence, if there are two factors, □ = ±1,4142; three factors, α = ±1,6818; four factors, α = ±2,0000, for example. A design with these axial points is named *Rotational Central Composite Design*. If there are two levels, it will result in 2^k factorial points + 2 k axial points + an arbitrary number of central points [40]. This strategy is represented in Figure 8, considering a 2^3 factorial: 2 levels, 3 factors (x_1, x_2 and x_3).

Another strategy is to use *Box-Behnken* design. This is very useful in evaluating response surfaces and uses two levels + central level in the experiments execution. It results in a fewer design points comparing to central composite design. Besides, the additional points fall in an operating zone within the determined levels while the axial points may fall beyond a safe operating limit. Figure 9 illustrates this design, considering 2^3 scheme as well. Another great advantage of this design is that it allows getting response surfaces and counter plots, leading to optimum point of operation.

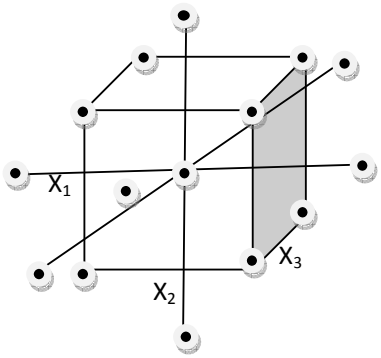

Figure 8 Rotational Central Composite design

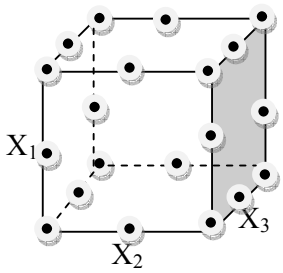

Figure 9 Box Behnken design

In all strategies of designs, when the model does not seem to fit well, it is worthwhile trying to transform the variables involved, before trying a different model or a different design [41]. If there are k factors involved at N levels, it will result on a N^k number of experiments, in a complete factorial scheme. Hence, it is almost impossible to run a complete scheme if there are 6 or more factors at 2 levels or 4 or more factors at 3 levels [40]. Besides, higher order interactions are evaluated, which is, frequently, unnecessary. In this case, fractional experiments can be used, carrying out a smaller set of experiments and considering only main effects and some interactions of lower order, which, in most of the times, domain the systems. This is called *Fractional Factorial Design*. It can be used 2^{k-1} experiments (half fraction), 2^{k-2} (1/4 fraction), 2^{k-3} (1/8 fraction) or less, according to the number of factors involved. Naturally, the smallest is the fraction, the smallest is the experimental resolution (order of interaction that can be obtained). It is important to make it clear that here it is given only a brief of some of the statistical techniques for developing a model. More details should be obtained in the specialized literature [39-42].

4.2 Empirical models for specific cases

Some examples of modeling powder quality properties that have already developed in the literature based on techniques discussed previously (item 4.1), can be seen in Table 1. Although only few works have already incorporated these empirical models into an integrated software to describe the entire spray drying process in order to control the powder formation and

its properties, this is a new feasible approach that begins to be developed, opening area for research and development.

Table 1 Statistical experiment design technique application to model powder quality in spray dryers.

Design technique	*Factors*	*Responses* (final powder)	Main quality required	Optimization performed	Ref.
Central composite	inlet air temperature liquid feed flow rate carrier agent concentration	process yield particle size hygroscopicity moisture content pigment content	minimize wall adherence maximize pigment retention	no	26
Full-factorial	inlet air temperature liquid feed flow rate air flow rate two-fluid nozzle gas flowrate	process yield particle size moisture content degradation protein, insulin (no-linear model)	reduce particle size for inhalation propose	yes, statistical models (maximize process yield; minimize other responses)	36
Full-factorial	inlet and outlet air temperatures liquid feed composition (starch, oil, glucose)	particle size particle surface particle density bulk density porosity lipid oxidation	improve micro-encapsulation (formulation of wall components)	no	25
Full-factorial	inlet air temperature liquid feed flow rate atomization speed rotation	particle size and dispersion index bulk density Hausner ratio internal porosity moisture content	maximize powder instantizing	yes, with incorporation of empirical models to the integrated software	38

5.0 Concluding remarks

As shown and discussed in this chapter, powders can be produced in spray dryers with a desirable product quality to attend requirements from market and consumers. This is performed by manipulating the spray-dryer operational variables, using a simulation-optimization model strategy. Product quality must be defined previously and quantified by the powder properties that best describe the desirable quality. Empirical models, developed using statistical experiment design techniques, provide the key to optimize the spray dryer operation conditions in order to reach the desirable powder product at high quality.

6.0 References

1. Filková, I.; Mujumdar, A. S. Industrial spray drying systems. In *Handbook of Industrial Drying*, 3rd edition, Mujumdar, A. S., Ed.; CRC Press Taylor and Francis Group, Boca Raton, Fl, 2006; pp.215-256.
2. Pisecky, J. Evaporation and spray drying in the dairy industry. In *Handbook of Industrial Drying*, 2rd edition, Mujumdar, A. S., Ed.; Marcel Dekker Inc.; New York, NY, 1995; pp.715-742.
3. Birchal, V.S.; Passos, M. L. Modeling and simulation of milk emulsion drying in spray dyers. Braz. J. Cem. Eng. **2005**, *22*, 293-302.
4. Mezhericher, M.; Levy, A.; Borde, I. Theoretical drying model of single droplets containing insoluble or dissolved solids. Drying Techn. **2007**, *25(6)*, 1.025-1032
5. Kim, E.H.J.; Chen, X. D.; Pearce, D. On the mechanisms of surface formation and the surface compositions of industrial milk powders. Drying Technol. **2003**, *21(2)*, 265-278.
6. Charlesworth, D. H.; Marshall Jr., W. R. Evaporating from drops containing dissolved solids. A. I. Ch. E. Journal **1960**, *6(1)*, 9-23.
7. Nešić, S. The evaporation of single droplets - Experiments and modelling. In *Drying'89*, Mujumdar, A.S., Ed.; Hemisphere Publishing Corp., New York, NY, 1990; pp.386–393.
8. Seydel, P.; Blömer, J.; Bertling, J. Modeling particle formation at spray drying using population balances. Drying Techn. **2006**, *24*, 137-146.
9. Refstrup, E. Recent advances in agglomeration during spray drying. http://niroinc.com/ drying_dairy_food/recent_advances_agglomeration.asp (accessed March 30, 2010).
10. King, C. J.; Kieckbusch, T. G.; Greenwald, C. G. Food-quality factors in spray drying. In *Advances in Drying*, vol. 3, Mujumdar, A. S., Ed.; Hemisphere Publishing Corp., New York, NY, 1984, pp. 71-120.
11. Knegt, R.J.; Brink, H. van den. Improvement of the drying oven method for the determination of the moisture content of milk powder. Int. Dairy J. **1998**, *8*, 733-738.
12. Beuchat, L. Microbial stability as affected by water activity. Cereal Foods World **1981**, *26*, 345-351.
13. Decagon Inc. AquaSorp - moisture sorption isotherm generator. Operator's Manual, version 3.0. http://www.decagon.com/pdfs/manuals/AquaSorp_v3.pdf (accessed March 30, 2010).
14. Passos, M. L.; Mujumdar, A. S. Mathematical models for improving spray drying processes for foods. Stewart Postharvest Review. **2005**, *1(4)*, 6:1-12.
15. Masters, K. *Spray Drying Handbook*, 5th ed.; Longman Group: Harlow, Essex, 1991.
16. Ré, M. I. Formulating drug delivery systems by spray drying. Drying Technol. **2006**, *24*, 433-446.
17. Medeiros, U. K. L.; Medeiros, M. F. D.; Passos, M. L. Goat milk production in small agro-cooperatives. In *Innovation in Food Engineering New Techniques and Products*, Passos, M. L. and Ribeiro, C. P., Eds.; CRC Press Taylor and Francis Group, Boca Raton, Fl, 2010; pp.539-578.

18. Svarovsky, L. *Solid-liquid Separation*, 4th ed.; Butterworths: Witham, Essex, 2000.
19. Geldart, D. *Gas Fluidization Technology*, John Wiley & Sons Ltda.: Chichester, Sussex, 1986.
20. Hahne, L.C.C. Experimental studies about the particle drying and agglomerating in vibro-fluidized beds for milk powder production. Master Thesis. Federal University of Minas Gerais, 2001 (in Portuguese).
21. Ilari, J-L.; Mekkaoui, L. Physical properties of constitutive size classes of spray-dried skim milk powder and their mixtures. Lait. **2005**, *85*, 279-294.
22. Westergaard, V. *Milk Powder Technology – Evaporation and Spray Drying.* 5th ed., Niro A/S, Copenhagen, Denmark. 2004.
23. Birchal, V. S. Modeling and simulating of milk drying in spray dryers, Ph.D Thesis. Federal University of Minas Gerais, 2003 (in Portuguese).
24. Pisecky, J. Bulk density of milk powders. Dairy Industries Int. **1978**, *3*, 4-11.
25. Drusch, S.; Schwarz, K. Microencapsulation properties of two different types of *n*-octenylsuccinate-derivatised starch. Eur. Food Res. Technol. **2006**, *222*, 155-164.
26. Tonon, R.; Brabet, C.; Hubinger, M. Influence of process conditions on the physicochemical properties of açai (*Euterpe oleraceae* Mart.) powder produced by spray drying. J. Food Eng. **2008**, *88*, 411-418.
27. Langrish, T. A. G. New engineered particles from spray dryers: research needs in spray drying. Drying Techn. **2007**, *25(6)*, 971-983.
28. Ozmen, L., Langrish, T. A. C. An experimental investigation of the wall deposition of milk powder in a pilot-scale spray dryer. Drying Techn. **2003**, *21(7)*, 1253-1272.
29. Ozmen, L., Langrish, T. A. C. Comparison of glass transition temperature and sticky point temperature for skim milk powder. Drying Techn. **2002**, *20(6)*, 1177 – 1192.
30. Kota K.; Langrish T. A. G. Prediction of wall deposition behaviour in a pilot-scale spray dryer using deposition correlations for pipe flows. J. Zhejiang University Sci. A, **2008**, *8(2)*, 301-312.
31. Emery, E. Flow properties of selected pharmaceutical powders. Master Thesis, University of Saskatchewan, Saskatoon, Canada, 2008.
32. Fredlund, D.G.; Rahardjo, H. *Soil Mechanics Unsaturated Soils.* John Wiley & Sons Inc., New York, NY, 1993.
33. Castellanos, A.; Valverde, J. M.; Quintanilla, M.A.S. The Sevilla powder tester: a tool for characterizing the physical properties of fine cohesive powders at very small consolidations. Kona, **2004**, *22*, 66-81.
34. Hayes, G. D. *Food Engineering Data Book*, Longman Scientific and Technical, London, 1987.
35. Xinde, X.; Shanjiing, Y.; Ning, H.; Bin, S. Measurement and influence factors of the flowability of microcapsules with high-content β-carotene. Chin. J. Chem. Eng. **2007**, *15(4)*, 579-585.
36. Ståhl, K.; Claesson, M.; Lilliehorn, P.; Lindén, H.; Bäckström, K. The effect of process variables on the degradation and physical properties of spray dried insulin intended for inhalation. Int. J. Pharm. **2002**, *233*, 227-237.
37. Healy, A.M.; McDonald, B. F.; Tajber, L.; Corrigan, O. I. Characterization of excipient-free nanoporous microparticles (NPMPs) of bendroflumethiazide. European J. Pharm. Biopharm. **2008**, *69*, 1182-1186.

38. Birchal, V.S.; Passos, M. L.; Wildhagen, G.R.S.; Mujumdar, A.S. Effect of spray-dryer operating variables on the whole milk powder. Drying Techn. **2005**, *23(3)*, 611-636.
39. Montgomery, D. C. *Design and analysis of experiments.* 6ed., John Wiley & Sons Inc., New York, NY, 2005.
40. Rodrigues, M.I.; Iemma, A.F. *Experiment Design and Process Optimization: a sequential design strategy*. Casa do Pão, Campinas, SP, 2005 (in Portuguese).
41. Box, G.E.P; Hunter, J.S. *Statistics for Experimenters: An Introduction to designs, Data Analysis and Model Building*. Wiley. New York, N.Y, 1978.
42. Box, G.E.P; Drapper, N.R. *Empirical Model – Building and Response Surfaces*. John Wiley & Sons, New York, N.Y., 1987.

Langrish, T.A.G. Spray drying and crystallization - Volume 1, Ed. Woo, M.W., Mujumdar, A.S. and Daud, W.R.W., **2010**, ISBN - 978-981-08-6270-1, Published in Singapore, pp. 61-76.

Spray drying and crystaliization

Chapter 3

Langrish T.A.G.

Department of Chemical and Biomolecular Engineering
University of Sydney, Australia

Contents **Page**

1.0 Introduction

The benefits of crystallization-in-drying can be simply stated as giving an understanding of the basic form or state of the solids that arise after the drying process and how the drying process can be used to not only control the particle moisture content but also the solid form.

Regarding the industrial motivation for studying this process, it is possible to imagine a number of particle production methods that might contribute to manufacturing new engineered powders, as illustrated in Figure 1. Concentrating now on the use of crystallization during drying as a method to create particular solids structures from spray-dried products, Figure 2 illustrates the situation that a particular final moisture content may be produced through a number of different routes, and each different route may create different degrees of crystallinity and hence different solids structures.

1.1 Effect on particle-wall deposition

On the basis of the Williams-Landel-Ferry findings[1], the rate of this solid-phase crystallization process accelerates when the particle temperature is above the glass-transition temperature of the particle. This consideration implies that trying to crystallize materials inside spray dryers needs to consider the combination of heat and mass transfer processes, as illustrated in Figures 3 and 4. Figure 3 shows that there are several different outcomes for particles that hit the walls of spray dryers. In relatively low temperature drying (low relative to the glass-transition temperature of the particles), the amorphous particles from the atomizer are likely to remain amorphous as they travel through the gas. Providing that the particle temperatures are below their glass-transition temperatures, the amorphous particles will remain glassy and bounce off the walls of the spray dryer (case 1). At higher temperatures, the temperatures of the amorphous particles may exceed their glass-transition temperatures, making the amorphous particles sticky and rubbery so that they are more likely to stick to the walls of the spray dryer, decreasing the yield or recovery from spray drying (case 2). The amorphous particles that stick to the walls may then crystallize as they are present on the walls. However, at even higher temperatures, there is an opportunity for the particle temperatures to exceed the glass-transition temperatures sufficiently for the particles to crystallize before the particles hit the dryer walls. This situation means that the crystallized particles are likely to bounce off the walls, increasing the yield again (case 3). Hence, for a fixed liquid feed rate, concentration and composition of solids in the liquid, initial droplet size, gas flow rate and humidity, increasing the inlet gas temperature is likely to increase the particle temperatures throughout the dryer, initially increasing the yields with better drying, which decreases the particle moisture contents and increases the glass-transition temperatures of the particles (case 1). Then, with further increases in the particle temperatures above the glass-transition temperatures of the particles, the yields are likely to decrease as the particles become stickier (case 2). Finally, at high enough temperatures, the particles are likely to crystallize, increasing the yields as crystallized particles bounce off the dryer walls (case 3). In summary, we are likely to see the yields or recoveries from spray drying increase, then decrease, and finally increase again as the inlet gas temperature to the dryer is increased.

Experimental evidence exists to support these assertions, and Figure 4 includes real data for the spray drying of sucrose [2] that follows this predicted trend in terms of experimental observations. These data were obtained from a laboratory-scale spray dryer (Buchi 290) when spray drying sucrose. The region where the particles are very sticky and adhere to the dryer walls and cohere to particles already on the walls is described as “the stickiness barrier”.

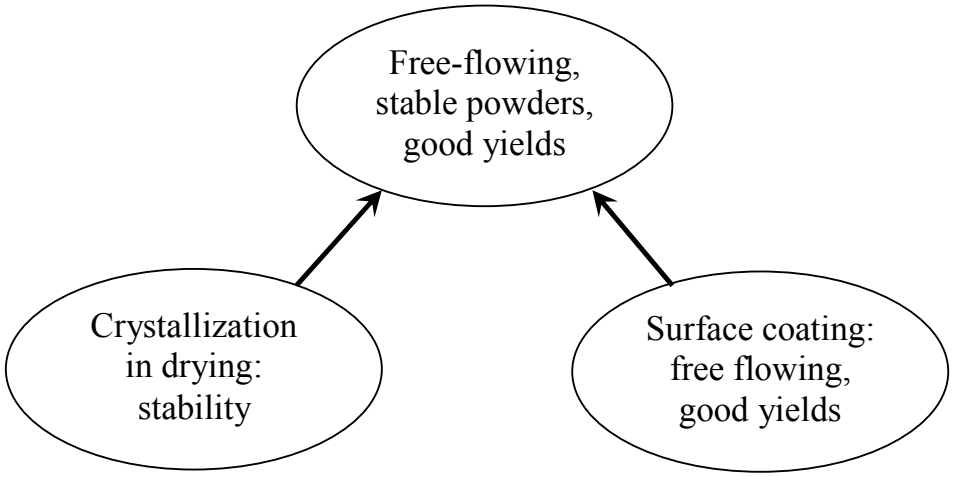

Figure 1 Combinations of particle engineering techniques for better engineered particles.

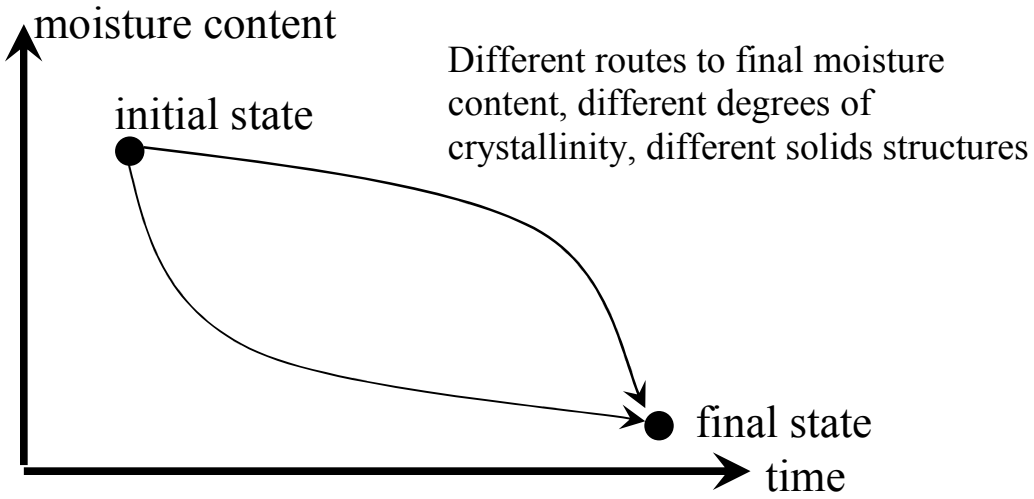

Figure 2 Different drying trajectories in spray drying for giving different solid structures while giving the same final moisture contents.

These considerations regarding the effects of particle and glass-transition temperatures mean that materials with very low glass-transition temperatures might be expected to crystallize during spray drying even with low inlet or outlet gas temperatures. Indeed, this is the case, with ascorbic acid (vitamin C) having a glass-transition temperature under -40°C [3] but crystallizing completely under all spray-drying conditions, even those involving inlet air temperatures as low as 110°C [4].

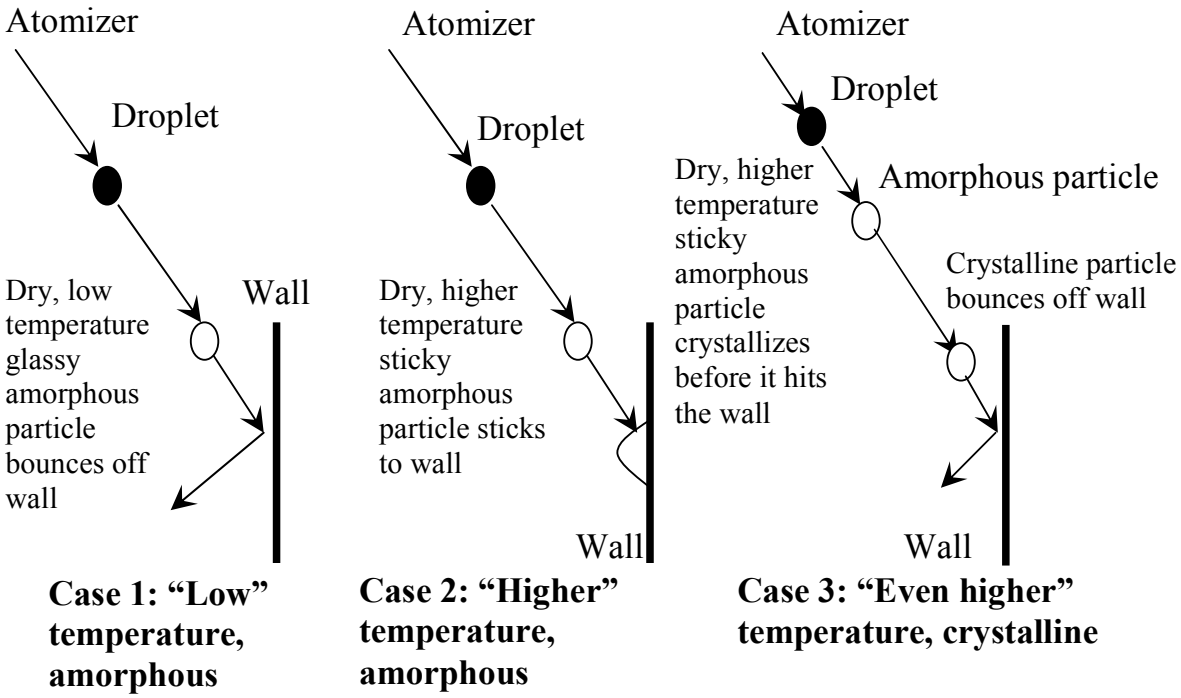

Figure 3 Different trajectories for spray-dried particles in spray dryers.

With higher inlet air temperatures and consequently higher particle temperatures leading to greater particle crystallization in spray dryers [5][6], there may be some suspicion that these high temperatures may lead to the spray-dried material being degraded as a result of the crystallization process. However, less than 5% degradation has been found for the spray drying of sucrose [2] and ascorbic acid [4]. The underlying reasons why the amount of degradation is so small can be understood by assessing the nature and extent of the temperature dependence of the solid-phase crystallization process[7] as quantified by the Williams-Landel-Ferry equation [1]. The logarithmic (base 10) and exponentiation (10^) terms in this equation mean that this equation predicts increases in the solid-phase crystallization rate that involve orders of magnitude increases in the crystallization rate with only a few degrees increase in particle temperature (Figure 5). This extremely rapid increase in predicted crystallization rate with increasing temperature should be contrasted with the normal behaviour of most reactions, including most degradation ones, that the rate doubles approximately with each ten degree increase in temperature. Hence the temperature dependence of the solid-phase crystallization process as predicted by the Williams-Landel-Ferry equation [1]

could be described as “super Arrhenius”. The practical outcome of this situation is simply that the material is more likely to crystallize before it degrades, as has been found experimentally.

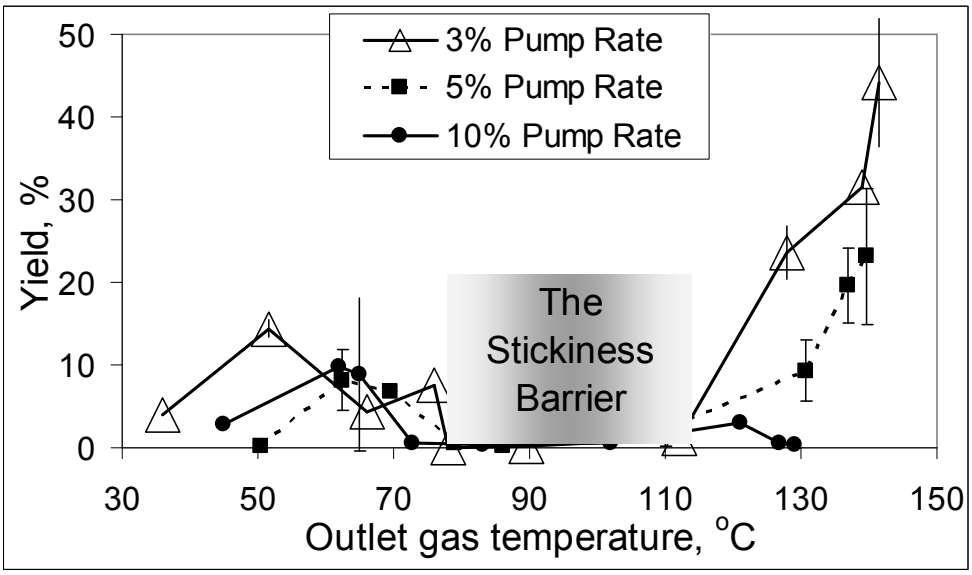

Figure 4 *Yield of the spray-dried products at different outlet gas temperatures for the spray drying of sucrose in a Buchi 290 spray dryer* [2]

So far, the discussion has focussed on what can be done to crystallize materials, but keeping materials amorphous is also potentially of interest. Amorphous material is more porous [8], more soluble [9-12], more bioavailable [11][13-15] and more sorptive [5][6][16]. Reducing the extent of crystallization during spray drying may be achieved by keeping the difference between the particle and the glass-transition temperatures as low as possible, but other methods are also possible. Formulatiing the material to be dried with additional proteins and/or fats will reduce the crystallization rates of sugars, since the\proteins and fats act to reduce the rate at which the sugar molecules rearrange themselves into a crystal matrix [17].

A key question is how to simulate the process of crystallization-in-drying within spray dryers so that it can either be maximized or minimized, and an answer to this question is explored in the following sections.

2.0 Parallel-flow design equations

The following framework treats spray dryers as having the gas and solids flowing in parallel to each other, and is more appropriate for tall-form spray dryers than for short-form ones, due to the overall flow patterns, as discussed above. Truong, Bhandari & Howes [18] have given a clear description of equations for these situations, and these equations are largely reproduced in the following sections. The approach, and the equations in it, was originally

reported by Keey & Pham [19]. This approach has been used by a number of authors [6][18]. The subscripts p, a, s have been used to represent the droplet, air and solids, respectively in the following equations.

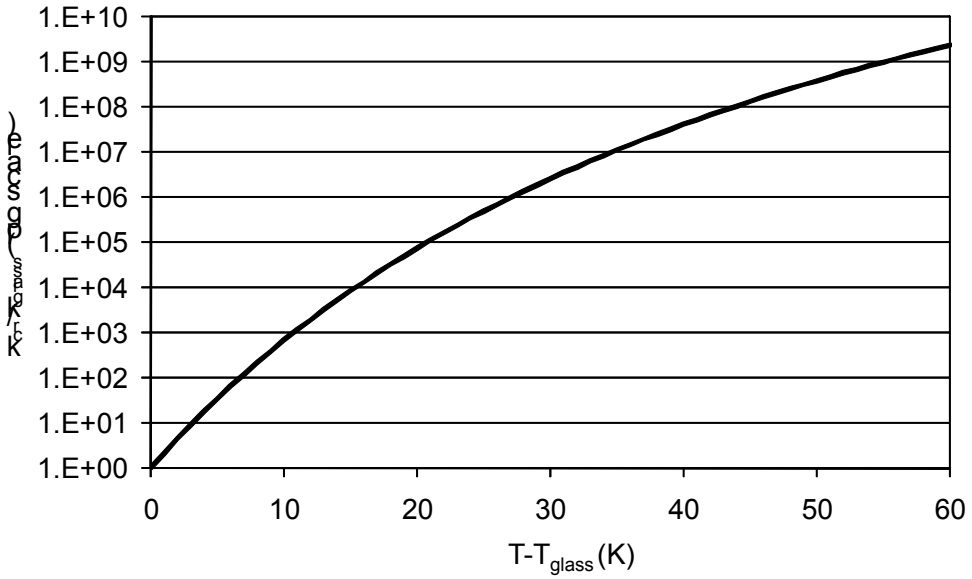

.Figure 5 *Predicted temperature dependence of the solid-phase crystallization process predicted from the Williams-Landel-Ferry equation [1] in terms of the increase in crystallization rate (k_{cr}) compared with the crystallization rate at the glass-transition temperature (k_g) as a function of the difference between the particle (T) and the glass-transition (T_{glass}) temperatures.*

2.1 Equation for droplet trajectories

Droplet axial, radial and tangential momentum balances give the droplet trajectory equations. The velocity (m s^{-1}) of the particles and the air are represented by U_p and U_a, respectively. The subscripts *x*, *r* and *t* represent the axial, radial and tangential components, respectively, and the axial distance from the atomiser has the symbol *h*.

$$\frac{dU_{px}}{dh} = \left[\left(1-\frac{\rho_a}{\rho_p}\right)g - \frac{3}{4}\frac{\rho_a C_D U_R\left(U_{px}-U_{ax}\right)}{\rho_p d_p}\right]\frac{1}{U_{px}} \quad (1)$$

$$\frac{dU_{pr}}{dh} = \left[-\frac{3}{4}\frac{\rho_a C_D U_R\left(U_{pr}-U_{ar}\right)}{\rho_p d_p}\right]\frac{1}{U_{px}} \quad (2)$$

$$\frac{dU_{pt}}{dh} = \left[-\frac{3}{4}\frac{\rho_a C_D U_R\left(U_{pt}-U_{at}\right)}{\rho_p d_p}\right]\frac{1}{U_{px}} \quad (3)$$

The density is ρ (kg m^{-3}), d_p is the droplet diameter (m), U_R is the relative velocity between the droplet and the air (m s^{-1}), and C_D is the drag coefficient. The air and the particle or droplet are referred to by the subscripts *a* and *p*, respectively. Equations given by Rhodes (1998) allow U_R and C_D to be calculated, as follows:

$$U_R = \sqrt{\left(U_{px} - U_{ax}\right)^2 + \left(U_{pr} - U_{ar}\right)^2 + \left(U_{pt} - U_{at}\right)^2} \tag{4}$$

$$C_D = \frac{24}{\mathrm{Re}_p}\left(1 + 0.15\,\mathrm{Re}_p^{\,0.687}\right) \tag{5}$$

By definition, the particle Reynolds number is given by the equation:

$$\mathrm{Re}_p = \frac{\rho_a U_R d_p}{\mu_a} \tag{6}$$

where the viscosity is μ (kg m^{-1} s^{-1}). The calculation of the radial distance, r, of droplets as a function of axial distance (*h*) from the atomiser is carried out as follows.

$$\frac{dr}{dh} = \frac{U_{pr}}{U_{px}} \tag{7}$$

2.2 Mass balance equations for the droplets

The unsteady-state mass balance for the droplets may be based on the concept of a characteristic drying curve [20], as follows:

$$\frac{dm_p}{dh} = -\xi \frac{A_p K_p}{U_{px}}\left(p_{vs} - p_{vp}\right) \tag{8}$$

The mass of the particle or droplet is m_p (kg), p_{vs} is the partial pressure of the surface of the droplet (Pa), p_{vb} is the partial pressure of water vapour in the bulk air (Pa), ξ is the relative drying rate (-), A_p is the droplet surface area (m^2), and K_p is the mass-transfer coefficient (partial pressure based) (kg m^{-2} s^{-1} Pa^{-1}). The droplet surface area (A_p) can be calculated as follows.

$$A_p = \pi d_P^2 \tag{9}$$

Shrinkage changes the droplet diameter. For some materials, such as salt, which do not form hollow particles, the assumption of balloon shrinkage without crust or skin formation (reasonable for salt [21]) allows the droplet diameter, d_p, to be updated, as follows.

$$d_p = d_{pi}\left(\frac{\rho_{pi} - 1000}{\rho_p - 1000}\right)^{\frac{1}{3}} \tag{10}$$

$$\rho_p = \frac{1 + X}{1 + X\dfrac{\rho_s}{\rho_w}}\rho_s \tag{11}$$

The variables that have not been defined previously are d_{pi}, the initial droplet diameter (m), ρ_{pi}, the initial droplet density (kg m^{-3}), and X is the moisture content (dry-basis). The following equations define the gas-phase mass-transfer coefficient:

$$K_p = \frac{M_w K_m}{M_a P} \tag{12}$$

$$K_m = \frac{\rho_a D_v Sh}{d_p} \tag{13}$$

K_p is the mass-transfer coefficient (partial pressure based, in kg m^{-2} s^{-1} Pa^{-1}), K_m is the mass-transfer coefficient (kg m^{-2} s^{-1}), D_v is the diffusivity of water in air (m^2 s^{-1}), Sh is the Sherwood number, M_w is the molecular weight of water (g mol^{-1}), M_a is the molecular weight of air (g mol^{-1}), and P is the total pressure (Pa). The following equation may be used to estimate the diffusivity (Perry's Chemical Engineering Handbook, 1997):

$$D_v = \frac{1.17564 \times 10^{-9} \times T_{abs}^{\ 1.75} \times 101325}{P} \tag{14}$$

The following equations define the Schmidt number (Sc) and allow the Sherwood number to be estimated:

$$Sc = \frac{\mu_a}{\rho_a D_v} \tag{15}$$

$$Sh = 2.0 + 0.6\,\mathrm{Re}_p^{\ 0.5}\, Sc^{0.33} \tag{16}$$

where T_{abs} is the absolute temperature of the droplet or particle (K).

2.3 Heat balance equations for the droplets

For the droplet or particle, the unsteady-state heat balance is given by the equation [18]:

$$\frac{dT_p}{dh} = \frac{\pi d_p k_a Nu\left(T_a - T_p\right) + \frac{dm_p}{dh} U_{px} H_{fg}}{m_s\left(C_{ps} + XC_{pw}\right) U_{px}} \tag{17}$$

The following equations define the Prandtl number (*Pr*) and allow the Nusselt number (*Nu*) to be estimated by the Ranz-Marshall equation:

$$Pr = \frac{C_{pa}\mu_a}{k_a} \tag{18}$$

$$Nu = 2.0 + 0.6\,\mathrm{Re}_p^{\,0.5}\,\mathrm{Pr}^{0.33} \tag{19}$$

Other product and particle properties are calculated as follows:

$$m_s = \frac{Xm_p}{100} \tag{20}$$

$$H_{fg} = 2.792\times10^6 - 160T_{abs} - 3.43T_{abs}^{\,2} \tag{21}$$

Here k_a is the thermal conductivity of humid air (W m^{-1} K^{-1}), H_{fg} is the latent heat of water evaporation (J kg^{-1}), m_s is the mass of solids in the droplet (kg) and C_p is the specific heat capacity (J kg^{-1} K^{-1}).

2.4 Balance equations for the drying medium

For the drying air, the mass-balance equation equates the mass of moisture lost by the droplets or particles with the mass of moisture gained by the gas:

$$\frac{dY_b}{dh} = \frac{\Sigma_{droplets}\left(-\frac{dm_p}{dh}\right) n_{droplets}}{G} \tag{22}$$

The mass flow rate of the dry air is G (kg s^{-1}), and $n_{droplets}$ is the flow rate of droplets (number s^{-1}). The corresponding heat-balance equation, again balancing the energy lost by the droplets or particles with the gain in humid heat capacity and heat loss from the dryer, is:

$$\frac{dH_h}{dh} = -\frac{1}{G}\left(\Sigma_{droplets}\left(m_s\left(C_{ps} + XC_{pw}\right)\frac{dT_p}{dh}\right) - \frac{UA\left(T_a - T_{amb}\right)}{L}\right) n_{droplets} \tag{23}$$

The enthalpy of the humid air is H_h (J kg^{-1}), UA is the heat-transfer coefficient for heat loss from the dryer, and L is the length of the spray-drying chamber.

2.5 Particulate drying kinetics

Correct quantitative prediction of the droplet and particle behaviour in the dryer requires proper modelling of the drying behaviour of the droplets. The temperature and moisture content of the droplets and particles affect all subsequent reactions, including crystallization. It is important to allow properly for hindered drying due to the presence of the solids. Various approaches exist in the literature, including the characteristic drying curve [19][22], A shortcut solution to the diffusion equation [23][24] and other diffusion models [25][26], Receding-plane type models [20] and others that include both convection and diffusion as transport processes [27] and reaction engineering approaches [28][29]. Both a characteristic drying curve (CDC) and the reaction engineering approach (REA) have been used to simulate drying behaviour and compared [28] with experimental data for whole and skim milk droplets, finding that the predictions from the REA model are closer to the experimental results from using CDC.

Although the predicted results from the REA model were closer to the experiments than those predicted by the CDC model, the difference was small, remaining under 5% for both models. Chen & Lin [28] recognised that the CDC model provided a good approximation to the experimental results, despite its simplicity. In addition, they recognised that the REA model includes initially incorrect activation energies, higher than the actual one, because the milk droplets initially behave in the same way as water, where the activation energy of drying is close to zero. The REA model overpredicts this value, thus underestimating the initial drying rate and predicting droplet temperatures that rise faster than in reality. This initial period of time, where over-prediction of the activation energy occurs, was found by Chen & Lin to be approximately the first 10% of the total drying time. Patel & Chen [29] used a parallel-flow approach to compare the two models, suggesting that the REA model gave better predictions at high relative humidities and high feed concentrations, but that the two models were similar under other conditions.

3.0 Crystallization in drying

3.1 A physical transformation

The extent of crystallization of a powder has a profound effect on properties relating to both use and handling. Studies of the properties of powders[30], have shown that fully crystalline powders have improved flowability and decreased wall deposition, whereas completely amorphous powders have the greatest bioavailability and adsorptive capacity [31] at the expense of flowability and stability[32]. A particle with a crystalline surface but an amorphous interior will retain much of the adsorptive capacity and bioavailability of an amorphous particle, with the crystalline flowability and decreased deposition characteristics. Hence the ability to control the degree

of crystallization will have significant benefits for those using spray-dried products as well as those operating the processes.

Background

Water-induced crystallization of lactose in storage has been known for a long time [33][34], but recently we have shown that water-induced crystallization of lactose occurs in spray dryers [5][6], due to the high temperatures involved and the control of humidity and product moisture content that is possible in this equipment. We have also shown [35] that water-induced crystallization occurs for a wide range of materials, including sucrose, coffee, tea, skim milk, maltodextrin and hibiscus extract. Most recently, we have shown [2] that sucrose can be fully crystallized inside a laboratory-scale (Buchi) spray dryer (small scale).

Basic Theory

Actual measurements of, and correlations for, the rate of crystallisation of polymers, organic glasses and inorganic were reported by Williams, Landel and Ferry[1] (WLF) and used to form the WLF equation. Roos and Karel [36] were able to apply the equation to food polymers, such as lactose. They found that the ratio (r) of the time for crystallisation (θ_{cr}) (time taken for the material to become 100% crystalline) at any temperature (T_p) to the time for crystallisation (θ_g) at the glass-transition temperature (T_{gt}) could be correlated by the following equation (the WLF equation):

$$\log_{10} r = \log_{10}\left(\frac{\vartheta_{cr}}{\vartheta_g}\right) = \frac{-17.44\left(T_p - T_{gt}\right)}{51.6 + \left(T_p - T_{gt}\right)} \tag{24}$$

Since the ratio, r, decreases when crystallisation becomes more rapid, the inverse of this ratio is a measure of the relative rate of crystallisation, compared with the crystallisation rate at the glass-transition temperature. The inverse of this ratio can be described as the "impact" of the particle temperature, T_p, and the glass-transition temperature, T_{gt}, which is a function of the particle moisture content, X, through the Gordon-Taylor equation. Both the particle temperature, T_p, and the particle moisture content, X, change through the dryer, as described in the previous sections, so the glass-transition temperature, T_{gt}, also changes as the droplets and particles dry out when they move through the dryer.

The Gordon-Taylor equation [37] can be used to predict the glass-transition temperature of food mixtures and pharmaceutical solids as a function of the composition and the glass-transition temperatures of the individual components that make up the mixture:

$$T_{gt} = \frac{w_1 T_{gt1} + k w_2 T_{gt2}}{w_1 + k w_2} \tag{25}$$

where, w_1 and w_2 are the respective weight fractions of the two components, T_{gt1} is the glass-transition temperature of one component, T_{gt2} is the glass-transition temperature of the other component, and k is a curvature constant, which can be determined empirically. One of these components

may be the solid material that is spray dried, while the other might be the moisture in the particle, and the equation can be extended to three or more components in the particle (Arvanitoyannis *et al.*, 1993). This equation is based on the assumption of perfect volume additivity, that is, the liquids mix without any change in volume, and there is no specific interaction between the components of the mixture. The equation has been used by many workers to predict that the glass-transition temperature decreases with increasing moisture content, as is found experimentally. The glass-transition temperature is affected by the nature and composition of the components [36][38]. The weight fraction of water, *w*, is related to the moisture content, *X*, expressed on a dry basis, through the equation w = *X* / (1 + *X*).

Both the particle temperature and the particle moisture content change through the dryer, and these changes are predicted by the simulation. These changes mean that the local value of the "impact", the inverse of the ratio of crystallisation times, needs to be integrated over the residence time for each particle in the dryer. In effect, this procedure treats the WLF equation (24) as representing the inverse of a rate equation for crystallisation, where the inverse of the ratio is equivalent to a relative rate for crystallisation, and the inverse of the ratio is integrated over the residence time of each particle in the dryer to predict the overall increase in crystallinity. It is important to note that the WLF equation (equation 24) makes no distinction between nucleation and crystal growth, meaning that it is implicitly assumed that nucleation of the material is non-rate limiting.

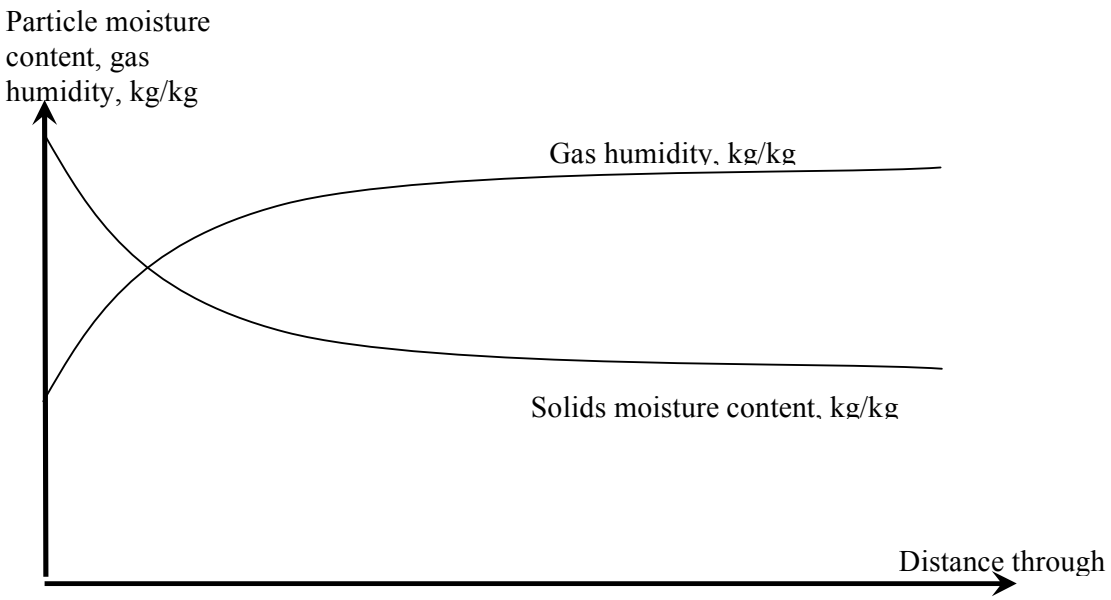

Figure 6 Typical drying prediction form the parallel flow design equations

3.2 Outcomes from using the simulation

Figure 6 shows the typical drying prediction obtained form the parallel flow model. Chiou *et al.* [5][6] have found that this simulation predicted the correct trends in terms of lactose crystallinity when lactose was spray dried in a Buchi B-290 spray dryer. Islam and Langrish [2] and Islam *et al.* [4] have found that the simulation also predicts the correct trends when spray drying lactose, sucrose and ascorbic acid, since the order of their glass-transition temperatures (a key part of the Gordon-Taylor equation) is 101°C for lactose, around 60-65°C for sucrose and -50°C for ascorbic acid. However, the simulation clearly does not allow for recirculation of particles, so its quantitative accuracy is likely to be modest.

4.0 References

1. Williams, M.L.; Landel, R.F.; Ferry, J.D. The temperature dependence of relaxation mechanisms in amorphous polymers and other glass-forming liquids. Journal of the American Chemical Society **1955**, *77(14)*, 3701-3707.
2. Islam, Md.I.; Langrish, T.A.G. Comparing the crystallization of sucrose and lactose in spray dryers. Transactions I.Chem.E., Foods and Bioproducts Engineering **2009**, *87(2)*, 87-95.
3. Migliardo, F.; Branca, C.; Magazu, S.; Migliardo, P.; Coppolino, S.; Villari, A.; Micali, N. Quasielastic and inelastic neutron scattering study of vitamin c aqueous solutions. Physica A: Statistical Mechanics and Its Applications **2002**, *304(1-2)*, 294-298.
4. Islam, Md.I.; Sherrell, R.; Langrish, T.A.G. An investigation of the relationship between glass-transition temperatures and the crystallinity of spray-dried powders. paper accepted for publication in *Drying Technology* (accepted for publication 25 September 2009).
5. Chiou, D.; Langrish, T.A.G. A comparison of crystallisation approaches in spray drying. Journal of Food Engineering **2008**, *88(2)*, 177-185.
6. Chiou, D.; Langrish, T.A.G.; Braham, R. Partial crystallisation behaviour during spray drying: simulations and experiments. Drying Technology **2008**, *26(1)*, 27-38.
7. Langrish, T.A.G. Assessing the rate of solid-phase crystallization for lactose: the effect of the difference between material and glass-transition temperatures. Food Research International **2008**, *41(6)*, 630-636.
8. Trivedi, P.; Axe, L. Ni and Zn sorption to amorphous versus crystalline iron oxides: macroscopic studies. Journal of Colloid and Interface Science **2001**, *244(2)*, 221-229.
9. Blagden, N.; De Matas, M.; Gavan, P.T.; York, P. Crystal engineering of active pharmaceutical ingredients to improve solubility and dissolution rates", Advanced Drug Delivery Reviews **2007**, *59(7)*, 617-630.

10. Pokharkar, V.B.; Mandpe, L.P.; Padamwar, M.N.; Ambike, A.A.; Mahadik, K.R.; Paradkar, A. Development, characterization and stabilization of amorphous form of a low Tg drug. Powder Technology **2006**, *167(1)*, 20-25.
11. Choi, W.S.; Kim, H.I.; Kwak, S.S.; Chung, H.Y.; Chung, H.Y.; Yamamoto, K.; Oguchi, T.; Tozuka, Y.; Yonemochi, E.; Terada, K. Amorphous ultrafine particle preparation for improvement of bioavailability of insoluble drugs: grinding characteristics of fine grinding mills. International Journal of Mineral Processing **2004**, *74(SUPPL)*, 165-172.
12. Hancock, B.C.; Parks, M. What is the true solubility for amorphous pharmaceuticals? Pharmaceutical Research **2000**, *17(4)*, 397-404.
13. Briggner, L.; Buckton, G.; Bystrom, K.; Darcy, P. The use of isothermal microcalorimetry in the study of changes in crystallinity induced during the processing of powders. International Journal of Pharmaceuticals **1994**, *105(2)*, 125-135.
14. Buckton, G.; Darcy, P. The influence of additives on the recrystallisation of amorphous spray dried lactose. International Journal of Pharmaceuticals **1995**, *121(1)*, 81-87.
15. Hancock, B.C.; Zografi, G. Characteristics and significance of the amorphous state in pharmaceutical systems. International Journal of Pharmaceuticals **1997**, *86(1)*, 1-12.
16. Lehto, V.-P.; Tenho, M.; Vaha-Heikkila, K.; Harjunen, P.; Paallysaho, M.; Valisaari, J.; Niemela, P.; Jarvinen, K. The comparison of seven different methods to quantify the amorphous content of spray dried lactose. Powder Technology **2006**, *167(2)*, 85-93.
17. Fitzpatrick, J.J.; Barry, K.; Cerqueira, P.S.M.; Iqbal, T.; O'Neill, J.; Roos, Y.H. Effect of composition and storage conditions on the flowability of dairy powders. International Dairy Journal **2007**, *17(4)*, 383-392.
18. Truong, V.; Bhandari, B.R.; Howes, T. Optimization of co-current spray drying process of sugar-rich foods. Part I - Moisture and glass transition temperature profile during drying. Journal of Food Engineering **2005**, *71(1)*, 55-65.
19. Keey, R.B.; Pham, Q.T. Behaviour of spray dryers with nozzle atomizers. Chemical Engineer (London), July/August, **1976**, *311*, 516-521.
20. Keey, R.B.; Suzuki, M. On the characteristic drying curve. Int. J. Heat Mass Transfer **1974**, *17(12)*, 1455-1464.
21. Langrish, T.A.G.; Zbicinski, I. The Effects of Air Inlet Geometry and Spray Cone Angle on the Wall Deposition Rate in Spray Dryers. Transaction of IChemE **1994**, *72(A)*, 420-430.
22. Langrish, T.A.G.; Kockel, T.K. The implementation of a characteristic drying curve for milk powder using a Computational Fluid Dynamics simulation", Chem. Engng. J. **2001**, *84(1)*, 69-74.
23. Liou, J.K.; Bruin, S. An approximate method for the nonlinear diffusion problem with a power relation between the diffusion coefficient and concentration. 1. Computation of desorption times. 2. Computation of the concentration profile. Int. J. Heat Mass Transfer **1982**, *25(8)*, 1209-1229.
24. Kieviet, F.G.**1997**. Modelling Quality in Spray Drying", Ph.D. Thesis, T.U. Eindhoven, The Netherlands, pp. 121-156.

25. Adhikari, B.; Howes, T.; Bhandari, B.R.; Truong, V. Surface stickiness of drops of carbohydrate and organic acid solutions during convective drying: experiments and modelling. Drying Technology **2003**, *21(5)*, 839-873.
26. Chen, X.D. Heat-mass transfer and structure formation during drying of single food droplets. Drying Technology **2004**, *22(1&2)*, 179-190.
27. Seydel, P.; Sengespeick, A.; Blömer, J.; Bertling, J. Experiment and mathematical modeling of solid formation at spray drying. Chem. Eng. Technol. **2004**, *27(5)*, 505-510.
28. Chen, X.D.; Lin, S.X.Q. Air drying of milk droplets under constant and time-dependent conditions. AIChE Journal **2005***, 51(6)*, 1790–1799.
29. Patel, K.C.; Chen, X.D. Prediction of spray-dried product quality using two simple drying kinetic models. Journal of Food Process Engineering **2005**, *28(6)*, 567-594.
30. Bhandari, B.R.; Datta, N.; Howes, T. Problems associated with spray drying of sugar-rich foods. Drying Technology **1997**, *15(2)*, 671-684.
31. Price, R.; Young, P.M. Visualization of the crystallization of lactose from the amorphous state. Journal of Pharmaceutical Sciences **2003***, 93(1)*, 155-164.
32. Chan, H.-K.; Chew, N.Y.K. Novel alternative methods for the delivery of drugs for the treatment of asthma. Advanced Drug Delivery Reviews **2003***, **55**(7)*, 793-805.
33. King, N. The physical structure of dried milk. Dairy Science Abstracts **1965**, *27(3)*, 91-104.
34. Bushill, J.H.; Wright, W.B.; Fuller, C.H.F.; Bell, A.V. The crystallization of lactose with particular reference to its occurrence in milk powder. Journal of the Science of Food and Agriculture **1965**, *16(10)*, 622-628.
35. Chiou, D.; Langrish, T.A.G. Crystallisation of amorphous components in spray-dried powders. Drying Technology **2007**, *25(9)*, 1423-1431.
36. Roos, Y.H.; Karel, M. Differential Scanning Calorimetry study of phase transitions affecting the quality of dehydrated materials. Biotechnology Progress **1990***, 6(2)*, 159-163.
37. Gordon, M.; Taylor, J.S. Ideal copolymers and the second-order transitions of synthetic rubbers. I Non-crystalline copolymers. Journal of Applied Chemistry **1952***, 2(9)*, 493-500.
38. Jouppila, K.; Roos, Y.H. Water sorption and time-dependent phenomena of milk powders. Journal of Dairy Science **1994***, **77**(7)*, 1798-1808.

Yoon, S.S. Lagrangian-based stochastic dilute spray modelling for drying applications - Volume 1, Ed. Woo, M.W., Mujumdar, A.S. and Daud, W.R.W., **2010**, ISBN - 978-981-08-6270-1, Published in Singapore, pp. 77-112.

Lagrangian-based Stochastic Dilute Spray Modelling for Drying Applications

Chapter 4

Yoon S.S.

School of Mechanical Engineering, Korea University,
Anamdong, 5-Ga, Sungbukgu, Seoul, 136-713, Korea

Contents **Page**

1.0 Introduction

Spray modeling has been a great interest in various fields of engineering, such as internal-combustion (IC) engine, pulverized coal power plant, solid rocket propellant, spray drying and cooling, ink-jet printing, crop spraying, meteorology, spray painting and coating, fire suppression, humidification, medicine inhalation and treatment devices, industrial cleaning, water treatment, and so on [1]. It is one class of the many classes of multiphase modeling that are associated with more general and wider ranges of multi-component (both in scale and phase) flow physics. Multiphase flow, in general, implies the involvement of two or more phases, such as liquid, gas (or bubble), solid, and even electrostatic and magnetic fields.

Bubble rising in a soda glass is a typical example of a (*i*) gas-liquid system. Pulverized coal powders for power plant applications are a typical (*ii*) solid-gas system. An electrostatic spray is a triple-phase system that involves liquid, gas, and electrostatics. A typical (*iii*) liquid-gas flow can be found in fire suppression and in IC fuel injection systems. A pneumatic pipe transport system for ocean mining applications typically involves the (*iv*) solid and liquid phases. A spray drying application initially involves a (*v*) liquid-gas system in the upstream, which later transforms into a solid-gas system due to the drying of the sprayed products, as shown in **Figure 1**. The spray modeling techniques reviewed in this report deal with liquid-gas or/and solid-gas systems in conjunction with (*ii*), (*iii*), and (*v*).

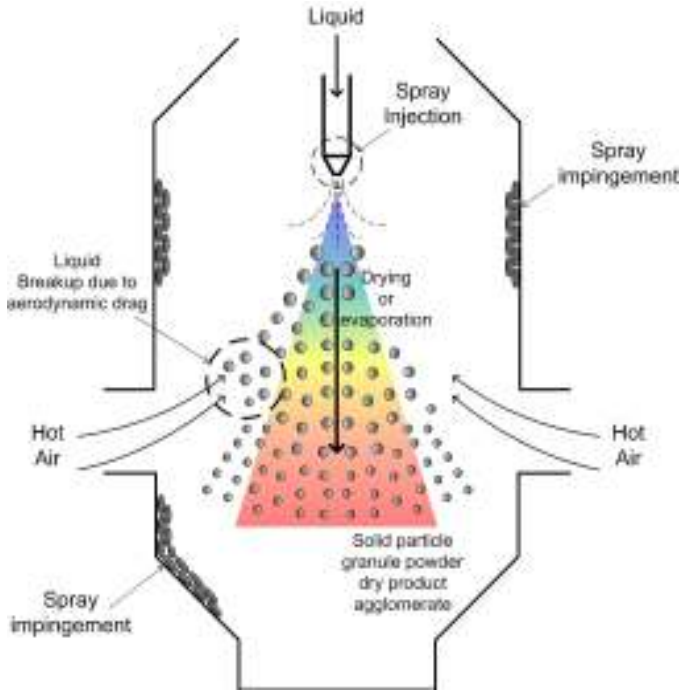

Figure 1 Description of the major physical processes inside a typical counter-current flow spray dryer

Modeling a multiphase flow poses a great computational challenge because the standardized sets of governing equations for coupled or interacting flow systems are still debatable. As for sprays, modeling the "small-scale" atomization phenomenon itself is a highly complex free-surface problem. The "large-scale" particle dynamics simulation (PDS) is possible only after receiving inputs regarding the small-scale atomization. Differences between the "small-scale" and the "larger-scale" atomization processes and their appropriate modeling are categorized in **Figure 2**.

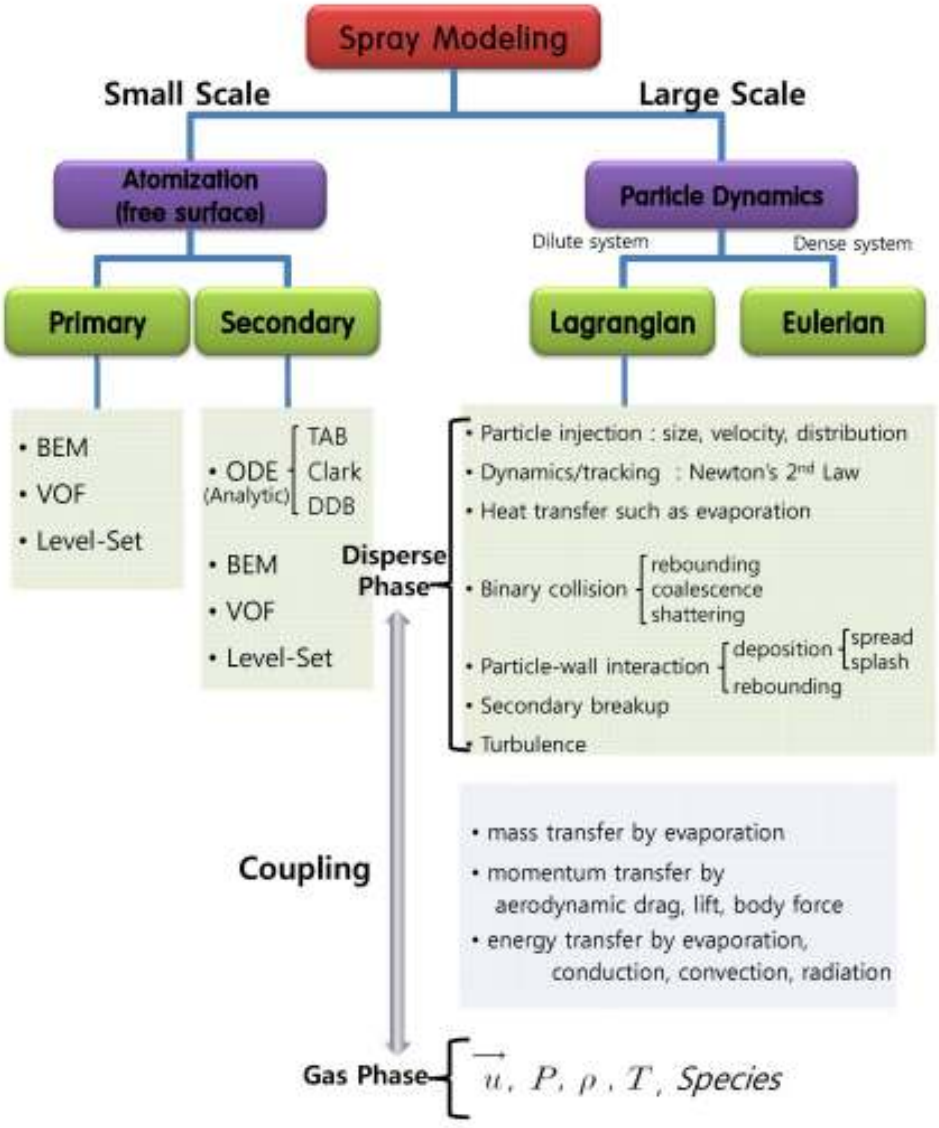

Figure 2 Guideline for spray modelling: sub-models may vary depending on the scale and the nature of the physical processes

As for the small-scale phenomena, capturing the fundamental instabilities that trigger the disintegration of the exiting liquid jet, which forms millions of particles (or drops), is an extremely challenging problem, especially for a high-speed jet, and this phenomenon is known as “primary” atomization. On the other hand, the atomization mechanism of a low-speed jet, as in inkjet printing, has been well understood through numerous instability theories and modelings. [2-11]. Various computational models, such as the boundary element method (BEM) [12-21], volume of fluid (VOF) [22-28], and the level-set method (LSM) [29-30], have given successful modeling of primary atomization, as shown in **Figure 3**.

a

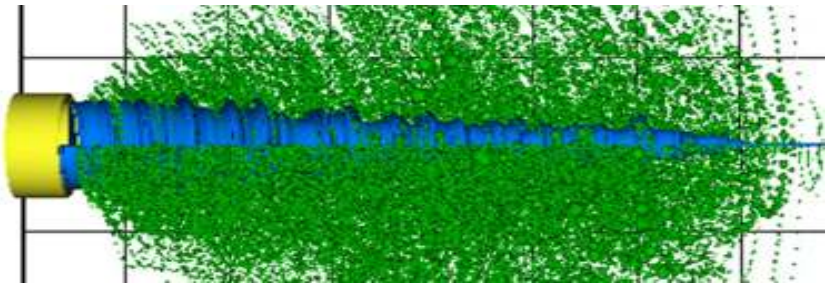

b

Figure 3 Modeling “small-scale” primary atomization using various models; (a) boundary element method [20] and (b) volume of fluid [28]. Images are re-printed under the permission of Wiley, Elsevier, and ILASS, respectively.

Once particles are detached from the exiting liquid, particles travel in gas and deform because of aerodynamic drag, and eventually, they breakup, and this breakup is known as “secondary” atomization. A simple ordinary differential equation (ODE) replicating a forced harmonic oscillator describes the deformation of a particle and its eventual breakup [31]. This ODE breakup model is simple enough to be coupled with PDS. More rigorous computations have been carried out by using BEM, VOF, and LSM for modeling breakup processes [12-30]. However, these models are impractical to couple with PDS due to their inordinate computational loads.

As for the large scale PDS, there are two major approaches, namely, the Eulerian-Eulerian approach and the Lagrangian-Eulerian approach. Basically, the physics of particle flow and that of the continuum gas phase, and their interaction (such as mass, momentum, and energy exchange) should be properly taken into account in modeling two-phase spray flows. Here, the continuum gas phase is always solved on an Eulerian reference frame, while the dispersed or discrete particle flow can be solved either on an Eulerian or Lagrangian frame of reference [32-38].

A spray system is either “dilute” or “dense,” depending on the particle number density at a fixed domain size. For example, a rule of thumb is that the spray system is dilute if the liquid phase volume is 10% or less than that of gas. Generally, the Lagrangian and Eulerian approaches are preferred for dilute and dense systems, respectively, although this preference is a matter of choice and not of principle. For a dilute spray system, drag and lift are the main driving force of the entire spray system. Conversely, for a dense spray system, particle collision is the main driving mechanism. To quantitatively distinguish the two systems, a dilute spray is assumed if $\tau_v<\tau_c$; otherwise, a dense spray is assumed, where τ_v is the momentum response time and τ_c is the average time required for the binary particle collision [39].

The Lagrangian approach is more popular than the Eulerian approach because the Lagrangian approach can be applied to both dilute and dense spray systems, as in **Figure 4** [19] and **Figure 5** [40,41]. On the other hand, the Eulerian approach is preferred for a dense system, such as a fluidized bed system (see **Figure 6),** and the corresponding Eulerian modeling result is seen in **Figure 7** [42]. The spray system is considered dense unless the fluidizing gas velocity is significant enough to yield a pneumatic transport (or conveying) scenario.

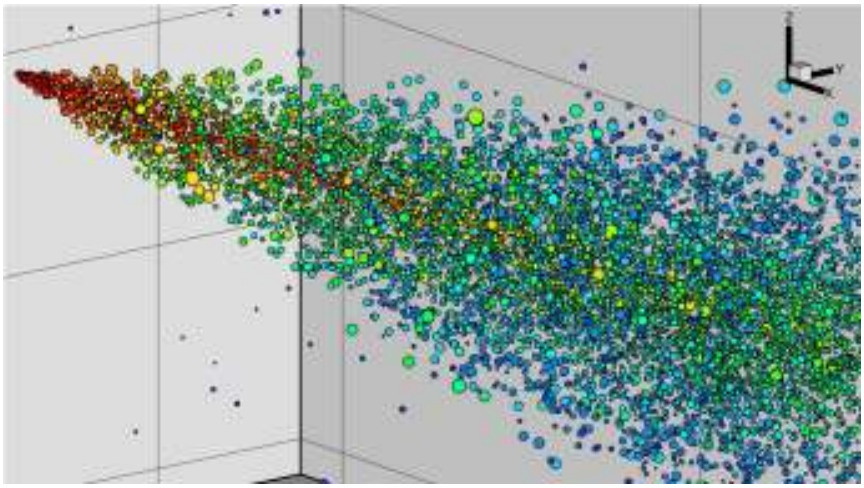

Figure 4 Lagrangian stochastic dilute spray modelling [19]

The Lagrangian approach is not suitable for a dense system because of the excessive computational load of tracking billions of particles. Furthermore, if the volume of a computational cell is mostly occupied by particles due to an excessive particle number resulting from the use of the Lagrangian approach, intractable numerical instability may be induced. To avoid this numerical instability, modelers are often forced to use an undesirably large or coarse grid, which leads to an inaccurate solution by the Lagrangian approach. On the other hand, the Eulerian approach must not be used for modeling a dilute spray because the particles of a dilute spray behave quite independently because of their large inter-particle distances. The use of the Eulerian approach would make sense only with respect to a dense spray in which the particles behave rather continuously as if the sprays are dense enough to be treated as a continuous medium.

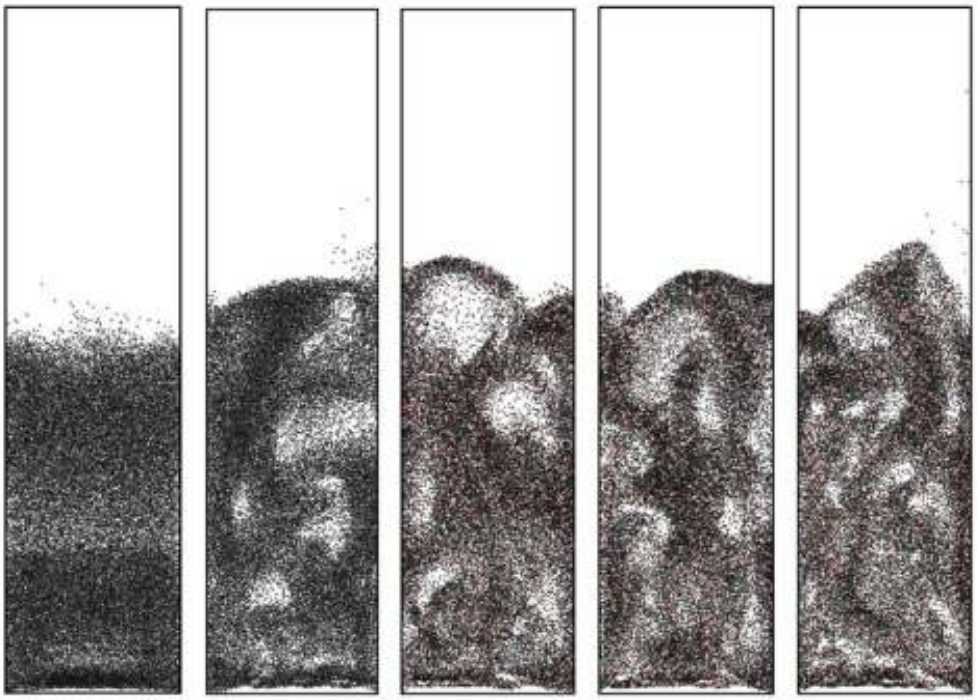

Figure 5 *Lagrangian approach for dense spray inside fluidized bed. The simulation shows the effect of gas pressure Pamb=1, 10, 21, 30, and 40 bar.* [40]

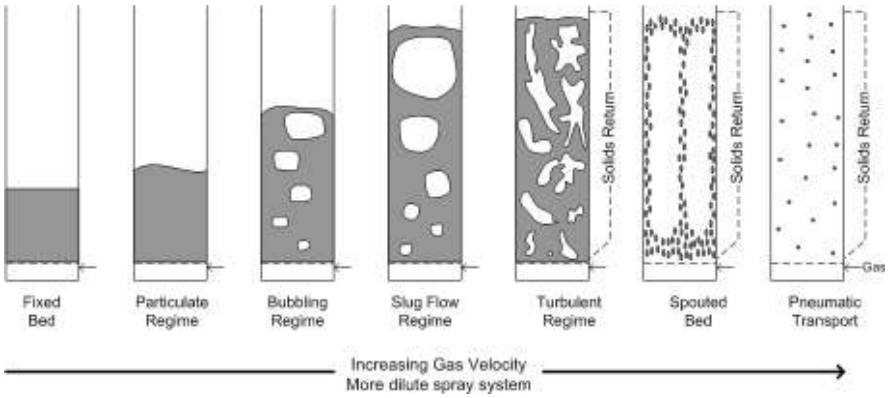

Figure 6 *Fludization regime change depending on the magnitude of the fluidizing gas*

In this report, the Largrangian-based dilute spray modeling in a "stochastic" sense is reviewed. This means that many of the mathematical formulations are based on probability functions. This modeling method was originally pioneered by O'Rourke [43] for use in IC-engine applications and has been widely used in most commercial codes, such as KIVA, CFX, Fluent, Star-CD, etc. General descriptions of particle phase transport equations (i.e., conservation of mass, momentum, and energy) are reviewed. Explanation on the interaction between the particle phase turbulence model and the *k-ε* RANS (Reynolds-Averaged Navier-Stokes) turbulence for the Eulerian phase is also provided. Various PDFs (probability density function) are introduced to model the initial particle size distribution. The actual computational load is

amenable with the stochastic approach that assumes “parcels,” which carry numerous particles. The difference between the parcel PDFs and particle PDFs are explicitly explained in this report. The basic mechanism of the aerodynamic breakup model of O’Rourke and Amsden [31], namely the TAB (i.e., Taylor analogy breakup) model, is provided. Within a locally-dense region, the binary collision between two particles may result in coalescence, bouncing, or separation. The collision physics of coalescence and grazing is modeled by the formulation of Brazier-Smith [44]. A general approach for the particle-wall interaction is also reviewed.

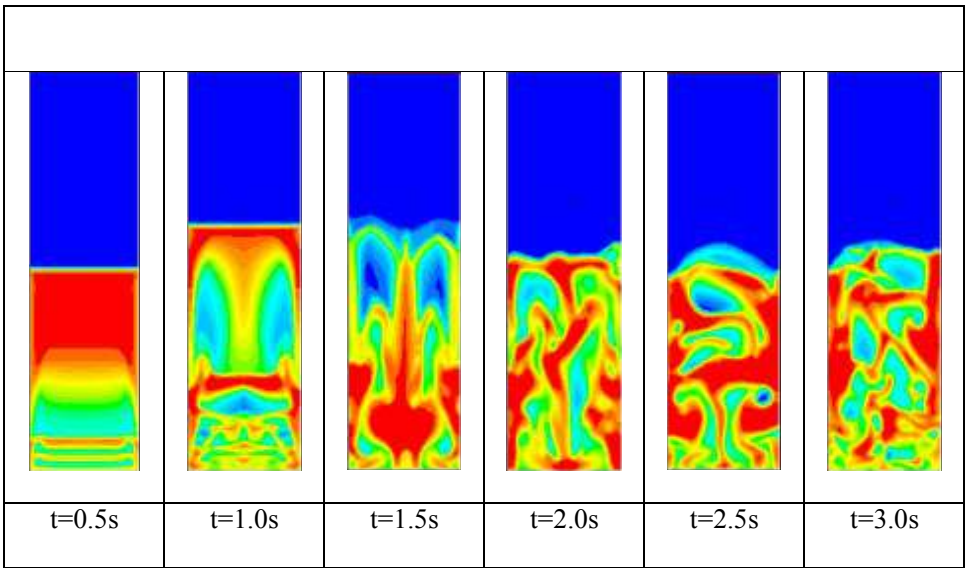

Figure 7 Eulerian approach for dense spray inside fluidized bed [41]

2.0 Modelling description

A two-phase system can be formulated by several approaches using either space averaging [45-52] or probabilistic descriptions [43, 53-54]. The approach taken here is based on spatial or phase-averaging. The specifics of phase-averaging are summarized in DesJardin and Gritzo [55]. In this approach, the governing equations of mass, momentum and energy are averaged in space by introducing additional terms that account for mass, momentum and energy transfer from the particles to the gas phase. These source terms are determined from the liquid phase transport equations, which track the dynamics of particles as they are transported in the carrier gas. The following subsections describe the modeling approaches for the Largrangian particle-phase only while details on its coupling with the Eulerian gas-phase is well described in Crowe [39].

2.1 Particle size distribution

In computational descriptions of a particulate flow, it is usually impossible to track all of the individual particles, and thus, alternative approaches are typically employed. One approach is to track parcels [56]. In the conservation equations describing these parcels to accurately represent the evolution of all particles, the particles in a parcel generally are restricted to a fixed diameter. If the number of particles in each parcel is identical, then the size distribution of the parcel should follow the size distribution of the particles. However, it is computationally more expedient to set the mass of each parcel to be identical for all parcels. Thus, the number of particles per parcel is inversely proportional to the particle mass. Equivalently, the number of particles per parcel is proportional to D^{-3} where D is the diameter of the particle. In this case, the parcel distribution, $f_c(D)$, differs from the particle distribution, $f_p(D)$.

$$f_c(D) = AD^3 f_p(D) \tag{1}$$

where A is a scaling factor used to properly normalize $f_c(D)$. O'Rourke [43] provides the corresponding parcel distribution for a given chi-square (χ^2) distribution while Hewson and Yoon [57] provide the corresponding parcel distributions for the Rosin-Rammler, log-normal, and Gaussian distributions, respectively. These PDFs are summarized in **Table 1,** and the corresponding expressions for the size distributions of particles and parcels are listed in **Table 2**.

Table 1 The PDFs for particle and parcel for the Rosin-Rammler, log-normal, Gaussian, and Nukiyama-Tanasawa distributions.

	Particle PDF, f_p	Parcel PDF, f_c
Rosin-Rammler	$f_{p,rr}(D) = q\frac{D^{q-1}}{X^q}\exp\left[-\left(\frac{D}{X}\right)^q\right]$ where q is the dispersion coefficient. $X = D_{10}/\Gamma(1/q+1)$ where Γ is the complete Gamma function.	$f_{c,rr}(D) = A_{rr}D^3 f_{p,rr}(D)$ $A_{rr} = \frac{1}{X^3\Gamma\left(\frac{3}{q}+1\right)}$
Log-normal	$f_{p,\ln}(D) = \frac{1}{\sqrt{2\pi}\sigma^*_{\ln}D}\exp\left[-\left(\frac{(\ln D - \ln D_{\ln})^2}{2\sigma^{*2}_{\ln}}\right)\right]$ where $D_{\ln} = \exp(\overline{\ln D}) = D_{10}/\exp(0.5\sigma^{*2}_{\ln})$ $\sigma^*_{\ln}$ is the dimensionless standard deviation of the logarithm of the diameter.	$f_{c,\ln}(D) = A_{\ln}D^3 f_{p,\ln}(D)$ $A_{\ln} = 1/\exp\left[3\bar{x} + (9/2)\sigma^{*2}_{\ln}\right] = \frac{1}{D^3_{\ln}\exp(9\sigma^{*2}_{\ln}/2)}$ where $\bar{x} = \ln D_{\ln}$
Gaussian	$f_{p,g}(D) = \frac{1}{\sqrt{2\pi}\sigma}\exp\left[-\frac{(D-\overline{D})^2}{2\sigma^2}\right]$ where σ is the dimensional standard deviation of the diameter. $\overline{D}$ is the mean diameter.	$f_{c,g}(D) = A_g D^3 f_{p,g}(D)$ $A_g\overline{D}^3 = A^*_g = \frac{\sqrt{2\pi}}{\left(2\sigma^{*3}+\sigma^*\right)a' + \sqrt{\pi/2}\left(3\sigma^{*2}+1\right)\left(1+c'\right)}$ $a' = \exp(-0.5/\sigma^{*2})$ $c' = erf\left(\frac{1}{\sqrt{2}\sigma^*}\right)$, note *erf* is the error function. $\sigma^* = \sigma/\overline{D}$ where $(\,)^*$ is the dimensionless quantity.
Nukiyama-Tanasawa	$f_{p,nt}(D) = a_{nt}D^p\exp\left[-bD^c\right]$ where $a_{nt} = \frac{cb^{(p+1)/c}}{\Gamma\left[\frac{p+1}{c}\right]}$ is the normalizing factor. The coefficients, b, c, and p are the dimensional parameters.	$f_{c,nt}(D) = A_{nt}D^3 f_{p,nt}(D)$ $A_{nt} = \frac{cb^{(p+4)/c}}{a_{nt}\Gamma\left[\frac{p+4}{c}\right]}$

An alternative method for predicting the particle size can be suggested by utilizing the linear theories particularly the Kelvin-Helmoltz and Rayleigh-Taylor instability theories. Further details of this alternative method are provided in **Section 2.3**.

Table 2 The size distributions for particle and parcel for the Rosin-Rammler, log-normal, Gaussian, and Nukiyama-Tanasawa distributions.

	Particle size	Parcel size
Rosin-Rammler	$D = X\left(\ln\left[\frac{1}{1-RN}\right]\right)^{1/q}$ RN is the random number ranging from 0 to 1.	$D = X\left(P^{-1}\left[\frac{3}{q}+1, RN\right]\right)^{1/q}$ where P^{-1} is the inverse of the incomplete gamma function (see Ref. [76]).
Log-normal	$D = D_{\ln}\exp\left[\sqrt{2}\sigma^*_{\ln} erf^{-1}(2RN-1)\right]$	$D = D_{\ln}\exp\left[\sqrt{2}\sigma^*_{\ln} erf^{-1}(2RN-1)+3\sigma^{*2}_{\ln}\right]$
Gaussian	$D = \overline{D}+\sqrt{2}\sigma erf(2RN-1)$	$RN = \frac{A^*_g}{\sqrt{2\pi}}\left\langle \sigma^*\left\{a'\left(1+2\sigma^2\right)-b'\left[\left(D^*-1\right)^2+2\sigma^{*2}\right]\right\}+ \frac{3\sigma^*}{2}\left\{\left(2-2D^*\right)b'-2a'+\sqrt{2\pi}\sigma^*\left(c'+d'\right)\right\}+ 3\sigma^*\left\{a'-b'\right\}+\sqrt{\frac{\pi}{2}}\left\{c'+d'\right\}\right\rangle$ $b' = \exp\left(-\frac{(D^*-1)^2}{2\sigma^{*2}}\right)$ $d' = erf\left(\frac{D^*-1}{\sqrt{2}\sigma^*}\right)$ note: This expression is implicit that it needs to be solved iteratively. Explicit expression for the parcel size of the Gaussian distribution cannot be obtained.
Nukiyama-Tanasawa	$D = \left\{\frac{1}{b}P^{-1}\left[\frac{p+1}{c}, 1-RN\right]\right\}^{1/c}$	$D = \left\{\frac{1}{b}P^{-1}\left[\frac{p+4}{c}, 1-RN\right]\right\}^{1/c}$

2.2 Spray transport equation

A stochastic separated flow (SSF) model [39] is used to represent the liquid phase of the flow. The SSF model is implemented using Lagrangian particles, which represent individual groups of particles referred to as parcels [56]. The dynamics of these particles are governed by a set of ordinary differential equation (ODE's) accounting for the conservation of mass, momentum and energy. The derivations of these ODE's can be found in several excellent literatures on particle transport [56,58] and so are not repeated in this report. Also, the transport equations introduced in this chapter are most suitable for a pure liquid drop, although they can indeed be applied to a solid particle or a liquid drop carrying solid particles inside. For the spray drying application, readers should be aware that a dissolved substance or agglomerates inside a liquid drop may impede the evaporation process for which the current transport equations lose some degree of accuracy.

A "thin-film" assumption [58] is used to approximate the two-phase liquid-gas interface at the surface of each particle. The following subsections summarize the transport equations for evaporating particles. In these equations, the subscripts "*p*", "*g*", and "*f*" denote the properties of the particle (or drop), gas and film, respectively, as shown in **Figure 8.**

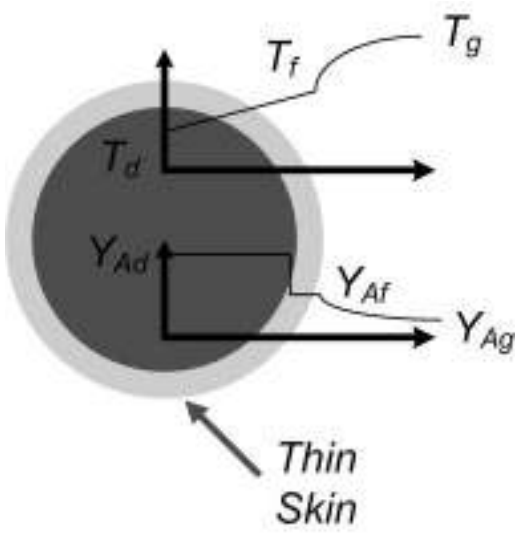

Figure 8 Property variations in particle using a thin skin model

Conservation of mass and species

The loss of mass from evaporation of the liquid particle is described using the following transport equation:

$$\frac{dm_p}{dt} = \dot{m}_p = -\pi D_p \frac{\mu_f}{Sc_f} B_m Sh_f \tag{2}$$

where $\dot{m}_p$ is the mass of the particle and ρ_f and μ_f are the density and dynamic viscosity of the film in thermodynamic state. The film is defined as the liquid-gas interface on the particle surface, as shown in **Figure 8**. The parameter, $B_m = (Y_f - Y_g)/(Y_p - Y_f)$, is the Spaulding or mass transfer number and characterizes the concentration gradients at the film interface. The Sherwood number, $Sc_f = h_m D_p / D_{mf}$, accounts for evaporation due to convection and is expressed in terms of the particle Reynolds number, and film Schmidt number, $Sc_f = v_f / D_{mf}$ using the Ranz-Marshall correction [59]: $Sc_f = 2\left[1 + \mathrm{Re}_p^{1/2}\, Sc_f^{1/3} / 3\right] \log\left(1 + B_m\right) / B_m$. The properties at the film still need to be specified and will be discussed in the evaluation of the film's thermophysical state in **Section 2.2**.

Conservation of momentum

The momentum equations for a small rigid sphere in non-uniform flow were derived by Maxey and Riley [60]. The momentum source terms for these equations include aerodynamic drag, static pressure gradient, virtual-mass, Basset, Saffman lift and body forces [61]. The full unsteady momentum equation for non-rotating, non-interactive, non-deforming, spherical liquid or solid particles [60], is

$$m_p \frac{du_{p_i}}{dt} = F_{D_i} + F_{P_i} + F_{A_i} + F_{H_i} + F_{L_i} + F_{B_i}, \tag{3}$$

where m_p is the particle mass, u_{p_i} is the particle velocity, and t is time. The forces on the right-hand side of this equation are defined as

$$\begin{aligned}
F_{D_i} &= \frac{\pi}{8}\rho_g D_p^2 C_D \left|u_{g_i} - u_{p_i}\right|\left(u_{g_i} - u_{p_i}\right) \quad \text{(Aerodynamic Drag)} \\
F_{P_i} &= \frac{\pi}{6}\rho_g D_p^3 \frac{Du_{g_i}}{Dt} \quad \text{(Pressure Gradient)} \\
F_{A_i} &= \frac{\pi}{6} C_A \rho_g D_p^3 \left(\frac{Du_{g_i}}{Dt} - \frac{du_{p_i}}{dt}\right) \quad \text{(Added Mass)} \\
F_{H_i} &= \frac{\pi}{4} C_H D_p^2 \sqrt{\frac{\rho_g \mu_g}{\pi}} \int_0^t \frac{\frac{d}{d\tau}\left(u_{g_i} - u_{p_i}\right)}{\sqrt{t-\tau}} d\tau \quad \text{(History)} \\
F_{L_i} &= 2.72 D_p^2 \sqrt{\rho_g \mu_g}\, \frac{S_{ij}}{\left(S_{lk} S_{kl}\right)^{1/4}}\left(u_{g_j} - u_{p_j}\right) \quad \text{(Saffman Lift)} \\
F_{B_i} &= \frac{\pi}{6} D_p^3 \left(\rho_p - \rho_g\right) g_j \delta_{ij} \quad \text{(Body Force),}
\end{aligned} \tag{4}$$

where ρ_g, μ_g, and u_{g_i} are the gas density, viscosity, and velocity, and ρ_p, D_p, and u_{p_i} are the particle density, diameter, and velocity, respectively. Gravitational acceleration is represented by g_j and the local carrier gas strain rate tensor is defined as $S_{ij} = \frac{1}{2}\left(\partial u_i / \partial x_j + \partial u_j / \partial x_i\right)$. Additionally, the two substantial derivatives of the gas velocity in these expressions are defined as

$$\begin{aligned}
\frac{Du_{g_i}}{Dt} &= \frac{\partial u_{g_i}}{\partial t} + u_{g_j} \frac{\partial u_{g_i}}{\partial x_j} \\
\frac{du_{g_i}}{dt} &= \frac{\partial u_{g_i}}{\partial t} + u_{p_j} \frac{\partial u_{g_i}}{\partial x_j}.
\end{aligned} \tag{5}$$

The original equation developed in Ref. [60] is only formally correct in the limit of zero particle Reynolds number, $\mathrm{Re}_p = \rho_g \left|u_{g_i} - u_{p_i}\right| D_p / \mu_g$. The additional coefficients C_D, C_A, and C_H in Eqs. (6) are added to adjust the respective terms for finite Reynolds numbers [62]. The coefficient of drag, C_D, is modeled using the standard drag coefficient relations for a sphere in uniform flow [58-60],

$$C_D = \begin{cases} \dfrac{24}{\mathrm{Re}_p}\left(1 + \dfrac{\mathrm{Re}_p^{2/3}}{6}\right) & \text{for } \mathrm{Re_p} < 1000 \\ 0.424 & \text{for } \mathrm{Re_p} \geq 1000 \end{cases} \tag{6}$$

More sophisticated treatments could be pursued to account for non-spherical particles [63-66].

When using the SSF model, the particle locations change according to a force balance, the Newton's second law, with the resultant leading to particle acceleration [60]. The full particle momentum equation contains a number of terms that can be categorized as either steady force or unsteady force. The unsteady forces approaches zero for a particle in a stationary flow field, but still often remain small with respect to the steady forces in commonly-encountered unsteady flows. For this reason, the unsteady terms are often safely neglected in particle simulations since they can be complex and computationally expensive to calculate. Therefore, as discussed by Faeth [58], if the ratio of particle to gas densities is large ($\rho_p / \rho_g \gg 200$), then the predominate forces consist of only the drag, F_{D_j}, and body forces, F_{B_j}, and this condition leads to a considerable simplification of the momentum equations to the form below:

$$m_p \frac{du_{p_j}}{dt} = F_{D_j} + F_{b_j} = \frac{\pi}{8} \rho_g D_p^2 C_D \left| u_{g_j} - u_{p_j} \right| \left(u_{g_j} - u_{p_j} \right) + g_j m_p \tag{7}$$

where u_{p_i} and u_{g_j} are the particle and gas phase velocities, D_p, is the particle diameter, and ρ_g is the gas phase density. The last term on the right hand side is the body force term due to gravity.

Conservation of energy

The particle energy, in terms of particle temperature, T_p, is related to the heat transfer due to convection ($\dot{Q}_c$) and evaporation ($\dot{Q}_e$) processes and has the form:

$$m_p C_{v_p} \frac{dT_p}{dt} = \dot{Q}_c + \dot{Q}_e = \pi D_p \frac{\mu_f C_{p_f}}{\mathrm{Pr}_f} \left(T_g - T_p \right) Nu_f + \dot{m}_p h_{\mathrm{lg}} \tag{8}$$

where C_{v_p} is the liquid particle specific heat, h_{lg}, is the heat of vaporization and $\mathrm{Pr}_f = C_{p_f} \mu_f / k_f$ is the film's Prandtl number. The thermal transfer number, $B_t = C_{p_f} (T_g - T_f) / h_{\mathrm{lg}}$, characterizes the temperature gradient at the film surface and can be expressed in terms of the Spaulding number under steady-state heat and mass transfer conditions as: $B_t = (1 + B_m)^{Le_f} - 1$, where $Le_f = Sc_f / \mathrm{Pr}_f = k_f / (\rho_f C_{p_f} D_{m_f})$ is the film's Lewis number [67]. The film's Nusselt number, ($Nu_f = h_p D_p / k_f$), characterizes the heat transfer due convection and is modeled similar to the Sherwood number as: $Nu_f = 2\left(1 + \mathrm{Re}_p^{1/2} Sc_f^{1/3} / 3\right) \log\left(1 + B_m\right) / B_m$.

2.3 Evaluation of film properties

In order to account for the mass and momentum of a particle and the heat exchange between the gas and the evaporating single particle (or drop) as in Eqs. (2)-(8), the film properties of ***species A*** in conjunction with **Figure 8** should be estimated. Drop evaporation always occurs in spray drying applications when the relative humidity is less than unity; evaporation takes place if the saturation pressure of a liquid drop is greater than the vapor pressure of the environment. To increase the evaporation rate, one may heat up the sprayed drops so that their saturation temperature increases, which in turn also increases the saturation pressure and decreases the relative humidity.

During the evaporation process of a single liquid particle, liquid mass is evaporated from the surface and diffuses as a vapor or film, properties of which can be found by utilizing the Spalding's thin-skin (or film) model [67]. The mass flux balance of the model assumes that the *total gaseous* Mass Flux of Fuel Species (MFFS) leaving the particle surface is equal to the sum of MFFS due to the *bulk velocity* of the mixture at the surface and MFFS due to *mass diffusion*. In addition, the basic assumptions of this thin-skin model are as follows: (*i*) the particle regression process is relatively slow; (*ii*) uniform temperature distribution exists around and within the particle surface; (*iii*) both particle and vapor are spherical in shape; (*iv*) the internal circulation, such as the Hill's vortex, within the particle is neglected; and (*v*) a complete saturation condition exists at the film. From **Figure 8**, the temperature and species distributions in and around the particle are broken into three regions. These regions consist of the temperature and species conditions at the particle center (Y_{A_p}, T_p), at the film interface or particle surface (Y_{A_f}, Y_{B_f}, T_f), and in the surrounding gas (Y_{A_g}, Y_{B_g}, T_g). Using this thin-skin model, along with the assumption of the Clausius-Clapeyron relation to describe the change in saturation conditions, an iterative procedure can be devised to determine the film's thermophysical properties as follows:

1. Guess an initial value for Y_{A_f}
2. Determine mass (Spaulding) and thermal transfer numbers: $B_m = (Y_{A_f} - Y_{A_g})/(Y_{A_d} - Y_{A_f})$ and $B_t = (1 + B_m)^{Le_f} - 1$.
3. Calculate film temperature assuming saturation conditions: $T_f = T_g - B_t h_{\lg_A} / C_{p_{A_f}}$.
4. Calculate the heat of vaporization using the relation from Watson [68-69]: $h_{\lg_A} = h_{\lg_{A_{ref}}} = [(T_{C_A} - T_f)/(T_{C_A} - T_{ref})]^{0.38}$ where T_{C_A} is the critical temperature for species ***A*** and $h_{\lg_{A_{ref}}}$ is a user specified reference heat of vaporization for ***species A*** at a given reference temperature, T_{ref}, and partial pressure $P_{A_{ref}}$.
5. Calculate saturation partial pressure using the Clausius-Clapeyron relation:

$\ln(P_{A_f} / P_{A_{ref}}) = -h_{\lg_A}\left(\left(\frac{1}{T_f} - \frac{1}{T_{ref}}\right) / R_A\right)$ where R_A is the gas constant for species A.

Note: If $P_{A_f} > P$, then P_{A_f} is set equal to *P* and iterate using Clausius-Clapeyron and Watson relations to find T_f, i.e., the fluid is boiling at the particle surface.

6. Recalculate species mass fraction using partial pressures:

$$Y_{A_f} = \frac{P_{A_f}}{P}\frac{MW_A}{MW_{mix_f}} \text{ where } MW_{mix_f} = \left[\frac{Y_{A_f}}{MW_A} + \frac{1 - Y_{A_f}}{MW_B}\right]^{-1}$$

7. Compare the calculated Y_{A_f} from step 6 with the guessed value from step 1. And repeat steps 1-6 using the Newton-Raphson-Secant iteration until convergence.
8. Once convergence is achieved, then calculate the mixture film surface density:

$$\rho_{mix_f} = \left(\frac{P_{A_f}}{R_A} + \frac{P - P_A}{R_B}\right) / T_f .$$

2.4 Turbulence model

For a particle-laden flow, the intrinsic characteristics of a two-phase flow (such as particle inertia, dissipation due to particle drag, effective viscosity, velocity fluctuation due to wake dynamics and self-induced vortex shedding, instabilities arising from shear and density gradients) cause turbulence. As to which characteristic is dominant is contingent on the relative strengths and scales (both in length and time) of the individual mechanisms. Whatever the reason, once turbulence exists, its effect on the dispersion of a parcel containing numerous particles should be properly taken into account. However, the time-averaged solution from RANS formulations for the gas phase lacks information regarding phenomenological details of turbulence because the solution is time-averaged and not instantaneously recorded. These unresolved turbulent motions are especially significant for the release of a high pressure spray that generates high levels of turbulent kinetic energy. Thus, turbulence models should be introduced in the course of particle trajectories to account for the unresolved turbulent eddies or local fluctuations in the velocity field and thus to mimics the particle dispersion while the rest of the thermo-physical variables are set equal to their corresponding time-averaged information.

There are a few well-known approaches which model the particle dispersion phenomenon arising from turbulence. The eddy lifetime (τ_e) approach has been widely used in many Lagrangian-based particle turbulence dispersion models [70-73] because of its simplicity. This eddy lifetime approach assumes that particles are responsive only to the low frequency fluctuation of the turbulent eddies. Another approach by Blumcke [74] introduces velocity fluctuations with the aid of the explicitly specified auto-correlation functions, *R(τ)* and *R(Δx)*, which are also the functions of integral

scales such as eddy lifetime and characteristic length-scale [75]. This auto-correlation approach requires the use of a digital filter that estimates the fluctuation quantities via a random generator. The approach by Berlemont et al. [32] differs from the eddy lifetime approach in that the suggested model explicitly introduces *any* shape (whether it is *linear* or *exponential*) of the Lagrangian time correlation function by using their correlation matrix technique. Here, in this report, the "eddy lifetime" is reviewed because of its simplicity and popularity.

The parcel turbulence model accounts for the effects of turbulent eddies perturbing the parcel trajectory and is based on the random walk model of Gosman and Ioannides [70], as modified by Shuen et al. [71]. The model assumes a Gaussian probability density function (PDF) for isotropic gas phase fluctuations that are parameterized by a zero mean and a variance that is proportional to the kinetic energy,

$$PDF_{u'_{g_j}} = \frac{1}{\sqrt{2\pi\sigma^2}} \exp\left(-\frac{u'_{g_j}}{2\sigma^2}\right) \tag{9}$$

which can be integrated and randomly sampled for each velocity component using the expression,

$$u'_{g_j} = \sqrt{2}\sigma erf^{-1}(2RN-1) \tag{10}$$

where the RMS is set equal to $\sigma = \sqrt{2k/3}$ and RN is a random number between 0 and 1. The sampled fluctuating velocities are used to determine one of two outcome events. First, the particle is light enough to be captured by the turbulent eddy and transported as a fluid particle over a time period equal to the eddy lifetime. Second, the particle has sufficient momentum to follow a ballistic trajectory and cross the eddy. The total time the particle interacts with the turbulent eddy (whose lifetime is τ_{eddy}) and the particle cross trajectory time (τ_{drift}) are the minimum of τ_{drift} and τ_{eddy}, as indicated below [71]:

$$\begin{aligned}
\tau &= \min\left(\tau_{drift}\ ,\ \tau_{eddy}\right) \\
\tau_{eddy} &= \sqrt{\frac{3}{2}}\ C_\mu^{3/4}\frac{k}{\varepsilon} \quad \text{or} \quad C_T\frac{k}{\varepsilon} \\
\tau_{drift} &= -\tau_p \ln\left(1-\frac{L_e}{\tau_p\left|\overrightarrow{u_p''}-\overrightarrow{u_g''}\right|}\right)
\end{aligned} \tag{11}$$

where L_e is the characteristic turbulent eddy length-scale, τ_p is the particle response time obtained by linearizing the Eq. (3), $\overrightarrow{u_g''} = \vec{u}_g + \overrightarrow{u_g'}$ is the instantaneous gas velocity, and the $\left|\overrightarrow{u_p''}-\overrightarrow{u_g''}\right|$ is the velocity at the start of the interaction. They are defined as below:

$$L_e = C_\mu^{3/4}\frac{k^{3/2}}{\varepsilon} \quad \text{or} \quad \sqrt{\frac{2}{3}}\,C_T\frac{k^{3/2}}{\varepsilon} \tag{12}$$

$$\tau_p = \frac{4}{3}\frac{\rho_g D_p}{\rho_p C_D\left|\overrightarrow{u_p''} - \overrightarrow{u_g''}\right|}$$

This turbulence time scale (τ) is used to determine the time step required to resolve the turbulence effect within the particle sub-cycling time marching steps. When $L_e > \tau_p\left|\overrightarrow{u_p''} - \overrightarrow{u_g''}\right|$, the characteristic eddy length is greater than the particle travel distance (i.e., the Stokes number is less than unity), implying that the eddy has captured the particle and the particle residence time in the eddy is equal to the eddy's lifetime and, thus, the particle time step can be set equal to the eddy lifetime; $\Delta t_p = \tau_{eddy}$. If $L_e < \tau_p\left|\overrightarrow{u_p''} - \overrightarrow{u_g''}\right|$, then a particle crosses the turbulent eddy and therefore Eq. (11) should be applied; $\Delta t_p = \tau = \min\left(\tau_{drift}\ ,\ \tau_{eddy}\right)$.

2.5 Primary atomization

Disintegration of a liquid jet emanating from a nozzle exit is attributed to several instability sources such as turbulence [76], cavitation [77], boundary layer instability [18,78,79], shear-driven KH-type instability [80], and buoyancy RT-type instability [81]. Among these, the KH-type instability is the most common one employed in spray modeling simply because it is believed that the shear instability between the emanating jet and the surrounding gas is the dominant destabilization source for primary atomization. The instability arises because of the relative velocity between a liquid jet and surrounding air. In the case of the RT instability, the wave growth rate is zero if the density of two fluids is identical; i.e., $\rho_l = \rho_g$, in which case the jet is unconditionally stable and there is no wave formation.

The drop size prediction by the KH theory is modified by an empirical constant that yields the initial drop size (D_p) and breakup time (τ_{KH}) as below [80]:

$$D_p = 9\lambda_{KH}$$

$$\tau_{KH} = \frac{3.726\ (40)a}{\omega_{r,KH}\lambda_{KH}} \tag{13}$$

where $\omega_{r,KH}$ is the growth rate of the most unstable wave whose length is λ_{KH}. The nozzle or jet radius is $d_{nozz}/2=a$.

$$\omega_{r,KH}\left(\frac{\rho_l a^3}{\sigma_l^{0.5}}\right) = \frac{0.34 + 0.38We_g^{1.5}}{(1+Z)(1+1.4T^{0.6})} \tag{14}$$

$$\frac{\lambda_{KH}}{a} = 9.02\frac{(1+0.45Z^{0.5})(1+0.4T^{0.7})}{(1+0.87We_g^{1.67})^{0.6}}$$

where $Z = We_l^{0.5} / \mathrm{Re}_l$, $T = ZWe_g^{0.5}$, $We_l = \rho_l u_{rel}^2 a / \sigma_l$ $We_g = We_l \varepsilon$, $\varepsilon = \rho_g / \rho_l$, $\mathrm{Re}_l = u_{rel} a / \nu_l$. One may consider using the RT theory if the jet system is dominated by buoyancy, for which acceleration of the light fluid toward the heavy fluid plays a key role in causing atomization [81]:

$$D_p = \lambda_{RT} = \frac{2\pi}{k_{RT}}(1.5) \tag{15}$$

$$\tau_{KH} = \frac{8}{\omega_{r,RT}}$$

Where

$$k_{RT} = \sqrt{\frac{a_c\left(\rho_l - \rho_g\right)}{3\sigma_l}} \tag{16}$$

$$\omega_{r,RT} = \sqrt{\frac{2}{3\sqrt{3\sigma_l}} \frac{\left[a_c\left(\rho_l - \rho_g\right)\right]^{1.5}}{\left(\rho_l - \rho_g\right)}}$$

where a_c is the acceleration of the interface from a light fluid (i.e., gas) to a heavy fluid (i.e., liquid).

2.6 Secondary atomization

As a drop moves through a gas, the pressure gradient causes its spherical shape to change and distort. As the distortion continues, the drop becomes an ellipsoid, or disk-shaped, until an upper limit is reached and breakup begins. This distortion plays a significant role in altering the drop's drag and drag coefficient as well as being the precursor to breakup. Neglecting deformation can lead to erroneously low drag and thus, incorrect drop trajectories.

Many models for this drop-breakup process are in use today, such as the Taylor analogy breakup (TAB) and drop deformation and breakup (DDB), and Clark models. Their breakup models are based on an analogy to a spring-mass system. The surface tension and gas aerodynamic forces are analogous to the resorting force of the spring and the external force on the mass, respectively. The liquid viscosity acts as the damping force. Other existing models of particle breakup include the wave breakup model of Reitz et al. [80,82], the Taylor Analogy Model (TAB) of O'Rourke and Amsden [31] and the extensions [83] and the stochastic spectral relaxation model of Gorokhavski et al. [84-85]. Here the breakup models of TAB, DDB, and Clark are reviewed. The second order ordinary governing equation for the TAB model can be written as:

$$m_p \frac{d^2 y}{dt^2} = m_p \frac{C_F}{C_b} \frac{\rho_g}{\rho_l} \frac{\left| u_{p_j} - u_{g_j} \right|}{r_{eq}^2} - m_p \frac{C_k \sigma}{\rho_l r_{eq}^3} y - m_p \frac{C_d \mu_l}{\rho_l r_{eq}^2} \frac{dy}{dt} \tag{17}$$

where ρ_l, μ_l and σ are the liquid particle density, viscosity and surface tension, respectively. The model constants, which are calibrated by combining theoretical considerations on particle oscillation frequencies with experimental data, have the values of C_F=1/3, C_b=1/2, C_k=8 and C_d=5 [86]. The left-hand-side of Eq. (17) represents the inertial term. The first, second, and third terms in the right-hand-side represent the driving force, spring, and damper terms, respectively. Equation (17) can also be re-written into the following form:

$$K \frac{d^2 y}{dt^2} + \frac{5N}{\mathrm{Re}_{eq}} \frac{dy}{dt} + \frac{8}{We_{eq}} y = \frac{2}{3} \tag{18}$$

where *K* and *N* are the are the liquid-to-gas ratio of density and dynamic viscosity ratio; i.e., $K = \rho_l / \rho_g$, and $N = \mu_l / \mu_g$, respectively. The Reynolds and Weber numbers are defined as: $\mathrm{Re}_{eq} = u_{rel} r_{eq} / \nu_g$ and $We_{eq} = \rho_g u_{rel}^2 r_{eq} / \sigma$, where r_{eq} and σ are the spherical drop's initial (or *equilibrium*) radius and surface tension. The dimensionless displacement, *y*, is defined as: $y = \Delta r_p / r_{eq}$ or $(r_p - r_{eq}) / r_{eq}$, as measured from the *equilibrium* edge to the edge of the elongated displacement (resulted from drag) in the major axis, as shown in **Figure 9**. The TAB model assumes that the breakup occurs if and only if the amplitudes of oscillation of the north and south poles equal the drop radius, yielding C_b=1/2 in Eq. (17).

Clark [87] re-defined the dimensionless displacement, *y*, with respect to the displacement of the *center of mass* of the half drop, r_{cm}, instead of the *equilibrium* radius, r_{eq}. Clark's linearized model for the drop oscillation phenomenon is:

$$(K+1) \frac{d^2 y}{dt^2} + \frac{9\pi^2 (N+1)}{4 \mathrm{Re}_{eq}} \frac{dy}{dt} + \frac{9\pi^2}{4 We_{eq}} \left(y - \frac{4}{3\pi} \right) = \frac{2}{\pi} \tag{19}$$

Ibrahim [83] also suggested a nonlinear breakup model, known as DDB, which was derived under the assumption that the drop kinetic energy and viscous dissipation are negligible as the drop approaches to the breakup mode. The nonlinear ordinary differential equation for the DDB model is:

$$K \frac{d^2 y}{dt^2} + \frac{4N}{\mathrm{Re}_{eq}} \frac{1}{y^2} \frac{dy}{dt} + \frac{27\pi^2}{16 We_{eq}} y \left\{ 1 - 2 \left(\frac{3\pi}{4} y \right)^{-6} \right\} = \frac{3}{8} \tag{20}$$

which needs to be solved numerically because of its nonlinear form. The fourth order Runge-Kutta method can be applied to solve this nonlinear differential equation of the DDB model. The analytic solution of both TAB and Clark's models can be obtained because they are linear differential equations. Here, to further investigate the details of the TAB model (for the reason of its popularity), the analytical solution to Eq. (17) is that of a simple harmonic

oscillator where y and $\dot{y}$ at time t are advanced to $t+\Delta t$ using the following relations [86].

$$y\left(t+\Delta t\right)=\frac{We_{eq}}{C}+\left\{\left(y(t)-\frac{We_{eq}}{C}\right)\cos(\omega t)+\frac{1}{\omega}\left(\dot{y}(t)+\frac{y(t)-We_{eq}/C}{\tau_b}\right)\sin(\omega\Delta t)\right\}\exp\left(-\frac{\Delta t}{\tau_b}\right) \tag{21}$$

$$\dot{y}\left(t+\Delta t\right)=\frac{We_{eq}/C-y(t)}{\tau_b}+\left\{\frac{1}{\omega}\left(\dot{y}(t)+\frac{y(t)-We_{eq}/C}{\tau_b}\right)\cos(\omega\Delta t)-\left(y(t)-\frac{We_{eq}}{C}\right)\sin(\omega\Delta t)\right\}\omega\exp\left(-\frac{\Delta t}{\tau_b}\right) \tag{22}$$

In Eqs. (21) and (22), $C=C_kC_b/C_F=12$ is a grouping of the TAB modeling constants, $\tau_b=2\rho_l r_{eq}^2/(C_d\mu_l)$ is the particle oscillation relaxation time, and $\omega=\sqrt{C_k\sigma/(\rho_l r^3)-(1/\tau_b)^2}$ is the particle oscillation frequency. It should be noted that, in the O'Rourke and Amsden's original paper, there is a typographical error; $y(t)$ and $\dot{y}(t)$ in the $\cos(\omega\Delta t)$ term from Eq. (22) are incorrectly switched in their original paper, but are corrected in this report.

The implementation details of Eqs. (21) and (22) are provided in Ref. [86] and expanded on here for additional clarify. The numerical procedure consists of first calculating the value of ω. For very small particles, $\omega^2<0$ and distortions in the particle are negligible. For this case, $y(t+\Delta t)$ and $\dot{y}(t+\Delta t)$ are simply set equal to zero. When $\omega^2>0$, the oscillation amplitude of the un-damped oscillation is first determined using the relation: $A=\sqrt{\left(y(t)-We_{eq}/C\right)^2+\left(\dot{y}(t)/\omega\right)^2}$ (i.e., assume $\tau_b\to\infty$ and add the squares of the factors in front of the sine and cosine terms of Eq. (21)). If $A+We_{eq}/C<1$, then the amplitude of the disturbance cannot cause particle breakup over a time period, $t+\Delta t$; that is, set $y(t+\Delta t)$=1 in Eq. (21), allow $\tau_b\to\infty$, and then combine the sine and cosine terms into a single cosine term with phase, Φ, as: $y(t+\Delta t)=We_{eq}/C+A\cos\left(\omega\Delta t+\Phi\right)$. In this case, Eqs. (21) and (22) are used to update the values of y and $\dot{y}$ for the current time step. If $A+We/C>1$, then breakup is possible and the breakup time, t_{bu}, is determined by solving for the smallest root of the equation: $We_{eq}/C+A\cos\left(\omega\Delta t+\Phi\right)=1$, where Φ is determined from the relations: $\cos(\Phi)=\left(y(t)-We_{eq}/C\right)/A$ and $\sin(\Phi)=-\dot{y}(t)/(A\omega)$ [86]. If $\Delta t<t_{bu}$, then no breakup occurs and y and $\dot{y}$ are updated. If $t_{bu}<\Delta t$, then breakup occurs, as illustrated in **Figure 9**, with the size and number of the newly formed particles determined from mass and energy conservation principles [31].

$$r_p(t+\Delta t) = r_p(t)\left(1+\frac{8K}{20}+\frac{\rho_l r(t)^3}{\sigma}\frac{6K-5}{120}\dot{y}^2\right)^{-1}$$
$$n_p(t+\Delta t) = \left[\frac{r_p(t)}{r_p(t+\Delta t)}\right]^3 \qquad (23)$$

The model constant K in Eq. (23) represents the ratio of the total energy in the distorted particle to the particle oscillation energy in the fundamental mode and has the value of K=10/3 [31].

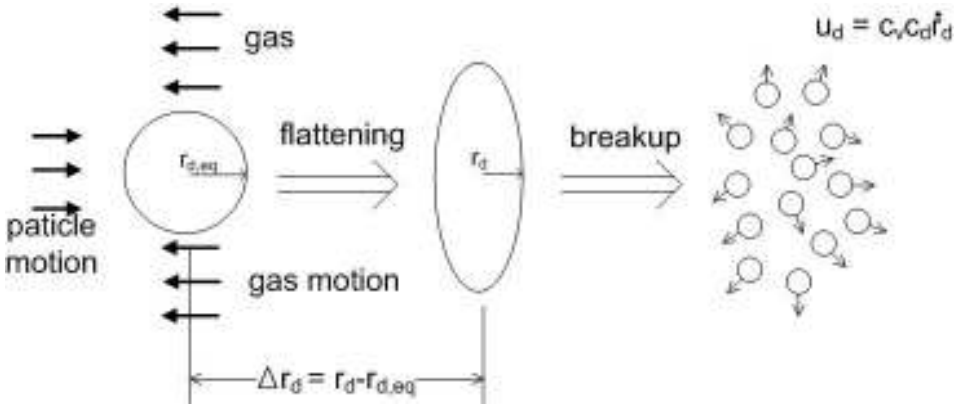

Figure 9 Taylor analogy breakup model

2.7 Binary collision model

Collisions between drops can result in the following regimes: (*i*) bouncing, (*ii*) permanent coalescence, (*iii*) separation (or grazing), and (*iv*) shattering; see **Figure 10**. These regimes are listed in the order of increasing the relative speed between the colliding binary drops [88]. Bouncing results from the gas film trapped between two colliding drops at relatively low collision speed. Permanent coalescence occurs when two drops combine into one single drop. At relatively high collision speed, separation follows a temporary coalescence, resulting in the formation of a string of two or more drops [89]. Shattering may occur at the high speed collision, resulting in the disintegration of two drops and subsequent formation of a cloud of numerous satellite drops.

These aforementioned collision regimes significantly differ depending on the liquid properties; water drop binary collision is quite different from hydrocarbon binary collision. The models reviewed in this section are applicable only for the water drop collision. The model should be modified according to the collision regimes if it is to be used for the analysis of the hydrocarbon drop collision [90-91].

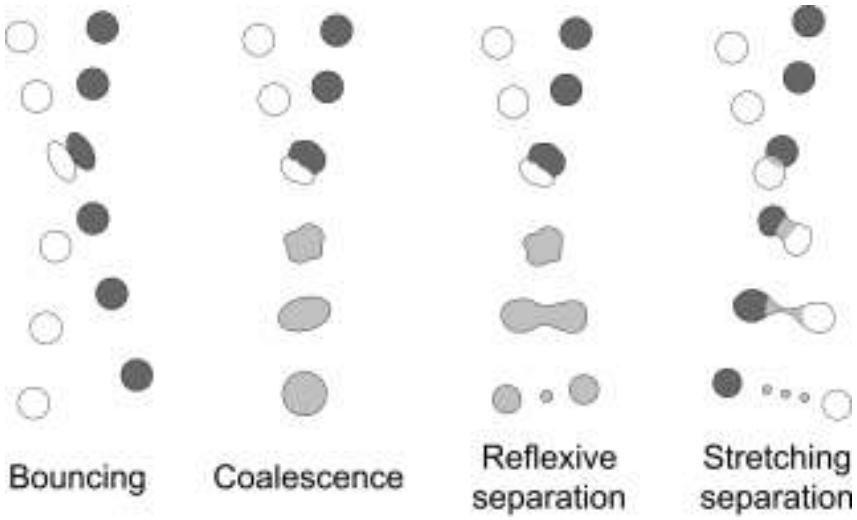

Figure 10 Various collision regimes in the order of increasing the relative sped between the colliding binary drops.

Coalescence-Separation Model by Ashgriz & Poo

Three major collision phenomena (or regimes) are considered herein: coalescence, reflexive separation, and stretching separation. Coalescence refers to the phenomenon of two drops combining into a single drop. Reflexive separation refers to two drops combining temporarily and then repelling each other, resulting in rebounding. Stretching separation occurs at a relatively high value of the impact parameter (defined as "χ" in **Figure 11(a)**), at which most of the mass of the colliding drops manages to flow toward their initial trajectory direction. Because of the nature of their off-centered collision (large value of χ), the collision triggers the spinning of both drops. The following model by Ashgriz and Poo [89] gives the criteria that distinguish one regime from another and, therefore, the status of the post-collision can be obtained analytically.

To illustrate the most general scenario for a binary collision, the necessary parameters are introduced in **Figure 11(a)**. The subscript "*s*" and "*l*" refer to small and large drops, respectively. The relative quantity is denoted with "*r*." d and u are the diameters and velocities of the drops. b is the distance between the centers of the drops before the collision. β is the angle between the trajectory of the small drop and the center-to-center line. γ is the angle between the trajectory of the small drop and the relative velocity vector. χ is the impact parameter, the projection of the separation distance between the droplet center in the direction normal to that of u, or χ can be thought of as the distance from the center of one drop to the relative velocity vector placed on the center of the other drop. B is the dimensionless impact parameter. The relative velocity of the two colliding drops is:

$$u_r = \sqrt{u_l^2 + u_s^2 - 2u_l u_s \cos\alpha} \tag{24}$$

Where

$$B = \frac{2\chi}{d_l + d_s} = \frac{2b\sin|\beta - \gamma|}{d_l + d_s} \tag{25}$$

$$\gamma = \sin^{-1}\left(\frac{u_l}{u_r}\sin\alpha\right)$$

As ***B*** approaches zero, head-on collision occurs, and as ***B*** approaches unity, *grazing* or off-centered collision occurs. A small value of ***B*** results in reflexive separation and a large value of ***B*** results in stretching separation. If ***B*** exceeds unity, two drops pass by and not collide. Thus the range of ***B*** is $0 \le B \le 1$.

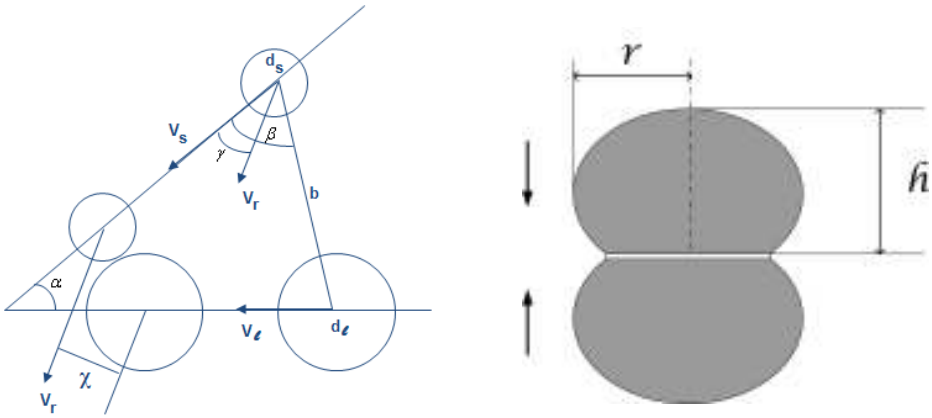

(a) (b)

Figure 11 (a) Schematic of the colliding binary drops. (b) Schematic of bouncing binary drops.

Reflexive separation results when the effective reflexive kinetic energy (K_r) is larger than 75% of its nominal surface energy:

$$K_r \ge 0.75\sigma\pi\left(d_l^3 + d_s^3\right)^{2/3} \tag{26}$$

Where

$$K_r = \sigma\pi d_l^2\left[\left(1+\Delta^2\right) - \left(1+\Delta^3\right)^{2/3} + \frac{We}{12\Delta\left(1+\Delta^3\right)^2}\left(\Delta^6\eta_1 + \eta_2\right)\right] \tag{27}$$

$$\Delta = d_s / d_l$$

$$\eta_1 = 2\left(1-\xi\right)^2\left(1-\xi^2\right)^{1/2} - 1$$

$$\eta_2 = 2\left(\Delta-\xi\right)^2\left(\Delta^2-\xi^2\right)^{1/2} - \Delta^3$$

$$\xi = \left(1+\Delta\right)B/2$$

This criterion can be rewritten in terms of the Weber number by setting the equal sign in Eq. (26).

$$\frac{We}{\Delta\left(1+\Delta^3\right)^2}\left(\Delta^6\eta_1+\eta_2\right)+3\left[4\left(1+\Delta^2\right)-7\left(1+\Delta^3\right)^{2/3}\right]=0 \tag{28}$$

This Eq. (28) distinguishes the regime of reflexive separation from the regime of coalescence; the regimes above and below the line from Eq. (28) are those of coalescence and reflexive separation, respectively. On the other hand, when the total effective stretching kinetic energy (K_{si}) is larger than the surface energy of the region of interaction, stretching separation occurs:

$$K_{si} \geq S_{si} \tag{29}$$

Where

$$K_{si}=\frac{1}{2}\rho U^2 V_l^2\left\{\frac{\Delta^3}{\left(1+\Delta^3\right)^2}\left[\left(1+\Delta^3\right)-\left(1-x^2\right)\left(\phi_s+\Delta^3\phi_l\right)\right]\right\} \tag{30}$$

$$S_{si}=\sigma\left[2\pi V_l d_l \tau\left(\Delta^3\phi_s+\phi_l\right)\right]^{1/2}$$

$$\phi_s=\begin{cases}1-\dfrac{1}{4\Delta^3}\left(2\Delta-\tau\right)^2\left(\Delta+\tau\right) & \text{for } h>\dfrac{1}{2}d_s\\[2ex] \dfrac{\tau^2}{4\Delta^3}\left(3\Delta-\tau\right) & \text{for } h<\dfrac{1}{2}d_s\end{cases}$$

$$\phi_l=\begin{cases}1-\dfrac{1}{4\Delta^3}\left(2-\tau\right)^2\left(1+\tau\right) & \text{for } h>\dfrac{1}{2}d_l\\[2ex] \dfrac{\tau^2}{4}\left(3-\tau\right) & \text{for } h<\dfrac{1}{2}d_l\end{cases}$$

$$h=\frac{1}{2}\left(d_l+d_s\right)\left(1-B\right)$$

$$V_{si}=\phi_s V_s$$

$$V_{li}=\phi_l V_l$$

Here the subscript "*i*" stands for "interacting" region. *V* represents the volume of the interacting regions. *h* is the width of the overlapping region. Eq. (30) can be rewritten in terms of the Weber number by setting the equal sign in Eq. (29).

$$We=\frac{4\left(1+\Delta^3\right)^2\left[3\left(1+\Delta\right)\left(1-B\right)\left(\Delta^3\phi_s+\phi_l\right)\right]^{1/2}}{\Delta^2\left[\left(1+\Delta^3\right)-\left(1-B^2\right)\left(\phi_s+\Delta^3\phi_l\right)\right]} \tag{31}$$

This Eq. (31) distinguishes the regime of stretching separation from that of coalescence; the regimes below and above the line from Eq. (28) are those of coalescence and stretching separation, respectively.

Bouncing Model by Estrade et al.

Estrade et al. [92] gives a criterion for the bouncing regime. Their model criterion assumes that a drop's initial kinetic energy of deformation does not exceed the energy required to produce the limit deformation. The model also assumes a short delay time during deformation, no energy exchange between gas and drop and little dissipative energy.

$$\text{If } \begin{cases} We < We_{crit} & \rightarrow \text{ Bouncing} \\ We > We_{crit} & \rightarrow \text{ Coalescence} \end{cases} \tag{32}$$

Where

$$We_{crit} = \frac{\Delta\left(1+\Delta^2\right)\left(4\phi' - 12\right)}{\chi_l\left(1-B^2\right)} \tag{33}$$

$$\chi_l = \begin{cases} 1 - \frac{1}{4}\left(2-\tau\right)^2\left(1+\tau\right) & \text{if } \tau > 1.0 \\ \frac{1}{4}\tau^2\left(3-\tau\right) & \text{if } \tau \le 1.0 \end{cases}$$

$$\phi' = 2\left(\frac{3}{\phi^2}+1\right)^{-2/3} + \left(\frac{3}{\phi^2}+1\right)^{1/3}$$

$$\tau = \left(1-B\right)\left(1+\Delta\right)$$

$$\Delta = d_s / d_l$$

The value of the shape factor, ϕ', depends on ϕ which is the critical ratio of the smallest height, *h*, and the largest radius, *r*, as $\phi = h/r$, as depicted in **Figure 11**. Thus, ϕ' is a function of the particles properties and the surrounding gas. The range of the critical ratio is $0 < \phi < 2$. If deformation is severe and nearly a "pancake" or "disk" is formed subsequent to the head-on collision, $\phi \rightarrow 0$. If the head-on collision is so insignificant that nearly no deformation results, then $\phi \rightarrow 2$ because *h* approaches the particle diameter, namely $h \rightarrow 2r$.

Coalescence-Separation Model by O'Rourke

The collision model by O'Rourke [43] accounts for grazing and coalescence of the colliding binary drops; it does not account for the shattering effect that may be important in high-speed collision scenarios [88]. The collision model is based on the stochastic parcel method, which assumes the collision of the two parcels residing in the same computational cell. It is also assumes that the particles inside each parcel are uniformly distributed over the computational cells where the particles reside. The particles with the larger diameters are named "collectors" while the particles with the smaller in

diameters are called “donors.” The expected frequency of collisions between one collector and all the donor particles is governed by a Poisson process with frequency parameter λ having the following function form.

$$f = \frac{n_s}{V_{cell}} \pi \left(r_s + r_l \right)^2 \left| \vec{u}_s - \vec{u}_l \right| \tag{34}$$

The subscripts “*l*” and “*s*” refer to the properties for the collectors (*large*) and donors (*small*) and, respectively. V_{cell} is the volume of the computational cell and n_s is the number of donors. For a Poisson process, the likelihood that a collector undergoes *n* collisions is defined with the following probability density function (PDF) distribution,

$$PDF = e^{-\bar{n}} \frac{\bar{n}^n}{n!} \quad , \quad \text{where} \quad \bar{n} = f \Delta t \tag{35}$$

Here, $\bar{n}$ refers to the averaged number of collisions that a collector undergoes with donors. Δ*t* represents the computational time step. When no collision occurs, the value of PDF approaches $PDF_o \to e^{-\bar{n}}$. The value of PDF is determined by sampling a random number, ranging $0 < RN_1 < 1$. If $RN_1 < PDF_o$, then no collision results. On the other hand, if $RN_1 > PDF_o$, then a second random number, $0 < RN_2 < 1$, is chosen to determine whether coalescence or grazing collision occurs.

The model outcome of the collision is based on the experimental and theoretical works of Brazier-Smith et al. [44] on the collision of water particles. In the Brazier-Smith study, three regimes (i.e., bouncing, coalescence, and separation) of particle collision are identified and found to be dependent on the impact parameter, $x = \sqrt{RN_2} \left(r_l + r_s \right)$, defined as the perpendicular distance between the center of one particle and the undeflected trajectory of the other [44]; see **Figure. 11(a)**. This impact parameter of each particle is represented stochastically because individual particles inside a parcel are not tracked during computation, but only parcels are tracked in Lagrangian simulation. The O’Rourke collision model assumes the follow post-collision state (see **Figure 12**);

$$\text{If} \begin{cases} x < x_{crit} \rightarrow \text{ Coalescence} \\ x > x_{crit} \rightarrow \text{ Separation or grazing} \end{cases} \tag{36}$$

The collision model of O’Rourke [43] only accounts for grazing collision without satellite particle formation. According to O’Rourke, the critical impact parameter, x_{crit}, is:

$$x_{crit} = \left(r_l + r_s \right) \sqrt{\min \left[\; 2.4 f\left(\gamma \right) \frac{1}{We_s}, \; 1.0 \; \right]} \tag{37}$$

where $f(\gamma) = \gamma^4 - 2.4\gamma + 2.7\gamma$ represents a curve-fit based on the data by Brazier-Smith et al for water drop collision. The ratio of the collector to donor is $\gamma = r_l / r_s = d_l / d_s$ or $\gamma = 1/\Delta = d_l / d_s$, and the Weber number is $We_s = \rho_{liq} |\vec{u}_l - \vec{u}_s|^2 r_s / \sigma$.

Once the outcome of the collision is known (suppose it is *coalescence*), then the number of coalescences for each collector is determined by satisfying the relation below:

$$\sum_{k=0}^{n-1} PDF(k) \le RN_1 \le \sum_{k=0}^{n} PDF(k) \tag{38}$$

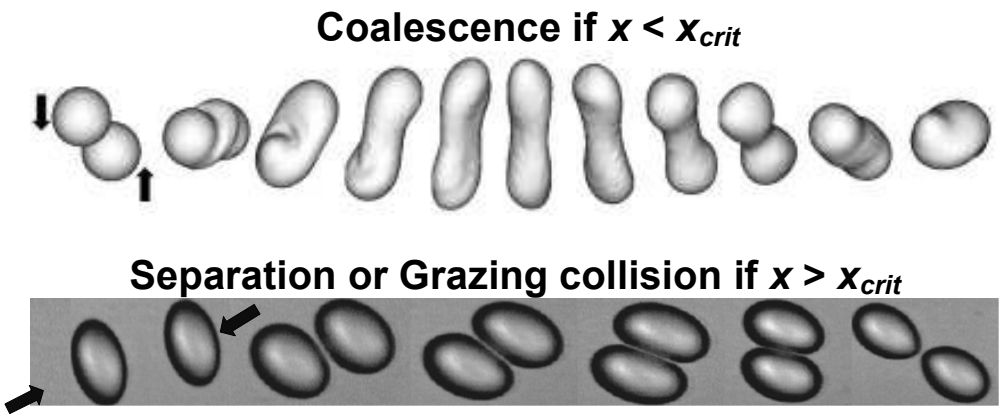

Figure 12 Collision criterion of binary drops by O'Rourke [43]

Satellite Model by Munnannur and Reitz

In the reflexive and stretching separation regimes, satellites (r_{sat}) are formed as a result of elongation of temporarily coalesced drops into a ligament (r_{lig}) which eventually breaks up into satellites. Based on the Rayleigh's linear jet breakup theory, all satellites formed are assumed to have the same size as r_{sat}=1.89r_{lig}, assuming that the nonlinear effect is negligible. Readers should be warned that multiple crests per wavelength due to nonlinearity can result in several satellites, which in turn yield r_{sat}<1.89r_{lig}.

Munnannur and Reitz [93] propose the model that determines the collision status:

$$\text{If } \begin{cases} C_{vs} > 0 \rightarrow \text{ Separation occurs} \\ C_{vs} \le 0 \rightarrow \text{ Grazing collision without fragmentation} \end{cases} \tag{39}$$

Where

$$C_{vs} = \frac{K_{si} - S_{si} - E_{diss}}{K_{si} + S_{si} + E_{diss}} \tag{40}$$

Once separation occurs, the time scale, which represents the ratio of the capillary time scale to the elongation time scale of the fluid ligament, is

introduced to determine whether there will be a *single* satellite or *multiple* satellites

$$\text{If } \begin{cases} \tau_{reflex} > 2 \rightarrow \text{ Multiple satellites} \\ \tau_{reflex} \le 2 \rightarrow \text{ A single satellite} \end{cases} \tag{41}$$

where $\tau_{reflex} = 0.75 k_2 \sqrt{We_0}$, k_2=0.45, and $We_0 = \rho_l (2r_0) u_{rel}^2 / \sigma_l$. If a single satellite is formed between the two end-drops, the drop radius is:

$$r_0 = \left[\left(\frac{4}{3} \right) \left(\psi_l r_l^3 + \psi_s r_s^3 \right) \right]^{1/3} \tag{42}$$

If multiple satellites are formed, then the satellites radius is $r_{sat} = 1.89 r_{lig}$ where ligament radius can be computed by solving the equation below:

$$\left(\frac{0.75}{\sqrt{2}} \right) (k_1 \alpha) We_0^{1/2} \bar{r}_{lig}^{-3.5} + \bar{r}_{lig}^{-2} - 1 = 0 \tag{43}$$

where k_1=8.5 and α=0.44, and $\bar{r}_{lig} = r_{lig} / r_0$. Note, the ligament (as a cylinder) is situated between the two end-drops. Prior to ligament stretching, the ligament is a *fat* cylinder whose radius is r_0 and its length is also r_0 and, thus, its volume is $V_{lig} = \pi r_0^3$. After the ligament is stretched to a *thin* cylinder, it eventually breaks up into multiple satellites, and their total volume is expressed as $V_{sat} = N_{sat} (4/3) \pi r_{sat}^3$. Because mass conserves as $V_{lig} = V_{sat}$, the total number of the satellites is:

$$N_{sat} = \frac{3}{4} \left(\frac{r_0}{r_{sat}} \right)^3 \tag{44}$$

Post-Collision Properties for Liquid Binary Drops

Once the type of collision and the number of particles in the collision are determined, then properties of the collector and donor parcels are updated based on mass, momentum and energy principles, which are detailed in refs. [86] and [43]. These relations are summarized below for, first, a collision event resulting in *coalescence*, in which the colliding donor (small) particles are coalesced with the collector (larger) particle and, thus, n_{coll} number of donors is zero in the donor parcel, where n_{coll} refers to the number of collisions.

$$\begin{aligned} m_t^{new} &= m_t = m_l + m_s \ n_{coll} \\ T_l^{new} &= \frac{1}{m_t} \left(T_l m_l + T_s m_s \ n_{coll} \right) \\ \vec{u}_l^{new} &= \frac{1}{m_t} \left(m_l \vec{u}_l + m_s \vec{u}_s \ n_{coll} \right) \end{aligned} \tag{45}$$

$$d_l^{new} = \left(\frac{6m_t}{\pi \rho_{liq}} \right)^{1/3}$$

$$n_s^{new} = n_s - n_{coll}$$

Here, the "*new*" superscript variables and m_t denotes the parcel properties and the total mass of the collector particles after collision. n_l and n_s refer to the number of large and small particles inside a computational parcel. If (n_{coll} n_l) > n_s, then there are physically not enough particles in the donor parcel to accommodate all of the collisions with the particles in the collector parcel. In this case, n_{coll} is reset to n_s/n_l and the mass of the particles associated with the particle parcel is set equal to zero and eventually removed from the calculation.

In a *grazing* collision event, only momentum exchange is considered since the time scales associated with heat exchange are much longer than the collision event. The particle velocities after collision are set as follows [43];

$$\text{If } n_l > n_s, \begin{cases} \vec{u}_s^{new} = \dfrac{1}{m_s + m_l} \left\{ m_s \vec{u}_s + m_l \vec{u}_l + m_l \left(\vec{u}_s - \vec{u}_l \right) \left(\dfrac{b - b_{crit}}{r_s + r_l - b_{crit}} \right) \right\} \\ \vec{u}_l^{new} = \dfrac{n_s \vec{u}_l + \left(n_l - n_s \right) \vec{u}_l}{n_l} \end{cases} \tag{46}$$

$$\text{If } n_l < n_s, \begin{cases} \vec{u}_s^{new} = \dfrac{1}{m_s + m_l} \left\{ m_s \vec{u}_s + m_l \vec{u}_l + m_s \left(\vec{u}_l - \vec{u}_s \right) \left(\dfrac{b - b_{crit}}{r_s + r_l - b_{crit}} \right) \right\} \\ \vec{u}_l^{new} = \dfrac{n_l \vec{u}_s + \left(n_s - n_l \right) \vec{u}_s}{n_s} \end{cases}$$

2.8 Particle-wall impact

Often, traveling particles collide with solid surrounding walls and the particle impact phenomena are investigated for various practical reasons: if particles do not deposit onto the surface (whether it is because of the liquid's high surface tension, hydrophobic substrate, a thin air-film, or the Leidenfrost effect), painting/coating quality becomes rather poor. For spray cooling applications, the particle rebound phenomenon decreases the cooling efficiency. In automobile applications, excessive fuel spray impingement onto walls of the IC engine forms a liquid film whose fuel-rich burning leads to unwanted pollutants. At high impact speeds, particles break up (often referred to as "splashing") into satellites, leaving scattered marks in the impacted region; this is detrimental for inkjet printing applications that requires a clean dot-printing onto a substrate. On the other hand, for spray drying applications, splashing should be promoted to produce powders by spraying mono-disperse drops onto various substrates. In these aforementioned applications, the particle impact phenomena should be controlled and understood properly to delineate their impact physics in the stochastic spray model.

Traditionally, surface tension, viscosity, and substrate roughness (i.e., *We*, *Re*, and R_a,) are the primary parameters that describe drop impact phenomena [94]. Bouncing occurs when the surface tension force greatly exceeds the dynamic force. When the dynamic force overcomes the surface tension force, the particle spreads upon impact and can splash if the dynamic force is too excessive; otherwise it simply spreads. In this report, outlines for the (*i*) bouncing, (*ii*) sticking, (*iii*) splashing phenomena are briefly are reviewed and the relevant references for the description of their detailed modeling approaches are suggested (see **Figure 13**).

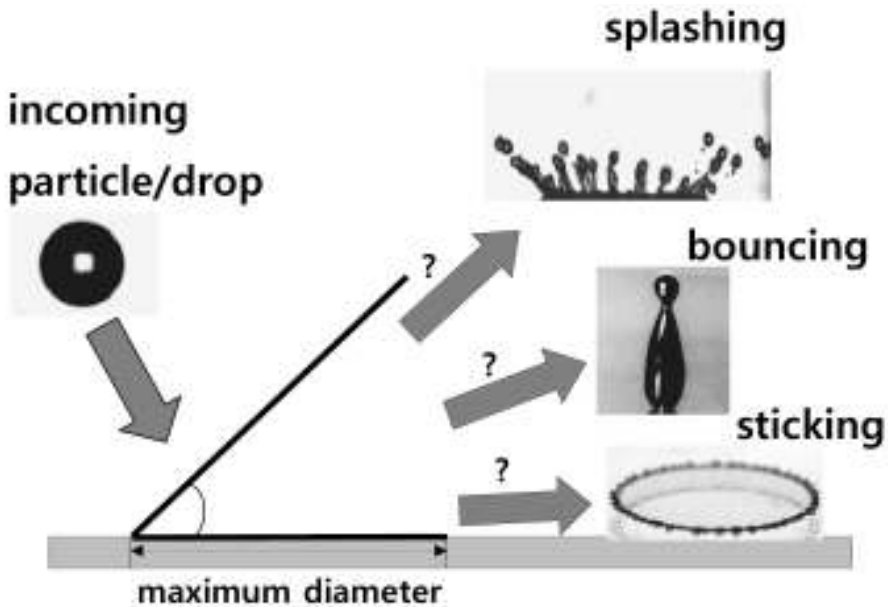

Figure 13 Configuration states during particle impact consisting of pre-impact (i.e., incoming stage), impact (i.e., maximum diameter), and post-impact (i.e., sticking, bouncing, and splashing)

Bouncing

Bouncing is commonly observed during a low speed impact, where the surface tension effect is pronounced. This phenomenon is of low interest because most of the present applications are concerned with high-speed impacts. Furthermore, it is of relatively low interest to industries, as opposed to sticking and splashing phenomena, because it has few practical applications. However, bouncing does occur in drop or spray impact and, thus, its mechanism needs to be correctly understood for accurate impact modeling. Aziz and Chandra [95] noted: If the surface energy of a drop at its maximum spreading is greater than the dissipation energy, then the drop rebounds; otherwise, the drop will stick. Mao et al. [96] also suggested a rebound criterion with the dimensionless rebound energy, E_r^* as an implicit function of the maximum spread factor and the equilibrium contact angle. If $E_r^*>0$, then the drop rebounds; otherwise, it sticks. More recently, Mukherjee and Abraham [97] presented a numerical simulation of rebounding using the lattice-Boltzmann model; but their study was limited to a case where the density ratios between the drop and surrounding gas were only 5 and 10. Ideally, the density ratio should reach an order of ~10^3 for water-drop impact

in air. Park et al. [98] used the boundary integral method to model the rebounding phenomenon for a range of air pressures.

Sticking

Among various subjects on drop impact, sticking has received much attention because of its broad applications such as inkjet-printing, coating, painting, and spray cooling. The maximum spreading diameter often needs to be predicted to estimate the coating area-coverage or painting performance. The accurate prediction includes the competition between the drop's inertia and surface tension energy and viscous dissipation energy. Chandra and Avedisian [99] predicted the maximum spreading diameter using an energy conservation concept. Healy et al. [100] compared various suggested models for experimental data (Ford and Furmidge, [101], Stow and Hadfield, [102]) and concluded that the model by Yang [103] yielded the best result. Mao et al. [96] also provided a correlation for the maximum spreading diameter as a function of the Reynolds, Weber number, and contact angle. Gong [104] also suggested another spreading model, but his results were not quantitatively compared with the results of other existing models. Sikalo et al. [105] utilized the VOF (Volume-of-Fluid) model for the maximum spreading diameter for highly viscous glycerin drops; their numerical results were compared with the experimental data of Stow and Hadfield [102]. For fire modeling applications, the sticking might be the source term for a fuel fire as a pool forms, and is, therefore, of interest. For solid propellant fires, the sticking can provide substantial deposition heat transfer to an object.

Splashing

Splash occurs for a relatively high speed impact, where inertia dominates over surface tension or/and viscosity. Various splash criteria were offered by Yarin and Weiss [106], Mundo et al. [107], and Cossali et al. [108]. Because of the dependence of splash on surface tension and viscosity, splashed droplets or satellites are normally scaled with the Weber, number and Reynolds or Ohnesorge (Oh) number (i.e., impingement characteristic parameter, $K_{crit}=aWe^{b}Re^{c}$, where a, b, and c are constants; as for a drop onto *film* for example, $K_{crit} = Oh^{-0.4}We = We^{0.8}Re^{0.4} = 2100 + 5880\ (\delta^{*})^{1.44}$, where δ^{*}= *film* thickness, non-dimensionalized by parent drop diameter, D_p), and so is the splashed liquid amount. At moderate impact speed, a corona is normally formed during spreading and the capillary waves along the rim of the corona in the azimuthal direction appear and eventually they snap-off, a phenomenon known as "corona splash." When the substrate is wet (liquid film), a rising corona sheet or crown is of larger relative size due to the mass added by the film. The related work on this topic includes: Stow and Stainer [109], Marmanis and Thoroddsen [110], Rioboo et al. [111], Xu et al. [112], Xu [113], and Kalantari and Tropea [114]. The splashed droplets size appears to obey a log-normal distribution, according to Stow and Hadfield [102]. Post-impact characteristics of the splashed droplets, such as their speed and size, were also studied by Cossali et al. [108] and Roisman et al. [115].

Surface roughness

Stow and Hadfield [102], Mundo et al. [107,116], Range and Feuillebois [117], Rioboo et al. [111] noted that the splashing criteria could change with surface roughness. Cossali et al. [108] provided an empirical fit for K_{crit} for a *dry* surface, based on the previous data; $K_{crit}=649+3.76/R^*$, where R^* is the surface roughness, non-dimensionalized by D_p. When the surface is sufficiently rough, "prompt splash" occurs, which is immediately followed by spreading. Breakthrough research was conducted by Xu et al. [112], who first showed that splash is a function of air pressure while conventional wisdom suggested that splash is dependent only on substrate roughness and the drop's physical properties. Their finding provides a new degree of freedom in controlling splash.

3.0 Conclusion

A general description of the particle phase transport equation (i.e., conservation of mass, momentum, and energy) was reviewed on the basis of Eulerian-Lagrangian particle tracking method. In this modeling approach, suitable for the dilute two-phase flow system, the particle phase is modeled on a Lagrangian reference frame and the gas phase is modeled on an Eulerian reference frame. Explanation on the interaction between the particle phase turbulence model and the *k-ε* RANS (Reynolds-Averaged Navier-Stokes) turbulence for the Eulerian phase was also provided. A stochastic approach utilizing PDFs was adopted for several sub-models, such as drop size distribution, turbulence, and binary collision. Furthermore, various models for the particle-wall interaction were reviewed.

4.0 Acknowledgement

This research was supported by Research Center of Break-through Technology Program through the Korea Institute of Energy Technology Evaluation and Planning (KETEP) funded by the Ministry of Knowledge Economy (2009-3021010030-11-1). The author also acknowledges that a partial support was made for this project by the National Research Foundation of Korea NRF Grant (NRF-2010-D00013). The author is indebted to Prof. Paul DesJardin at University of Buffalo for his support in writing this review chapter.

5.0 References

1. Chigier, C. Challenges for Future Research in Atomization and Spray Technology: Arthur Lefebvre Memorial Lecture. Atomization and Sprays **2006,** *16,* 727–736.
2. Drazin, P.G.; and Reid, W.H. Hydrodynamic Stability. Cambridge University Press, New York, NY **1981**, 14–28.
3. Rayleigh W.S. On the Instability of Jets, Proceedings of London Mathematical Society Lecture Note Series **1878**, *10* (4)
4. Weber , C. Zum Zerfall eines Flussigkeitsstrahles. Angewandte Zeitschrift fur Mathemetischelogik und Mechnika **1931**, *11,* 138–245.

5. Batchelor ,G.K. Collected Works of G. I. Taylor. Cambridge University Press, Cambridge, MA, **1958**.
6. Ponstein. J. Instability of Rotating Cylindrical Jets. Applied Sciencific Research **1959**, *8* (6), 425–456.
7. Levich, V.G. Physicochemical Hydrodynamics. Prentice Hall, Englewood Cliffs, NJ **1962**, 639–646
8. Sterling, A.M.; Sleicher, C.A. The Instability of Capillary Jets. Journal of Fluid Mechanics **1975**, *68* (3), 477–495.
9. Wu, K. J.; Reitz, R. D.; Bracco, F.V. Measurements of Particle Size at the Spray Edge near the Nozzle in Atomizing Liquid Jets. Physics of Fluids **1986**, *29* (4), 941–951.
10. Brennen, C. Cavity Surface Wave Patterns and General Appearance. Journal of Fluid Mechanics **1970**, *44* (1), 33–493.
11. Yoon, S.S.; Heister, S. D. Categorizing linear theories for atomizing round jets, Atomization and Sprays **2003**, *13*, 499-516.
12. Longuet-Higgins, M.S.; Cokelet, E.D. The deformation of steep surfaces waves on water. I. A numerical method of computation. Proceedings of the Royal Society of London Series A-mathematical and Physical Science **1976**, *350*, 1-26.
13. Lundgren, T.S.; Mansour, N.N. Oscillations of Particles in Zero Gravity with Weak Viscous Effects. Journal of Fluid Mechanics **1988**, *194,* 479-510.
14. Hilbing, J.H.; Heister, S.D.; Spangler, C.A.; Boundary Element Method for Atomization of a Finite Liquid Jet. Atomization and Sprays **1995**, *5*, 621-638.
15. Heister, S.D. Boundary Element Methods for Two-Fluid Free Surface Flows. Engineering Analysis Boundary with Elements **1997**, *19*, 309-317.
16. Yoon, S.S.,; Heister, S.D.; Analytic Solution for Fluxes at Interior Points for the 2D Laplace Equation. Engineering Analysis Boundary with Elements **2000**, *24*, 155-160.
17. Yoon, S.S.; Heister, S.D.; Epperson, J.T.; Sojka, P.E.; Modeling Multi-jet Mode Electrostatic Atomization using Boundary Element Methods. Journal of Electrostatics **2001**, *50*, 91-108.
18. Yoon, S.S.; Heister, S.D. A Nonlinear Atomization Model Based on a Boundary Layer Instability Mechanism. Physics of Fluids **2004**, *16,* 47-61.
19. Yoon, S.S. Particle Distributions at the Liquid Core of a Turbulent Spray. Physics of Fluids **2005**, 035103.
20. Park, H.; Yoon, S.S.; Heister, S.D. A Nonlinear Atomization Model for Computation of Particle-Size Distributions and Complete Spray Simulation, International Journal for Numerical Methods in Fluids **2005**, *48*, 1219-1240.
21. Park, H.; Heister, S.D. Nonlinear Simulation of Free Surfaces and Atomization in Pressure Swirl Atomizers. Physics of Fluids **2006**, *18*, 052103.
22. Ashraf, A. I.; Milind, A. J. Nonlinear Breakup Model for a Liquid Sheet Emanating From a Pressure-Swirl Atomizer. Journal of Engineering for Gas Turbines and Power **2007**, *129*, 945-953.
23. Boeck, T.; Li, J.; López-Pagés, E.; Yecko, P.; Zaleski, S. Ligament formation in sheared liquid–gas layers. Theoretical and Computational Fluid Dynamics **2007**, *21*, 59–76.
24. Huawei, H.; Kamiel, G. A Numerical Study of Entrainment Mechanism in Axisymmetric Annular Gas-Liquid Flow **2007**, *129*, 293-301.
25. Ishimoto, J.; Ohira, K.; Okabayashi, K.; Chitose, K. Integrated numerical prediction of atomization process of liquid hydrogen jet. Cryogenics **2008**, *48*, 238–247.
26. Mandal, A.; M, A. Jo; J, Xue; A, A. Ibrahim. Flow of power-law fluids in simplex atomizers. International Journal of Heat and Fluid Flow **2008**, *29*, 1494–1503.
27. Siamas, G.A.; Jiang, X.; Wrobel, L.C. A numerical study of an annular liquid jet in a compressible gas medium. International Journal of Multiphase Flow **2008**, *34*, 393–407
28. Lebas, R.; Menard, T.; Beau, P.A.; Berlemont, A.; Demoulin, F.X.; Numerical simulation of primary break-up and atomization: DNS and modeling study. International Journal of Multiphase Flow **2009**, *35*, 247-260.
29. Pan, Y; Suga, K. A numerical study on the breakup process of laminar liquid jets into a gas, physics of fluid **2006**, *18*, 052101.
30. Gorokhovski, M.; Herrmann, M. Modeling Primary Atomization. Annual. Review of Fluid Mechanics **2008**, *40*, 343-366.
31. O'Rourke, P.J.; Amsden, A.A., The Tab Method for Numerical Calculation of Spray Particle Breakup. SAE Technical **1987**, 872089.

32. Berlemont, A.; Desjonqueres, P; Gouesbet, G. Particle lagrangian simulation in turbulent flows. International Journal of Multiphase Flow **1990**, *16* (1), 19-34.
33. Berlemont, A.; Grancher., M.S.; Gouesbet, G.; On the Lagrangian simulation of turbulence influence on particle evaporation. International Journal of Heat and Mass Transfer **1991**, *34*, 280-2812.
34. Berlemont, A.; Grancher, M.S.; Gouesbet, G. Heat and mass transfer coupling between vaporizing particles and turbulence using a Lagrangian approach. International Journal of Heat and Mass Transfer **1995**, *38*, 3023-3034.
35. Berlemont, A.; Achim, P.; Chang, Z.; Lagrangian approaches for particle collisions: The colliding particle velocity correlation in the multiple particles tracking method and in the stochastic approach. physics of fluids **2001**, *13* (10), 1396845.
36. Crowe, C.T.; Sharma, M.P.; Stock, D.E. The particle-source-in cell (PSI-CELL) model for gas-particle flows. Journal of Fluids Engineering **1977**, *99*, 325-332.
37. Crowe, C.T.; Chung, J.N.; Troutt, T.R. Particle mixing in free shear flows. Progress in energy and combustion Science **1988**, *14*, 171-194.
38. Crowe, C.T.; Troutt, R.; and Chung, J.N. Numerical models for two-phase turbulent flows. Annual Review Fluid Mechanics **1996**, *28*, 1143.
39. Crowe, C.; Sommerfeld, M.; Tsuji, Y. Multiphase Flows with Particles and Particles. CRC Press, New York, NY, **1998**.
40. Li, J.; Kuipers, J.A.M. On the origin of heterogeneous structure in dense gas–solid flows. Chemical Engineering Science **2005**, *60*, 1251 – 1265.
41. Helland, E.; KOccelli, R.; Tadrist, L. Numerical study of cluster formation in a gas-particle circulating fluidized bed. Powder Technology **2000**, 110, 210-221
42. Lee. M.W. Numerical Studies on the Behavior Characteristics of Bi-dispersed Particle in Gas-Solid Fluidized Bed. M.S., Korea University **2009**.
43. O'Rourke, P. Collective Particle Effects on Vaporizing Liquid Sprays. Los Alamos National Laboratory Report **1981**, No. LA-9069-T
44. Brazier-Smith, P.R.; Jennings, S.G.; Latham, J. The Interaction of Falling Water Particles: Coalescence. Proceedings of the Royal Society of London Series A-mathematical and Physical Science **1972**, *326*, 393-408.
45. Anderson, T. B. and Jackson, R., A Fluid Mechanical Description of Fluidized Beds, I&EC Fundamentals **1967***, 6* (4), 527–539.
46. Gray, W.G.; Lee, P.C.Y. On the Theorems for Local Volume Averaging of Multiphase Systems. Int. J. Multiphase Flow **1977**, *3*, 333-340.
47. Gough, P.S.; Zwarts, F.J. Modeling Heterogeneous Two-Phase Reacting Flow. AIAA Journal **1979**, *17* (1), 17-25.
48. Slattery, J.C. Flow of Viscoelastic Fluids Through Porous Media. AICHE Journal **1966**, 13, 1066-MS.
49. Slattery, J.C. Momentum Energy and Mass Transfer in Continua, second edition. Robert E. Krieger Publishing Company, Inc **1981**.
50. Whitkar, S. Advances in the Theory of Porous Media. Industrial and Engineering Chemistry **1969**, 61, 14-28.
51. Whitkar, S. The Transport Equations for Multi-phase Systems. Chemical Engineering Science, **1973**, *28*, 139-147.
52. Oefelein, J.C.; Yang, V. Simulation of High-Pressure Spray Field Dynamics, in Recent Advances in Spray Combustion: Spray Atomization and Particle Burning Phenomena in Progress in Astronautics and Aeronautics **1996**, *2*.
53. Zhu, M.; Bray, K.N.; Rumberg, O.; Rogg, B.; PDF Transport Equations for Two-Phase Reactive Flows and Spray. Combustion and Flame **2000**, *122*, 327-338.
54. Archambault, M.R.; Edwards, C.F. Computation of Spray Dynamics By Direct Solution of Moment Transport Equations. 38th Aerospace Sciences Meeting & Exhibit, Reno, NV **2000**.
55. DesJardin P.E.; Gritzo. A dilute spray model for fire simulations: formulation, usage and benchmark problems. Sandia National Laboratories Technical Report, L.A **2002**, SAND2002-3419,.
56. Faeth, G.M.; Evaporation and Combustion of Spray. Progress in energy and combustion Science **1983**, 1-76.
57. Hewson, J.C.; Yoon, S.S. On sampling from prescribed particle pdfs using computational parcels. Atomization and Sprays, **2005**, *15*, 119-131.
58. Faeth, G.M.; Mixing, Transport and Combustion in Sprays. Progress in energy and combustion Science **1987**, *13*, 293-345.

59. Ranz, W.E.; Marshall, W.R.; Evaporation from Particles, Chemical Engineering Progress **1952**, 141-173.
60. Maxey, M.R. and Riley, J.J., Equation of Motion for a Small Rigid Sphere in a Nonuniform Flow, Physics of Fluids **1983***, 26* (4), 883-889.
61. Loth, E. Numerical Approaches for Motion of Dispersed Particles, Particles, and Bubbles. Progress in Energy and Combustion Science **2000**, *26*, 161-223.
62. Odar, F.; Hamilton, W.S. Forces on a sphere accelerating in a viscous fluid. Journal of Fluid Mechanics **1964**, *18*, 302-314
63. Chhabra, R.P.; Agarwal, L.; Sinha, N.K. Drag on Non-spherical Particles: An Evaluation of Available Methods. Powder Technology **1999**, *101*, 288-295.
64. Lazaro, B.J.; Lasheras. J.C. Particle dispersion in a turbulent, plane, free shear layer. Physics of Fluids A **1989**, *6*, 1035-1044.
65. Vojir, D.J.; Michaelides, E.E. Effect of the history term on the motion of rigid spheres in a viscous fluid. International Journal of Multiphase Flow **1994**, *20 (3)*, 547-556.
66. Ganser, G.H. A rational approach to drag prediction of spherical and nonspherical particles. Powder Technology **1993**, *77*, 143-152.
67. Kuo, K.K. *Principles of Combustion*; A Wiley-Interscience Publication, John Wiley & Sons: New York, 1986.
68. Watson, K.M. Predication of Critical Temperature and Heats of Vaporization. Industrial and Engineering Chemistry **1931**, *23*, 360-364.
69. Lefebvre, A.H. *Atomization and Sprays*; Hemisphere Publishing Corporation: New York, **1989**.
70. Gosman, A.D.; Ioannides, E. Aspects of Computer Simulation of Liquid-Fueled Combustion. 19th American Institute of Aeronautics and Astronautics Aerospace Sciences Meeting **1981**, 810323.
71. Shuen, J-S.; Chen, L-D.; Faeth, G.M. Evaluation of a Stochastic Model of Particle Dispersion in a Turbulent Round Jet. AICHE Journal **1983**, *29*, 167-170.
72. Durst, F.; Milojevic, D.; Schonung, B. Eulerian and Lagrangian Predictions of Particulate Two-phase Flows: a Numerical Study. Applied Mathematical Modelling **1984**, *8*, 101-115.
73. Milojevic, D. Lagrangian Stochastic-Deterministic (LSD) Predictions of Particle Dispersion in Turbulence. Particle & Particle Systems Characterization **1990**, *7*, 181-190.
74. Blumcke, E.; Brandt, M.; Eickhoff, H.; Hassa, C. Particle Dispersion in Highly Swirling, Turbulent Flows. Particle & Particle Systems Characterization **1993**, *10*, 182-190.
75. Klose, G.; Rembold, B.; Koch, R.; Wittig, S. Comparison of State-of-the-art Droplet Turbulence Interaction Models for Jet Engine Combustor Conditions. International Journal of Heat and Fluid Flow **2001**, *22*, 343-349.
76. Hinze, J. O. *Turbulence*; McGraw Hill Book Company: New York, 1975.
77. Bergwerk, W. Flow Patterns in Diesel Nozzle Spray Holes. Proceedings of the Institution of Mechanical Engineers Series **1959**, *173*, 655.
78. Brennen, C. Cavity Surface Wave Patterns and General Appearance. Journal of Fluid Mechanics **1970**, *44*, 33.
79. Hoyt, J.W.; Taylor, J.J. Turbulence Structure in a Water Jet Discharging in Air. Physics of Fluids **1977**, *20*, S253
80. Reitz, R.D. Modeling Atomization Processes in High-Pressure Vaporizing Sprays. Atomisation and Spray Technology **1987**, *3*, 309-337.
81. Su, T.F.; Patterson, M.A.; Reitz, R.D.; Farrell, P.V. Experimental and numerical studies of high pressure multiple injection sprays. SAE paper **1996,** 960861
82. Liu, A.B.; Mather, D.; Reitz, R.D. Modeling the Effects of Particle Drag and Breakup on Fuel Sprays. SAE Technical **1993**, 930072.
83. Ibrahim, E.A.; Yang, H.Q.; Przekwas, A.J. Modeling of Spray Particles Deformation and Breakup. Journal of Propulsion and Power **1993**, *9*, *4*, 651-654.
84. Gorokhavski, M. Stochastic Spectral Relaxation Model of Particles Break-Up in Liquid Spray Compuations. 38th Aerospace Sciences Meeting & Exhibt Reno NV **2000**, 0198.
85. Gorokhovski, M.; Apte, S. Stochastic Sub-grid Modeling Particle Breakup for LES of Atomizing Spray. Center for Turbulence Research Annual Research Briefs **2001**, 169-176.
86. Amsden, A.A.; Ramshaw, J.D.; O'Rourke, P.; Dukowicz, J.K. KIVA: A Computer Program for Two-and Three-Dimensional Fluid Flows with Chemical Reactions and Fuel Sprays. Los Alamos Report **1985**, 10245.

87. Clark, M.M. Drop Breakup in a Turbulent Flow-I. Conceptual and Modeling Considerations. Chemical Engineering Science **1988**, *43*, 671-679.
88. Georjon, T.L.; Reitz, R.D. A Particle-Shattering Collision Model for Multidimensional Spray Computations. Atomization and Sprays **1999**, *9*, 231-254.
89. Ashgriz, N.; Givi, P. Coalescence Efficiencies of Fuel Particles in Binary Collisions. International Communications in Heat and Mass Transfer **1989**, *16*, 11-20.
90. Qian, J.; Law, C.K. Regimes of Coalescence and Separation in Particle Collision. Journal of Fluid Mechanics **1991**, *331*, 59-80.
91. Jiang, Y.J.; Umemura, A.; Law, C.K. An Experimental Investigation on the Collision Behaviour of Hydrocarbon Droplets. Journal of Fluid Mechanics **1992**, *234*, 171-190.
92. Estrade, J.P.; Carentz, H. Experimental Investigation of Dynamimc Binary Collision of Ethanol Droplets - A Model from Droplet Coalescence and Bouncing. International Journal of Heat and Fluid Flow **1999**, *20*, 486-491.
93. Munnannur, A.; Reitz, R.D. A New Predictive Model for Fragmenting and Non-fragmenting Binary Droplet Collisions. International Journal of Multiphase Flow **2007**, *33*, 873-896.
94. Rein, M.; Delplanque, J.P. The role of air entrainment on the outcome of drop impact on a solid surface. Acta Mechanica **2008**, *201*, 105-118.
95. Aziz, S.D.; Chandra S. Impact, recoil and splashing of molten metal droplets. International Journal of Heat and Mass Transfer **2000**, *43*, 2841-2857.
96. Mao, T.; Kuhn, D.; Tran, H. Spread and rebound of liquid droplets upon impact on flat surfaces. AICHE Journal **1997**, *43*, 2169-2179.
97. Mukherjee, S.; Abraham, J. Investigations of drop impact on dry walls with a lattice-Boltzmann model. Journal of Colloid and Interface Science **2007**, *312*, 341-354.
98. Park, H.; Yoon, S.S.; Jepsen, R.A.; Heister, S.D.; Kim, H.Y. Droplet bounce simulations and air pressure effects on the deformation of pre-impact droplets, using a boundary element method. Engineering Analysis with Boundary Elements **2008**, *21*, 21-31.
99. Chandra S.; Avedisian C.T. On the collision of a droplet with a solid surface. Proceedings of the Royal Society of London Series A-Mathematical and Physical Sciences **1991**,*432*, 13-41.
100. Healy, W.M.; Hartley, J.G.; Abdel-Khalik, S.I. Comparison between theoretical models and experimental data for the spreading of liquid droplets impacting a solid surface. International Journal of Heat and Mass Transfer **1996**, *39*, 3079-3082.
101. Ford, R.E.; Furmidge, C.G.L. Impact and spreading of spray drops on foliar surfaces. Society of Chemical Industry Monograph **1967**, *25*, 417.
102. Stow, C.D.; Hadfield, M.G. An experimental investigation of fluid flow resulting from the impact of a water drop with an unyielding dry surface. Proceedings of the Royal Society of London Series A-Mathematical and Physical Sciences **1981**, *373*, 419-441.
103. Yang, W.J. Theory on vaporization and combustion of liquid drops of pure substances and binary mixtures on heated surfaces. Institute of Space and Aeronautical Science University of Tokyo Rpt **1975**, *535*, 423-455.
104. Gong, S. Spreading of droplets impacting on smooth solid surface. Japanese Journal of Applied Physics **2005**, *44*, 3323-3324.
105. Sikalo, S.; Wilhelm, H.D.; Roisman, I.V.; Jakirlic, S.; Tropea, C. Dynamic contact angle of spreading droplets: experiments and simulations. Physics of Fluids **2005**, *17*, 062103.
106. Yarin, A.L.; Weiss, D.A. Impact of drops on solid surfaces: self-similar capillary waves, and splashing as a new type of kinematic discontinuity. Journal of Fluid Mechanics **1995**, *283*, 141-173.
107. Mundo, C.; Sommerfeld, M.; Tropea, C. Droplet-wall collisions: experimental studies of the deformation and breakup process. International Journal of Multiphase Flow **1995**, *21*, 151-173.
108. Cossali, G.E.; Coghe, A.; Marengo, M. The impact of a single drop on a wetted solid surface. Experiments in Fluids **1997**, *22*, 463-472.
109. Stow, C.D.; Stainer, R.D. The physical products of a splashing water drop. Journal of the Meteorological Society of Japan **1977**, *55* (5), 518-531.
110. Marmanis, H.; Thoroddsen, S.T. Scaling of the fingering pattern of an impacting drop. Physics of Fluids **1996**, *8*, 1344-1346.
111. Rioboo, R.; Tropea, C.; Marengo, M. Outcomes from a drop impact on solid surfaces. Atomization and Sprays **2001**, *11*, 155-165.

112. Xu, L.; Zhang, W.W.; Nagel, S.R. Drop splashing on a dry smooth surface. Physical Review Letters **2005**, *94*, 184505.
113. Xu, L. Liquid drop splashing on smooth, rough, and textured surfaces. Physical Review E **2007**, *75*, 056316.
114. Kalantari, D.; Tropea, C. Spray impact onto flat and rigid walls: empirical characterization and modeling. International Journal of Multiphase Flow **2007**, *33*, 525-544.
115. Roisman, I.V.; Horvat, K.; Tropea, C. Spray impact: rim transverse instability initiating fingering and splash, and description of a secondary spray, Physics of Fluids **2006**, *18*, 102104.
116. Mundo, C.; Sommerfeld, M.; Tropea, C. On the modeling of liquid sprays impinging on surfaces, Atomization and Sprays **1998**, 8, 625-652.
117. Range, K.; Feuillebois, F. Influence of surface roughness on liquid drop impact, Journal of Colloid and Interface Science **1998**, *203*, 16-30.

Oliveira, W.P., Souza, C.R.F., Kurozawa, L.E., Park, K.L. Spray drying of food and herbal products - Volume 1, Ed. Woo, M.W., Mujumdar, A.S. and Daud, W.R.W., **2010**, ISBN - 978-981-08-6270-1, Published in Singapore, pp. 113-156.

Spray drying of food and herbal products

Chapter 5

Oliveira W.P.[1], Souza C.R.F.[1], Kurozawa L.E.[2], Park K.J.[2]

[1] University of São Paulo/FCFRP, Ribeirão Preto, SP, Brazil
[2] University of Campinas/FEAGRI, Campinas, SP, Brazil

Contents **Page**

1.0 Introduction

Spray drying is a one-step processing operation for turning a liquid feed into a dried particulate form, by spraying the feed into a hot drying gas medium. While reduces the product bulk weight and size, spray drying minimizes handling and also preserves the product by reducing its water activity to a low level, required to stop bacterial degradation.[1,2] The production of dried particles from a liquid feed in a single processing step makes spray drying an exceptional and important process.

Spray drying is widely applied in several industrial sectors including the food, pharmaceutical and chemical. Several biological and thermal-sensitive materials, liquid materials, such as milk, fruit juices and pulps, herbal extracts, enzymes, essential oils, aromas and various pharmaceuticals have been dried by this process.[3,4] Its adequacy to process thermal-sensitive materials is mainly due to the short residence time of the product inside the dryer (in the order of a few seconds).

One of the most remarkable advantages of the spray drying is the capacity of process several kinds of materials and the possibility of obtain a dried product with pre-specified properties. These characteristics are particularly important when we are interested to obtain dried products of good quality and high content of healthy enhancing substances, such as the phenolic compounds, flavonoids, carotenoids and so on.

Nowadays, the consumers are very concerned in the attributed health benefits of the phytochemicals present in the so-called functional foods and nutraceuticals, including the herbal dried extracts.[5] Several terms have been used with similar meanings to these products, such as 'functional foods', medical foods, dietary supplements and health foods, but the term nutraceutical is more frequently used. Nutraceutical can be defined as a food or parts of foods that provide medical-health benefits including the prevention and/or treatment of disease. These products may vary from isolated nutrients, dietary supplements and diets to genetically engineered designed foods, functional foods, herbal products, and include processed foods such as cereals, soups and beverages.[6,7] The significantly growing interest of this market has forced the industries to improve the quality control of these products in order to guarantee the stability, efficacy and safety of the claimed health promoting substances.

In this chapter it will be presented some general aspects of the use of spray drying for drying of selected foods and herbal extracts and also for encapsulation of some plant derived products, including essential oils, flavors, plant pigments and oleoresins.

2.0 General aspects of spray drying

Drying is generally applied in nutraceutical processing, aiming the reduction of the product water activity to a safe level, which assures its microbial stability and minimizes physical and chemical changes during storage. Several drying systems can be employed for dehydration of foods and

nutraceuticals, including vacuum drying, convective drying, freeze drying, spout and fluidized bed dryers, and spray dryers. The selection of a particular equipment depends on the type and properties of the material to be processed as well as the desired product properties.

Spray drying is highly suitable for the continuous production of dry powders, granules or other agglomerated products from liquid pumpable feedings, such as solutions, suspensions and emulsions. The concept of spray drying is based on the high increase in the surface area of the contact area between the material to be dried and the drying medium promoted by the atomization. Different spray drying configurations exist, which varies in size and shape of the drying chamber, type of atomizing devices (rotary atomizers, pressure nozzles, pneumatic nozzles, ultrasonic devices and so on), air-droplet contact system (co-current, conter-current and mixed flow), and product collecting systems. Interesting reviews of the spray drying technique, focusing in hardware and process parameters as well as in current applications on pharmaceutical technology were presented by Krzysztof and Krzysztof.[8,9] The design of a spray drying process includes the establishment of operating conditions that increase product recovery and produce an end product of a pre-defined quality specification.[10] The short residence time of the product inside the dryer makes the spray drying suitable for the processing of themosensitive materials, including pharmaceuticals and biological materials. The spray drying is widely used in the preparation of dried powders from extracts of medicinal plants, fruit pulps, plants oleoresins, essential oils, and so on.[11-18]

The variables generally monitored during spray drying include the inlet and outlet drying gas temperature and humidity and the feed flow rate of drying gas and liquid material. These data can be used to predict and to improve the efficiency of the drying process, through performing mass and energy balances, statistical analysis and/or process simulations. The thermal efficiency is a parameter commonly used for process optimization. Higher thermal efficiencies are obtained when the temperature of the effluent gas are closer to their saturation temperature. However, in most situations the process is guided by the needs of product quality, instead of equipment efficiency.

In general, the moisture content of spray dried product is directly linked to the temperature of the gas leaving of the drying chamber. Lower moisture content can be obtained through the increasing in the outlet gas temperature and/or augmenting the product residence time inside drying chamber. The moisture content has effect on several properties of the dried product, such as product solubility and density.[19] However, the exposure of thermosensitive substances to high temperatures for long time periods can lead to product degradation. Thus, the control of the processing conditions are extremely important, since the product properties are dependent on the processing conditions used.[20] Thermosensitive products could be processed under low pressure and temperatures, and the production of particles relatively uniform and spherical with composition similar to the one present in the infeed can be achieve.[21]

3.0 Relevant physical-chemical properties

The physical-chemical properties of powders produced by spray drying depend on some process variables, such as the characteristics of the liquid feed (viscosity, flow rate) and of the drying air (temperature, pressure), as well as the type of atomizer. The knowledge and understanding of powder properties is essential to optimize processes, functionality, and reduce costs.[22] Properties of food powders can be classified as physical or chemical properties. Physical properties include the particle shape, density and porosity, surface characteristics, hardness, diameter and size. Chemical properties are related to the food composition and its interaction with others substances, such as water or components within the food structure. Instant properties and stickiness characterize certain processes like dissolution and caking powders, which are involved in different processing operations (agglomeration, drying, mixing and storing).

Bulk density and porosity

The knowledge of product density is of fundamental use for material properties studies and industrial processes in selecting storage, processing, packaging and distribution conditions. Bulk density includes the volume of the solids and liquids materials and all porous closed or open to the surrounding atmosphere, and generally is used to characterize a final product obtained by milling or drying.[22]

For packaging and shipping considerations, the knowledge of bulk density is very important, because this property shows how much material, by weight, will fit into a container. Lower bulk density of product is not interesting, resulting in a greater size of package. Moreover, the lower the bulk density, the more occluded air within the powders and, therefore, there was a greater possibility for product oxidation and reduced storage stability.[23,24] This volume fraction of air is indicated by the porosity, and, generally the internal, external and interparticle pores of food powders provide a high porosity (40 – 80%).[22]

Therefore, it is necessary to know the influence of variables on bulk density of a spray dried product. In general, this powder property can be increased with an increase in the feed rate, solid contents and outlet air temperature. On the other hand, it can be decreased with increase in inlet air temperature.[25]

Particle size

The particle size is one of the most important physical parameters of powders with regard to handling. Particle size can influence the flow out of storage bins, the blending of different components, compaction and the segregation of a mixture, in which smaller particles keep on distributed in the bottom and greater particles, in the top. In addition, this property significantly influences essential properties to food products such as smell, texture and appearance.[26] As particle size decreases, the increase in the particle surface area causes higher affinity with moisture and ability to agglomeration during the

drying process. Moreover, powders with reduced particles size present low solubility and flowability.[27]

Generally, in a spray drying system, the size of the dried particles depends on the size of the atomized droplets. The droplet size is affected by the atomization type, physical properties of the feed solution and feed solids concentration. Droplet size usually increases as the feed concentration or viscosity increases and the energy available for atomization decreases, resulting in the formation of greater particles.[19] During the drying of droplets, the drying rates can affect size of particles. Drying at conditions that result in faster drying rates (e.g. high air temperature) produces larger particles than drying under slower drying conditions.[24] When a particle is subjected to higher drying rates, there is a rapid formation of a dried layer surface. This hardening skin does not allow the particles shrinking during drying process, resulting in higher particles sizes.

Particle shape

Particle shape is an important physical property and can affect some factors, such as flowability of powder, packing and interaction with fluids.[22] In general, powders produced by spray drying present particles with spherical shape and several sizes. Spherical and smooth particles are desirable owing to aroma retention (least surface to volume ratios), highest bulk densities (best packing) and best flowability.[24] On the other hand, surface imperfections, such as wrinkle, cracks or collapses, occur when there is a slow film formation during drying of atomized droplets. The presence of dents has an adverse effect on the flow properties of particles powders.[29] Thus, process conditions that eliminate or minimize dent formation should be preferred. The shrinkage of the particles is related to the differences in the drying rate, which is higher for higher temperature, resulting in faster water evaporation and, consequently, causing formation of a smooth and hard crust.

Flowability

Powder flowability is a measure of the capacity of powders to be flow. This property is important in many units operations involving flow of powders, such as: pneumatic transport to other equipment or silos, mixing and packaging. The factors that influence powder flowability are: particle size (lower size, worse flowability, because there is more surface area or surface contact available for cohesive forces and frictional forces to resist flow); particle shape (surface imperfections, such as wrinkle, cracks or dents have an adverse effect on the flow properties of particles powders) and moisture content (high moisture content leads to poor flowability, due to the increase in liquid bridges and capillary forces acting between particles).[30]

Stickiness

Stickiness may be defined as the tendency of a product to adhere to a contact surface.[22] Spray drying and handling of sticky products is difficult, because the particles tend to sticky together and to the surface of materials they come to contact with, such as wall chamber dryer and cyclones.[31] This fact can lead to problems related to lower product recovery during spray drying, operating problems and powder caking. Stickiness in spray dried powders is attributed to

the rapid drying of the liquid feed droplets. There is a formation of amorphous particles, which have sticky properties.[32] Sticky powders are more hygroscopic and less free flowing than nonsticky powders. Some of the examples of sticky products are fruit and vegetable juice powders, honey powders and amorphous lactose powder.[33]

The problem of powder stickiness is mainly due to the low glass transition temperature (Tg) of the components with low molecular weight, such as some sugars (glucose, fructose, sucrose) and organic acids. The glass transition temperature is defined as the temperature at which an amorphous system changes from the glassy to the rubbery state. Molecular mobility in the glassy state is extremely slow, due to the high viscosity of the matrix (about 10^{12} Pa.s). The Tg can be taken as a reference parameter to project spray drying systems and characterize the properties, quality, stability and safety of food systems. Structural alterations, such as stickiness, agglomeration, caking and crystallization, occur in amorphous food powders when stored and processed at temperatures above the Tg. Since glass transition temperature increases with molecular weight, the addition of carriers agents (drying aids) has been used in the production of powders, reducing the stickiness and wall deposition in spray drying.[34,35]

Instant properties

Instant properties of spray dried food are related to ability of the powder to dissolve in water. Each particle must be wetted, sunk in the liquid and dissolved. Therefore, properties such as wettability, sinkability, dispersibility and solubility are of importance for the reconstitution of powders. Their definitions are:[4,22,25]

- *Wettability*: Capacity of particles powder to adsorbed water on their surface. Depends of particle size (higher size, lower incidence of clumping) and surface composition (presence of fat reduces wettability);
- *Sinkability*: Ability of powder to sink below the water surface after it has been wetted. This property depends on particle density (denser particles sink faster than light ones);
- *Dispersability*: Ability of powder to be distributed throughout the water, without formation of lumps;
- *Solubility*: This property refers to the rate and extent to which the components of powder particles dissolve in water. Depends of the chemical composition of powder and its physical state.

4.0 Quality changes during spray drying

Significant physical and chemical changes occur during drying of a liquid material. Since most foods, herbal extracts and other biomaterials have a complex composition these changes can not be described in a simple manner, and can continue to occur during the product storage. In general terms, drying is a process during which there is a transition of a viscoelastic or liquid material to a solid form. The dried material may be either a crystalline or an amorphous

solid.[36] Usually, amorphous behavior has been observed in spray dried materials.[37,38] A mechanism of formation of amorphous structures in dehydration and the relationships between equilibrium (solution, crystalline solid) and nonequilibrium (amorphous solid and liquid) states was proposed by Roos[39] and is presented in Figure 1. This phenomenon is known to be linked to glass transition temperatures and environmental conditions.[40]

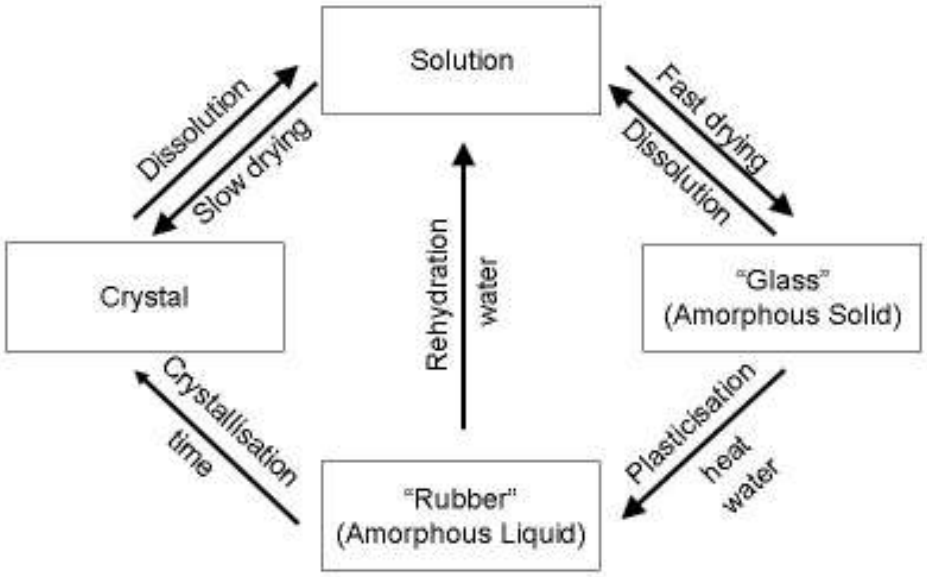

Figure 1 Formation of amorphous structures in dehydration and the relationships between equilibrium (solution, crystalline solid) and nonequilibrium (amorphous solid and liquid) states.[39]

During spray drying, the dehydration of atomized liquid occurs from the droplets surface to the inner core. There is an increase in the solutes concentration at particles surface and a consequently fall in the particle temperature caused by evaporation. The viscosity of this layer of concentrated solutes increases quickly and the particle surface passes to the glassy state before collide with other particles or with the dryer wall. The fast formation of glassy powders during spray drying reduces the cohesion/adhesion inter-particles and between particles and dryer wall, guaranteeing the free flow of the particles inside the drying chamber. At end of the process the product temperature and moisture content should be keep under restrict intervals, in order to maintain the powdered product at the glassy state.[39]

The temperature at which the transition from glassy to the rubbery state occurs is defined as the glass transition temperature, Tg. At temperatures higher than Tg, there are an increase in the mobility of the molecules present in the material, and with the increase in the moisture content due to water absorption, the material structure could collapse. The type of behavior depends on the material composition.[41] Herbal dried extracts and several fruit products show propensity to water absorption, which is mainly due to the presence of significant amounts of low molecular weight carbohydrates, such as fructose, glucose, and so on.[42] Thus, the increase in the moisture content could result in dissolution and/or recrystallization of these substances contributing for the physical

degradation of the product during storage.[41] These events can cause product *caking*. The *caking* is characterized by the powder solidification due to particle-particle interaction attributed to Van der Waals, capillary and electrostatic forces and can occur during stages of drying, packing and/or storage.

Losses and/or degradation of bioactive compounds are associated with the spray drying of herbal extracts and nutraceuticals, which depend on the processing stages involved and of the composition fed to the dryer (extractive solutions associated with drying adjuvants). These factors should be optimized in order to generate a product with concentration of marker compounds within specified intervals.

Drying aids (carriers or adjuvants) such as starches of corn, manioc and rice, modified starches, maltodextrins, silicon colloidal dioxide, acacia gum (gum arabic), cyclodextrins and solid corn syrups are frequently used aiming to minimize the losses of bioactive compounds (acting as encapsulating agent) and to improve or modify the physical and chemical product properties. The drying aids can be used alone or in associations, being the ideal composition established for each specific situation. A concise review of some drying aids frequently used for spray drying is presented following.

5.0 Drying aids

Drying aids are also known as drying carriers, drying adjuvants, and wall materials (in microencapsulation). The addition of drying carriers to the feed solution is important in the spray drying process, due to its influence on the powders properties and product stability. Carbohydrates of high molecular weight such as starch and modified starches, maltodextrins, solid corn syrups, gum arabic and cyclodextrins are in general used as drying carriers. One of the main function of the drying carriers is to increase the glass transition temperature of the product, reducing its stickiness and wall deposition in spray drying, and its agglomeration tendency during spray drying and storage, reducing product stickiness and generating a more stable product.[34,35,43] Following, different types of carrier agents used in spray drying of foods, herbal extracts and other nutraceuticals are described.

Starches and modified starches

Starch is one of the most common natural polymers, is cheap and has been commercially extracted from several sources, such as corn, tapioca, potato, wheat, rice and waxy maize. Starch consists of linear amylose and branched amylopectin, two polysaccharides based on α-(D)-glucose. Both polymers are organized in a semicrystalline structure, and in the starch granule, amylopectin forms the crystalline portion. The exact structure of starch is not yet fully understood. Starch is cold water insoluble and, when is mixed with water and heated, forms pastes with high viscosity.[44] One method used to modify starch is pyroconversion, in which the starch is heated, usually in the presence of acid or alkali. Partial hydrolysis of the starch takes place as well as repolymerization to form more highly branched polymers. The resulting product is the modified starches, which have higher cold water solubility and lower solution viscosity

than gelatinized native starch, and can be applied at concentrations up to 50 %, without substantial increase of the feed viscosity.[45]

Maltodextrins and solids corn syrup

Maltodextrins [$(C_6H_{10}O_5)_nH_2O$] are non-sweet saccharide polymers, obtained by acid or enzymatic hydrolysis of starch, consisting of D-glucose units linked primarily by α-1-4 bonds.[44] Hydrolysis of starch with acid or enzymes results in formation of maltodextrins. These products are usually classified according to their dextrose equivalency, DE.[44,46,47] Dextrose equivalent (DE) is a measure of the degree of starch polymer hydrolysis and is inversely related to its average molecular weight.[44] Maltodextrins with DE between 20 and 60 are generally denoted as solids corn syrup.

The glass transition temperatures of maltodextrins increase conversely with DE, ranging from 100 ^oC for maltodextrin with DE 36 to 188 ^oC for products with DE 5. Consequently, maltodextrins with low DE are mainly used as drying adjuvant in materials that are difficult to dry, such as sugar rich fruit juices, flavorings and sweeteners, in order to increase their glass transition temperature. Products spray dried with these materials as carrier agents are more free-flowing. The other advantages of maltodextrins solutions are: non-sweet, low viscosity at high solids ratio, excellent cold water solubility and low cost.[44,48]

Acacia gum (gum arabic)

Gum arabic is the dried gummy exudate obtained from the stems and branches of *Acacia senegal* (Linné) Willdenow or other species of Acacia (Fam. Leguminosae) that grow mainly in the Sudan and Senegal regions of Africa.[49] There are many acacia species but only few are able to provide the amount of gum required for industrial production. Chemically, gum arabic is a complex heteropolysaccharide with a highly ramified structure, with the main chain formed of D-galactopyranose units, linked by β-D glycosidic bonds (1$\rightarrow$3). The molecular weight of gum arabic ranges from 240000 to 580000. The side chains with variable chemical structure formed from D-galactopyranose, L-rhamnose, L-arabinofuranose and D-galacturonic acid are linked to the main chain β-(1$\rightarrow$6) bonds.[46] It has been used as an encapsulating agent in microencapsulation by spray drying, due to its good emulsifying capacity and low viscosity in aqueous solution. However, it is very expensive. Acacia is available as white or yellowish-white thin flakes, spheroidal tears, granules, powder, or spray dried powder. It is odorless and has a bland taste. Nowadays, there are a increasing need to find suitable substitutes for arabic gum, mainly due to unstable social and political conditions in the Sudan, the main supplier of acacia gum.[49,51]

Cyclodextrins

Cyclodextrins (CDs) are extensively used as solubilizing and stabilizing agent. Cyclodextrins are crystalline, nonhygroscopic, cyclic oligosaccharides obtained by enzymatic degradation of the starch due to the action of the enzyme cyclodextrin glycosiltransferase (CGT-ase). Among the most commonly used forms (α, β and γ-cyclodextrin, which have respectively 6, 7 and 8 glucose units, there are several cyclodextrin derivatives, such as dimethyl-β-cyclodextrin, 2-hydroxyethyl-β-cyclodextrin, and trimethyl-β-cyclodextrin.[49]

Cyclodextrins are 'bucketlike' or 'conelike' toroid molecules, with a rigid structure and a central cavity, which size depend on the cyclodextrin type. Due to the arrangement of hydroxyl groups within the molecule, the internal surface of the cavity is hydrophobic and the outside of the torus is hydrophilic, permiting the cyclodextrin to accommodate a guest molecule within the cavity, forming an inclusion complex. The formation of inclusion complex alters significantly the characteristics of the host molecule, changing its chemical reactivity, improving product solubility, fixing volatile substances, and stabilizing substances sensible to heat, light, and oxidation.[52-54]

The flip side of any CFD simulation is model validation, which is a big challenge in spray drying due to the harsh conditions within the chamber which make local measurements extremely difficult- even impossible. The task is further complicated with the presence of droplets or particles which might foul measurement equipments inserted into the chamber. This section aims to introduce the current validation method available and also some of the experimental data available for comparison.

6.0 Spray drying of selected food & herbal products

In this section is presented a revision about the drying of several foods and plant derived products, including fruit pulps, herbal extracts, natural colorants, and the microencapsulation of essential oils and oleoresins.

6.1 Fruit pulps

In tropical and subtropical countries, a large amount of fruits and vegetables are produced, which are very attractive from of commercial point of view. However, nowadays, changes in food consumption can be noted. Consumers have been looking for healthier and more natural foodstuffs in order to have a balanced and nutritious diet. In this context, consumers have been encouraged to increase their daily intake of fruits and vegetables since their nutritional value as sources of vitamins and minerals is recognized. However, in association with the seasonal shortages, most of these products present high water content, making them more susceptible to decomposition by microorganisms, to chemical and enzymatic reactions. These products are extremely perishable and it is difficult to be marketed or exported as fresh produce, and therefore has to be processed in order to improve their shelf life and prevent post-harvest losses.

In the last few decades, novel processed fruit products have been introduced onto the market. In order to be competitive and to provide more convenience, food safety, healthy benefits and sensory quality, food industry have been developed new products to satisfy emerging consumer demands and to increase profitability. Therefore, an increasing demand for fruit juices has been observed, but most of consumers do not have time to spend in preparing them, requiring ready-to-use or easy-to-prepare products.

Juices, nectars and frozen pulps are the principal products obtained from the fruits. Juices and nectars are costly to transport, because of their high volume, and frozen pulps require the additional cost related to an adequate cold chain. Juice powders are interesting exportation products, at the same time being cheap to transport and with a prolonged shelf life.

Fruit and vegetable powders provide a stable, natural, easy dosing ingredient which generally finds consumers in many foods and pharmaceutical products such as flavoring and coloring agents. Among the several drying methods, spray drying is a process widely used to produce fruit juices powders and involves both particle formation and drying, where the feed is transformed from the fluid state into droplets and then into dried particles, by spraying it continuously into a hot drying medium.[55]

However, fruit juice powders may have problems in their properties, such as stickiness and hygroscopicity, due to the presence of low molecular weight sugars and acids. These components are present in high proportion (90 % of dry substances) in juices and consist of different hydrocarbons such as monosaccharides (glucose, fructose), disaccharides (sucrose), polysaccharides and organics acids.[56] The Tg values of pure fructose, glucose and sucrose are 5, 31 and 62 °C, respectively, and, for pure malic, citric and tartaric acids, are 11.03, 15.73 and 20.57 °C, respectively.[35,57] These temperatures values are much lower than the normal operating temperatures in spray drying.[31] Thus, they can stick on the dryer chamber wall during drying, leading to low product yield and operating problems. Moreover, structural alterations, such as stickiness, agglomeration, caking and crystallization, occur in amorphous food powders when stored at temperatures above the Tg.[34,35,58-61]

Since the Tg increases with molecular weight, part of these problems can be solved by the addition of some carrier agents, like polymers and gums to the product before drying. The addition of these carrier agents reduces powder hygrocopicity and stickiness, increasing product recovery during spray drying.

Tonon et al.[62], working with spray drying of açai pulp (*Euterpe oleraceae* Mart.), observed that the increase on maltodextrin 10 DE concentration (10 to 30 %) caused a reduction on powder hygroscopicity (about 16 to 12.5 g of adsorbed water/100g solids) at inlet air temperature of 160 °C and feed flow rate of 15 g/min. Similar behavior was observed by Oliveira et al.[63] when studied the effect of drying aid (maltodextrin 10 DE and cashew tree gum) concentration on cashew apple juice powder hygroscopicity. Papadakis et al.[64] compared different average molecular weights of maltodextrin (6, 12 and 21 dextrose equivalent - DE) on the hygroscopicity of raisin juice powder. From their results, they concluded that as the DE decreased, the hygroscopicity increased, since the lower molecular weight maltodextrins contain shorter chains and more hydrophilic groups. Moreover, these authors verified that an increase in the maltodextrin concentration (from 33/67 to 50/50, raisin juice solids/maltodextrin solids ratio) resulted in an increase of the recovery of feed solids in the powder (43 to 73 %, 51 to 73 % and 56 to 74 % for maltodextrin with 21 DE, 12 DE and 6 DE, respectively), showing that the problem of stickiness in the drying chamber was overcome through the use of maltodextrin. During spray drying of lime juice, the stickiness problem was only overcome with the use of drying additives, mainly due to low glass transition temperature of the product.[56] To solve this problem and produce free-flowing powder, silicon dioxide and maltodextrin 5 DE

were used as drying carriers. Their investigation revealed that an addition of silicon dioxide and maltodextrin to lime juice (lime juice-soluble solids:additives ratio of 70/30) is the optimum amount for a complete and successful drying of this product. When the ratio was 80/20, the powders were produced but deposited on the cone wall and were a little sticky. Spray drying behavior of orange juice concentrate with several levels of maltodextrin 6 DE was studied by Shrestha et al.[61] The use of 50 % maltodextrin concentration did not help in spray drying of the orange juice (only 20 % powder was recovery) and its powder was sticky. The recovery of orange juice powder increased as the amount of maltodextrin in powders increased.

Besides reducing powders hygroscopicity, such agents, normally used for microencapsulation, can protect sensitive food components against unfavorable ambient conditions, mask or preserve flavors and aromas, reduce the volatility and reactivity and provide additional attractiveness for the merchandising of food products.[28] Spray drying of immature acerola juice, using maltodextrin 25 DE, gum arabic or a mixture of both as carrier agents, showed that these components offered equivalent contributions to the powder physical stability[66]. Oliveira et al.,[63] working with spray drying of cashew apple juice using maltodextrin and cashew tree gum as aid drying, observed that ascorbic acid retention was increased from 72 % to 95 % by increasing drying aid:juice ratio from 3 to 5.

Other alternatives can also be tried to reduce stickiness problems such as using appropriate outlet drying air temperature, introducing of cold air into the bottom part of the dryer, dehumidifying the drying gas or cooling of the dryer wall. Introduction of cooling air at the lower part of the dryer chamber results in the formation of a solid particle surface, reducing the stickiness of the powder particles. However, only a limited amount of air can be introduced because the cooling process will raise the air relative humidity, which can once again aggravate the situation.[43,67] Other authors have dehumidified the inlet air by taking it into an absorption air dryer.[68] This method reduced residue accumulation of tomato juice powder on the cone walls and allowed the product to be dried at lower outlet air temperatures. On other work, Goula and Adamopoulos[33] investigate the influence of maltodextrin addition on the stickiness during spray drying of tomato pulp in dehumidified air. The product recovery (80 – 90 %) obtained by these authors were much higher than those reported by others researchers, who added maltodextrins to sugar-rich foods. This difference, according to the authors, occurs due to the lower outlet air temperature and higher drying rates when dehumidified air is used. It was concluded that this combination (maltodextrin addition and use of dehumidified air) can be the solution of the wall depositions during spray drying of tomato pulp. An overview in the literature shows several other studies on spray drying of different kinds of fruit pulps. A resume of some studies are shown in Table 1.

Table 1 Selected studies on spray drying of fruit pulps

Pulp fruit	Spray drying conditions	Carrier agent	Ref.
Apricot, blackcurrant and raspberry	*Laboratory-scale spray dryer:* T_{in} = 130 - 200°C T_{out} = 75 –- 100°C $\dot{m}_{air}$ = 64 kg/min Evaporative capacity = 3.5 kg/h *Leaflash 100 spray dryer:* T_{in} = 160 - 250°C T_{out} = 90 - 100°C $\dot{m}_{air}$ = 83 kg/min Evaporative capacity = 7 kg/h	Maltodextrins 6 DE, 12 DE and 19 DE	[34]
Açai (*Euterpe oletaceae* Mart.)	*Laboratory scale spray dryer* T_{in} = 138 - 202°C T_{out} = 82 - 114°C $\dot{m}_{feed}$ = 5 - 25 g/min Atomization pressure = 0.06 MPa	Maltodextrin 10 DE	[62]
Apple	T_{in} = 150°C T_{out} = 65°C	Maltodextrin 6 DE	[31]
Bayberry (*Myrica rubra* Sieb. Et Zucc)	T_{in} = 140 - 160°C T_{out} = 65 - 85°C T_{feed} = 50°C $\dot{V}_{feed}$ = 30 ml/min	Maltodextrins 12 DE and 19 DE	[69]
Cactus pear (*Opuntia streptacantha*)	T_{in} = 205 and 225°C Atomization pressure = 0.1 and 0.2 MPa $\dot{V}_{feed}$ = 20 ml/min	Maltodextrins 10DE and 20DE	[70]
Cactus pear (*Opuntia ficus-indica*)	T_{in} = 165°C T_{out} = 90°C	Maltodextrin 18-20 DE	[71]
Camu-camu (*Myrciaria dúbia*)	T_{in} = 100 - 160°C T_{out} = 85°C $\dot{V}_{feed}$ = 25 - 30 ml/min	Arabic gum and maltodextrin 10DE	[72]
Cashew apple	T_{in} = 185°C T_{out} = 90°C $\dot{V}_{feed}$ = 840 ml/h	Maltodextrin 10DE and cashew tree gum	[63]
Durian (*Durio zibethinus*)	T_{in} = 160°C T_{out} = 85°C	Not used	[73]
Guava (*Psidium guajava* L.)	T_{in} = 160°C T_{out} = 80°C	Maltodextrins 9-12DE and 15-19.9DE	[74]
Immature acerola (*Malpighia emarginata*)	T_{in} = 120°C T_{out} = 80 - 82°C $\dot{V}_{feed}$ = 3 - 3.5×10^{-5} m^3/s	Gum Arabic and maltodextrin 25DE	[66,75]

to continue

continuation

Lime	T_{in} = 135 - 160°C T_{out} = 59 - 63°C $\dot{m}_{feed}$ = 3.7 kg/min T_{feed} = 25°C $\dot{m}_{air}$ = 317 kg/h Atomizer speed = 5.000 rpm	Maltodextrin 5 DE and silicon dioxide	[56]
Mango	T_{in} = 160°C T_{out} = 70 - 75°C $\dot{V}_{feed}$ = 10 ml/min $\dot{V}_{air}$ = 0.7 m^3/min	Maltodextrin 20 DE, gum Arabic and starch waxy	[76]
Orange	T_{in} = 110 - 190°C $\dot{V}_{feed}$ = 150 - 450 ml/min Atomizer speed = 10.000 – 25.000 rpm	Maltodextrin, liquid glucose and methylcellulose	[77]
	T_{in} = 160°C $\dot{V}_{feed}$ variable to maintain T_{out} of 65°C T_{feed} = 50°C Atomizer speed = 20.000 rpm	Maltodextrin 6DE	[65]
Pineapple	T_{in} = 190°C T_{out} = 90°C $\dot{m}_{feed}$ = 0.18 kg/min Atomizer speed = 25.000 - 35.000 rpm	Maltodextrin 10DE	[78]
	T_{in} = 150°C T_{out} = 65°C Atomizer speed = 20.000 rpm	Maltodextrin 6DE	[67]
Pomegranate (*Punica granatum* L.)	T_{in} = 130°C T_{feed} = 20°C $\dot{V}_{air}$ = 600 L/h	Maltodextrins 10DE, gum Arabic, waxy starch and microcrystalline cellulose	[79]
Raisin	T_{in} = 110 - 200°C T_{out} = 86 - 115°C $\dot{V}_{feed}$ = 8.2 - 15 ml/min Atomizer speed = 10.000 - 25.000 rpm	Maltodextrins 6DE, 12DE and 21DE	[64]
Tomato	T_{in} = 130 - 150°C T_{feed} = 32°C $\dot{m}_{feed}$ = 1.75 g/min $\dot{V}_{air}$ = 22.75 m^3/h	Maltodextrins 6DE, 12DE and 21DE	[33]
	T_{in} = 110 - 140°C T_{feed} = 32°C $\dot{m}_{feed}$ = 1.75 g/min $\dot{V}_{air}$ = 17.50 and 22.75 m^3/h $\dot{V}_{compressed\ air}$ = 500 - 800 L/h	Not used	[19,68,80,81]
	T_{in} = 130 - 160°C $\dot{V}_{feed}$ = 8 - 16 ml/min $\dot{V}_{air}$ = 630 - 800 cm^3/s Atomizer speed = 25.000 - 35.000 rpm	Not used	[82]
Watermelon (*Citrulus lanatus*)	T_{in} = 145 - 175°C T_{feed} = 20°C	Maltodextrin 10DE	[83]

6.2 Herbal extracts and nutraceuticals

Vegetable materials are the source of many phytochemicals compounds, many of which with proved healthy enhancing and therapeutic properties. Depending on the region, these plant derived products can be classified by using several terms such as botanicals, functional foods, nutraceuticals, medical food, dietary supplements and health foods. The food companies favored the term functional foods and nutritional foods, approaching the discussion from a nutritional concept. In the other hand, the pharmaceuticals companies prefer medical foods, nutraceuticals, and functional foods, and approach the topic from a medicinal point of view. The term nutraceutical, resulted from the combination of the words “nutrition” and “pharmaceutical” is widely used. This discussion falls outside of the scope of this chapter, but is well covered in the recent literature.[6,84]

Phytochemicals are secondary metabolites synthesized by plants including carotenoids, phenolics, alkaloids, terpenes, sterols, saponins, nitrogen-containing compounds, and organosulfur compounds.[85] Secondary metabolites are organic substances not directly essential for the normal plant life, but are but may be useful for the plant as a whole. Phenolics and carotenoids are the most studied phytochemicals, and involve substances as phenolic acids, flavonoids, stilbenes, coumarins, tannins, lycopene, curcumin, β-carotene, lutein, and so on. Several of these compounds can exhibit potent biological properties such as antioxidant, antimicrobial, anti-inflammatory, and anti-tumoral, which are promising to be exploited in the pharmaceutical, food and cosmetics industries. Polyphenols are found in many dietary plant products, including fruits, vegetables, beverages, herbs, and spices.[86]

In the last few decades, the world demand for plant derived products has increased significantly. The phenomenal growth in the use of phytochemicals as functional and nutraceutical foods has forced the food and pharmaceutical industry to control the quality of those claiming to be health promoting ingredients in terms of efficacy and safe.[87]

Nowadays, the herbal and nutraceutical processing sectors are moving more and more toward commercialization of standardized extracts, or dried extract that is manufactured to a specified phytochemical concentration (also known as marker concentration). Thus, the production of standardized dried extracts represents a field in expansion, since the current tendency of the pharmaceutical industry is the substitution of traditional fluid forms by dry plants extracts. Among the reasons in favor of this tendency, the following should be highlighted: greater concentration, stability and easy of standardization of the bioactive compounds; ease of transportation; reduced space required for product storage; and lower risk of microbial contamination.

Herbal dried extracts are much better adapted to the demands of modern therapeutic practice, given the ease of standardization and handling, which contribute to guaranteeing the homogeneity of pharmaceutical preparations. In the pharmaceutical sector, dried extracts are used in the preparation of pills, capsules, granulates, ointments and as intermediary products. Dried extracts can be prepared from the dehydration of a concentrated extractive solution from

herbal materials (leaves, roots, seeds, whole plant, inflorescence, fruits, etc.), resulting in a dried powder. Several drying techniques can be used including freeze-drying, spray drying and spouted bed drying.[89-97] Nevertheless, the operating conditions used in the drying and thermal processing of bioproducts like herbal dried extracts and nutraceuticals, might have a considerable impact on the properties and cost of the product, generating different degrees of loss of active compounds.[87, 96]

Spray dryers are traditionally used in the herbal processing industries. This equipment is widely used in industrial processes involving the generation and drying of small liquid droplets. Dry fine powders, granulates or agglomerates can be continually produced by the drying of solutions, emulsions or suspensions. The spray drying process basically consists of the atomization of a diluted solid-fluid mixture in a heated gaseous current that promotes solvent evaporation, leading to a dry product. The quality of the powder obtained depends on the processing variables and operating conditions used. The final moisture content, solubility and apparent density are of fundamental importance. In general, the products obtained by spray drying are more soluble and concentrated.[4]

Since most of the dried extracts and nutraceuticals are intended for oral administration, there are acceptable limits of bacterial contamination. Remili et al.[98] studied the microbial contamination of spray dried extracts of medicinal plants and the process effects on product quality. The authors reported that, qualitatively, the spray dried extracts present low microbial contamination. However, the total viable bacterial content remained relatively high, exceeding 10^3 CFU/g (colony-forming units per gram) in 35 out of 82 of the samples analyzed.

The occurrence of stickiness (adhesion or cohesion) is a common problem during drying of herbal extracts. This issue has been extensively investigated for foodstuffs and occurs more frequently for materials with a high concentration of sugars.[40] Medicinal plant extracts in general contains higher amounts of sugars, carbohydrates and organic acids.[42] Due to the significant presence of reducing sugars, the addition of drying aids to the extractive solution before drying is almost mandatory, in order to improve the product properties and drying performance. The drying aids should have chemical inertia, innocuously, and thermal stability.[89] Drying aids that are widely used in the dehydration process of herbal extracts include: corn, cassava and rice starches, modified starches, maltodextrins, colloidal silica, gum arabic, cyclodextrins, and κ-carrageenan. These compounds can be used for drying processes alone or in association, such that the ideal proportions should be established for each specific case, both in terms of the extract composition and drying method used.

De Paula et al.[99] studied three combinations of drying aids, namely colloidal silicon dioxide alone, and its combination with microcrystalline cellulose and β-cyclodextrin at 1:1 ratio during the production of spray dried extracts of *Achyrocline satureioides* (marcela). Twenty percent of polysorbate 80 plus 80 % of drying aid relative to solid contents were added to 80 mL of water and homogenized under magnetic stirring. Then, 100 g of extractive solution were added to the drying aid suspension and the resulting formulations were concentrated under reduced pressure at temperature lower than 50 ^{o}C until 40 % of the initial mass of the extractive solution. The masses of the concentrated

extracts were completed with distilled water to 50 g, and spray dried in a Büchi mini spray dryer at a feed flow rate of extractive solution of 3.0 mL/min, and inlet and outlet temperatures of drying gas of 150 – 160 ^{o}C and 95 – 96 ^{o}C, respectively. The powdered extracts were incorporated in an ointment base, and it was evaluated the effects of the drying aids used on ointment properties such as spreadibility, oleosity index, viscosity, and pH. Although all compositions evaluated maintained its plastic behavior, the drying aids showed effects on the physical parameters at different levels. The use of colloidal silicon dioxide alone promoted a small oleosity index and an intermediary spreadibility. The substitution of part of the colloidal silicon dioxide by microcrystalline cellulose or β-cyclodextrin increased the oleosity index and improved the ointment spreadibility.

Gum arabic and aerosil® 200 were evaluated as drying aid for preparation of spray dried extracts of *Fraxinus excelsior*.[101] The liquid extracts were obtained by steeping 570 g of dried leaves in 10 L of boiling water (E1) or 710 g of dried leaves in 10 L of boiling 70 % ethyl alcohol (E2) for 1 h, followed by filtration. The aqueous extract was spray dried in presence of 88 g (dry weight) of gum arabic, and the alcoholic extract in presence of 80 g (dry weight) of Aerosil 200. The spray drying was carried out in a Niro Atomizer (type Minor), with turbine drive and countercurrent flow regime at inlet temperature of the drying gas of 130 – 140 ^{o}C, and outlet drying gas temperature of 65 – 70 ^{o}C. The dried product showed physicochemical, organoleptic and pharmacological properties good enough to qualify them as useful medicinal products. The product obtained from the hydroalcoholic extract appeared to be superior compared to the originated from the aqueous extract. Thin-layer chromatograms showed no effect of the spray drying on marker compounds present in the extractive solutions. The addition of drying aids improved the product shelf life.

An evaluation of the spray drying performance and product properties during spray drying of *Bauhinia forficata* Link extracts was presented by Souza and Oliveira.[101] The extractive solution was obtained from dried and powdered *Bauhinia forficata* leaves placed in contact with an ethanol:water solution (70:30 in weight) at temperature of 50 ^{o}C. The extraction time was 1 h at the stirring rate of 200 rpm. The extract was filtered under vacuum and concentrated three times in a rotary evaporator (vacuum pressure of 600 mmHg and 50 ^{o}C), and its density, solids concentration, alcohol, and total flavonoid contents were determined. The concentrated extractive solution were added with 80 % of colloidal silicon dioxide (Tixosil® 333, related to solid contents), and submitted to drying in a SD-05 spray dryer (Lab-plant, Huddersfield, UK). The spray drying variables were: the inlet gas temperature (80 and 150 ^{o}C), the ratio of the mass feed flow rate of the concentrated extract to the evaporation capacity of the dryer (15, 45, 75, and 100 %), and the feed flow rate of the drying gas (0.0118, 0.0168, and 0.0227 kg/s). The atomizing air feed flow rate was fixed at 15 L/min at a pressure of 1 bar. Significant impact of the spray drying conditions on product properties and on dryer performance during production of standardized dried extract of *Bauhinia forficata* was observed, confirming the real need for more research focused on this theme. In general, the drying conditions that give an end product with the desired specification are not linked with the optimal dryer performance. Therefore, product quality and system behavior should be

taken in account simultaneously during optimization of drying conditions for production of dried extracts of medicinal plants.

A comparison of the spray and spouted-bed dryer performance and the physicochemical product properties during drying of hydro-alcoholic extracts of three plants used in the Brazilian traditional medicine: *Passiflora alata*, *Bauhinia forficata*, and *Maytenus ilicifolia* was present by Oliveira et al.[102] Extractive solutions from the three plants studied, were obtained by placing dried and milled plant leaves in contact with ethanol:water mixtures for 1 hour. The ratio between plant to solvent mass were at at 1:5 for *Bauhinia forficata* and *Passiflora alata*, and 1:6 for *Maytenus ilicifolia*. The extraction temperatures were respectively 50, 70 and 60 ^{o}C. The extractive solutions were filtered vacuum filtration system and concentrated in a rotary evaporator (vacuum pressure of 600 mmHg and 50 ^{o}C) until to achieve a solid contents of 9 %. Colloidal silicon dioxide (Tixosil® 333, Rhodia, São Paulo, Brazil) was added to the concentrated extracts before the drying to improve the process performance (40 % of the solid contents for the extracts of *Passiflora alata* and *Maytenus ilicifolia* and 80 % for the *Bauhinia forficata* extract). The final compositions were submitted spray and spouted bed drying at optimized processing conditions. The spouted bed gave an end product with higher concentration of the chemical markers and lower moisture content compared to the spray dried product; even both processes working at similar relation liquid to drying gas ratio and inlet gas temperatures. Both dryers produced free-flowing polydisperse powdered particles within a limited range (0 to 30 μm). The spouted bed leads to the formation of irregular particles with flake shapes, whereas a high proportion of near rounded particles were obtained in the spray dryer.

The literature shows several other examples of the spray drying of herbal extracts of several plant species.[103-109] Table 2 presents a brief review of some studies reported. The losses of volatile compounds (ex. flavors and essential oils) are another problem that could occur during the drying of herbal extracts, mainly derived from aromatic plants. High losses of total phenol and flavonoid contents were observed during spray and spouted bed drying of *Rosmarinus officinalis* extracts added with a blend of colloidal silicon dioxide (Tixosil 333®) and maltodextrin DE 14 at a 40:20 ratio (related to the solid contents in the extract).[110] In these situations, the correct selection of drying adjuvants associated to microencapsulation techniques are valuable tools in the minimization the losses of volatiles during dehydration of extracts from aromatic plants. Some aspects of the microencapsulation of essential oils, flavors and oleoresins during spray drying will be covered in the next section.

Table 2 Selected studies on spray drying of herbal exrtacts

Material	Spray drying parameters	Drying carriers	Main findings	Ref.
Pinneaple stem extract	Lab-Plant SD-05 T_{in} = 70, 110 and 150 °C $\dot{V}_{feed} / \dot{V}_{max}$ = 24, 36 and 48 % $\dot{m}_{air}$ = 0.0227 kg/s P_{at} = 2 kgf/cm^2 $\dot{V}_{at}$ = 1.20 m^3/h Cs = 11.46 % m/m	Maltodextrin (DE14) at proportions of 60 to 100 % relative to solids content in the crude extract.	Significant effects of the processing parameters on the retention of the proteolytic activity of the powdered extract were observed. High processing temperatures lead to a product with a smaller moisture content, particle size and lower agglomerating tendency. A product with insignificant losses of the proteolytic activity (≈ 10 %) and low moisture content (less than 6.5 %) is obtained at selected drying conditions.	[105]
Soybean extract	Lab-Plant SD-05 T_{in} = 80, 115 and 150 °C $\dot{m}_{feed}$ = 240. g/h $\dot{m}_{air}$ = 0.0227 kg/s $\dot{V}_{at}$ = 0.90 m^3/h P_{at} = 1 bar Cs = 25.0 % m/m	Colloidal silicon dioxide (Tixosil 333® Rhodia), maltodextrin and starch, 2.5 % relative to the solids content in the extract.	The correct choice of drying adjuvant has significant impact on spray dried soybean extract properties. The product using colloidal silicon dioxide as carrier showed high polyphenol, genistein contents and antioxidant activity. The chemical and antioxidant activities of spray dried product showed to be affected by the drying temperature. High losses on total polyphenol (67 %) and genistein (75 %) compared to the initial contents were observed.	[106]
Lippia sidoides extract	Lab-Plant SD-05 T_{in} = 140 - 160 °C P_{at} = 5 kgf/cm^2 $\dot{V}_{feed}$ = 240. mL/h Cs = 20 % m/m T_{feed} = 50 °C	Maltodextrin DE10 and gum arabic in different proportions (4:1, 3:2, 2:3, 0:1) (m/m)	Dried extracts showed average particle sizes ranged from 7.8 to 10.6 μm, regular and spherical morphology and moisture content between 7.8 and 9.4 %. Thymol retentions from 70.2 to 84.2 % (in relation to liquid extract) were observed. Higher thymol retention was related to increase of gum arabic ratio. *Lippia sidoides* extractive solutions and dried extracts showed antifungal activity, indicating their potential as a natural product for medicinal or even cosmetic purposes.	[107]
Radix salvia	Büchi B-290 mini-spray dryer T_{in} = 70, 80 and 90 °C T_{out} = 44 to 62 °C $\dot{V}_{feed}$ = 3.0, 3.5 and 4.0 mL/min	Gelatin and sodium salt of carboxy-methyl-cellulose at different proportions. Relation between core and wall material varied from 1/2 to 1/6.	The results showed that spray-dried microcapsules had a regular spherical shape but the majority presented rough surfaces or invaginations with a diameter of 2-5 μm. *R. salvia* miltiorrhiza nanoparticles were embedded in the wall system consisting of gelatin and CMC-Na. Higher encapsulation yield and encapsulation efficiency were obtained under the inlet temperature of 80 °C and the ratio between core:wall material of 1/4. In vitro release study showed that *R. salvia* miltiorrhiza microcapsules could regulate drug release of bioactive compounds.	[108]

6.3 Microencapsulation of essential oils, flavour and oleoresins

Many plants derived products of commercial interest, particularly in the food and pharmaceutical industries, contain high amount of volatile and/or thermosensitive compounds, susceptible to oxidation and often occur in liquid form under normal environmental conditions. These substances can undergo irreversible alterations in their physicochemical properties when exposed to contact with other materials or external agents without adequate protection. The microencapsulation technology is a method that can be applied to transform these substances into more stable materials (lower volatility and less susceptibility to oxidation) providing easy handling (solid form).

Microcapsules incorporate new properties into active substances, as well as improve the quality of the final product. Encapsulation is applied in several industrial sectors, such as food, pharmaceutical, chemical and agricultural. Examples of application involve the microencapsulation of essential oils, vitamins, mineral salts, colorants, enzymes, hormones and chemotherapy drugs.

Microencapsulation can be defined as a process where a continuous thin coating is formed around solid particles, liquid drops, or gas cell that are fully contained within the capsule wall.[111] The coating is denominated as wall material, coating material, carrier, encapsulation or matricial agent. The coated material is called active or core material.[112]

The term microparticles is widely used, including the microcapsules and microspheres. In the microcapsules, the core material is concentrated near the center of the microcapsule, and coated by a continuous film of the coating material, while in the microspheres the active material is uniformly dispersed through the matrix.[28,112,113]

The microparticles properties depend on the encapsulation method and physical and chemical properties of the core and wall materials. Therefore, the capsules can present as amorphous or crystalline materials, having compact or porous structures, with spherical or irregular shapes, and size varying from micrometers to millimeters.[113-115]

The retention of bioactive and volatile compounds is directly linked to factors related with the chemical properties of the core and wall materials such as molecular weight, polarity and relative volatility, chemical structure, proportion core/wall material, and so on. The end use of the microencapsulated product also affects the selection of the encapsulation method and encapsulation materials. The spray drying is the method commonly used for microencapsulation. The main process variables are the composition of the encapsulation formulation, the inlet and outlet drying air temperatures, the gas flow rate, the distribution of temperature and humidity inside the dryer, the residence time, and the geometry of the drying chamber.[115] In general, matricial microparticles are generated by spray drying, in which the core (active material) is distributed in a matrix of the wall material.[111]

The encapsulation system is designed to protect the active product from factors that cause their deterioration, reducing the possibility of interaction between the nucleous and other compounds of the formulation, losses caused by volatilization and to permit the controlled release under defined conditions .[112-114]. The diversity of wall materials permits the obtaining products with the desired functional properties. Wall materials can be selected from a wide variety of natural or synthetic polymers, depending of the material to be encapsulated and the desired product properties. Several types of materials can be used: polysaccharide derivatives of cellulose, such as carboxymethyl cellulose, methylcellulose, hydroxypropyl cellulose, hydroxymethylcellulose phthalate and cellulose acetate phthalate; polysaccharides not derived from cellulose, such as alginates, chitosan, gum arabic, maltodextrin and modified starch; derivatives of acrylic/methacrylic acid; derivates of polylactic/polyglycolic acid; and non-polymeric materials, such as vegetable fats, sugars, organic acids and hydrogenated vegetable oils.[3,47] It is desired that the wall material show good emulsifying and film-forming properties, be easy to dry (permeable to the solvent system used), low viscosity at high solid concentrations, chemically inert, and so on.[112,113] The water solubility is also a factor to be considered, since aqueous feedings are more commonly used.[116]

The main wall materials used in the encapsulation of volatile materials can be divided in four groups, namely mono and disaccharides, the gums (acacia, gum agar, sodium alginate), hydrolyzed starches (maltodextrins and solid corn syrup), and chemically modified starches.[114,117,118] In general, wall materials that are effective emulsifiers and/or film formers yield better volatile retention than materials that do not present these characteristics.[28,47,112,113] Since most wall materials do not present these properties together, blends of distinct wall materials are frequently used to enhance microencapsulation efficiency.[119,120] Gum arabic provides very good volatile retention during spray drying. Maltodextrin is a good compromise between cost and effectiveness because of its low viscosity at a high solid ratio. However, its major shortcomings are the lack of emulsifying capacity and low retention of volatile compounds.

There are correlation between the maltodextrin dextrose equivalency number (DE) and the retention of aromatic compounds during spray drying microencapsultation. Bangs and Reineccius[121] reported a decrease in the retention capacity with increasing DE from 10 to 36.5. However, Yoshii et al.[122] observed higher retention of volatile compounds during storage with the increase in DE. Anandaraman and Reineccius[123] verified that maltodextrins with higher DE showed superior protective effect against oxidation on the encapsulated orange oil. Thus, the effect of maltodextrin DE on the microencapsulation process depends on the evaluated properties.

Blends between gum arabic, maltodextrin and modified starch are known to give a better encapsulation efficiency and stability than gum arabic alone.[120] Sankarikutty et al.[124] evaluated the effect of different proportions maltodextrin: gum arabic on the spray drying microencapsulation of cardamom oil, and found the best result for the 1:2.3 ratio. Bhandari et al.[125] showed good retention levels during spray drying microencapsulation of citral and of the lynalil acetate

in mixtures of gum arabic and maltodextrins at different ratios. The feed emulsions at solid concentrations of 50 % were spray dried in a Leaflash system at temperatures ranging from 300 to 400 °C. The volatile retention showed a tendency to increase with the proportion of arabic gum.

Vaidya et al.[120] investigated the effects of binary and ternary blends of gum arabic, maltodextrin (DE-18) and modified starch (HI-CAP 100) on the content and stability of volatiles during microencapsulation of cinnamon oleoresin by spray drying. The feed emulsions at 30 % of wall material and 10 % of cinnamon oleoresin (based on wall material) were spray dried in a JISL LSD-48 mini spray dryer, at inlet and outlet drying temperatures of 160 ± 2 and 120 ± 5 °C, respectively. The feed flow rate of emulsion was 300 g/h and the atomizing pressure of 3 bars. Results indicated gum arabic as the better wall material for encapsulation of cinnamon oleoresin, compared to the others carriers, when used alone. A 4:1:1 blend of gum arabic:maltodextrin:modified starch offered better protection than the pure gum arabic and other blends evaluated.

The effects of different mixtures between maltodextrin and gum arabic (4:1, 3:2, 2:3, 0:1 m/m) on the spray drying encapsulation of *Lippia sidoides* essential oil were evaluated by Fernandes et al.[119] Content of essential oil related to wall material were 20 and 25 % in weight. The feed emulsions having solid concentrations from 30 to 60 % m/m were spray dried in a Lab-Plant SD-05 spray dryer, at inlet drying temperatures of 140 to 160 °C, feed flow rate of 15 % of the maximum evaporation capacity, and atomizing pressure of 5 kgf/cm^2. The best thermal efficiency and powder recovery were found at 160 °C. The best encapsulation efficiency was related to experimental parameters as follow: solid content of the encapsulating composition of 50 % (m/m), maltodextrin:gum arabic ratio of 0:1 (m/m) and wall material:essential oil ratio of 4:1 (m/m), giving an optimal thymol retention of 12.8 mg/100 mg of microcapsules.

Several other materials have been tested to encapsulate volatile compounds, such as mesquite gum,[126] blends of maltodextrin (DE 16-20) and whey protein/or modified starch/or small molecule surfactant,[127] skimmed milk powder and whey protein concentrate[128] and the entrapment in cyclodextrins.[119,129] Beristain et al.[126] evaluated the ability of mesquite (*Prosopis juliflora*) gum to act as an encapsulating agent for the production of spray dried emulsions of cardamom (*Elettaria cardamomum*) essential oil. Emulsions containing oil:gum ratios of 1:5, 1:4 and 1:3 w/w were prepared by homogenizing 300 g of mesquite gum/kg in deionized water with the essential oil. The emulsions were spray dried in a Büchi-190 mini spray dryer, at inlet and outlet drying temperatures of 200 ± 5 and 110 ± 5 °C, respectively. Results showed the feasibility of spray drying microencapsulation of cardamom oil using mesquite gum as wall material. High flavour retention efficiency (83.6 %) was obtained when a ratio 4:1 gum:essential oil was used, confirming the good emulsifying and encapsulation properties of mesquite gum, as an alternative encapsulating material.

Jafari et al.[127] used blends of maltodextrin (DE 16-20) and whey protein/or modified starch/or small molecule surfactant (Tween 20) to encapsulated nanoparticles of d-limonene by spray drying. Pre-emulsions having 40 % of solid contents (30 % of maltodextrin and 10 % of emulsifiers) were prepared and the core material at proportion of 1:4 core:wall material were continuously added to the continuous phase and stirred for 10 minutes. Then, the pre-emulsions were further emulsified by microfluidization or ultrasound, and then submitted to spray drying in a pilot plant spray dryer (model SL 20, Au), at inlet and oultlet drying temperatures of 180 and 65 °C, respectively, and atomizing pressure of 300 kPa. Emulsions obtained by microfluidization technique showed the highest d-limonene retention, and presented good processing stability. Biopolymers as HI-CAP and whey protein concentrate are more efficient than small molecules surfactants, like tween 20.

Baranauskiene et al.[128] used skimmed milk powder (SMP) and whey protein concentrate (WPC) to encapsulate essential oil of oregano, and aroma extracts of citronella and sweet marjoram by spray drying. Solutions containing 30 % of solids were prepared by reconstituting and dispersing the wall materials in deionized water at 40 ^{o}C, and after cooling were mixed overnight to enhance hydration. The essential oil at 1:4 ratio relative to wall materials was emulsified into hydrated material and submitted to spray drying in an A/S Niro Atomizer, at inlet and outlet drying temperatures of 190 ± 5 and 90 ± 5 °C, atomizer wheel speed of 30 - 40 rps. The percentage of flavoring entrapped into the microcapsules varied from 54.3 % (marjoram in WPC) to 80.2 % (oregano in SMP). Changes in the composition of individual flavor compounds and the content of flavoring remaining on the surface of microparticles during encapsulation in SMP and WPC matrixes were remarkably lower for encapsulated oregano essential oil. The scanning electron microscopy and particle size analysis revealed that microcapsules were well-formed spherically shaped particles. SMP coated products had smoother surface as compared to WPC, which contain more dents and wrinkles on the capsule surface. Particle size varied from 6 to 280 μm for SMP and from 2 to 556 μm for WPC microencapsulated products.

Cyclodextrins have also been successfully used to form inclusion complexes with essential oils using spray drying. Fernandes et al.[107] investigated the formation of inclusion complexes of *Lippia sidoides* essential oil in β-cyclodextrin by spray drying. The β-cyclodextrin slurry containing 50 % of solid (m/m on the wet basis) was prepared by blending the β-cyclodextrin powder in warm distilled water at 50 °C under continuous stirring with a magnetic bar. *Lippia sidoides* essential oil was added to the slurry to reach 3 different essential oil: β-cyclodextrin ratios (1:10; 1.33:10 and 2:10). The slurry was cooled down to room temperature and left for 12 h under agitation to reach the equilibrium condition. The slurry was fed to a bench-top spray dryer (Lab-Plant SD-05, Huddersfield, U.K.), at inlet drying temperature of 160 ^{o}C, at a flow rate of 15 % of the maximum evaporation capacity at 50 ^{o}C at atomizing pressure of 5 kgf/cm^2, and air flow rate of 60 m^3/h. Thermoanalytical techniques (TG, EGD, TG-MS) were used to support the formation of inclusion complex

and to examine their physicochemical properties after accelerated storage conditions (RH of 66.09 % at 40 °C). The results showed that inclusion complex of β-cyclodextrin:essential oil microparticles was successfully produced by spray drying. The optimum ratio between β-cyclodextrin:essencial oil with regard to the total oil retention and thermal stability of the product was 1:10. The thermal properties of the complexes were influenced by the different essential oil/β-cyclodextrin ratio and also by the storage conditions.

Lemon oil was successfully encapsulated by kneading with β-cyclodextrin at a ratio of lemon oil to β-cyclodextrin of 88:12 (w/w).[125] The resulting paste at ≈ 18 % solids content was submitted to vacuum or spray drying. The spray drying was carried out in an APV Lab I Spray dryer, at inlet and outlet temperatures of 160 and 60 °C, respectively. Volatile composition was monitored periodically and no significant difference was found, irrespective of kneading time or drying method used. An optimum mixing time was found to be 15 min, giving an encapsulation of lemon oil of 97.7 mg/g of β-cyclodextrin in the complex powder. Several other examples of the use of spray drying for microencapsulation of volatile materials using several wall materials are presented in Table 3.

6.4 Natural colorants and coloring extracts

Some vegetal materials have valuable applications as source of natural dyes and coloring extracts aiming to replace artificial dyes due to legislation restrictions and consumers preferences.[15,135] Substances as anthocyanins and carotenoids are commonly used as natural colorants in food, cosmetics and animal feed.[136] These substances have also beneficial effects to human healthy and have low toxicity. Carotenoids comprise a large class of natural plant pigments having important biological activities. Among carotenoids commonly found in vegetables and fruits, and detectable in human plasma, are α-carotene, β-carotene, γ-carotene, lycopene, lutein, zeaxanthin, and β-cryptoxanthin. The carotenoids are largely used as food additives, and are recommended due to their pro-A vitamin content and antioxidant activity.[135] Carotenoids can be divided into carotenes containing only carbon and hydrogen, and xanthophylls made up of carbon, hydrogen, and oxygen. Pigments are rather unstable because they strongly absorb light and are highly unsaturated molecules and present low water solubility.[137] The most applied alternative to increase stability of carotenoids and to allow their incorporation in hydrophilic environment is the microencapsulation technique, which provides a physical barrier protecting the pigment. Among the available microencapsulation techniques, the most used process is spray drying.[138] Several wall materials have been used in the microencapsulation of natural colorants and coloring extracts, such as maltodextrins, gum arabic, β-cyclodextrin, gelatin, sucrose, gellan gum, mesquite gum, and some lipids.

Table 3 Studies on spray drying microencapsulation of essential oils and flavors

Material	Spray drying parameters	Drying carriers	Main findings	Ref.
Cumin oleoresin	JISL LSD-48 mini SD T_{in} = 160 ± 2 °C T_{out} = 120 ± 5 °C P_{at} = 3 bars $\dot{m}_{feed}$ = 300 g/h	Maltodextrin DE18, gum arabic and modified starch (Hi-Cap 100) and their blends	Microcapsules were evaluated for the content and stability of volatiles > p-cymene > cuminaldheyde > γ-terpinene for six weeks. Gum Arabic showed greater protection than maltodextrin and modified starch. A 4/6:1/6:1/6 blend of gum arabic, maltodextrin and modified starch offered better protection than gum Arabic does. However, protective effect of ternary blend was not similar for all constituents, and follows the order of volatiles > p-cymene > cuminaldheyde > γ-terpinene.	[130]
Black pepper oleoresin	Büchi-190 mini SD T_{in} = 178 ± 2 °C T_{out} = 110 ± 5 °C P_{at} = 5 bars $\dot{V}_{feed}$ = 300. mL/h	Gum arabic and comercial modified starch (Hi-Cap)	Extend of entrapment of piperine and volatiles and non volatiles depend on the nature of carrier material used. Gum Arabic was found to be a better wall material for encapsulation of peper oleoresin than is modified starch.	[131]
d-limonene, ethyl butyrate and ethyl propionate (model flavors)	Ohkawara-L8 T_{in} = 200 °C T_{out} = 110 ± 10 °C Wheel speed = 30000rpm $\dot{m}_{air}$ = 100 kg/h (at T_{out}) $\dot{V}_{feed}$ = 2700. mL/h	Binary blends of maltodextrin DE15-20 (30 %), and gum arabic, modified starch (Hi-Cap 100) and soybean water soluble polysaccharide, at concentration of 10%.	The emulsion droplet size affects the volatiles retention during encapsulation. Smaller emulsion size of the insoluble flavor shows higher retention and lower surface oil content after encapsulation. The reduction of the size of the large emulsion droplets during atomization is one of the main causes of loss of flavors. However, the preparation of smaller emulsions is not mandatory for moderately soluble flavors that show the highest retention for optimum values of the mean emulsion droplet size.	[132]
l-menthol	Ohkawara-L8 T_{in} = 180 °C T_{out} = 100 ± 5 °C Wheel speed = 30000rpm $\dot{m}_{air}$ = 11000 kg/h $\dot{V}_{feed}$ = 2700. mL/h	Gum arabic and modified starch (CAPSUL and Hi-Cap 100)	Microencapsultion of l-menthol was carried out proportions of l-menthol to the wall material of 1:9, 2:8, and 3:7. The solids concentration of the feed emulsion was set at 30 % (w/w). Results showed an higher retention of l-menthol for increasing the proportion of wall material. Hi-Cap 100 showed a higher retention of l-menthol than the other wall materials, but shows the presence of oil residue on the powder surface, mainly at high content of l-menthol in the feed. The release characteristics of l-menthol microparticles depended on the relative humidity and temperature.	[133]
Monoterpenes (limonene, β-pinene, β-myrcene, citral and linalool)	Lab-Plant SD-04 T_{in} = 150 °C T_{out} = 93 °C P_{at} = 5 bars $\dot{V}_{feed}$ = 900. mL/h	Gum arabic	Increasing the concentration of limonene, β-pinene, β-myrcene, citral and linalool from 10 to 30 % with respect to the wall material decrease the percentage of retention of essencial monoterpenes in the product. β-pinene was better retained than limonene, and β-myrcene showed the small retention. Stability of the capsules to temperature was checked for 33 days, and the degradation products were evaluated.	[134]

Ersus and Yurdagel[135] investigated the spray drying microencapsulation of anthocyanin pigments extracted from black carrot (*Daucus carota* L.) with maltodextrins of different DE number, namely MDX 29 (28-31 DE), Glucodry 210 (20-23 DE) and Stardri 10 (10 DE). Maltodextrin were incorporated to acidified ethanol anthocyanin extract (at 6 % solid contents) until to reach final solid concentrations of 20 % and stirred for complete homogenization. The feed mixtures were submitted spray drying in a SD-04 spray dryer, at inlet drying gas temperatures of 160, 180 and 200 °C and outlet temperatures of 107, 118 and 131 ± 2 °C. The flow rate of the feed composition was 300. mL/h at temperature of 25 °C. Spray dried acidified ethanol anthocyanin extracts of black carrots content showed greater anthocyanin losses at higher inlet/outlet temperatures. 20-21 DE maltodextrin (Glucodry 210) gave the product with higher anthocyanin contents. Product stored at 4 °C showed a half-life 3 times higher compared to 25 °C storage.

Larroza et al.[138] encapsulated lycopene in a blend of gum arabic and sucrose (8:2) by spray drying. Emulsion was prepared by dissolving the wall materials in warm water and adding the lycopene previously dissolved in dichloromethane. The emulsion was submitted to spray drying at inlet and outlet temperatures of 170 ± 2 and 113 ± 2 °C, respectively. The encapsulation efficiency ranged from 94 to 96 %, with an average yield of 51 %, with microcapsules showing superficial indentations and lack of cracks and breakages. Lycopene purity increased from 96.4 to 98.1 % after spray drying, which yielded a pale-pink, dry, free-flowing powder.

Shu et al.[139] studied the encapsulation of lycopene by spray drying using blends of edible gelatin and sucrose at several ratios (1/9 to 4/6). The relation between core and wall material varied from 1/2 to 1/16. Gelatin and sucrose were dissolved in hot distilled water and the lycopene (purity from 6 to 90 %), previously dissolved in acetone, was added under stirring to form a coarse emulsion, and then homogenized. The resulting emulsion was submitted to spray drying, under inlet drying temperatures ranging from 170 - 210 ^{o}C, feed flow rate of emulsion of 100. mL/h, feed temperature from 35 to 65 ^{o}C, and drying air velocity of 2 m/s. Encapsulation yield and encapsulation efficiency were significantly affected by the ratio between core and wall materials, gelatin:sucrose ratio, homogenization pressure, inlet drying temperature, feed temperature, and lycopene purity. The optimal condition was determined as follows: gelatin/sucrose ratio of 3/7, ratio of core:wall material of 1/4, feed temperature of 55 °C, inlet drying temperature of 190 °C, homogenization pressure of 40 MPa, and lycopene purity of not less than 52 %, at which the microencapsulated lycopene showed some isomerization, but a good storage stability.

Wang et al.[15] encapsulated curcumin pigments in blends of gelatin and porous starch at proportions of 1/20, 1/3 and 1/40 curcumin:wall material ratio, varying the emulsification time and temperature. The emulsions were fed to a YC-105 spray dryer. The inlet drying temperature ranged from 180 to 200 °C, the gas flow rate from 50 to 70 m^3/h, and the feed flow rate of microencapsulating composition from 60 to 80 mL/min. Encapsulation efficiencies were significantly affected by the ratio of curcumin (core) to wall materials, embedding temperature, inlet drying gas temperature and feed flow rate. Statistical analysis of the encapsulation and spray drying process permitted the determination of optimum conditions, namely: ratio core to wall material of 1/30, embedding temperature of 70 °C, embedding time of 2 h,

inlet drying gas temperature of 190 °C, feed flow rate of 70 mL/min, and drying gas flow rate of 70 m^3/h. In these conditions microencapsulated curcumin before and after spray drying showed good solubility and stability.

Oleoresins containing natural carotenoids (from red chilies and Aztec marigold petals) were microencapsulated in a water /oil/water (W/O/W) multiple emulsions based on blends of gellan gum, arabic gum, mesquite gum and maltodextrin DE10, with total solids content 25 and 35 %, and 0.25 % m/m theoretical carotenoid concentration.[140] The multiple emulsions were spray dried in a Mobile Minor Niro-Atomizer at inlet and outlet drying temperatures of 170 ± 5 and 80 ± 3 °C, at feed flow rate of emulsion of 20 mL/min at atomizing pressure of 2.8 bar. Microcapsules obtained by spray drying of W/O/W multiple emulsions with high solid contents showed the best morphology, highest microencapsulation efficiency, and retention of total carotenoids. High encapsulation efficiency was obtained for a high biopolymer blend to primary emulsion ratio. However, a lower kinetics of carotenoid degradation longer carotenoid half life was obtained with the lowest solids concentration and ratio biopolymer blend to primary emulsion. The storage conditions affect the microcapsules morphology and stability of encapsulated carotenoids.An overview in literature shows several other examples of spray drying of natural colorants and coloring extracts such as bixin[141], carotenoid pigments from rosa mosqueta (Rosa rubiginosa),[142] and anthocyanin from grape (Vitis labrusca) bagasse,[143] using distinct drying conditions and wall materials.

6.5 Drying of miscellaneous food products

This section will present studies on the spray drying of important miscellaneous products, such as egg, cheese, inulin, honey, milk, protein hydrolysate and so on, not covered in the previous sections.

Egg

Egg products have a range of applications in baking, dressing and confectionery products, due to its functional properties, such as foaming, gelling and emulsifying properties. Recently, instead of traditional liquid eggs, an increase of demand of dried egg products (whole egg, egg yolk and egg white) in the food industry has been observed, due to the growing importance of ready-for-use food products. The advantage of dried semi-finished products over traditional liquid eggs is respect to storage, handling and microbiological safety.[144]

However, the spray drying process can lead to changes in sensitive egg components, such as proteins, affecting the functional properties of whole egg after reconstitution. Therefore, the knowledge of influence of drying conditions on functional properties of powder egg is essential to obtain a product with desirable properties for applications in different food products. Ayadi et al.[144] and Franke and Kieβling[145] evaluated the effect of inlet air temperature, feed flow rate and nozzle pressure on foaming, gelling and emulsifying properties of spray dried white and whole eggs. Masters[4] recommends that the egg spray

dried be cooled down to 30 °C or less as soon as possible to avoid heat damage.

Cheese

In almost every cheese factory, spray drying is an important process. However, spray dryers are mostly used for the by-product drying, such as whey, while is little used for making cheese powder. Cheese powder is mainly utilized as flavoring in dips, dressings, biscuits, chips and hot dishes, like spaghetti and soups. Before spray drying, it is necessary converting cheese to pump able fluid and not too viscous for atomization. This step is done by melting process, where the cheese is disintegrated and, during heating and agitation, melting salts such as phosphates and citrates are added together with water. For spray drying of cheese, aged cheese is recommended as a feed material, since a certain quantity of aroma is inevitably lost during process.[146]

Inulin

Inulin is a reserve carbohydrate and consists of a chain of fructose molecules with a terminal glucose molecule. This substance was used as an ingredient on foods, with reduced or no sugar and fat, such as chocolates, ice creams and yogurts, and others. Its use on products with low calories and reduced fat levels, in Europe, United States and Canada, is already quite extending. Moreover, inulin also presents some functional properties, acting in the organism similarly way to dietary fibers and contributing to the improvement of the gastrointestinal system conditions.[147] Due to these properties, the food and pharmaceutical industries have been using inulin in the production of functional foods, nutritional composites and medicines. The most stable form for the commercialization of the inulin is the extract in powder.[148]

Honey

Similarly fruit juices, honey are composed of several sugars (90 % honey are glucose and frutose) and organic acids. The glass transition temperature of honey is around - 45 °C (with 16 % moisture w/w, proximately). Considering the Tg of the principal components of honey (glucose and fructose), the glass transition temperature of anhydrous honey may lie between the Tg of fructose (16 °C) and glucose (32 °C). This mean that spray drying is impossible and the addition of carrier agents are unavoidable to dry this product.[36] Bhandari et al.[67] verified the effect of addition maltodextrin 6 DE, at different concentrations, on product recovery. Increasing honey:maltodextrin ratio from 0.47:0.53 to 0.55:0.45, product recovery decreased from 56.5 to 20.3 %. According to Bhandari and Hartel,[36] the addition of higher carrier content causes a dilution of the honey, but in terms of flavor it may not matter much if a strong honey is selected for spray drying. Spray dried honey with maltodextrin is already commercially available and is used mainly in premixes and for flavoring purposes.

Milk

Fresh milk has a high nutritional value; however this product has a limited shelf-life and therefore should be processed in order to become microbiologically stable. Spray drying of milk is a very important process in the

dairy industries. The disadvantage of milk drying is that the energy consumption is high; no other process in the dairy industry demands a high energy per ton of final product.[149] This fact occurs due to high moisture content of milk (about 90 %), and practically all that water has to be removed by heat. The advantage of spray drying is a relatively gentle drying process that has replaced drum dryers, which causes more product denaturing. The quality of milk powder is an important parameter to be considered, that will determine the acceptance of product in the market. These aspects are related to the: microbiological safety, chemical quality and physical-chemical properties (moisture and fat content, bulk density, particles size) of the powder. The physical-chemical properties are important, because they affect the powder reconstitution (sinkability, solubility, dispersability and wetability) in water.

Protein hydrolysate

Protein hydrolysates are sources of biologically active peptides.[150,151] Bioactive peptides can affect numerous physiological functions of the organism, such as antihypertensive, immunomodulating, antithrombotic, antioxidative, anticancer, and antimicrobial activities.[152] Moreover, protein hydrolysates are applied in the nutritional management of individuals who cannot digest whole/intact protein. Hydrolysates rich in low molecular weight peptides, especially di- and tri-peptides with as little as possible free amino acids, have been shown to have more dietary uses due to their high nutritional and therapeutic values.[153]

However, due to their high moisture and protein content, protein hydrolysates are very perishable and could be converted to powder to improve their shelf life. Due to low molecular weight peptides, protein hydrolysates present low Tg values and, consequently, high hygroscopicity and thermoplasticity. So, the addition of carrier before spray drying is necessary. Kurozawa et al.[154] evaluated the effect of addition carrier agent on Tg and physical stability of chicken protein hydrolysate spray dried. The powder, without carrier agents, presented a low Tg and low critical values for moisture content and water activity, indicating its vulnerability during processing, handling and storage. The Tg and critical moisture content values raised when maltodextrin or gum arabic were used as drying agents, showing their contribution to the powder stability.

Whey

In terms of volume and weight, whey is the largest amount of waste from the cheese industrial processing, becoming a problem, both for environment and processing plant. Therefore, the cheese industry is continuously looking for solutions to these problems caused by whey discharge, such as animal feeding and fertilizer. Therefore, it has been necessary to find alternative types of products made from whey that would be more attractive for consumers, together with alternative low-cost technologies that would be more attractive for producers. Spray drying of whey can be a solution for cheese industry, since the product has high protein content. There are two major whey proteins: α-lactalbumin and β-lactoglobulin, which plays an extremely important role in the food industry, as a result of its gelation and emulsification properties.[146,155] Spray drying of many food products have been studied by several researchers. An overview of some studies are shown in Table 4.

Table 4 Miscellaneous food products submitted to spray drying

Food products	Spray drying conditions	Carrier agent	Ref.
Egg	T_{in} = 110 - 125°C $\dot{m}_{air}$ = 0.18 kg/min $\dot{V}_{feed}$ = 0.2 - 0.3 L/h	Not used	[144]
	T_{in} = 130 - 190°C Nozzle pressure = 125 - 195 bar	Not used	[145]
Extract from ham by-products	T_{in} = 100 - 200°C $\dot{V}_{air}$ = 25 - 50 m^3/h $\dot{V}_{feed}$ = 2.5 - 10.0 mL/h	Not used	[156]
Honey	T_{in} = 150°C T_{out} = 65°C Atomizer speed = 20.000 rpm	Maltodextrin 6DE	[67]
	T_{in} = 150°C T_{out} = 65°C	Maltodextrin 6DE	[31]
Hydrolyzed sweetpotato puree	T_{in} = 150, 190 and 220°C T_{out} = 100°C T_{feed} = 60°C $\dot{m}_{feed}$ = 2 kg/h Atomizer speed = 20.000 rpm	Maltodextrin 11DE	[157]
Inulin	T_{in} = 186 - 193°C	Modified and hydrolyzed starch	[148]
Lactose hydrolysed skim milk	T_{in} = 130°C T_{out} = 65°C T_{feed} = 50°C	Not used	[65]
Whey protein	T_{in} = = 160 - 255°C T_{out} = 60 - 120°C $\dot{m}_{feed}$ = 4.7 - 17.5 kg/h $\dot{m}_{air}$ = 227 kg/h	Not used	[155]
Milk	T_{in} = 160 - 190°C $\dot{m}_{feed}$ = 1.4 - 2.4 kg/h Atomizer speed = 42.000- 50.000 rpm	Not used	[158]
	T_{in} = 120, 160 and 200°C T_{out} = 83, 107 and 128°C (for concentrate milk) T_{out} = 75, 103 and 119°C (for skim milk) $\dot{V}_{feed}$ = 8 mL/h $\dot{V}_{air}$ = 38 m^3/h	Not used	[159]
Protein hydrolysate from chicken breast	T_{in} = 180°C T_{out} = 91 - 102°C $\dot{m}_{feed}$ = 0.2 kg/h	Maltodextrin 10DE and gum Arabic	[154]
Protein hydrolysate from chicken breast	T_{in} = 88 - 136°C T_{out} = 91 - 102°C $\dot{V}_{feed}$ = 0.4 - 1.0 L/h	Maltodextrin 10DE	[160]
Protein hydrolysate from tilapia	T_{in} = 150 and 180°C T_{out} = 76 and 90°C	Maltodextrin	[161]
Protein hydrolysate from fermented shrimp by-products	T_{in} = 180°C T_{out} = 140°C T_{feed} = 80°C $\dot{V}_{feed}$ = 1.0 L/h	Not used	[162]
Shark cartilage gelatin	T_{in} = 127°C T_{out} = 100°C	Not used	[163]
Soymilk	T_{in} = 255 - 275°C $\dot{V}_{feed}$ = 0.37 and 0.58 L/min Atomizer speed = 19.300 and 26.800 rpm	Not used	[164]

7.0 Final remarks

Currently, the market for natural products has increased considerably, since consumers become more interested in a healthy life. Products having high concentration of phytochemicals can help to improve our healthy or are used even for medicinal purposes. These products have received much attention from the consumers, scientific community, industry and government worldwide. Several terms have been used to classify these products, such as 'functional foods', medical foods, dietary supplements health foods, nutraceutical, and includes botanicals and phytomedicines, being the term nutraceutical more frequently used. It is obvious that the term adopted will be related to the final use of the product.

Natural products are also used as food, pharmaceutical, and cosmetic excipients, in most varied applications such as natural colorants, natural antioxidants, flavoring agents, and food preservatives. Generally, these products are composed by a complex mixture of substances, for which little information on physical and chemical properties is available. Thus the standardization of these products is challenging, and is a fascinating research subject.

Most natural products contains high amount of volatile and/or thermosensitive compounds, susceptible to oxidation and often have high water activity and/or occur in liquid form under normal environmental conditions. These substances can undergo irreversible alterations in their physicochemical properties when exposed to contact with other materials or external agents without adequate protection.

Spray drying is a key technology in natural products processing since it is one-step processing operation for turning a liquid feed into a dried particulate form, by spraying the feed into a hot drying gas medium. While reduces the product bulk weight and size, spray drying minimizes handling and also preserves the product by reducing its water activity to a low level, required to stop bacterial degradation, generating an attractive, marketable and often long shelf-life product. The technology is also widely used for microencapsulation, transforming reactive substances into more stable materials (lower volatility and less susceptibility to oxidation) providing easy handling (solid form).

In this chapter was presented an overview of recent applications and concepts involved in field of spray drying of several foods and plant derived products. Topics of general character were approached, including aspects of spray drying, relevant physical-chemical properties of spray dried product, quality changes, and drying carriers. Finally, the spray drying of food and herbal products, emphasizing fruit pulps, herbal extracts, and also encapsulation of essential oils, flavors, plant pigments and oleoresins was presented.

8.0 Nomenclature

Cs	solid concentrations in the feed composition	[-]
$\dot{m}_{air}$	mass flow rate of drying air	[MT^{-1}]
$\dot{m}_{feed}$	mass flow rate of the feed composition	[MT^{-1}]
P_{at}	atomizing air pressure	[$ML^{-1}T^{-2}$]
T_{in}	inlet drying gas temperature	[θ]
T_{feed}	temperature of the feed composition	[θ]
T_{out}	outlet drying gas temperature	[θ]
$\dot{V}_{air}$	volumetric flow rate of drying gas	[L^3T^{-1}]
$\dot{V}_{at}$	volumetric flow rate of atomizing gas	[L^3T^{-1}]
$\dot{V}_{feed}$	volumetric flow rate of the feed composition	[L^3T^{-1}]
$\dot{V}_{max}$	maximum volumetric evaporation capacity of the dryer	[L^3T^{-1}]

9.0 References

1. Hayashi, H. 1989. Drying technologies of foods - their history and future, Drying Technology **1989**, *7(2)*, 315-369.
2. Chiou, D.; Langrish, T.A.G. Crystallisation of amorphous spray-dried powders. In Proceedings of 15th International Drying Symposium (IDS 2006), Budapest, Hungary, **2006**, pp. 562-569.
3. Barbosa-Cánovas, G.V.; Ortega-Rivas, E.; Juliano, P.; Yan, H. Encapsulation Processes, In: Food powders: Physical Properties, Processing, and Functionality, Chapter 8, 199-219, **2005**.
4. Masters, K. Spray drying. An introduction to principles, operational practice and applications. Leonard Hill Books; London, **1972**.
5. Orsat, V.; Raghavan, V. Dehydration technologies to retain bioactive components. In: J. Shi (Ed.) Functional Food Ingredients and Nutraceuticals - Processing Technologies, Chapter 7, 173-191, Taylor & Francis, Boca Raton; USA, **2007**.
6. Kwak, N.S.; Jukes, D.J. Functional foods. Part 2: the impact on current regulatory terminology. Food Control **2001**, *12*, 109-117.
7. Wildman, R.E.C.; Kelley, M. Nutraceutical and functional foods. In Wildman, R.E.C. (ed.) Handbook of Nutraceuticals and Functional Foods – 2nd Ed., Chapter 1-21, CRC Press, Taylor & Francis Group, Boca Raton, USA, **2006**.
8. Krzystof, C.; Krzystof, S. Spray drying technique: I. Hardware and process parameters. Journal of Pharmaceutical Sciences **2009**, *99*, 575-586.

9. Krzystof, S.; Krzystof, C. Spray drying technique: II. Current applications in pharmaceutical technology. Journal of Pharmaceutical Sciences **2009**, *99*, 587-597.

10. Langrish, T.A.G. New Engineered particles from spray dryers: Research needs in spray drying. Drying Technology **2007**, *25*, 971-983.

11. Souza, C.R.F.; Georgetti, S.R., Salvador, M.J.; Fonseca, M.J.V.; Oliveira, W.P. Antioxidant activity and physical-chemical properties of spray and spouted bed dried extracts of *Bauhinia forficata*. Brazilian Journal of Pharmaceutical Sciences **2009***, 45(2)*, 209-218.

12. Soares, L.A.L.; Ortega, G.G.; Petrovick, P.R.; Schmidt, P.C. Optimization of tablets containing a high dose of spray-dried plant extract: A technical note. AAPS PharmSciTechnology **2005**, *6*, E367-E371.

13. Edris, A.; Bergnståhl, B. Encapsulation of orange oil in a spray dried double emulsion, Nahrung/Food **2001**, *45*, 133-137.

14. Angel, R.C.M.; Espinosa-Muñoz, L.C.; Aviles-Aviles, C.; González-García, R.; Moscosa-Santillán, M.; Grajales-Lagunes, A.; Abud-Archila, M. Spray-drying of passion fruit juice using lactose-maltodextrin blends as the support material. Brazilian Archives of Biology and Technology **2009**, *52*, 1011-1018.

15. Wang, Y.; Lu, Z.; Lv, F.; Bie, X. Study on microencapsulation of curcumin pigments by spray drying. European Food Research and Technology **2009**, *229*, 391-396.

16. Wiesenborn, D.; Zbikowski, Z.; Nguyen, H. Process conditions affect pigment quality and yield in extracts of purple sunflower hulls. Journal of the American Oil Chemists' Society **1995**, *72*, 183-188.

17. Fernandes, L.P.; Oliveira, W.P.; Sztatisz, J.; Novák, C. Thermal properties and release of *Lippia sidoides* essential oil from gum arabic/maltodextrin microparticles, Journal of Thermal Analysis and Calorimetry **2008**, *94*, 461-467.

18. Acosta-Esquijarosa, J.; Jáuregui-Haza, U.; Amaro-González, D.; Sordo-Martínez, L. Spray drying of aqueous extract of *Mangifera indica* L (Vimang): Scale up for the process. World Applied Sciences Journal **2009**, *6(3)*, 408-412.

19. Goula, A.M.; Adamopoulos, K.G. Spray drying of tomato pulp: Effect of feed concentration. Drying Technology **2004**, *22*, 2309-2330.

20. Chegini, G.R.; Ghobadian, B. Spray dryer parameters for fruit juice drying. World Journal of Agricultural Sciences **2007**, *3*, 230-236.

21. Filková, I.; Mujumdar, A.S. Industrial Spray Drying Systems. In: Handbook of Industrial Drying, edited by A.S. Mujumdar, 2nd edition, vol. 1, Marcel Dekker, USA, Chapter 9, 263-308, **1995**.

22. Barbosa-Cánovas, G.V.; Juliano, P. Physical and chemical properties of food powders. In: C. Onwulata (Ed.), Encapsulated and powdered foods, Chapter 3, 39-71, Taylor & Francis, Boca Raton, USA, **2005**.

23. Cai, Y.Z.; Corke, H. Production and properties of spray-dried *Amaranthus* betacyanin pigments. Journal of Food Science **2000**, *65(7)*, 1248-1252.

24. Reineccius, G.A; Multiple-core encapsulation – The spray drying o food ingredients. In: Vilstrup, P. (Ed.). Microencapsulation of food ingredients. Leatherhead Publishing; Surrey, 151-185, **2001**.

25. Barbosa-Cánovas, G.V.; Vega-Mercado, H. Dehydration of food. Chapman & Hall; New York, **1996**.

26. O'Hagan, P.; Hasapidis, K.; Coder, A.; Helsing, H.; Pokrajac, G. Particle size analysis of food powders. In: Onwulata, C. (Ed.). Encapsulated and powdered foods, Chapter 9, 215-246, Taylor & Francis: Boca Raton; USA, **2005**.

27. Tóth, J.; Pallai-Varsányi, E. Drying of bovine serum albumin on inert particle surface in msb dryer. In Proceedings of the 15th International Drying Symposium, Budapeste, Hungria, 1216-1222, **2006**.

28. Ré, M.I. Microencapsulation by spray drying. Drying Technology **1998**, *16 (6)*, 1195-1236.

29. Rosenberg, M.; Kopelman, I.J.; Talmon, Y. A scanning electron microscopy study of microencapsulation. Journal of Food Science **1985**, *50(1)*, 139-144.

30. Fitzpatrick, J.J. Food powder flowability. In: C. Onwulata (Ed.), Encapsulated and powdered foods, Chapter 11, 247-260,. Taylor & Francis, Boca Raton; USA, **2005**.

31. Boonyai, P.; Howes, T.; Bhandari, B. Application of the cyclone stickiness test for characterization of stickiness in food powders. Drying Technology **2006**, *24*, 703-709.

32. Chiou, D.; Langrish, T.A.G. Crystallisation of amorphous spray-dried powders. In Proceedings of 15th International Drying Symposium (IDS 2006), Budapest, Hungary, 562-569, **2006**.

33. Goula, A.M.; Adamopoulos, K.G. Effect of maltodextrin addition during spray drying of tomato pulp in dehumidified air: I. Drying kinetics and product recovery. Drying Technology **2008**, *26*, 714-725.

34. Bhandari, B.R.; Snoussi, A. Dumoulin, E.D.; Lebert, A. Spray drying of concentrated fruit juices. Drying Technology **1993**, *11(5)*, 1081-1092.

35. Roos, Y., Karel, M. Applying state diagrams to food processing and development. Food Technology **1991**, *45(12)*, 66-71.

36. Bhandari, B.R.; Hartel, R.W. Phase transitions during food powder production and powder stability. In: Onwulata, Charles (Ed.). Encapsulated and Powdered Foods, Chapter 11, pp. 261 – 292, Boca Raton: Taylor & Francis, **2005**.

37. Jouppila, K.; Roos, Y.H. Glass transition and crystallization in milk powders. Journal Dairy Science **1994**, *77*, 1798-1808.

38. Mani, S.; Jaya, S.; Das, H. Sticky issues on spray drying of fruit juices. Saskatoon, Canada Presented at the 2002 ASAE/CSAE North-central Intersection Meeting – Paper MBSK 02-201, 1-18, **2002**.

39. Roos, Y. H. Importance of glass transition and water activity to *spray-drying* and stability of dairy powders. Lait **2002**, *82*, 475-484.

40. Bhandari, B.R.; Howes, T. Implication of glass transition for the drying and stability of dried foods. Journal of Food Technology **1999**, *40*, 71-79.

41. Labuza, T.P.; Labuza, P.S. Influence of temperature and relative humidity on the physical states of cotton candy. Journal of Food Preservation **2004**, *28*, 274-287.

42. Chu, K.K.W.; Chow, A.H.L. Impact of carbohydrate constituents on moisture sorption of herbal extracts. Pharmaceutical Research **2000**, *17 (9)*, 1133-1137.

43. Truong, V., Bhandari, B.R, Howes, T. Optimization of co-current spray drying process of sugar-rich foods. Part I – Moisture and glass transition temperature profile during drying. Journal of Food Engineering **2005**, *71*, 55-65.

44. Kenyon, M.M. Modified starch, maltodextrin and corn syrup solids as wall materials for food encapsulation. In: S. J. Risch, G. A. Reineccius (Eds.), Encapsulation and controlled released of food ingredients (pp. 42-50). Society American Chemical; Washigton, DC, USA, **1995**.

45. Reineccius, G.A. Carbohydrates for flavor encapsulation. Food Technology **1991**, *45*, 144-147.

46. BeMiller, J.N.; Whistlers, R.L. Carbohydrates. In; Fennema, O. (Ed.), Food Chemistry, 3rd Ed., Marcel Dekker; New York, 157-224, 1996.

47. Shahidi, F.; Han, X.Q. Encapsulation of food ingredients. Cristal Reviews in Food Science and Nutrition **1993**, *33(6)*, 501-547.

48. Kenyon, M.M.; Anderson, J. Maltodextrins and low dextrose-equivalence corn syrup solids. In: RISCH, S. J.; REINECCIUS, G. A. (Eds.) Flavor encapsulation, American chemical Society, Washington DC, USA, 87-102, **1988**.

49. Rowe, R.C.; Sheskey, P.J.; Quinn, M.E.; Handbook of Pharmaceutical Excipients, 6th Edition, Pharmaceutical Press, London, UK, **2009**.

50. Thevenet, F. Natural encapsulation agent for food ingredients. In: S. J. Risch, G. A. Reineccius (Eds.), Encapsulation and controlled released of food ingredients, pp. 51-59, Society American Chemical; Washigton, DC, USA, **1995**.

51. Scheindlin S. Acacia - a remarkable excipient: the past, present, and future of gum arabic. JAMA **2001**, *41*, 669-671.

52. Szejtli, J. Introduction and general overview of cyclodextrin chemistry. Chemistry Review **1998**, *98*, 1743-1753.

53. Martin Del Valle, E.M. Cyclodextrin and their uses: a review. Process Biochemistry **2004**, *39*, 1033-1046.

54. Venturini, C.C.; Nicolini, J.; Machado, C.; Machado, V.G. Propriedades e aplicações recentes das ciclodextrinas. Química Nova **2008**, *31(2)*, 360-368.

55. Masters, K. Spray Drying Handbook; Longman: New York, **1990**.

56. Dolinsky, A.; Maletskaya, K.; Snezhkin, Y. Fruit and vegetable powders: Production technology on the bases of spray and convective drying methods. Drying Technology **2000**, *18(3)*, 747-758.

57. Roustapour, O.R.; Hosseinalipour, M.; Ghobadian, B. An experimental investigation of lime juice drying in a pilot plant spray dryer. Drying Technology **2006**, *24*, 181-188.

58. Khalloufi, S.; El-Maslouhi, Y.; Ratti, C. Mathematical model for prediction of glass transition temperature of fruit powders. Journal of Food Science **2000**, *65(5)*, 842-848.

59. Roos, Y.H. Water activity and physical state effects on amorphous food stability. Journal of Food Processes and Preservation **1993**, *16(6)*, 433-447.

60. Roos, Y.H. Glass transition – Related physicochemical changes in foods. Food Technology **1995**, *49(10)*, 97-102.

61. Shrestha, A.K.; Ua-arak, T.;Adhikari, B.P.; Howes, T.; Bhandari, B.R. Glass transition behavior of spray dried orange juice powder measured by differential scanning calorimetry (DSC) and thermal mechanical compression test (TMCT). International Journal of Food Properties **2007**, *10(3)*, 661-673.

62. Tonon, R.V.; Brabet, C.; Hubinger, M.D. Influence of process conditions on the physicochemical properties of açai (*Euterpe oleraceae Mart*.) powder produced by spray drying. Journal of Food Engineering **2008**, *88(3)*, 411-418.

63. Oliveira, M.A.; Maia, G.A.; Figueiredo, R.W.; Souza, A.C.R.; Brito, E.S.; Azeredo, H.M.C. Addition of cashew tree gum to maltodextrin-based carriers for spray drying of cashew apple juice. International Journal of Food Science and Technology **2009**, *44*, 641-645.

64. Papadakis, S.E.; Gardeli, C.; Tzia, C. Spray drying of raisin juice concentrate. Drying Technology **2006**, *24(2)*, 173-180.

65. Shrestha, A.K.; Howes, T.; Adhikari, B.P.; Bhandari, B.R. Water sorption and glass transition properties of spray dried lactose hydrolysed skim milk powder. LWT – Food Science and Technology **2007**, *40*, 1593-1600.

66. Righetto, A.M.; Netto, F.M. Effect of encapsulating materials on water sorption, glass transition and stability of juice from immature acerola. International Journal of Food Properties **2005**, *8(2)*, 337-346.

67. Bhandari, B.R.; Datta, N.; Howes, T. A semi-empirical approach to optimize the quality of drying aid required to spray dry sugar-rich foods. Drying Technology **1997**, *15(10)*, 2509-2525.

68. Goula, A.M.; Adamopoulos, K.G. Spray drying of tomato pulp dehumidified air: I. The effect on product recovery. Journal of Food Engineering **2005**, *66*, 25-34.

69. Gong, Z.; Zhang, M.; Mujumdar, A.S.; Sun, J. Spray drying and agglomeration of instant bayberry powder. Drying Technology **2008**, *26*, 166-121.

70. Rodríguez-Hernández, G.R.; González-García, A.; Grajales-Lagunes, A.; Ruiz-Cabrera, M.A. Spray drying of cactus pear juice (*Opuntia streptacantha*): Effect on the physicochemical properties of powder and reconstituted product. Drying Technology **2005**, *23(44)*, 955-973.

71. Moβhammer, M.R.; Stintzing, F.C.; Carle, R. Evaluation of different methods for the production of juice concentrates and fruit powders from cactus pear. Innovative Food Science and Emerging Technologies **2006**, *7*, 275-287.

72. Dib Taxi, C.M.A.; Menezes, H.C.; Santos, A.B.; Grosso, C.R.F. Study of the microencapsulation of camu-camu (*Myrciaria dubia*) juice. Journal of Microencapsulation **2003**, *20*, 443-448.

73. Chin, S.T.; Nazimah, S.A.H.; Quek, S.Y.; Man, Y.B.C.; Rahman, R.A.; Hashim, D.M. Changes of volatiles' attribute in durian pulp during freeze- and spray-drying process. LWT – Food Science and Technology **2008**, *41*, 1899-1905.

74. Chopda, C.A.; Barret, D.M. Optimization of guava juice and powder production. Journal of Food Processing Preservation **2001**, *25*, 411- 430.

75. Righetto, A.M.; Netto, F.M. Vitamin C stability in encapsulated green west Indian cherry juice and in encapsulated synthetic ascorbic acid. Journal of the Science of Food and Agriculture **2006**, *86*, 1202-1208.

76. Cano-Chauca, M.; Stringheta, P.C.; Ramos, A.M.; Cal-Vidal, J. Effect of the carriers on the microstructure of mango powder obtained by spray drying and its functional characterization. Innovative Food Science and Emerging Technologies **2005**, *6*, 420-428.

77. Chegini, G.R.; Ghobadian, B. Effect of spray-drying conditions on physical properties of orange juice powder. Drying Technology **2005**, *23(3)*, 657-668.

78. Abadio, F.D.B.; Domingues, A.M.; Borges, S.V.; Oliveira, V.M. Physical properties of powdered pineapple (*Ananas comosus*) juice – effect of maltodextrin concentration and atomization speed. Journal of Food Engineering **2004**, *64(3)*, 285-287.

79. Youssefi, S.; Emam-Djomeh, Z.; Mousavi, S.M. Comparison of artificial neural network (ANN) and response surface methodology (RSM) in the prediction of quality parameters of spray-dried pomegranate juice. Drying Technology **2009**, *27*, 910-917.

80. Goula, A.M.; Adamopoulos, K.G. Spray drying of tomato pulp dehumidified air: II. The effect on powder properties. Journal of Food Engineering **2005**, *66*, 35-42.

81. Goula, A.M.; Adamopoulos, K.G.; Kazakis, N.A. Influence of spray drying conditions on tomato powder properties. Drying Technology **2004**, *22(5)*, 1129-1151.

82. Al-Asheh, A.; Jumah, R.; Banat, F.; Hammad, S. The use of experimental factorial design for analyzing the effect of spray dryer operating variables on the production of tomato powder. Food and Bioproducts Processing **2003**, *81(2)*, 81-88.

83. Quek, S.Y.; Chok, N.K.; Swedlund, P. The physicochemical properties of spray-dried watermelon powders. Chemical Engineering and Processing **2007**, *46*, 386-392.

84. Kwak, N.S.; Jukes, D.J. Functional foods. Part 1: the development of a regulatory concept. Food Control **2000**, *12*, 99-107.

85. Cacace, J.E.; Mazza, G. Pressurized low polarity water extraction of biologically active compounds from plant products. In: J. Shi (Ed.) Functional Food Ingredients and Nutraceuticals - Processing Technologies, Chapter 5, 135-155, Taylor & Francis, Boca Raton; USA, **2007**.

86. Yoon J.H.; Baek, S.J. Molecular targets of dietary polyphenols with anti-inflammatory properties. Review. Yonsei Medical Journal **2005**, *6*, 585-596.

87. Raghavan, G.S.V.; Orsat, V., Recent advances in drying of biomaterials for quality of bioproducts. Asia-Pacific Journal of Chemical Engineering **2007**, *2*, 20-29.

88. Gertenback, D.D. Solid-liquid extraction technologies for manufacturing nutraceuticals. In: Shi, J.; Mazza, G.; Maguer, M. (Eds). Functional Foods - Biochemical and processing aspects, Chapter 11, 1-36, CRC Press, Boca Raton; USA, **2002**.

89. Teixeira, H.F. Avaliação da influência de adjuvantes farmacêuticos sobre as características físicas, químicas, tecnológicas e farmacológicas de extratos secos nebulizados de *Achyrocline satureioides* (Lam.) DC. Compositae – marcela. PPGCF/UFRGS, Porto Alegre, RS, (Dissertação), **1996**, 146p.

90. Souza, K.C.B. Desenvolvimento de metodologias analíticas e tecnológicas na obtenção de extratos secos nebulizados de *Passiflora edulis* variedade *flavicarpa* (maracuja). PPGCF-UFRGS, Porto Alegre, Rio Grande do Sul, (Dissertação), **1997**, 156p.

91. Senna, E.L.; Petrovick, P.R.; Ortega, G.G.; Bassani, V.L. Preparation and characterization of *spray dried* powders from *Achyrocline satureoides* (Lam) DC extracts. Phytotherapy Research **1997**, *11(2)*, 123-127.

92. Cordeiro, D.S. Produção de extrato seco de *Maytenus ilicifolia* Martius ex Reiss pelo processo leito de jorro. PPGCF-FCFRP/USP, Ribeirão Preto, SP, (Dissertação), **2000**, 80p.

93. Cordeiro, D.S.; Oliveira, W.P. Technical aspects of the production of dried extract of *Maytenus ilicifolia* leaves by jet spouted bed drying. International Journal of Pharmaceutics **2005**, *299(1-2)*, 115-126.

94. Runha, F.P.; Cordeiro, D.S.; Pereira, C.A.M.; Vilegas, J.; Oliveira, W.P. Production of dry extracts of medicinal Brazilian plants by spouted bed process: development of the process and evaluation of thermal degradation during drying operation, Transaction Ichem **2001**, *79(C)*, 160-168.

95. Souza, C.R.F. Estudo comparativo da produção de extrato seco de *Bauhinia forficata* Link pelos processos *spray dryer* e leito de jorro. PPGCF-FCFRP/USP, Ribeirão Preto, SP, (Dissertação), **2003**, 179p.

96. Souza, C.R.F.; Oliveira, W.P. Spouted bed drying of *Bauhinia forficata* Link extract: effect of the position of the feed atomizer and operating conditions on equipment performance and product properties. Brazilian Journal of Chemical Engineering **2005**, *22(2)*, 239-247.

97. Bott, R.F.; Labuza, T.P.; Oliveira, W.P. Stability testing of spray and spouted bed dried extracts of *Passiflora alata*. Drying Technology **2010**, (*In Press*).

98. Remili, H.; Boussard, P.; Devleeschouwer, M., Microbiological quality of spray-dried pharmaceutical plants extracts, European Journal of Pharmaceutical Sciences **1994**, *1*, 265-268.

99. Paula, I.C.; Ortega, G.G.; Bassani, V.L.; Petrovick, P.R. Development of ointment formulation prepared with *Achyrocline satureoids* spray dried extracts. Drug Development and Industrial Pharmacy **1998**, *24(3)*, 235-241.

100. Casadebaig, J.; Jacob, M.; Cassanas, G.; Gaudy, D.; Baylac, G.; Puech, A. Physicochemical and pharmacological properties of spray dried powders from *Fraxinus excelsior* leaf extracts. Journal of Ethnopharmacology **1989**, *26*, 211-216.

101. Souza, C.R.F.; Oliveira, W.P. Powder properties and system behavior during spray drying of *Bauhinia forficata* Link extract. Drying Technology **2006**, *24(6)*, 735-749.

102. Oliveira, W.P.; Bott, R.F.; Souza, C.R.F. Manufacture of standardized dried extracts from medicinal Brazilian plants. Drying Technology **2006**, *24(4)*, 523-533.

103. Martins, A.G.; Guterres, S.S.; Ortega, G.G. Anti-ulcer activity of spray dried powders prepared from leaf extracts of *Maytenus ilicifolia* Martius ex Reiss. Acta Farmaceutica Bonaerense **2003**, *22(1)*, 39-44.

104. Vargas, A.J.; Geremias, D.S.; Provensi, G.; Fornari, P.E.; Reginatto, F.H.; Gosmann, G.; Schenkel, E.P.; Fröde, T.S. *Passiflora alata* and *Passiflora edulis* spray dried aqueous extracts inhibit inflammation in mouse model of pleurisy. Fitoterapia **2007**, *78*, 112-119.

105. Cabral, A.C.S.; Said, S.; Oliveira, W.P. Retention of the enzymatic activity and product properties during spray drying of pineapple stem extract in presence of maltodextrin. International Journal of Food Properties **2009**, *12*, 536-548.

106. Georgetti, S.R.; Casagrande, R.; Souza, C.R.F.; Oliveira, W.P.; Fonseca, M.J.V. Spray drying of the soybean extract: effects on chemical properties and antioxidant activity. Food Science and Technology/Lebensmittel-Wissenschaft + Technologie **2008**, *41(8)*, 1521-1527.

107. Fernandes, L.P.; Oliveira, W. P.; Sztatisz, J.; Szilágyi, I. M.; Novák, C. Solid state studies on molecular inclusions of *Lippia sidoides* essential oil obtained by spray drying. Journal of Thermal Analysis and Calorimetry **2009**, *95*, 855-863.

108. Su, Y.L.; Fu, Z.Y; Zhang, J.Y; Wang, W.M.; Wang, H.; Wang, Y.C.; Zhang, Q.J. Microencapsulation of *Radix salvia miltiorrhiza* nanoparticles by spray-drying, Powder Technology **2008**, *184*, 114-121.

109. Krishnaiah, D.; Sarbatly, R.; Hafiz, A.M.M.; Hafeza, A.B.; Rao, A.R.M. Study of retention of bioactive components of *Morinda citrifolia* I. using spray-drying, Journal of Applies Sciences **2009**, *9*, 3092-3097.

110. Souza, C.R.F.; Schiavetto, I.A.; Thomazini, F.C.F.; Oliveira, W.P. Processing of *Rosmarinus officinalis* Linne extract on spray and spouted bed dryers. Brazilian Journal Chemical Engineering **2008**, *25*, 59-69.

111. King, C.J. Spray drying: retention of volatile compounds revisited. Drying Technology **1995**, *13(5-7)*, 1221-1240.

112. Madene, A.; Jacquot, M.; Scher, J.; Desobry, S. Flavour encapsulation and controlled release – a review. International Journal of Food Science and Technology **2006**, *41*, 1-21.

113. Desai, K.G.H.; Park, H.J. Recent developments in microencapsulation of food ingredients. Drying Technology **2005**, *23*, 1361-1394.

114. Gharsallaoui, A.; Roudaut, G.; Chambin, O.; Voilley, A.; Saurel, R. Applications of spray-drying in microencapsulation of food ingredients: an overview. Food Research International **2007**, *40*, 1107-1121.

115. Wendel, S.; Çelik, M. Uma visão geral sobre o uso da tecnologia de spray-drying. Pharmaceutical Technology **1998**, 31-45.

116. Gouin, S. Microencapsulation: industrial appraisal of existing technologies and trends. Trends in Food Science and Technology **2004**, *15*, 330-347.

117. Reineccius, G.A. The spray drying of food flavors. Drying Technology **2004**, *22(6)*, 1289-1324.

118. Funchs, M.; Turchiuli, M.; Bohin, M.; Cuvelier, M.E.; Ordonnaud, C.; Peyrat-Maillard, M.N.; Dumoulin, E. Encapsulation of oil in powder using spray drying and fluidized bed agglomeration. Journal of Food Engineering **2006**, *75*, 27-35.

119. Fernandes, L.P.; Turatti, I.; Lopes, N.P.G.; Ferreira, J.; Candido, R.C.; Oliveira, W.P. Volatile retention and antifungal properties of spray-dried microparticles of *Lippia sidoides* essential oil. Drying Technology **2008**, *26*, 1534-1542.

120. Vaidya, S.; Bhosale, R.; Singhal, R.S. Microencapsulation of cinnamon oleoresin by spray drying using different wall materials. Drying Technology **2006**, *24*, 983-992.

121. Bangs, W.M.; Reineccius, G.A. The influence of dryer infeed matrices on the retention of volatile flavor compounds during spray drying. Journal of Food Science **1982**, *47(1)*, 254-259.

122. Yoshii, H.; Soottitantawat, A.; Liu, X.D; Atarashi, T.; Furuta, T.; Aishima, S.; Ohgawara, M; Linko, P. Flavor release from spray-dried maltodextrin/gum arabic or soy matrices as a function of storage relative humidity. Innovative Food Science and Emerging Technologies **2001**, *2*, 55-61.

123. Anandaraman, S.; Reineccius, G.A. Stability of encapsulated orange peel oil. Food Technology **1986**, *40(11)*, 88-93.

124. Sankarikutty, B.; Sreekumar, M.M.; Narayanan, C.S.; Mathew, A.G. Studies on microencapsulation of cardamom oil by spray drying technique. Journal of Food Science and Technology **1988**, *25(6)*, 352-356.

125. Bhandari, B.R.; Dumoulin, E.D; Richard, H.M.J; Noleau, I.; Lebert, A.M. Flavor encapsulation by spray drying: application to citral and linaryl acetate. Journal of Food Science **1992**, *57(1)*, 217-221.

126. Beristain, C.I.; Garcia, H.S.; Vernon-Carter, E.J. Spray-dried encapsulation of Cardamom (*Elettaria cardamomum*) essential oil with mesquite (*Prosopis juliflora*) gum. LWT – Food Science and Technology **2001**, *34*, 398-401.

127. Jafari, S.M.; HE, Y.; Bhandari, B. Encapsulation of nanoparticles of d-limonene by spray drying: role of emulsifiers and emulsifying techniques. Drying Technology **2007**, *25*, 1079-1089.

128. Baranauskiene, R.; Venskutonis, P.R.; Dewettinck, K.; Verhe, R. Properties of oregano (*Origanum vulgare* L.), citronella (*Cymbopogon nardus* G.) and marjoram (*Majorana hortensis* L.) flavors encapsulated into milk protein-based matrices. Food Research International **2006**, *39*, 413-425.

129. Bhandari, B.R.; D'arcy, B.R.; Padukka, I. Encapsulation of lemon oil by paste method using β-cyclodextrin: encapsulation efficiency and profile of oil volatiles. Journal of Agricultural and Food Chemistry **1999**, *47*, 5194-5197.

130. Kanakdande, D.; Bhosale, R.; Singhal, R.S. Stability of cumim oleoresin microencapsulated in different combination of gum arabic, maltodextrin and modified starch. Carbohydrate Polymers **2007**, *67*, 536-541.

131. Shaikh, J.; Bhosale, R.; Singhal, R. Microencapsulation of black pepper oleoresin. Food Chemistry **2006**, *94*, 105-110.

132. Soottitantawat, A.; Yoshii, H.; Furuta, T; Ohkawara, M.; Linko, P. Microencapsulation by spray drying: Influence of emulsion size on the retention of volatile compounds. Journal of Food Science **2003**, *68*, 2256-2262.

133. Soottitantawat, A.; Takayama, K.; Okamura, K.; Muranaka, D.; Yoshii, H.; Furuta, T; Ohkawara, M.; Linko, P. Microencapsulation of l-menthol by spray drying and its release characteristics. Innovative Food Science and Emerging Technologies **2005**, *6*, 163-170.

134. Bertolini, A.C.; Iani, A.C.; Grosso, C.R.F. Stability of monoterpenes encapsulated in gum arabic by spray-drying. Journal of Agricultural and Food Chemistry **2001**, *49*, 780-785.

135. Ersus, S.; Yurdagel, U. Microencapsulation of anthocyanin pigments of black carrot (*Daucus carota* L.) by spray dried. Journal Food Engineering **2007**, *80*, 805-812.

136. Tanaka, Y.; Sasaki, N.; Ohmiya, A. Biosynthesis of plant pigments: anthocyanins, betalains and carotenoids. The Plant Journal **2008**, *54*, 733-749.

137. Mortensen, A. Carotenoids and other pigments as natural colorants. Pure Applied. Chemistry **2006**, *78*, 1477-1491.

138. Nunes, I.L.; Mercadante, A.Z.; Encapsulation of lycopene using spray-drying and molecular inclusion processes. Brazilian Archives of Biology and Technology **2007**, *50*, 893-900.

139. Shu, B.; Yu, W.; Zhao, Y.; Liu, X. Study on microencapsulation of lycopene by spray-drying. Journal Food Engineering **2006**, *76*, 664-669.

140. Rodriguez-Huezo, M.E.; Pedroza-Islas, R.; Prado-Barragán, L.A.; Beristain, C.I.; Vernon-Carter, E.J. Microencapsulation by spray drying of multiple emulsion containing carotenoids. Journal Food Science **2004**, *69*, E351-E359.

141. Barbosa, M.I.M.J.; Borsarelli, C.D.; Mercadante, A.Z. Light stability of spray-dried bixin encapsulated with different edible polysaccharide preparations, Food Research International **2005**, *38*, 989-994.

142. Robert, P.; Carsson, R.M.; Romero, N.; Masson, L. Stability of spray-dried encapsulated carotenoid pigments from Rosa Mosqueta (*Rosa rubiginosa*) oleoresin. JAOCS **2003**, *80*, 1115-1120.

143. Valduga, E.; Lima, L.; Prado, R.; Padilha, F.F.; Treichel, H. Extraction, spray drying and microencapsulating of 'Isabel' grape (*Vitis labrusca*) bagasse anthocyanin. Ciência e Agrotecnologia, Lavras **2008**, *32*, 1568-1574.

144. Ayadi, M.A.; Khemakhen, M.; Belgith, H.; Attia, H. Effect of moderate spray drying conditions on functionality of dried egg white and whole egg. Journal of Food Science **2008**, *73(6)*, 281-287.

145. Franke, K.; Kieβling, M. Influence of spray drying conditions on functionality of dried whole egg. Journal of the Science of Food and Agriculture **2002**, *82*, 1837-1841.

146. Písecký, J. Spray drying in the cheese industry. International Dairy Journal **2005**, *15*, 531-536.

147. Roberfroid, M.; Gibson, G.R.; Delzenne, N. The biochemistry of oligofructose, a nondigestible fiber: an approach to calculate its caloric value. Nutrition Reviews **1993**, *51(5)*, 137-146.

148. Leite, J.T.C.; Park, K.J.; Ramalho, J.R.P. Obtainment of the inulin extract by lowering temperature and the inulin powder by spray drying. In Proceeding of the 13th International drying Symposium (IDS 2002), Beijing, China, 662-669, **2002**.

149. Verdurmen, R.E.M.; Jong, P. Optimisation product quality and process control for powdered dairy products. In Smit, Gerrit (Ed.). Dairy Processing: Improvement Quality, Chapter 16, Boca Raton; CRC Press, **2003**.

150. Friedman, M. Nutritional value of proteins from different food sources. A review. Journal of Agricultural and Food Chemistry **1996**, *44(1)*, 6-29.

151. Gildberg, A; Stenberg, E. A new process for advanced utilization of shrimp waste. Process Biochemistry **2001**, *36(8-9)*, 809-812.

152. Clare, D.A.; Swaisgood, H.E. Bioactive milk peptides: A prospectus. Journal of Dairy Science **2000**, *83(6)*, 1187-1195.

153. Bhaskar, N.; Modi, V.K.; Govindaraju, K.; Radha, C.; Lalitha, R.G. Utilization of meat industry by products: Protein hydrolysate from sheep visceral mass. Bioresource Technology **2007**, *98(2)*, 388-394.

154. Kurozawa, L.E.; Park, K.J.; Hubinger, M.D. Effect of maltodextrin and gum arabic on water sorption and glass transition temperature of spray

dried chicken meat hydrolysate protein. Journal of Food Engineering **2009**, *91*, 287-296.

155. Anandharamakrishnan, C.; Rielly, C.D.; Stapley, A.G.F. Loss of solubility of α-lactalbumin and β-lactoglobulin during the spray drying of whey proteins. LWT **2008**, *38*, 270-277.
156. Fernández-Pérez, V.; Tapiador, J.; Martín, A.; Luque de Castro, M.D. Optimization of the drying step for preparing a new commercial powdered soup. Innovative Food Science and Emerging Technologies **2004**, *5*, 361-368.
157. Grabowski, J.A.; Truong, V.D.; Daubert, C.R. Spray drying of amylase hydrolyzed sweet potato puree and physicochemical properties of powder. Journal of Food Science **2006**, *71*, E209-E217.
158. Birchal, V.S.; Passos, M.L.; Wildhagen, G.R.S.; Mujumdar, A.S. Effect of spray-dryer operating variables on the whole milk powder quality. Drying Technology **2005**, *23*, 611-636.
159. Nijdam, J.J.; Langrish, T.A.G. An investigation of milk powders produced by a laboratory-scale spray dryer. Drying Techonology **2005**, *23*, 1043-1056.
160. Kurozawa, L.E.; Morassi, A.G.; Vanzo, A.A.; Park, K.J.; Hubinger, M.D. Influence of spray drying conditions on physicochemical properties of chicken meat powder. Drying Technology **2009**, *11*, 1248-1257.
161. Abdul-Hamid, A.; Bakar, J.; Bee, G.H. Nutritional quality of spray dried protein hydrolysate from Black Tilapia (*Oreochromis mossambicus*). Food Chemistry **2002**, *78*, 69-74.
162. Bueno-Solano, C.; López-Cervantes, J.; Campas-Baypoli, O.N.; Lauterio-García, R.; Adan-Bante, N.P.; Sánchez-Machado, D.I. Chemical and biological characteristics of protein hydrolysates from fermented shrimp by-products. Food Chemistry **2009**, *112*, 671-675.
163. Kwak, K.S.; Cho, S.M.; Ji, C.I.; Lee, Y.B.; Kim, S.B. Changes in functional properties of shark (*Isurus oxyrinchus*) cartilage gelatin produced by different drying methods. International Journal of Food Science and Technology **2009**, *44*, 1480-1484.
164. Perez-Munoz, F.; Flores, R.A. Characterization of a spray drying system for soymilk. Drying Technology **1997**, *15*, 1023-1043.

Sadikoglu, H. Spray freeze drying - Volume 1, Ed. Woo, M.W., Mujumdar, A.S. and Daud, W.R.W., **2010**, ISBN - 978-981-08-6270-1, Published in Singapore, pp. 157-182.

Spray freeze drying

Chapter 6

Sadikoglu H.

Department of Chemical Engineering, Gebze Institute of Technology, Gebze-Kocaeli, Turkey

Contents **Page**

1.0 Introduction

Spray freeze drying (SFD), a combination of two different drying processes, spray drying (SD) and freeze drying (FD), is an emerging technology for drying of foods, pharmaceutials, biochemicals, ceramics and fine chemicals. In order to understand the spray freeze drying, both freeze drying and spray drying were overviewed.

1.1 Freeze drying

Freeze drying also known as “lyophilization” or “cryodesiccation” is a dehydration process mainly used for pharmaceutical, fine chemical and food industries to preserve heat sensitive and perishable materials or make the material more convenient for transportation. The freeze-drying of a certain product of interest includes the following steps [1]:

1. Preparation and formulation step (addition of the optimal amount of bulking agents, stabilizers, antioxidants, emulsifiers, cryoprotectors, and/or moisture-buffering agents to the material to be freeze-dried)
2. Freezing step (liquid solutions, gel suspensions, or foodstuffs are cooled down to their solidification temperature to freeze the free water in the material)
3. Primary drying step (free or frozen water in the material being freeze-dried is removed by sublimation under high vacuum),
4. Secondary drying step (certain amount of bound water of the material being freeze-dried is removed by desorption under moderately high vacuum)
5. Packaging and final storage (packing the certain amount of freeze-dried product with an appropriate packaging material in a sterile environment and storing the packed product in a controlled conditions to prevent water vapor and oxygen ingress and light).

The freeze drying process requires intensive energy for sublimation of frozen solvent (water) during the primary drying stage, for removing of bound (unfrozen) solvent (water) during the primary and secondary drying stages and for supporting the vacuum during the entire drying process. In freeze drying process, heat input to the material being dried, drying chamber pressure, and, ice condenser temperature are natural control variables. The magnitude of heat input to the material being dried depends on the value of the heating plates temperatures. Therefore, the value of the heating plate temperatures must be in admissible range to prevent unacceptable product quality[2-3]. This means that, during primary drying stage, temperature of dried region must not exceed scorch point while temperature of the frozen region must be less than the melting point of the product of interest. During secondary drying stage, temperature at anywhere in the dried sample must not exceed the scorch point of the product.

The drying chamber pressure is the another natural control variable and affects significantly the mass and heat transfer mechanisms of the freeze-drying process. The drying chamber pressure is equal to the sum of the partial pressures of water vapor and inerts in the drying chamber. Thus, the value of drying chamber pressure can be changed by adjusting the partial pressure of water vapor in the chamber (the partial pressure of water vapor can be changed by adjusting the temperature of the ice condenser) and by increasing or decreasing the partial pressure of the inerts in the chamber (the partial pressure of the inerts increases by opening a bleeding valve, and decreases through the use of a vacuum pump).

Supplying enough sublimation energy to the moving interface from the heating plate located at the top of the product being freeze dried through porous dried layer without scorching the dried layer and from the heating plate located at the bottom of the product through frozen layer without melting the frozen layer is a difficult task. The primary drying stage of the freeze drying process is mass transfer limited process and control of drying chamber pressure becomes dominant. Drying chamber pressure should be close to its minimum value of 1-10 Pa to keep mass transfer rate in the dried region of material being dried relatively high. As a result of low drying chamber

pressure which is close to the absolute vacuum, the main mechanism of energy transfer from top heating plate to the upper surface of the material being freeze dried takes place by radiation. The amount of energy (heat) that reached at the top surface of the material being freeze dried is transfered to the moving interface through porous dried layer by conduction. The thermal conductivity of dried layer is very low due to the porous structure. Energy input to the material being freeze dried from the heating plate located at the bottom of the tray occurs by conduction. The heat that enters to the bottom surface of the material conducted through the frozen layer to the moving interface. The thermal conductivity of the frozen layer is about one order of magnitute greater than the thermal conductivity of the frozen layer, but constraint for the frozen layer, which is the melting temperature, is much lower than the constraint for the dried layer which is the scorch temperature of the dried layer. Hence, the great amount of heat required for sublimation at the moving interface comes from the bottom of the product being freeze dried. During the entire freeze drying period, the heating plate temperatures must be monitored and controlled properly to prevent any melting and scorching in the frozen and dried layers, respectively. Low thermal conductivity of the dried layer and low melting temperature of the frozen layer cause gradual heat input to the system resulting in extending the duration drying period.

Even though freeze drying is both slow and expensive (initial investment and operating cost is high), it has wide range of application especially for drying heat sensitive products in the food, pharmaceutical, biochemical and biomedical industries.

1.2 Spray drying

Another widely used drying from the chemical industry (amino acid, nitrates, titaniun dioxide, paint pigments, ammonium salts, etc.) to the food industry (milk, tea, coffee, whey, egg, etc.) and from the pharmaceutical industry (penicillin, blood products, vaccinees, etc) to the biochemical industry (yeast extract, algea, enzymes, etc.) is spray drying which has been used since 1850's. In spray drying, a solution, slurry, emulsion, gel or paste pumped into an atomizer that uses a rotating wheel or pressurize nozzle, which is generally located at the top of the drying chamber to obtain highly dispersed sprayed droplets. The air used in spray drying is drawn from the atmosphere by a fan, passed through filters and sometimes dehumidified. Air is heated to a desired temperature by using an oil furnace, a steam heater or an electrical heater. Highly dispersed sprayed droplets meet the hot air in the cyclone type drying chamber. After the droplets come in contact with the hot air, the moisture is transformed into the air, and majority of the dried product falls into the bottom of the drying chamber where are they collected. The air that leaves the drying chamber conveys some of the dried products. Therefore, it is passed through a cyclone separator to catch the dried particles in the air stream.

There are three fundamental stages in spray drying:

1- Atomization of liquid product of interest to highly dispersed droplets,

2- Mixing of sprayed droplets with hot gas stream (generally air) to evaporate moisture of the product to obtain fine dried product,

3- Separation of the dried products from the exhaust air.

Atomization

The atomizing device, which breaks bulk liquid into small droplets to form a spray, is the most important equipment in the spray drying process. The main functions of the atomizer are to create a high surface to mass ratio to facilitate evaporation and to produce particles with desired shape, size and density. The quality of the product produced in a spray dryer and the energy required to maintain the atomization of liquid to form a spray depend heavily on the selection of the atomizer. There are different types of atomizers used commercially in spray drying processes:

1- *Rotary or wheel atomizer:* Liquid is fed into the center of a high speed rotating wheel to break fluid into small droplets by using centrifugal energy. The main advantage of the rotary or wheel atomizer is the ability of producing homogeneous spray within a wide range of mean droplet size. They are flexible, and can be used for different products. They are easy to operate, and desired droplet size can be obtained by adjusting wheel speed. The capital and operational costs are high compare to the other atomizers. They are not suitable for atomizing highly viscous materials. Rotary or wheel atomizers can not be utilized in the horizontal dryers.

2- *Pressure nozzle:* Pressure nozzle is the most widely used atomizer for spray dryers. The material being spray dried is supplied to the nozzle under pressure produced from a high pressure pump. The rotating fluid allows the nozzle to convert pressure energy of liquid into the kinetic energy to form a thin, high-speed film at the exit of the nozzle[4]. The quality of the thin film heavily depends on viscosity, surface tension of the liquid feed, the amount of feed per unit time and the medium where material is sprayed. A single pressure nozzle capacity generally does not exceed 100 l/h, but several nozzles can be utilized in the drying chamber to increase production capacity. The capital and operational costs of pressure nozzles are lower than the other atomizers. They are simple, easy to construct and flexible. Operation pressure for the pressure nozzles can vary from 250 psi (17.4 bar) to 10,000 psi (690) bar [4].

3- *Pneumatic or two-fluid nozzle:* Pneumatic or two-fluid nozzles combine liquid feed material and compressed air (0.15 MPa to 0.8 Mpa) or steam in a two-fluid nozzle to atomize the fluid. In general, liquid material to be spray dried is mixed with the compressed air at the outside of the nozzle, but there are few applications where mixing occurs inside the nozzle. These types of nozzles are able to atomize highly viscous fluids to produce fine particles. The size of the spray droplets produced by the pneumatic or two-fluid nozzles can be altered

by adjusting air-liquid ratio. The high cost for producing compressed air makes pneumatic or two-fluid nozzles expensive to operate.

4- *Ultrasonic atomization:* The conventional atomizers such as rotary (or wheel), pressure and two-fluid (or pneumatic) atomizers are not sufficient to atomize highly viscous, non-Newtonian and long molecular chain structured liquids. Some of these liquids form filaments instead of spherical droplets when conventional atomizers are used. Recent studies show that ultrasonic energy and vibration obtained from a sonic resonance cup placed in front of the nozzle can be used to disintegrate highly viscous liquids to obtain droplets with desired size. Ultrasonic atomizers can be used to produce fine droplets below 50 μm. Commercial application of ultrasonic atomizers is limited, but expected to grow over the coming years.

Drying Chamber

The design and shape of the drying chamber depends heavily on the final characteristics of the dried product, production rate, selected atomizer, required time for air-dispersed droplet contact. Data obtained from experimental laboratory or pilot scale spray dryers to determine some basic design parameters are usually used to design industrial scale spray dryer chambers. Stainless steel metal sheets are generally used to construct spray dryer chambers. The outer surface of chamber can be insulated when needed. The mixing of the dispersed droplets and air inside the drying chamber could be co-current or countercurrent or mixed flow. Co-current contact where atomized droplets fall down with the flowing air, is common when wheel (or rotary) and nozzle type atomizers are used in the design. Countercurrent contact where air comes in contact with the spray dried particles counter currently is suitable for heat sensitive products. The mixed flow contact consists of both co-current and countercurrent contact, and this type of design is usually used when the space for drying chamber is limited and coarse product is desired [5].

Powder Collection and Separation

The dried product is collected at the bottom of the drying chamber in the form of powder and discharge. The bottom part of the drying chamber is generally in cone shape to facilitate collection of the dried product and also acts as a cyclone separator. Majority of the dried product is taken from the bottom of the drying chamber, but some of the dried powder goes to the discharged gas stream and must be separated by a high efficiency cyclone separator prior to filtration.

Compared with other drying processes, the spray drying has some advantages. The fine dried powder products with required size and shape can be produced from any pumpable liquids such as solution, slurry, paste, gel and suspension. Spray dryers can be designed at any capacity from few kg/h to tons/h for heat-resistant products (ceramic powders, fertilizers and etc.) and heat sensitive products (pharmaceuticals, bio-chemicals and etc). Automatic control of the process is possible because process parameters in spray drying can be measured and monitored during the entire drying period. By choosing appropriate atomizer, altering feed to drying air ratio and adjusting rotational speed or pressure of the compressed air in atomizer, uniform porous spherical particles in required size and shape can be produced.

2.0 Spray freeze drying

Spray freeze drying combines the best features of both spray and freeze drying to produce high quality and spherical porous particles in a wide range of sizes, especially for pharmaceutical and bio-chemical uses. The first step in spray freeze drying is to prepare spherical frozen droplets with the required properties. In general, two-fluid nozzles or pneumatic nozzles that are the same nozzles used in spray drying are also used in spray freeze drying to obtain droplets. By adjusting the compressed air to feed liquid ratio for intended size of frozen particles, the material to be spray freeze dried is atomized into the cryogenic liquid nitrogen or very cold gas stream for freezing. Short after the sprayed droplets is in contact with the frozen medium, they form slurries of frozen particles. The collected frozen particles packed in trays of freeze dryer to remove both the free (frozen) and bound (sorbed) water content of the materials (Figure 1). The rest of the procedure is the same as that of the conventional freeze drying where the free solvent (water) content of the material is removed by sublimation and bound water content is removed by desorption during primary and secondary drying stages, respectively. The initial investment and operational costs of the spray freeze drying process is higher than both spray and freeze drying processes because the spray freeze drying requires atomization of frozen particles in addition to the conventional freeze drying process. Also, the duration of the drying process in spray freeze drying is higher than the conventional freeze drying as a result of low heat and mass transfer capabilities of the porous structure formed by packing sprayed frozen particles in a tray. The main cost apportioned are the energy to produce compressed air for atomizing the liquid feed to produce fine droplets, the energy to maintain freezing medium at sub-zero temperatures to obtain frozen slurry, the energy for sublimation of the frozen solvent during primary drying stage, the energy for removal (desorption) of bound (unfrozen) solvent during primary and secondary drying stages, and the energy to support vacuum during entire drying cycle. Despite of its low productivity and high cost, the spray freeze drying is becoming more popular process for producing relatively large porous microparticles which are ideal for pulmonary drug delivery, processing of low water soluble drugs [6-8], producing of powders for epidermal immunization [7,9], and the preparation of particles for micro-encapsulation[7,10].

The history of the spray freeze drying can be dated back to 1940's when Benson and Ellis [11] have studied the surface area of protein particles prepared by spray freezing subsequently freeze drying. In 1964, Werly and Baumann [12] have produced sub-micronized powder by spray-freezing. The idea of producing fine solid micron or sub-micron sized particles using spray freezing followed by the freeze drying inspired many inventors, and many patents issued over the years [13-16]. The variations of the effective parameters such as the pressure of nitrogen, pressure of liquid feed, flow of nitrogen and flow of liquid were studied [17], and the mass flow ratio which is defined as the ratio mass of nitrogen to the liquid feed was found to be the most important parameter that affects the size and stability of spray freeze dried product. The

effects of excipients such as trehalose, mannitol, surfactants and ammonium sulfate incorporated into the protein solution for stabilization during atomization and drying of protein solution were studied [18] and it was shown that incorporation of excipient into the bovin serum albumin (BSA) stabilized the solution during spray freeze drying by lowering the specific surface area in the dried powder. Spray freeze drying technique can increase the solubility of the low water soluble drugs by reducing the size of the drug particles [6]. The spray freeze dried powder with smaller particle size and higher surface area results from porous structure of particles which have better wettability and faster dissolution rates in aqueous medium [19]. Specific surface areas of various powders obtained from different techniques were compared [20] and the spray freeze dried powders were found to have largest specific area.

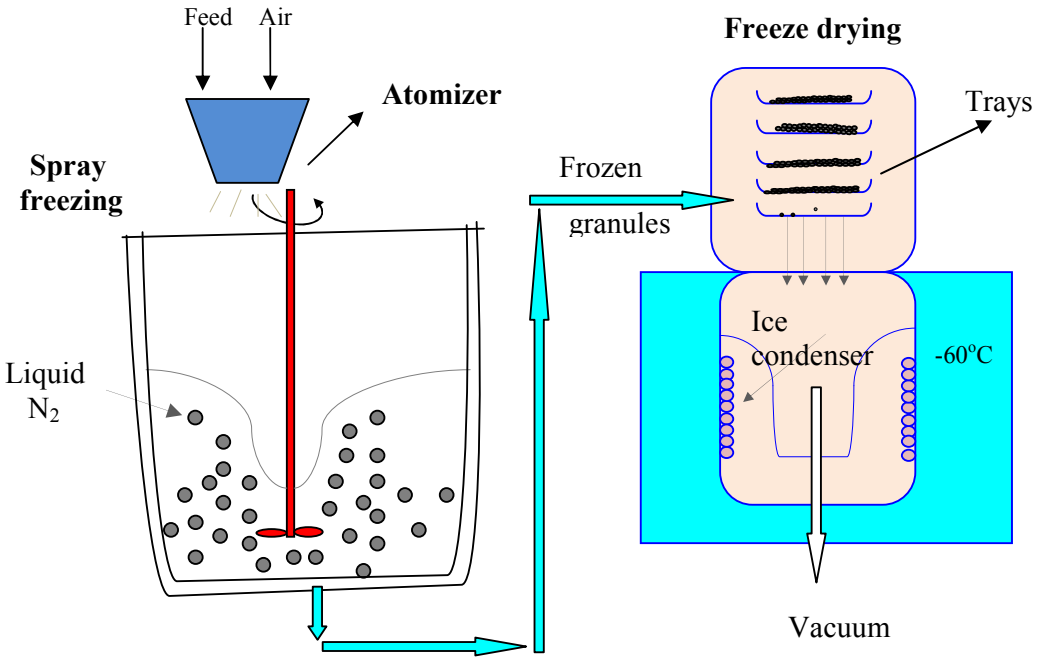

Figure 1 Diagram of the spray drying process

Another current and potential use of the spray freeze drying is in micro-encapsulation which is defined as a process for coating of very small droplets or particles of liquid or solid materials with polymeric films. The micro-encapsulation process has a wide range application in chemical, material science, food and pharmaceutical industries. Micro-encapsulation can be used to isolate core material such as vitamins from the destructive effect of oxygen, to prevent evaporation of a volatile core such as aroma and flavor, to improve the handling of the sticky materials and to buffer reactive core from a chemical attack. In the pharmaceutical industry, micro-encapsulation is used for protection, stabilization and controlled release of drugs. The model protein bovine serum albumin (BSA) obtained from spray freeze drying process successfully encapsulated into poly (D,L lactide-*co*-glycolide) (PLG) micro-spheres for controlled release of native protein[21]. A water soluble drug,

procaine hydrochloride, was successfully encapsulated in a microcapsule core, porous structured biodegradable poly(DL-lactide) (PLA) that was prepared by spray freeze drying. The particle morphology, the amount of solvent used, solvent exposure time, the amount of the surfactant and the method of dispersing the freeze-dried particles in water were found to the amount of the effective parameters in the encapsulation process [22]. The effective process parameters for producing spray freeze dried therapeutic protein such as, recombinant human growth hormone (rhGH) for encapsulation were studied[10] and the mass flow ratio of atomization was found to be the most important factor. High mass flow rates contribute the production sprayed protein powders with a very fine and friable microstructure that helps controlled release of therapeutic proteins. The impact of various excipients to stabilize human immunoglobulin G (IgG) during atomization period of spray freeze drying followed by subsequent encapsulation into polylactide-co-glycolide (PLGA) microspheres were studied and mannitol and trehalose were found as appropriate additives protecting IgG from degradation [23]. Lam et al.[23] encapsulated recombinant human nerve growth factor (rhNGF) into poly (lactic-co-glycolic) acid (PLGA) microspheres using a spray freeze drying technique.

Micro-encapsulation is also one of the promising processes to produce functional foods fortified with health-promoting additives. By using spray freeze drying procedure, *Lactobacillus paracasei* was successfully microencapsulated with high viability for probiotic use[25]. Even though the spray freeze drying is considered to be the most suitable process to prepare friable solid powders with high specific surface area for encapsulation, some researchers reported that the spray freeze drying is not a suitable process to produce darbepoetin alfa particles for encapsulation as a result of high aggregation during drying and reconstitution [26,27].

Producing advanced ceramics with unique electrical properties such as superconductivity or superior mechanical properties (enhanced toughness and high-temperature strength) depends on using highly pure synthetic precursor powders with desired properties. The ability of producing granules with a density and homogeneity that directly corresponds to the characteristics of the original suspension makes the spray freeze drying technique significant process for producing precursor powders. In order to prepare homogenous and reactive precursor powders for advanced ceramics, a mixture of water-soluble salts such as sulfates are dissolved in water to obtain a highly dispersed solution. Prepared salt solution is sprayed into chilled organic liquids such as hexane with an atomizer to obtain frozen droplets for desired size and property. The frozen material separated from the liquid hexane is passed through the sieves and packed in a tray then undergoes the freeze drying to remove solvent (water) by sublimation under vacuum. Particle shrinkage, strong inter-particle bonds, and the migration of additives that occur during the conventional drying can be eliminated by using freeze drying technique. Similar to other use of the spray freeze drying, the shape and size of the granules can be controlled by the solution rheology, spray flow rate and applied gas pressure at atomizer.

Highly porous and temperature resistant the magnesia ceramics for combustion catalyst support was obtained by spraying magnesium sulfate aqueous solution into cooled n-hexane and subsequently freeze dried [28]. The water based nitrate solutions sprayed from an atomizer into liquid nitrogen to

obtain fine frozen particles were dried in an industrial freeze dryer to produce precursors for synthesizing superconducting Bi-2223 ceramic [29]. Lee et al.[30] have prepared perovskite-type $LaCoO_3$ oxides by spray freeze drying of citrate precursor. They have reported that spray freezing of precursor followed by freeze drying reduced calcination temperature, enhanced amount of the precursor, and increased surface area of the product (LaCoO3). Itatani et al.[31] reported that the spray freeze drying technique can be used to produce various calcium-phosphate powders with minimal agglomeration.

Even though spray freeze drying has a wide range of application in ceramics industry to produce fine precursors for synthesizing advanced ceramics such as superconductors [32], temperature resistant and highly durable materials, and in the food industry to produce functional foods such as probiotics and high value foods, it has undisputed future in the pharmaceutical industry especially in producing pulmonary inhalable drugs. The pulmonary delivery of biopharmaceuticals requires to produce particles with the optimal properties for deep lung deposition without violating active ingredient of molecules. There are several ways such as milling (vibration milling, ball milling, and jet milling), controlled solvent crystallization, supercritical fluid processing, liquid dispersion systems, spray drying and spray freeze drying to obtain inhalation powder drug for pulmonary delivery. The overall efficiency of the inhalation powder drugs depends on the amount of fine particles delivered to lung and lung bioavailability [33]. The size, morphology, dispersability and aerodynamics behavior of the particles play an important role on the efficiency of inhalation process. Incorporating desirable attributes, such as narrow size distribution, enhanced protein stability, improved dispersability, sustainable release, or enhanced targeting into the particles are the main challenge to prepare inhalable powder drugs for pulmonary drug delivery [33-35]. Safe and novel excipients such as poly (lactic-co-glycolic) acid (PLGA), dipalmitoylphosphatidyl-choline (DPPC), lactose, mannitol, trehalose, albumin, and etc., or should be used to improve the performance of inhalation powder drugs. Producing inhalation powder drug and excipients with required characteristics may regulate the release in lung, target certain areas in the lung, avoid macrophage uptake, increase particle mass inhaled per breath, facilitate epithelial permeability and drug absorption, and improve therapeutic action[35].

The success of inhaled medical powders commonly used to cure diseases of the lung such as asthma and cystic fibrosis depends heavily on the particle characteristics of the powders such as aerodynamic diameter that can be altered to deliver drug particles to different areas of the lung. Aerodynamic diameter is a physical property of a particle in a viscous fluid such as air. In general, particles have irregular shapes with actual geometric diameters that are difficult to measure. Aerodynamic diameter characterizes the aerodynamic behavior of the particle by taking into account the shape, size and density of the particles. The aerodynamic diameter d_{ae} can be derived by employing Stoke's Law and is defined as Eq. (1):

$$d_{ae} = \sqrt{\frac{\rho_p}{\chi \rho_0}} d_p \qquad (1)$$

where ρ_p is the particle density (g/cm^3), χ is the dynamic shape factor (dimensionless), ρ_0 is standard particle density (g/cm^3) and d_p is the geometric diameter of the particle (cm). The dynamic shape factor, χ, is the ratio of the drag force on a particle to the drag force on the particle volume-equivalent to the sphere at the same velocity[33]. The value of the dynamic shape factor for a perfect spherical particle is 1, but as the shape of the particle diverges from the sphere, the dynamic shape factor can take a value greater than 1. For example, the value of dynamic shape factor for non-spherical shapes such as platelets, rods or fibers can be as high as 10. The aerodynamic diameter for a spherical particle, as it is given in Eq. (1), is proportional to the geometric the diameter of particle and the square root of the particle density. The value of the aerodynamic diameter can be reduced by either decreasing the geometric diameter of the particle, reducing the particle density or both. The aerodynamic diameter is the key parameter for pulmonary drug delivery. Many experimental and theoretical studies have showed that the particles with mean aerodynamic diameter of 1–3 μm have a tendency to deposit mainly in alveolar region (deep lung) of the lung which is the primary target to deliver therapeutic dose for different lung diseases. The inhalation powder drug of mean aerodynamic diameter of 1–3 μm is considered to be optimal size for inhalation drug delivery and deposits minimally in the mouth and throat. On the other hand, particles with aerodynamic diameter greater than 6 μm tend to deposit Tracheobronchial region, generally not desired for an inhalation therapy. Particles with small aerodynamic diameter such as 1 μm or less are mostly exhaled as breathing while particles with large aerodynamic diameter such as 10 μm or more have little chance to reach beyond the mouth[36].

Large porous particles with small mass density and large geometric diameter obtained by using the spray freeze drying method is considered to be highly effective for pulmonary drug delivery. Having nearly identical aerodynamic diameters, the inhalation ability of the small size and high mass density non-porous particles is better than the large size and low mass density porous particles as a result of smaller surface to volume ratio and less deposition in dry powder inhaler (DPI). Increasing particle size reduces phagocytosis of particles by macrophages. Large particles have tendency to deposit in the pulmonary region that may escape clearance by alveolar macrophages and; therefore, permit drug release for longer periods of time [36].

The spray freeze drying method has a promising future for producing therapeutics inhalation powders for pulmonary drug delivery compare to spray drying and milling. The micro-particles produced by the spray freeze drying have relatively large porous structure and better fine particle fraction. The spray freeze drying is the combination of both spray and freeze drying processes; hence, productivity is low and initial investment and operation all costs are high. The spray freeze drying involves the packing of frozen slurry in a container. Thus, a packed bed of frozen particles have porous structure that make it complicated to supply enough heat to the material being freeze dried for sublimation. As a result of poor transport properties, the duration of spray freeze drying cycle is much greater than the conventional freeze drying process. The operation cost is a function of drying time, and reducing the drying time without causing any loss in quality of product is the main challenge for the spray freeze drying process to have a future in the production of pulmonary inhalable drugs. In order to construct operational control policies to optimize the spray freeze drying process by reducing both

duration of drying time and intensive energy usage without violating any constraint, knowledge about the heat and mass transfer mechanisms involved in the primary and secondary drying stages are crucial. Previous studies have shown that establishing both qualitative and quantitative control policies on natural control variables such as drying chamber pressure, heat input and condenser temperature of conventional freeze drying can substantially reduce drying times and costs of each drying batch [2,3, 37].

3.0 Mathematical modelling of spray freeze drying

3.1 Primary drying stage

In order to predict duration of the drying, temperature distributions, water vapor pressure, inert gas pressure and bound water content at any given time, during both the primary and secondary drying stages of spray freeze drying process, some dynamic multi-dimensional mathematical models were proposed. Among these, the model developed by Liapis and Bruttini[7] is an advanced mathematical model to qualitatively and quantitatively describe the dynamic behavior of spray freeze drying process. In Figure 2, the diagrams of a material on a tray during spray freeze drying and descriptions of the frozen solvent (water) in a frozen particle and the pores resulting from the sublimation of frozen water during the primary drying stage to form a porous dried particle are given. The variable Z(t) represents the position of the moving interface between partially saturated porous frozen region II formed by packing frozen particles and porous dried layer I of a material on a tray. During the primary drying stage of spray freeze drying, water vapor resulted mainly from the sublimation of frozen free water, and negligible amount obtained from desorbing bound water content while during the secondary drying stage the water vapor resulted from only desorbing bound water of the material being spray freeze drying moves through the pores dried layer I to reach condenser part of the drying chamber for removal. The disappearance of the partially saturated porous frozen region II is considered to be the end of the primary drying stage that is the starting of the secondary drying stage. As it is shown in Figure 2 q_I, q_{II} and q_{III} represent the amount of heat fluxes to the material being spray freeze dried in a packed bed from the top, bottom and side surfaces of the tray, respectively.

In primary drying stage, the energy balance equation that represents temperature distribution in dried region I of the packed bed is as follows:

$$\frac{\partial T_I}{\partial t} = \alpha_{Ie} \frac{\partial^2 T_I}{\partial z^2} - \frac{c_{pg}}{\rho_{Ie} c_{pIe}} \left(T_I \frac{\partial N_{t,I}}{\partial z} - N_{t,I} \frac{\partial T_I}{\partial z} \right) + \frac{\Delta H_V \rho_I}{\rho_{Ie} c_{pIe}} \left(\frac{\partial C_{sw}}{\partial t} \right) \quad (2)$$

The numerical values for the parameters used in Eq. (2) are given in Table 1 by employing volume-averaging theory [7, 38] that uses physical properties of the gas and solid phases. The last term in the Eq. (2) accounts for the removal of sorbed water during primary drying stage and it has shown

to be negligible [7,37,39]. The parameter ρ represents the density of the solid in dried region I while ρ_{Ie}, c_{pIe} and k_{Ie} represent effective parameters. The variable $N_{t,I}$ is the sum of water vapor and inerts mass flux vectors and represents the total amount of mass removed from the unit square of the material being spray freeze dried in unit time (in second). The constitutive equations for water vapor and inerts mass flux in the pores of dried layer I can be obtain from dusty-gas model [2,7,39].

$$N_{w,1} = -\frac{M_w}{R_g T_I}\left(k_{1,II}\frac{\partial p_{w,1}}{\partial z} + k_{2,II}\, p_{w,1}\left(\frac{\partial p_{in,1}}{\partial z} + \frac{\partial p_{w,1}}{\partial z}\right)\right) \tag{3}$$

$$N_{in,1} = -\frac{M_{in}}{R_g T_I}\left(k_{3,II}\frac{\partial p_{in,1}}{\partial z} + k_{4,II}\, p_{in,1}\left(\frac{\partial p_{in,1}}{\partial z} + \frac{\partial p_{w,1}}{\partial z}\right)\right) \tag{4}$$

The parameters k_1 and k_3 are the bulk diffusivity constants, k_2 and k_4 are the self-diffusivity constants and p_w and p_{in} are the partial pressures for water vapor and inerts, respectively, in dried layer I. The dusty-gas model does not require detailed information about the porous structure of the dried layer I [7], and it is easy to use. The Darcy's flow permeability, C_{01} that is parameter for self-diffusivity constants (k_2, k_{34}) could be obtained from the Blake-Kozeny correlation [7,40].

$$C_{01} \cong -\frac{\varepsilon_{pb}^3}{150(1-\varepsilon_{pb})^2} d_p^2 \tag{5}$$

Where, d_p denotes the diameter of the frozen particles packed on a tray while ε_{pb} represents the porosity of the packed bed formed by packing frozen particles.

$$\varepsilon_{pb} = \frac{\text{volume of pores in the particle}}{\text{volume of the particle}}$$

Experimently proven [7] that dimensional change of spray frozen particle during both primary and secondary drying stages is negligible and the value of the d_p is considered to be constant during entire drying run. As a result of the minimal dimensional change in the diameter of frozen particle, macroporosity, ε_{pb}, of packed considered to be the same for both dried layer I and partially saturated porous frozen layer II. The heat and mass transfer resistances in dried layer of a material undergoing spray freeze drying is larger than that could be encountered in dried layer of the same material undergoing the conventional freeze drying, because, the porosity of the dried layer I in spray freeze drying is significantly lower than the conventional freeze drying. The expression for the removal of the bound water is as follows:

$$\frac{\partial c_{sw}}{\partial t} = -k_{des} c_{sw} \tag{6}$$

where, the parameter k_{des}, represents desorption rate constant of the linear rate mechanism that could be used to describe the desorption (removal) of bound water [7,39].

The ice saturation, S, that is defined as the fraction of the ice volume to the pore volume in the particle is given by:

$$S = \frac{\frac{4}{3}\varepsilon_p \pi d_{ice}^3}{\frac{4}{3}\varepsilon_p \pi d_p^3} = \left(\frac{d_{ice}}{d_p}\right)^3 \tag{7}$$

where, the parameter, d_{ice}, represents the diameter of an ice core in the particle. The continuity equations for the water vapor and the inert gas in the pores of the porous dried layer I can be expressed as follows:

$$\frac{\partial p_{w,I}}{\partial t} = -\frac{R_g T_I}{\varepsilon_{t,I} M_w}\left(\frac{\partial N_{t,I}}{\partial z} + \rho_I \frac{\partial C_{sw}}{\partial t}\right) \tag{8}$$

$$\frac{\partial p_{in,1}}{\partial t} = -\frac{R_g T_I}{\varepsilon_{t,1} M_{in}}\left(\frac{\partial N_{t,I}}{\partial z}\right) \tag{9}$$

The parameter, ε_{pb}, represents the total porosity of the dried layer I, and can be expressed as follows:

$$\varepsilon_{t,I} = \varepsilon_{pb} + (1-\varepsilon_{pb})\varepsilon_p \tag{10}$$

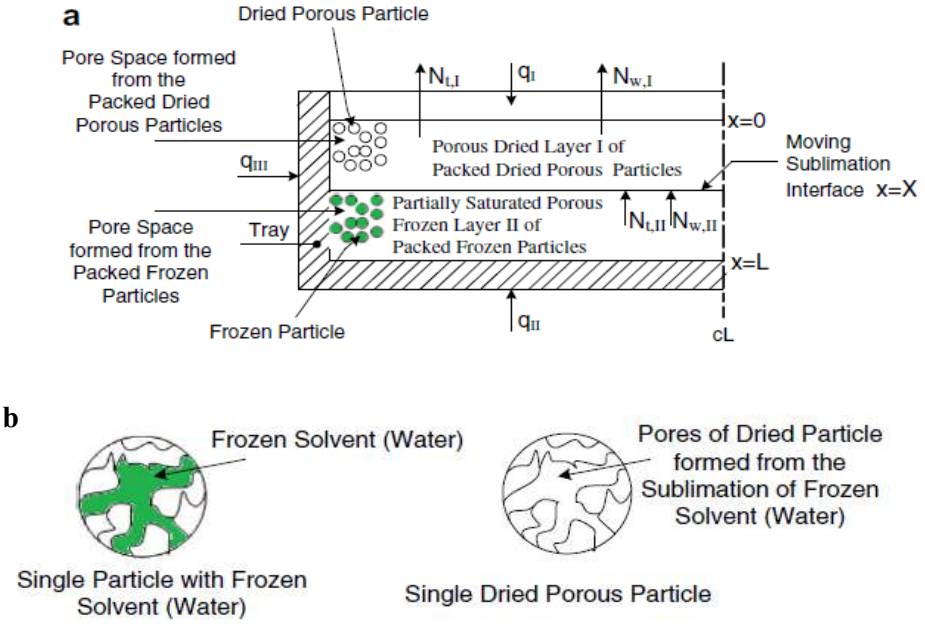

Figure 2 *(a) Diagram of a material being spray freeze dried in a tray. (b) Depictions of the frozen solvent (water) in a frozen particle and the pores resulting from the sublimation of frozen water during the primary drying stage to form a porous dried particle.*

The energy and material balances in the porous frozen layer II are as follows[7]:

$$\frac{\partial T_{II}}{\partial t}=\alpha_{II}\frac{\partial^2 T_I}{\partial z^2}-\frac{c_{pg}}{\rho_{II}c_{pII}}\left(T_{II}\frac{\partial N_{t,II}}{\partial z}-N_{t,II}\frac{\partial T_{II}}{\partial z}\right)+\frac{\Delta H_s}{\rho_{II}c_{pII}}\left(\rho_f-\rho_d\right)\frac{\partial S}{\partial t}+\frac{\Delta H_V\rho_I}{\rho_{II}c_{pII}}\left(\frac{\partial C_{sw}}{\partial t}\right) \quad (11)$$

$$\frac{\partial\left(\varepsilon_{t,II}p_{w,II}\right)}{\partial t}=-\frac{R_gT_{II}}{M_w}\left(\frac{\partial N_{w,II}}{\partial z}+\rho_I\frac{\partial C_{sw}}{\partial t}-\left(\rho_f-\rho_d\right)\frac{\partial S}{\partial t}\right) \quad (12)$$

$$\frac{\partial\left(\varepsilon_{t,II}p_{in,II}\right)}{\partial t}=-\frac{R_gT_{II}}{\varepsilon_{t,II}M_{in}}\left(\frac{\partial N_{in,II}}{\partial z}\right) \quad (13)$$

Water vapor and inerts mass flux in unsaturated porous frozen layer II can be determined using Eq. (14) and Eq.(15), respectively.

$$N_{w,II}=-\frac{M_w}{R_gT_{II}}\left(k_{1,II}\frac{\partial p_{w,II}}{\partial z}+k_{2,II}p_{w,II}\left(\frac{\partial p_{in,II}}{\partial z}+\frac{\partial p_{w,II}}{\partial z}\right)\right) \quad (14)$$

$$N_{in,II}=-\frac{M_{in}}{R_gT_{II}}\left(k_{3,II}\frac{\partial p_{in,II}}{\partial z}+k_{4,II}p_{in,II}\left(\frac{\partial p_{in,II}}{\partial z}+\frac{\partial p_{w,II}}{\partial z}\right)\right) \quad (15)$$

The parameters used in Eq. (11) through Eq. (15) can be calculated by using volume- averaged approach [7,40].

$$\varepsilon_{\mathrm{t,II}}=\varepsilon_{\mathrm{pb}}+(1-\varepsilon_{\mathrm{pb}})\varepsilon_{\mathrm{p}}(1-S_{av}) \quad (16)$$

$$\rho_{\mathrm{II}}\cong S_{av}\rho_f+(1-S_{av})\rho_d=(1-\varepsilon_{\mathrm{pb}})\left(S_{av}\rho_{f,s}+(1-S_{av})\rho_{d,s}\right) \quad (17)$$

$$\rho_{\mathrm{II}}c_{\mathrm{pII}}\cong S_{av}\rho_fc_{pf}+(1-S_{av})\rho_dc_{pd}=(1-\varepsilon_{\mathrm{pb}})\left(S_{av}\rho_{f,s}c_{pf,s}+(1-S_{av})\rho_{d,s}c_{pd,s}\right) \quad (18)$$

$$k_{\mathrm{II}}=S_{av}k_f+(1-S_{av})k_d=S_{av}(1-\varepsilon_{\mathrm{pb}})^{3/2}k_{f,s}+(1-S_{av})(1-\varepsilon_{\mathrm{pb}})^{3/2}k_{d,s} \quad (19)$$

$$\rho_{\mathrm{f}}=(1-\varepsilon_{\mathrm{pb}})\rho_{f,s} \quad (20)$$

$$\rho_{\mathrm{d}} = (1-\varepsilon_{\mathrm{pb}})\rho_{d,s} \tag{21}$$

$$\rho_{\mathrm{d,s}} = (1-C_{\mathrm{sw}})\rho_{d,s,f} \tag{22}$$

$$\rho_{\mathrm{I}} = (1-\varepsilon_{\mathrm{pb}})\rho_{d,s,f} \tag{23}$$

The parameter, S_{av}, represents the volume-averaged ice saturation ($0 \le S_{\mathrm{av}} \le 1$) and equal to integral mean of dimensionless ice saturation, S, over the volume of the porous frozen region II occupied by particles. In Eq. (16), $\varepsilon_{p,II}$, represents the total porosity of the porous frozen layer II, and its value varies with time because the value of the volume-averaged ice saturation, S_{av}, varies with time.

$$S_{av} = \frac{1}{V_{II,p}} \int_0^{V_{II,p}} S dV_{II,p} \tag{24}$$

The parameters, ρ_f, c_{pf}, and k_f, defined in Eqs. (17) through (20) represent the apparent density, heat capacity and thermal conductivity of a frozen particle based material (S_{av}=1), respectively, while the parameters ρ_d, c_{pd}, and k_d defined in Eqs. (17) through (19) and (21) denote apparent density, heat capacity and thermal conductivity of a dried particle based material, respectively, after the primary drying (S_{av}=0). The parameters, $c_{pf,s}$ and $k_{f,s}$, defined in Eqs. (18)-(19) represent the heat capacity and thermal conductivity of a frozen solution based material, respectively, while the parameters $c_{pf,d}$ and $k_{f,d}$ that defined in Eqs. (18)-(19) denote heat capacity and thermal conductivity of a dried solution based material, respectively. Finally, the parameter, $\rho_{d,s,f}$, denotes the density of the solution based material when it is fully dried and both forms of frozen and sorbed water have been removed [7]. The water vapor pressure in porous frozen layer II can be calculated directly from the following expression [7,40]:

$$p_{w,II} = p_w^{sat}\left(T_{II}\right) = 10^{(-2663.5/T_{II})+12.537} \tag{25}$$

When the value of S>0, the term $\partial p_{w,II}/\partial t$ in Eq. (12) could be determined from the following equation:

$$\frac{\partial p_{w,II}}{\partial t} = \frac{dp_w^{sat}}{dT_{II}} \frac{\partial T_{II}}{\partial t} \tag{26}$$

where, the term $\partial T_{II}/\partial t$ can be obtained by solving of Eq. (11). The evolution of ice saturation, S, can be obtained by solving of Eq. (12). An energy balance at the moving interface, whose thickness is taken infinitesimal, can be express as follows:

$$k_{II}\frac{\partial T_{II}}{\partial z} - k_{Ie}\frac{\partial T_I}{\partial z} + \left(\rho_{II}c_{pII}T_{II} - \rho_I c_{pI}T_I\right)\frac{\partial Z}{\partial t} + c_{pg}T_{\mathrm{int}erf}N_{t,\mathrm{int}erf} = \Delta H_s N_{w,\mathrm{int}erf} \tag{27}$$

In Eq.(27), T_{interf}, denotes the temperature of the interface ($T_{interf} = T_I = T_{II}$), $N_{w,interf}$ represents water vapor mass flux at the moving interface and $N_{t,interf}$ represents total mass flux (sum of water vapor mass flux and inert mass flux) at the moving interface. $\partial Z/\partial t$ denotes the velocity of the moving interface and can be defined as follows [2-3,7,37, 39]:

$$\frac{\partial Z}{\partial t} = -\frac{N_{w,interf}}{\rho_{II} - \rho_I} \tag{28}$$

Table 1 Expressions and values for the physical parameters

$c_{pd,s}$ = 2590 J/kg K
$c_{pf,s}$ = 1930 J/kg K
c_{pg} = 1616.6 J/kg K
C_{sw}^0 =0.6415 kg water/kg solid
$\left(D_{w,in}\right)_i = \left(4.342\text{x}10^{-6}\left(T_i^{2.334}\right)\right)/P_i$ m^2/s for I and II
$k_{Ie} = \left(1-\varepsilon_{pb}\right)^{3/2}\left(2.596\text{x}10^{-4}\left(P_I\big\vert_{z=0} + P_I\big\vert_{z=Z}\right) + 0.039806\right)$ W/m K
k_{des} = 6.48x10^{-7} s^{-1} during the primary drying stage
k_{des} = 7. 80x10^{-5} s^{-1} during the secondary drying stage
$k_{d,s} = 2.596\text{x}10^{-4}(P_{II}\vert_{z=Z} + P_{II}\vert_{z=L}) + 0.039806$ W/m K
$k_{f,s}$ = 2.56 W/m K
L = 0.01 m
M_{in} = 28.82 kg/kmol
M_w = 18.00 kg/kmol
p_i^0 =5.07 Pa, at t = 0 and 0≤z≤ L for i = I, II
$p_{in,i}^0$ =4.0 Pa, at t = 0 and 0≤z≤ L for i = I, II
$p_{w,i}^0$ =1.7 Pa, at t = 0 and 0≤z≤ L for i = I, II
R_g = 8.314 J/K mol
$T_{lp} = T_{up}$ = 253.15 K for primary drying stage
$T_{lp} = T_{up}$ = 293.15 K for secondary drying stage
T_m = 263.15 K
T_{scor} = 313.15 K
T_i^0 =233.15 K, at t = 0 and 0≤z≤ L for i = I, II
ΔH_s =2687.4 kJ/kg
ΔH_v=2840 kJ/kg
ε_p = 0.785
ε_{pb} = 0.50
$\mu_{mx} = 18.4558x10^{-7}\left(T_i^{1.5}/\left(T_i + 650\right)\right)$ kg/ms, for i = I, II
$\rho_{d,s} = 328\left[\left(1+C_{sw}\right)/\left(1+C_{sw}^0\right)\right]$ kg/m^3
$\rho_{d,s,f}$ = 199.817 kg/m3
$\rho_{f,s}$ = 1030 kg/m3
$\rho_{Ie}c_{pIe} \cong 328\left(1-\varepsilon_{pb}\right)\rho_{d,s}c_{pd,s}$
$\tau_I = \sqrt{2}$ dimensionless

$\tau_{II} = \sqrt{2}$ dimensionless

The initial and boundary conditions for Eqs.(2), (6), and (8) through (13) for spray freeze frying on a tray are as follows:

$$T_I = T_{II} = T_Z = T^0 \ at \ t = \ 0 \ , \ 0 \le z \le L \tag{29}$$

$$p_w = p_w^0, \quad p_{in} = p_{in}^0 \ at \ t = \ 0 \ , \ 0 \le z \le Z(t) \tag{30}$$

$$C_{sw} = C_{sw}^0 \ at \ t \ = \ 0 \ , \ 0 \le z \le L \tag{31}$$

$$q_I = k_{Ie} \left. \frac{\partial T_I}{\partial z} \right|_{z=0} \ at \ z = 0 \ , \ t \ge 0 \quad \text{where} \quad q_I = \sigma F \left(T_{up}^4 - T_I^4(0,t) \right) \tag{32}$$

$$T_I = T_{II} = T_Z \quad at \ \ z = Z(t), \quad t \ge \ 0 \tag{33}$$

$$q_{II} = k_{II} \left. \frac{\partial T_{II}}{\partial z} \right|_{z=L} \ at \ z = L \ , \ t \ge 0 \tag{34}$$

For radiation heat transfer to the bottom of tray,

$$q_{II} = \sigma F \left(T_{lp}^4 - T_{II}^4(L,t) \right) \tag{35}$$

For a thin film between the frozen material and lower plate,

$$q_{II} = h \left(T_{Lp} - T_{II}(L,t) \right) \tag{36}$$

The value of the thermal film conductivity, h, could be found in [2,3,39], and suitably adjusted to account for the lowered pressure in the freeze-drying process. The variable, p_{w0}, is the partial pressure of water vapor in the chamber, usually determined by the condenser design and assumed constant within the drying chamber[39]. The variable, P_0, denotes the sum of partial pressure of water vapor and inerts ($P_0 = p_{w0} + p_{in0}$) at z = 0, and is usually considered to be approximately equal to the total pressure in the drying chamber.

$$p_w = p_{w0}, \quad p_{in} = P_c - p_{w0} \ at \ z = \ 0 \ , \ t \ge 0 \tag{37}$$

$$p_w = f\left(T\big|_{z=Z(t)}\right) \; at \; z = \; Z(t) \; , \; 0 \le t \le t_{pd} \tag{38}$$

$$\left.\frac{\partial p_{in}}{\partial z}\right|_{z=Z(t)} = 0 \quad at \; z = Z(t), \;\; 0 \le t \le t_{pd} \tag{39}$$

The initial condition for Eq. (28) is as follows:

$$Z = 0 \; at \; t = \; 0 \tag{40}$$

The initial and boundary conditions for Eqs. (12) and (13) are as follows:

$$S = 1 \; at \; t = \; 0 \tag{41}$$

$$p_{in,II} = p_{in,II}^{0} \quad at \; t = \; 0 \tag{42}$$

$$\frac{\partial p_{in,II}}{\partial z} = 0 \quad \text{at impermeable surfaces} \tag{43}$$

The equations given from Eq. (2) through Eq. (42) represent the mathematical model and the parameters that could be used to describe the dynamic behavior of the primary drying stage of spray freeze drying in a tray. The heat input from the upper heating plates to the top surface of the sample (q_I), the heat input from lower heating plates to the bottom surface of the sample (q_{II}), and drying chamber pressure (P_0) are the natural control variables. The control variables must be selected from set of admissible controllers that (i) the temperature, T_{interf}, of moving interface and the temperature, T_{II}, in the region of the porous frozen layer II (S>0) must be less than the melting temperature, T_m, of the frozen material, (ii) and the temperature, T_I, in porous dried layer I and the temperature, T_{II}, in the porous frozen layer II (S=0) must be less than the scorch temperature, T_{scor}, of the material being spray freeze dried.

3.2 Secondary drying stage

In the secondary drying stage, there is no longer porous frozen layer II available, and thus, there is no moving sublimation interface. The secondary drying stage involves the removal of bound (unfrozen) water. The thickness of the dried layer is L, and the energy balance in this layer is as follows:

$$\frac{\partial T_I}{\partial t} = \alpha_{Ie} \frac{\partial^2 T_I}{\partial z^2} - \frac{c_{pg}}{\rho_{Ie} c_{pIe}} \left(T_I \frac{\partial N_{t,I}}{\partial z} - N_{t,I} \frac{\partial T_I}{\partial z} \right) + \frac{\Delta H_V \rho_I}{\rho_{Ie} c_{pIe}} \left(\frac{\partial C_{sw}}{\partial t} \right) \tag{44}$$

The initial and boundary conditions of Eq.(43) are:

$$T_I = \gamma(z) \; at \; t = t_{pd}, \; 0 \le z \le L \tag{45}$$

$$q_I = k_{Ie} \left.\frac{\partial T_I}{\partial z}\right|_{z=0} \quad at\ z = 0\ ,\ t \geq 0 \quad \text{where} \quad q_I = \sigma F\left(T_{up}^4 - T_I^4(0,t)\right) \tag{46}$$

$$q_{II} = k_{Ie} \left.\frac{\partial T_I}{\partial z}\right|_{z=L} \quad at\ z = L\ ,\ t \geq 0 \tag{47}$$

For radiation heat transfer to the bottom of tray,

$$q_{II} = \sigma F\left(T_{lp}^4 - T_I^4(L,t)\right) \tag{48}$$

For a thin film between the frozen material and lower plate,

$$q_{II} = h\left(T_{Lp} - T_I(L,t)\right) \tag{49}$$

The continuity equations for water vapor and inert gas are given in Eqs. (7) and (8) while the equation for the removal of bound water is given in Eq. (6). The initial and boundary conditions for the material balance equations for the secondary drying stage are given by the following expressions [39]:

$$p_w = \delta(z)\ at\ t = t_{pd},\ 0 \leq z \leq L \tag{50}$$

$$p_{in} = \mu(z)\ at\ t = t_{pd},\ 0 \leq z \leq L \tag{51}$$

$$C_{sw} = \theta(z)\ at\ t = t_{pd},\ 0 \leq z \leq L \tag{52}$$

$$p_w = p_{w0},\quad p_{in} = P_c - p_{w0}\ at\ z = 0\ ,\ t \geq t_{pd} \tag{53}$$

$$\left.\frac{\partial p_w}{\partial z}\right|_{z=L} = 0 \quad at\ z = L,\ \ t > t_{pd} \tag{54}$$

$$\left.\frac{\partial p_{in}}{\partial z}\right|_{z=L} = 0 \quad at\ z = L,\ \ t > t_{pd} \tag{55}$$

The functions γ(z), δ(z), μ(z), and θ(z) provide the profiles of T_I, p_w, p_{in}, and C_{sw} at the end of the primary drying stage or at the beginning of the secondary drying stage in which; these profiles are obtained by the solution of the model equations for the primary drying stage. Eqs. from (43) through (54), (7) and (8) represent the mathematical model that could be used to describe the dynamic behavior of the secondary drying stage of spray freeze drying in a tray. It should be noted that the control variables q_I, q_{II}, and P_0, must have dynamic values during the secondary drying stage such that the temperature everywhere in the sample ($0 \leq z \leq L$) should be kept below the scorch temperature, T_{scor}, ($T_I \leq T_{scor}$) of the material being dried.

4.0 Conclusion

The current studies have shown that the utilization of the spray freeze drying process in pharmaceutical, bio-chemicals, food, ceramics and fine chemicals industries will increase dramatically. The ability of producing sprayed protein powders with a very fine and friable microstructure that controlled release of therapeutic proteins. This makes spray freeze drying process of favorable for micro-encapsulation. In ceramics the industry, precursor powders that have similar density and homogeneity of original suspension can be produced by using the spray freeze drying. The spray freeze drying has a wide range of application from the ceramics industry (production of fine precursors to synthesize advanced ceramics such as superconductors, temperature resistant and highly durable materials) to the food industry (production of functional foods such as probiotics and high value foods), but it has undisputed future in pharmaceutical industry especially in producing pulmonary inhalable drugs. Large porous particles with small mass density, large geometric diameter and optimal aerodynamic diameter (1–3 μm) are highly effective for pulmonary drug delivery, and they can be produced by using spray freeze drying method. Reducing the operation cost which is the function of drying time, without causing any loss in product quality will be the main challenge for future of the spray freeze drying process.

5.0 References

1. Sadikoglu, H.; Ozdemir, M.; Seker, M. Freeze-Drying of Pharmaceutical Products: Research and Development Needs. Journal of Drying Technology, **2006**, *24*, 849-861.
2. Sadikoglu, H.; Liapis, A. I. and Crosser, O. K. Optimal Control of the Primary and Secondary Drying Stages of Bulk Solution Freeze Drying in Trays. Journal of Drying Technology **1998**, *16*, 399-431.
3. Sadikoglu, H.; Ozdemir, M.; Seker, M. Optimal control of the primary drying stage of freeze drying process in vials using variational calculus. Journal of Drying Technology, **2003**, *21(7)*, 1307-1331.
4. Gohel, M. C.; Parikh .R.K, Nagori, S.A. Spray Drying: A Review. Pharmaceutical Review **2009**, *5(7)*, http://www.pharmainfo.net/volumes-and-issues/2009/vol-7-issue-5
5. Filkova, I.; Huang, L. X.; Mujumdar, A. S. Industrial Spray Drying Systems. in AS. Mujumdar (ed), Handbook of Industrial Drying, (Second Edition). Marcel Dekker, New York and Basel, pp. 309-343.
6. Leuenberger, H. Spray freeze-drying – the process of choice for low water soluble drugs?, Journal of Nanoparticle Research **2002**, *4*, 111–119.
7. Liapis, A. I.; Bruttini, R. A mathematical model for the spray freeze drying process: the drying of frozen particles in trays and in vials on trays. International Journal of Heat and Mass Transfer **2009**, *52(1-2)*, 100-111.

8. Sonner C, Maa Y-F, Lee G. Spray-freezing-drying for protein powder preparation: particle characterization and a case study with trypsinogen stability. Journal of Pharmaceutical Science **2002**, *91(10)*, 2122-2139.
9. Maa, Y.-F.; Nguyen, P.-A.; Sweeney, T.; Shire, S.J.; Hsu, C.C. Protein inhalation powders: spray drying vs spray freeze drying, Pharmaceutical Research **1999**, *16*, 249–254.
10. Costantino, H.R.; Johnson, O.L.; Zale, S.E. Relationship between encapsulated drug particle size and initial release of recombinant human growth hormone from biodegradable microspheres. Journal of Pharmaceutical Science **2004**, *10*, 2624-2634.
11. Benson, S.W.; Ellis, D.A. Surface areas of proteins. I. Surface areas and heat of adsorption. Journal of the American Chemical Society **1948**, *70*, 3563-3569.
12. Werly, E.F.; Baumann, E.K. Production of sub-micronized powder by spray-freezing. Archives of environmental health **1964**, *9*, 567-571.
13. Maa,Y.-F.; Nguyen, P.-A. Method of spray freeze drying proteins for pharmaceutical administration, US Patent 6,282,282 (**2001**).
14. Wang, Z.; Finlay, H. F. Powder formation by atmospheric spray freeze drying. US Patent 2008/0155853 A1 (**2008**).
15. Maa,Y.-F.; Prestreski, S. J.; Burkoth, T. L. Spray freeze dried compositions. US Patent 2003/0202978 A1 (**2003**).
16. Gombotz, W. R.; Healy, M. S.; Brown , L. R.; Auer, H. E. Process for producing particles of biologically active molecules. US Patent 6,569,458 B1 (**2003**).
17. Costantino, H.R.; Firouzabadian, L.; Hogeland, K.; Wu, C.; Beganski, C.; Carrasquillo, K.G.; Cordova, M.; Griebenow, K.; Zale, S.E.; Tracy, M.A. Protein spray freeze drying. Effect of atomization conditions on particle size and stability, Pharmaceutical Research **2000**, *17*, 1374–1382.
18. Costantino, H.R.; Firouzabadian, L.; Wu, C.; Carrasquillo, K.G.; Griebenow, K.; Zale, S.E.; Tracy, M.A. Protein spray freeze drying. 2. Effect of formulation variables on particle size and stability. Journal of Pharmaceutical Science **2002**, *91(2)*, 388-395.
19. Rogers, T.L.; Nelsen, A.C.; Hua, J.; Brown, J. N.; Sarkari, M.; Young, T.J.; Johnston, K. P.; Williams III, R.O. A novel particle engineering technology to enhance dissolution of poorly water soluble drugs: spray-freezing into liquid. European Journal of Pharmaceutics and Biopharmaceutics **2002**, *54*, 271–280.
20. Rogers, T.L.; Nelsen, A.C.; Sarkari, M.; Young, T.J.; Johnston, K. P.; Williams III, R.O. Enhanced aqueous dssolution of a poorly water soluble drug by novel particle engineering technology: spray-freezing into liquid with atmospheric freeze-drying. Pharmaceutical Research 2003, *3(20)*, 485-493.
21. Carrasquillo, K.G.; Stanley, A.M.; Aponte-Carro, J.C.; De Jésus, P.; Costantino, H.R.; Bosques, C.J.; Griebenow K. Non-aqueous encapsulation of excipient-stabilized spray-freeze dried BSA into poly(lactide-co-glycolide) microspheres results in release of native protein. Journal of Control Release **2001,** *76(3)*,199-208.

22. Yin, W.; Yates, M.Z. Encapsulation and sustained release from biodegradable microcapsules made by emulsification/freeze drying and spray/freeze drying. Journal of Colloid and Interface Science **2009**, *336*, 155–161.

23. Wang, J.; Chua, K.M.; Wang, C.H. Stabilization and encapsulation of human immunoglobulin G into biodegradable microspheres. Journal of Colloid Interface Science **2004**, *71(1)*, 92-101.

24. Lam, X.M.; Duenas, E.T.; Cleland, J,L.Encapsulation and stabilization of nerve growth factor into poly (lactic-co-glycolic) acid microspheres. Journal of Pharmaceutical Science **2001**, *90(9)*, 1356-1365.

25. Semyonov, D.; Ramon, D.; Kaplun, Z.; Levin-Brener, L.; Gurevich, N.; Shimoni, E. Microencapsulation of Lactobacillus paracasei by spray freeze drying. Food Research International **2010**, *43*, 193–202.

26. Nguyen, X.C.; Herberger, J.D.; Burke, P.A. Protein powders for encapsulation: a comparison of spray-freeze drying and spray drying of darbepoetin alfa. Pharmaceutical Research **2004**, *20(3)*, 507-514.

27. Burke, P.A.; Klumb, L.A.; Herberger, J.D.; Nguyen, X.C.; Harrell, R.A.; Zordich, M. Poly(lactide-co-glycolide) microsphere formulations of darbepoetin alfa: spray drying is an alternative to encapsulation by spray-freeze drying. Pharmaceutical Research **2004**, *3(20)*, 500-506.

28. Yokota, T.; Takahata, Y.; Katsuyama, T.; Matsuda, Y. A new technique for preparing ceramics for catalyst support exhibiting high porosity and high heat resistance. Catalysis Today **2001**, *69*, 11–15.

29. Badica, P.; Aldica, G. Bi-2223 freeze-dried ceramic: specific features, related problems and search for new solutions. Journal of Optoelectronics and Advanced Materials **2003,** *4(5)*, 1029 – 1039.

30. Lee, S. H.; Lee, J. Y.; Park, Y.M. Complete oxidation of methane and CO at low temperature over LaCoO3 prepared by spray-freezing/freeze-drying method. Catalysis Today **2006**, *117*, 376–381.

31. Itatani, K.; Iwafune, K.; Howell, F. S.; Aizawa, M. Preparation of various calcium-phosphate powders by ultrasonic spray freeze-drying technique. Materials Research Bulletin **2000,** *35*, 575–585.

32. Badica, P.; Aldica, G.; Morozov, V.V.; Popa, S.; Mandache, S. The influence of sintering environment and Intermediate grounding on the scattering of the superconducting characteristics in BSCCO Ceramic produced by spray-frozen, freeze drying method. Applied Superconductivity **1996**, *12(4)*, 583-589.

33. Chow, A. H. L.; Tong, H. H. Y.; Chattopadhyay, P.; Shekunov, B. Y. Particle Engineering for Pulmonary Drug Delivery. Pharmaceutical Research **2007**, *3(24)*, 411-437.

34. Edwards, D.A.; Dunbar C. Bioengineering of therapeutic aerosols. Annual Review of Biomedical Engineering 2002, *4*, 93-107.

35. Koushik, K.; Kompella, U. B. Particle and device engineering for inhalation drug delivery. Drug Delivery Technology **2004**, *2(4)*, 40-50.

36. Edwards, D. A.; Ben-Jebria, A.; Langer, R. Recent advances in pulmonary drug delivery using large, porous inhaled particles. Journal of Applied Physiology **1998***, 85*, 379-385.

37. Sheehan, P.; Liapis, A. I. Modeling of the primary and secondary drying stages of the freeze drying of pharmaceutical products in vials: numerical results obtained from the solution of a dynamic and spatially multi-dimensional lyophilization model for different operational policies. Biotechnology and Bioengineering **1998**, *60*, 712–728.

38. Whitaker, S. Simultaneous Heat, Mass, and Momentum Transfer in Porous Media: A Theory of Drying, Advances in Heat Transfer, vol. 13, Academic Press, New York, NY, USA, **1977**, 119–203.

39. Sadikoglu, H.; Liapis, A. I. Mathematical Modelling of the Primary and Secondary Drying Stages of Bulk Solution Freeze-Drying in Trays: Parameter Estimation and Model Discrimination by Comparison of Theoretical Results with Experimental Data. Drying Technology **1997**, *15*, 791-810.

40. Marti, J.; Mauersberger, K. A survey and new measurements of ice vapor pressure at temperatures between 170 and 250 K, Geophysical Research Letters **1993**, *20*, 363–366.

5.0 Nomenclatures

c_p	heat capacity (kJ/kg)
C_{sw}	concentration of bound (sorbed) water (kg water/kg solid)
C_{01}	constant dependent only upon the structure of the porous medium and giving relative Darcy flow permeability (m^2)
C_1	constant dependent only upon the structure of the porous medium and giving relative Knudsen flow permeability (m)
C_2	constant dependent only upon the structure of the porous medium and giving the ratio of bulk diffusivity within the porous medium to the free gas bulk diffusivity (dimensionless)
d_{ice}	diameter of ice core in particle (m)
d_p	diameter of particle (m)
d_{pore}	mean pore diameter of porous layer formed from the packing of the particles (m)
$D_{w,in}$	free gas mutual diffusivity in a binary mixture of water vapor and inert gas (m^2/s)
$D^0_{w,in}$	$D_{w,in}P$ (N/s)
Z(t)	geometric shape (as per Fig. 1b) of the moving interface, a function of time (m)
k	thermal conductivity (W/K m)
k_1	bulk diffusivity constant, $k_1 = C_2 D^0_{w,in} K_w / \left(C_2 D^0_{w,in} + K_{mx} P \right)$ (m2/s)
k_2, k_4	self-diffusivity constant, $k_2 = k_4 = \left(K_w K_{in} / \left(C_2 D^0_{w,in} + K_{mx} P \right) \right) + \left(C_{01} / \mu_{mx} \right)$ (m^4/N s)
k3	bulk diffusivity constant, $k_3 = C_2 D^0_{w,in} K_{in} / \left(C_2 D^0_{w,in} + K_{mx} P \right)$ (m^2/s)

k_{des} rate constant in the desorption mechanism of bound water, Eq. (6) (s^{-1})

K_w Knudsen diffusivity for water vapor, $K_w = C_1\sqrt{R_g T / M_w}$ (m^2/s)

Kin Knudsen diffusivity of inert gas, $K_{in} = C_1\sqrt{R_g T / M_{in}}$ (m^2/s)

K_{mx} mean Knudsen diffusivity for binary gas mixture, $K_{mx} = y_w K_{in} + y_{in} K_w$ (m^2/s)

L length (height) of material in tray (m)

m_w amount of free water in material (kg/m^2)

M molecular weight (kg/kmol)

N mass flux (kg/m^2 s)

p partial pressure (Pa)

p_w^{sat} saturated water vapor pressure (Pa)

P total pressure (Pa)

P_{dcham} pressure in drying chamber (Pa)

q heat flux (W/m^2)

R radius of vial (m)

R_g ideal gas constant (J/K mol)

S ice saturation, Eq. (7) (dimensionless)

S_{av} volume-averaged ice saturation, Eq. (16) (dimensionless)

t time (s)

T temperature (K)

T_Z temperature at surface of moving interface (K)

V velocity of moving interface (m/s)

z space coordinate of distance along the length (height) of the material in the tray (m)

Z position of moving interface in the material in the tray (m) y mole fraction (dimensionless)

Greek letters

ΔH_s heat of sublimation of ice (J/kg)

ΔH_v heat of vaporization of bound water (J/kg)

ε_p particle porosity (dimensionless)

ε_{pb} porosity of the bed formed by the packed particles (dimensionless)

μ_{mx} viscosity of vapor phase in the pores (kg/m s)

ρ density (kg/m^3)

τ tortuosity (dimensionless)

Superscripts

o initial value

Subscripts

d dried particle based material after primary drying

d,s dried solution based material after primary drying

d,s,f dried solution based material when frozen and sorbed water have been removed

e effective

f frozen particle based material

f,s frozen solution based material

g gas

I region I, porous dried layer

II	region II, unsaturated porous frozen layer
in	inert gas
interf	moving interface
lp	lower heating plate
m	melting
mx	binary mixture of water vapor and inert gas
pd	primary drying stage
scor	scorch
t	total
up	upper heating plate
w	water vapor

Chen, X.D., Lin, S.X.Q., Patel, K.C., Woo, M.W. A simplified design procedure for spray dryers for milk powder manufacture - Volume 1, Ed. Woo, M.W., Mujumdar, A.S. and Daud, W.R.W., **2010**, ISBN - 978-981-08-6270-1, Published in Singapore, pp. 183-196.

A simplified design procedure for spray dryers for milk powder manufacture

Chapter 7

Chen X.D.[1,2], Lin S.X.Q.[1], Patel K.C.[1], Woo M.W.[1]

[1] Department of Chemical Engineering, Monash University

[2] Department of Chemical and Biochemical Engineering, College of Chemistry and Chemical Engineering, Xiamen University, Xiamen City, P.R. China

Contents **Page**

1.0 Introduction

Spray drying is by definition the transformation of feed from a fluid state into a dried particulate form by spraying the feed into a hot drying medium [1]. Application of this process can be widely found in the manufacture of powdered food: for example, milk powder, instant coffee, dried eggs, soups, baby foods and sweeteners. This chapter provides a simplified practical tool or approach in designing a spry dryer for milk manufacture. Steps involved in the proposed design approach, in chronological order, are: (1) overall component selection, (2) performing an overall heat and mass balance for the dryer, (3) scaling of the dryer length based on the required particle residence time and (4) determining the required dryer diameter. Discussion on step 1 and 2 can be found in a few established literatures on spray drying [1][2]. Therefore, they will only be briefly included here for completeness.

4.1 Heat balance

The heat balance of the drying air for individual cell is:

Heat in - Heat out = Heat used for heating droplet and evaporation + Heat loss

$$G_{in}C_{p,in}\left(T_{in}-T_{ref}\right)\Delta t_{air}-G_{out}C_{p,out}\left(T_{out}-T_{ref}\right)\Delta t_{air} = hA_{droplet}(T_{bulk}-T_{droplet})N_{droplet}\Delta t_{droplet}+KA_{cell}(T_{bulk}-T_{ambient})\Delta t_{air} \quad (9)$$

where G_{in} and G_{out} (kg/s) are mass flow rates at the cell inlet and outlet, $C_{p,in}$ and $C_{p,out}$ (kJ/kgK) are specific heat of the drying air at cell inlet and outlet humidity, T_{in} and T_{out} (^{o}C) are drying air temperature at cell inlet and outlet, T_{ref} (^{o}C) is the reference temperature for heat balance calculation (it can typically be taken as 0^{o}C), $A_{droplet}$ (m^2) is droplet surface area, T_{bulk} and $T_{droplet}$ (^{o}C) are bulk air temperature and droplet temperature respectively, $N_{droplet}$ is the number of droplet passing the cell, A_{cell} (m^2) is cell surface area exposure to ambient, Δt_{air} (s) is the residence time of drying air in the cell and $\Delta t_{droplet}$ (s) is the residence time of the droplet in the cell.

The residence time of the drying air in the cell can be calculated as follows:

$$\Delta t_{air}=\frac{A_{cell,cross}\Delta L}{V_{air}} \quad (10)$$

where ΔL (m) is the length of the cell (along the axis of a spray dryer), V_{air} (m^3/s) is the volumetric flow rate of the drying air and $A_{cell,cross}$ (m^2) is the cross section area of the cell. The residence time of the droplet in the cell can be calculated as follows:

$$\Delta t_{droplet}=\frac{\Delta L}{v_{droplet}} \quad (11)$$

where $v_{droplet}$ (m/s) is the velocity of the droplet travelling the distance of cell's length. The number of the droplet passing through the cell can be calculated as follows:

$$N_{droplet}=N\Delta t_{air} \quad (12)$$

where N (1/s) is the total droplet number generated per second.

4.2 Mass balance

Similar to the heat balance, the following equation can be used to calculate the outlet humidity of the cell.

these configurations, the direction of the drying air can be concurrent or count-current in relation to the atomized liquid spray.

There are three conventional configurations with regards to atomization options, i.e., open mode design with single point powder discharge, open mode design with two point powder discharge and close cycle design with single point powder discharge. Three types of atomizers can be used, i.e., rotary atomizer, pressure nozzle atomizer and two-fluid nozzle atomizer. The selection of the atomization device depends mainly on the desired characteristics of the powder as well as the properties of the bulk liquid feed to be atomized. The designer should consult with nozzle manufacture and literature [2]. This selection of an atomization system will be important in providing the preliminary design information, initial droplet size distribution and feed rate, for subsequent estimation of the particle residence time.

There are five options for post-operation on the powder, i.e., no treatment, pneumatic transport, external fluid bed, integrated fluid bed and integrated belt [2]. Various options are available for powder separation. However, from the consideration of hygienic and safety, only cyclone separator, bag filter and wet scrubber are used in milk powder production.

The capability of the spray dryer is determined by the type of the chamber and by the components integrated. For example, the selection of different type of the nozzle and different post-operations of the powder will result in different powder size and size distribution and functionality. Detailed discussion on the capabilities of different spray drying installations in terms of the combinations of the type of chamber, after treatment and atomization device, can be found elsewhere [2].

3.0 Heat balance of a spray dryer

For continuous operation of a spray dryer, the mass flow rate of the input air and feed equals the mass rate of the output of air and product. Heat input of air and feed equals the sum of heat output of air and product and heat losses from the dryer. The physical input components are:

- Drying air;
- Auxiliary air, for example, cooling air (for cooling the atomizer to avoid overheating) and fine powder transport air etc.;
- Liquid feed to be dried.

The physical output components are exhaust air and powder. For a given amount of feed to be dried to a certain level of moisture content, the amount of air required can be calculated by collating the individual heat requirements for evaporating the moisture from the droplet, heating or cooling each individual component from its inlet to its outlet temperature and heat losses. The inlet and outlet parameters are as follows:

- Drying air inlet temperature t_{inlet} (^{o}C) and humidity $H_{ambient}$ (kg/kg);
- Ambient air temperature $t_{ambient}$ (^{o}C) and humidity $H_{ambient}$ (kg/kg);
- Drying air feed rate (which has to be calculated) G_{inlet} (kg/s);
- Atomization device cooling air temperature $t_{cooling}$ (^{o}C), humidity $H_{ambient}$ (kg/kg) and mass flow rate $G_{cooling}$ (kg/s);

- Fine powder transport air temperature $t_{transport}$ (^oC), humidity $H_{ambient}$ (kg/kg) and mass flow rate $G_{transport}$ (kg/s);
- Feed concentrate temperature t_{feed} (^oC), mass flow rate G_{feed} (kg/s) and solids content TS (wt%);
- The ratio of the recycled fines to the total powder production R_{fine}. Fine powder returns to the dryer at $t_{transport}$, i.e., the same temperature as the fines transport air temperature);
- Powder moisture content m_{powder} (wt%);
- Dryer wall surface area A_{dryer} (m^2);
- Exhaust air temperature t_{outlet} (^oC) and humidity H_{outlet} (kg/kg);
- Heat loss coefficient K (W/m^2K)

The inlet and outlet conditions need to be initially fixed. Normally this is determined by manufacturing experience on the product of interest, knowledge on inlet drying air temperature and the required outlet air temperature for the desired powder moisture content. With the other operation parameters outlined above, the heat balance can be estimated as follows:

Heat of evaporation of water:

$$Q_{evap} = G_{feed} \times \left(1 - \frac{TS}{1 - m_{powder}}\right)\left[\Delta H_{water} + C_{v,outlet} \times \left(t_{outlet} - t_{feed}\right)\right] \quad (1)$$

where ΔH_{water} (kJ/kg) is the latent heat for water evaporation and $C_{v,outlet}$ is the specific heat capacity of water vapour at the dryer's outlet temperature.

Heat of powder/product:

$$Q_{powder} = G_{feed} \times \frac{TS}{1 - m_{powder}} \times \left[C_{powder}\left(1 - m_{powder}\right) + C_{water} m_{powder}\right] \quad (2)$$

where C_{powder} (kJ/kgK) and C_{water} (kJ/kgK) are specific heat capacity of dry powder and water.

Heat of cooling air:

$$Q_{cooling} = G_{cooling}\left(\frac{t_{outlet} C_{a,outlet} - t_{ambient} C_{a,ambient}}{1 + H_{ambient}} + H_{ambient}\left(t_{outlet} C_{v,outlet} - t_{ambient} C_{v,ambient}\right)\right) \quad (3)$$

where $C_{a,outlet}$ (kJ/kgK) and $C_{a,ambient}$ (kJ/kgK) are specific heat capacity of air at dryer's outlet temperature and ambient temperature respectively, $C_{v,ambientt}$ is specific heat capacity of water vapour at ambient temperature.

Heat of fines transport air:

$$Q_{fine-transport} = G_{transport} \times \left(\frac{t_{outlet} C_{a,outlet} - t_{transport} C_{a,transport}}{1 + H_{ambient}} + H_{ambient} \times \left(t_{outlet} C_{v,outlet} - t_{transport} C_{v,transport}\right)\right) \quad (4)$$

where $C_{a,transport}$ and $C_{a,transort}$ are specific heat capacity of the transport air and water vapour at the dryer's outlet temperature respectively.

Heat of fine powder:

$$Q_{fine} = G_{feed} \times \frac{TS}{1 - m_{powder}} \times R_{fine}\left(t_{outlet} - t_{transport}\right)\left[C_{powder} \times \left(1 - m_{powder}\right) + C_{water} m_{powder}\right] \quad (5)$$

Heat loss to the ambient:

$$Q_{loss} \approx KA_{dryer}\left(t_{outlet} - t_{ambient}\right) \quad (6)$$

Total energy required:

$$Q_{total} = Q_{evap} + Q_{powder} + Q_{cooling} + Q_{fine-transport} + Q_{fine} + Q_{loss} \quad (7)$$

Drying air thus required:

$$G_{inlet} = \frac{Q_{total}}{t_{inlet} C_{a,ambient} - t_{outlet} C_{a,outlet} + H_{ambient}\left(t_{inlet} C_{v,inlet} - t_{outlet} C_{v,outlet}\right)} \quad (8)$$

The following is an example heat balance of a pilot scale dryer. The specifications of the pilot scale dryer are as follow:

- Drying chamber dimension: Ø 2500x2000 mm, 60° cone
- Nominal main process gas flow: 1250 kg/hr
- Water evaporation capacity: 20-110 kg/h
- Typical mean particle size range: 30-300 micron (for the drying of large particle a very high temperature must be used. This is not suitable to food products)
- atomizing devices: rotary atomizer, two-fluid nozzle and pressure nozzle

Based on these overall specifications above, some of the possible operating parameters calculated with equation (1) to (8) are shown in Table 1.

Table 1 Case studies of operating parameters obtained by overall mass and energy balance

	Case 1	**Case 2**	**Case 3**
Inlet temperature (°C)	250	200	200
Outlet temperature (°C)	110	90	100
Water evaporation rate (kg/hr)	60	50	44
Latent heat of evaporation (kJ/kg)	2260	2260	2260
Specific heat capacity of air (kJ/kg K)	1.022 (at 180°C)	1.013 (at 140°C)	1.013 (at 140°C)

Nominal main process air flowrate (kg/hr)	1250	1250	1250
Specific heat capacity of air (kJ/kg K)	1.013 (at 130°C)	1.009 (at 100°C)	1.009 (at 100°C)
Ambient air temperature (°C)	15	15	15
Water evaporation rate without heat loss (kg/hr)	79.1	61.6	56.0
Net power input (kW)	82.7	64.8	64.8
Heat loss (kW)	12.0	7.3	7.6
Temperature difference between average chamber temperature and ambient temperature (^{o}C)	150	115	120
Maximum required combustor power output/drying air power consumption @350°C (kW)	**117.8**		

4.0 Estimation of particle residence time

For successful drying operation, under the actual drying air temperature and humidity, it is essential to have sufficient residence time to dry particles to the required moisture content. Heat balance only provides information on the required drying air flow rate through the dryer. However, whether or not the droplets can be sufficiently dried in the chamber is determined by the droplet residence time alongside with the drying air temperature and humidity.

Simulation is a technique or tool that can provide predictions and trends of process and product parameters with acceptable accuracies. Simulation techniques are increasingly becoming popular within the software development community to optimize the spray drying process and predict product properties before conducting real and usually expensive spray drying trials [3].

However, the spray drying process is complex, involving atomization of the feed, spray air contact/mixing, and spray evaporation/drying [1]. Due to this complexity, it is difficult to mathematically capture the entire physical phenomena in a single simulation. One solution is to use CFD simulation in conjunction with single droplet drying kinetics. However, undertaking of CFD simulation requires special training and resources which might not be easily accessible. Furthermore, there is limited verification of CFD prediction in the industrial scale. One alternative is a simple one-dimensional simulation of the spray dryer.

The main assumption of this approach is a plug-flow behaviour of the particles [3]. In this approach, mass, heat and momentum are applied to individual droplet moving through the length of the dryer which is dicretized axially into many small adjacent cells. Within these discretized cells, the

drying air is assumed well mixed. The drying air and droplets are assumed to be moving in parallel.

4.1 Heat balance

The heat balance of the drying air for individual cell is:

Heat in - Heat out = Heat used for heating droplet and evaporation + Heat loss

$$\begin{aligned} &G_{in}C_{p,in}\left(T_{in}-T_{ref}\right)\Delta t_{air}-G_{out}C_{p,out}\left(T_{out}-T_{ref}\right)\Delta t_{air} \\ &=hA_{droplet}(T_{bulk}-T_{droplet})N_{droplet}\Delta t_{droplet}+KA_{cell}(T_{bulk}-T_{ambient})\Delta t_{air} \end{aligned} \quad (9)$$

where G_{in} and G_{out} (kg/s) are mass flow rates at the cell inlet and outlet, $C_{p,in}$ and $C_{p,out}$ (kJ/kgK) are specific heat of the drying air at cell inlet and outlet humidity, T_{in} and T_{out} (^{o}C) are drying air temperature at cell inlet and outlet, T_{ref} (^{o}C) is the reference temperature for heat balance calculation (it can typically be taken as 0^{o}C), $A_{droplet}$ (m^2) is droplet surface area, T_{bulk} and $T_{droplet}$ (^{o}C) are bulk air temperature and droplet temperature respectively, $N_{droplet}$ is the number of droplet passing the cell, A_{cell} (m^2) is cell surface area exposure to ambient, Δt_{air} (s) is the residence time of drying air in the cell and $\Delta t_{droplet}$ (s) is the residence time of the droplet in the cell.

The residence time of the drying air in the cell can be calculated as follows:

$$\Delta t_{air}=\frac{A_{cell,cross}\Delta L}{V_{air}} \quad (10)$$

where ΔL (m) is the length of the cell (along the axis of a spray dryer), V_{air} (m^3/s) is the volumetric flow rate of the drying air and $A_{cell,cross}$ (m^2) is the cross section area of the cell. The residence time of the droplet in the cell can be calculated as follows:

$$\Delta t_{droplet}=\frac{\Delta L}{v_{droplet}} \quad (11)$$

where $v_{droplet}$ (m/s) is the velocity of the droplet travelling the distance of cell's length. The number of the droplet passing through the cell can be calculated as follows:

$$N_{droplet}=N\Delta t_{air} \quad (12)$$

where N (1/s) is the total droplet number generated per second.

4.2 Mass balance

Similar to the heat balance, the following equation can be used to calculate the outlet humidity of the cell.

Moisture in + Moisture removed from droplets = Moisture out

$$\frac{G_{in}\Delta t_{air}}{1+H_{in}} \times H_{in} + \dot{m}N_{droplet}\Delta t_{droplet} = \frac{G_{out}\Delta t_{air}}{1+H_{out}} \times H_{out} \quad (13)$$

where G_{in} (kg/s) and G_{out} (kg/s) are the mass flow rates at cell inlet and outlet, H_{in} (kg/kg) and H_{out} (kg/kg) are the humidity at cell inlet and outlet, $\dot{m}$ is drying rate of the droplet which can be estimated from Equation (17). The mass flow rate of the outlet of the cell can be calculated as follows:

$$G_{outlet} = G_{inlet} + \dot{m}N_{droplet}\Delta t_{droplet} \quad (14)$$

4.3 Momentum balance

The axial velocity of the droplet $v_{droplet}$ (m/s) can be estimated with the following equation [3]:

$$\frac{dv_{droplet}}{dt} = \frac{(\rho_{droplet} - \rho_{air})g}{\rho_{droplet}} - \frac{0.75C_D\rho_{air}(v_{droplet} - v_{air})}{d_{droplet}v_{droplet}} \quad (15)$$

where $\rho_{droplet}$ (kg/m^3), ρ_{air} (kg/m^3) is density of the droplet and air respectively, C_D (-) is the drag coefficient, $d_{droplet}$ (m) is the diameter of the droplet and t (s) is the time.

4.4 Implementation of the one-dimensional model

The discretized heat, mass and momentum equations above can be easily implemented in a spreadsheet. In implementing the one-dimensional model, it is important that the dryer length is sufficiently discretized to ensure accuracy and stability of the computation. Depending on the predicted product moisture, the length of the dryer can then be varied under different operating conditions to give different design combinations. In the heat and mass balance equation, it can be seen that the evaporation mass transfer source terms links the particle and the air phase. This source term can be calculated using the Reaction Engineering Approach [9] drying model which will be outlined below. Case studies of the residence time predicted for different particle sizes are listed in Table 2.

Table 2 Residence time of the milk droplet drying from 50 wt% to 9 wt%

Initial partial size (mm)	50	100	200	300
Residence time (sec)	0.4	6	12.2	26

Note: mass ratio of drying air to feed: 9.17; drying air inlet temperature: 204°C; drying air outlet temperature: 60°C.

4.5 Reaction engineering approach

Accurate description of the drying kinetic is a key element in such spray drying simulation. There are four types of drying kinetic approaches which are commonly used in drying modelling.

- Reaction engineering approach (REA);
- Characteristic drying curves (CDC) approach;
- Internal moisture diffusion-based approaches;
- Receding interface (or moving boundary) approaches.

The REA model has been reported to be robust among various studies and will be the choice of our approach for the design [4][5].

The reaction engineering approach assumes that evaporation is an 'activation' process having to overcome an 'energy barrier' whilst condensation or adsorption is not [4]. It uses a simple equation to describe the relationship between the droplet surface vapour concentration and the water content and temperature of the droplet:

$$\rho_v = \rho_{v,sat} \exp\left(-\frac{\Delta E_v}{RT_d}\right) \tag{16}$$

where ΔE_v (J/kmol) is essentially a 'correction factor' of the apparent activation energy for drying due to the increasing difficulty in removing the moisture at low moisture content levels, ρ_v (kg/m^3) and $\rho_{v,sat}$ (kg/m^3) are the vapour concentration at the particle-gas interface and saturation vapour concentration respectively, and R (J/mol.K) is the universal gas constant. The interface temperature can be approximated to be equal to the droplet temperature T_d (°C) as the Biot number [10] is normally very small for such application. Thus the mass balance can be expressed as follows:

$$\dot{m} = \frac{dm}{dt} = m_s \frac{dX}{dt} = -h_m A[\rho_{v,sat} \exp\left(-\frac{\Delta E_v}{RT_d}\right) - \rho_{v,b}] \tag{17}$$

where m (kg) and m_s (kg) are the droplet weight and droplet mass respectively, t (s) is the drying time, h_m (m.s^{-1}) is the external mass transfer coefficient and $\rho_{v,b}$ (kg/m^3) is the bulk vapour concentration. The heat transfer coefficient h (W/m^{-2}.K).and the mass transfer coefficient h_m can be

obtained from established correlations such as the Ranz-Marshall correlation [6], which takes the following form:

$$Nu=2+0.60Re^{1/2}Pr^{1/3} \quad (18)$$

$$Sh=2+0.60Re^{1/2}Sc^{1/3} \quad (19)$$

The energy balance used for the model is given by the following form:

$$mC_{p,d}\frac{dT_d}{dt} = hA(T_b - T_d) + \Delta H_{water} m_s \frac{dX}{dt} \quad (20)$$

where $C_{p,d}$ (kJ/kgK) is the specific heat capacity of the droplet, T_b (°C) is the drying air temperature, m_s (kg) and X (kg/kg) are dry mass per droplet and average water content, respectively. The activation energy was calculated from the droplet weight loss versus time curves, which were obtained experimentally for the product of concern. The resulting correlations of the normalized activation energy versus moisture content difference for skim and whole milk were reported by Chen and Lin [4], taking the following form (initial solids content 20 wt% and 30 wt%):

Skim milk
$$\frac{\Delta E_v}{\Delta E_{v,b}} = 0.998\exp\left[-1.405(X - X_b)^{0.930}\right] \quad (21)$$

Whole milk
$$\frac{\Delta E_v}{\Delta E_{v,b}} = 0.957\exp\left[-1.291(X - X_b)^{0.934}\right] \quad (22)$$

where $\Delta E_{v,b}$ (J/kmol) is the 'equilibrium' activation energy (the maximum value) and X_b (kg/kg) is the equilibrium moisture content on dry basis corresponding to the air humidity and temperature). It is noteworthy that As examples, equation 21 and 22 are initial solid concentration specific. For 40 wt% and higher solid concentrations these profiles were approximated using a method shown by Patel et al. [5]. Equation 21 and 22 are relative activation energy correlations for the air drying of skim milk [3].

40 wt% milk solids:

$$\frac{\Delta E_v}{\Delta E_{v,b}} = 0.9975 - 1.28962\times(X - X_b) - 0.0096\times(X - X_b)^2 + 2.8014\times(X - X_b)^3 - 4.6627\times(X - X_b)^4 + 3.2613\times(X - X_b)^5 - 0.8469\times(X - X_b)^6 \quad (23)$$

50 wt% milk solids:

$$\frac{\Delta E_v}{\Delta E_{v,b}} = 1.0063 - 1.5828\times(X - X_b) + 3.3561\times(X - X_b)^2 - 9.389\times(X - X_b)^3 + 12.22\times(X - X_b)^4 - 5.5924\times(X - X_b)^5 \quad (24)$$

The parameter $\Delta E_{v,b}$ can be calculated using the relative humidity and temperature of drying air.

$$\Delta E_{v,b} = -RT_b \ln\left(\frac{\rho_{v,b}}{\rho_{v,sat}}\right) \tag{25}$$

The equilibrium vapour concentration $\rho_{v,b}$ is related to the corresponding equilibrium water content of milk at different temperatures through the desorption isotherm. The GAB model, which was fitted at elevated temperatures of up to 90 °C and a wide range relative humidities up to 100%, can be used to estimate X_b of skim and whole milk [7]:

$$X_b = \frac{Ckm_0 a_w}{(1-ka_w)(1-ka_w+Cka_w)} \tag{26}$$

where X_b (kg/kg) is the equilibrium moisture content, m_0 (kg/kg) is the monolayer moisture content, a_w is the water activity (which is the same as the relative humidity in this case, a_w=*RH*), *C* and *k* and are temperature dependent constants.

$$C = C_0 \exp\left(\frac{\Delta H_1}{RT}\right) \tag{27}$$

$$k = k_0 \exp\left(\frac{\Delta H_2}{RT}\right) \tag{28}$$

where *T* (K) is the temperature, ΔH_1 (J/mol) and ΔH_2 (J/mol) are heats of sorption of water in milk and c_0 and k_0 are constants. These constants are listed in Table 3.

Table 3 GAB constant for skim milk and whole milk

	m_0 (kg/kg)	C_0	k_0	ΔH_1(J/mol)	ΔH_2 (J/mol)
Skim milk	0.06156	0.001645	5.710	24831	-5118
Whole milk	0.04277	0.1925	2.960	10485	-3215

The REA parameters above can be used for the simulation of droplet drying under changing ambient drying air humidity and temperature typically found in spray dryers. Implementation of the REA approach can be undertaken using the finite difference procedures given below [4]:

1. The droplet weight, temperature, diameter and moisture content at the entry of the discretized cell are set as initial values.
2. Average droplet film temperature can be calculated. The heat and mass transfer coefficients were then computed from the *Nu* and *Sh* number using Equation 18 and 19.
3. The saturated vapour concentration can then be determined at the droplet temperature and the activation energy can be calculated using Equation 21 and 22 for skim or whole milk, respectively. Then the

droplet surface vapour concentration was calculated using Equation 16.

4. The drying rate *dm/dt* is further calculated using Equation 17 and the rate of the droplet temperature change *dT/dt* determined using Equation 20.
5. Based on the rate of drying and temperature change, the particle mass and temperature was updated. The time interval in determining the magnitude change of these properties is obtained by comparing the particle velocity with the spatial length of the discretized section.
6. At the inlet of the next discretized cell, the initial droplet weight and temperature were calculated using the values at the previous cell exit. The droplet diameter change can be calculated using the experimental correlation given below.
7. This calculation cycle can be repeated until the last discretized section of the dryer.

Droplet diameter change data was reported by Lin and Chen [8]. The data were correlated approximately against the solids content using the following equation:

$$\frac{D}{D_o} = b + (1-b)\frac{X}{X_o} \tag{29}$$

where D (m) is the droplet diameter at drying time t (s), D_0 (m) is the droplet initial diameter, X (kg/kg) is the water content of the droplet at drying time t, X_0 (kg/kg) is the initial water content of the droplet and b is the shrinkage coefficient. Under the circumstances of limited data, the coefficient b values were correlated as following [8]:

Skim milk: $$b = 0.0117X_0^2 - 0.1295X_0 + 1.00 \tag{30}$$

Whole milk: $$b = 0.0083X_0^2 - 0.1036X_0 + 1.00 \tag{31}$$

Validations of the experimental data for the above correlations are up to 40 wt% for the solids content. The drying air temperature is up to 110°C and drying air velocity is up to 1 m/s. extrapolation is possible but may require some caution.

5.0 Estimation of the dryer diameter

The dryer can be designed more compact by careful estimation of its diameter (to same material for construction). This diameter may evaluated by the spray nozzle coverage along with the droplets deceleration path length. Four terms are commonly used to describe spray coverage and they are available from nozzle manufacturers (Figure 2):

- Spray Angle: the included angle of the spray as measured close to the nozzle orifice. Due to the gravity and air flow affects, this parameter is useful only for determining spray coverage close to the nozzle.

- Actual spray coverage: the actual coverage at a specified distance from the nozzle.
- Effective spray angle: the angle calculated from the actual coverage at a distance.
- Theoretical spray coverage: the spray coverage at a specified distance if assuming spray moving in straight lines.

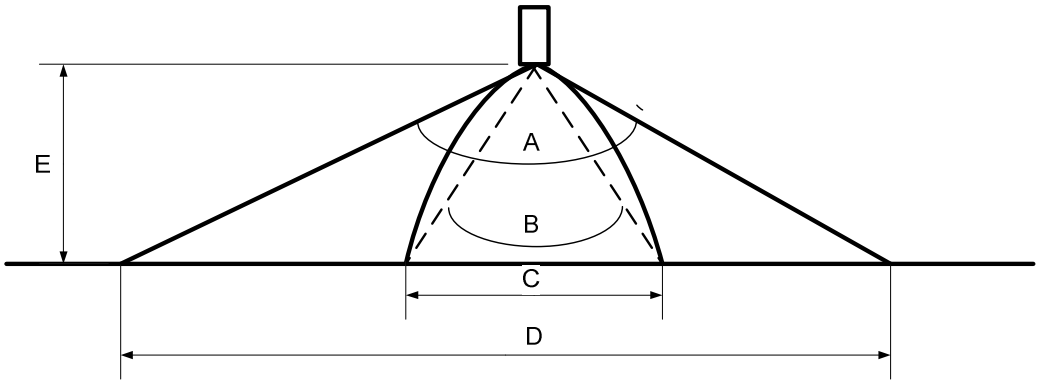

Figure 2 Spray angle and coverage (A: spray angle; B: effective spray angle; C: the actual coverage at a specified distance; D: the theoretical coverage at distance E)

Milk concentrate leaves the atomizing device at a very high speed. The droplets contact with the drying air immediately and decelerate to reach the velocity of the surroundings. In milk powder production, the smallest droplets take about 0.1 m to decelerate and the largest droplets take about a 1 m path [2]. The actual spray coverage data at the distance when droplets reach the surrounding air velocity can be used to evaluate the diameter of the dryer. This data might be available from the nozzle manufacturer or determined through experiment (if nozzle is available). A safety factor of 0.2 to 0.4 m might be necessary to avoid wall deposition. If the actual spray coverage is not available, the theoretical spray coverage/angle and 1 meter deceleration path can be used to estimate the diameter of the spray coverage. If more than one nozzle are used, overlap of the spray coverage should be avoided.

6.0 References

1. Masters, K. **1979**. *Spray Drying Handbook. p1*, London: George Godwin Limited
2. Pisecky, J. **1997**. Handbook of Milk Powder Manufacture. P44-51, 79. Copenhagen, Denmark: Niro A/S.
3. Patel, K.; Chen, X. D.; Jeantet, R.; Schuck, P. One-dimensional simulation of co-current, dairy spray drying systems – pros and cons. Dairy Science Technology **2010**, *90(2-3)*, 181-210.
4. Chen, X. D.; Lin, S. X. Q. Air drying of milk droplet under constant and time-dependent conditions. AIChE Journal **2005**, *51*, 1790–1799.

5. Patel, K.C.; Chen, X. D.; Lin, S. X. Q.; Adhikari, B. A composite reaction engineering approach to drying of aqueous droplets containing sucrose, maltodextrin (de6) and their mixtures. AIChE Journal **2009**, *55*, 217-223.
6. Ranz, W.E.; Marshall, W.R. Evaporation from drops, Chemical Engineering Progress **1952**, *48(3)*, 141-146.
7. Lin, S. X. Q.; Chen, X. D.; Pearce, D. L. Desorption isotherm of milk powders at elevated temperatures and over a wide range of relative humidity. Journal of Food Engineering **2005***, 68*, 257-264.
8. Lin, S. X. Q.; Chen, X. D. Engineering data of diameter change during air drying of milk droplets with 40 wt% initial solids content. Drying Technology **2009**, *27*, 1028-1032.
9. Chen, X. D. The basics of a reaction engineering approach to modelling air-drying of small droplets or thin later materials. Drying Technology, **2008**, 26, 627-639.
10. Chen, X. D. Critical *Biot* number for uniform temperature assumption in transient heat and mass transfer calculations. International Journal of Food Engineering, **2005**, 1(3), Article 6, 1-8.

Perea-Flores, M.J., Chanona-Perez, J.J., Terres-Rojas, E., Calderon-Dominguez, G., Garibay-Febles, V., Alamilla-Beltran, L., Gutierrez- Lopez, G.F. A simplified design procedure for sprya dryers for milk powder manufacture - Volume 1, Ed. Woo, M.W., Mujumdar, A.S. and Daud, W.R.W., **2010**, ISBN - 978-981-08-6270-1, Published in Singapore, pp. 197-218.

Microstructure characterization of milk powders and their relationshp with rehydration properties

Chapter 8

Perea-Flores M.J.[1], Chanona-Perez J.J.[1], Terres-Rojas E.[1], Calderon-Dominguez G.[1], Garibay-Febles V.[2], Alamilla-Beltran L.[1], Gutierrez- Lopez G.F.[1]

[1]Departamento de Ingeniería Bioquímica, Sección de Graduados e Investigación. Escuela Nacional de Ciencias Biológicas del Instituto Politécnico Nacional

[2]Laboratorio de Microscopia Electrónica de Ultra-Alta Resolución del Instituto Mexicano de Petróleo

Contents **Page**

1.0 Introduction

The demand of food powder products with better functional properties, has increased as a result of the market globalization, playing their physicochemical and microstructure properties a very important role on their overall reconstitution properties. Nowadays, it is expected that when reconstituting a food powder, it can be easily rehydrated with water, preserving its original properties. In this context, several factors have been reported to contribute to the reconstitution of food powders[1], such as composition, and physical (size, shape, surface properties, density) and microstructure (uniformity, air content) properties, being the microstructure a very important factor to understand the rehydration phenomena; however it was barely considered during the last century by food engineers, maybe as a result of the few knowledge about the underlying sciences linking food structure to product properties and the lack of techniques that allow acquiring better food structure images to be able to quantify [2][3].

Nowadays, image analysis has been applied to food images, as acquired by different microscopic systems, to obtain numerical data about morphology, structure and microstructure of the analyzed foods. The extracted information has been useful to improve the understanding of structure-function relationships of these complex systems, such as food and biological materials. On the other hand, fractal analysis has been successfully applied for the quantitative evaluation of irregular surfaces and textures of biological materials, and also to characterize ruggedness and geometric complexities of different food particles, such as instant coffee, skim milk, potato starch powder, maltodextrin particles and others. The key to quantify the irregularity of the contours and surfaces of food materials is by evaluating the apparent fractal dimension (FD) by extracting structural and microstructural features from different microscopy images. These results are important to understand the architecture and microstructure-functionality properties of food products.

For this reason, microscopy and image analysis techniques could be considered as proper tools to evaluate qualitatively and quantitatively the food microstructure, making possible to carry out numerical correlations between microstructure data, as obtained from the images, and the functional properties of food powders. The objective of this contribution was to illustrate the application of image analysis to the study of milk powder microstructure.

2.0 Physical properties of powder

There are several characteristics of single particles or agglomerates that are important for physicochemical and functional properties such as moisture, particle size and shape, density, roughness, texture, rehydration capability, wettability, insolubility index, among others [4]. According to Bhandari [5], powder properties can be classified into fundamental, functional, defects and image parameters. Some powder properties are illustrated in Table 1.

2.1 Moisture

Milk powder show very low moisture content (<5%), as measured by vacuum oven drying methods or infrared lamps (rapid testing), as well as water activity (a_w) values, varying from 0.12 to 0.15 [5][6].

Table 1 Classification of powder properties (adapted from Bhandari,[5])

Basic properties	***Functional properties***	***Product faults***	***Image parameters from microscopy techniques***
• Moisture • Particle size and distribution • Particle density • Particle shape • Bulk density • Hygroscopicity • Color	• Reconstitution properties - Wettability - Sinkability - Dispersibility - Solubility percentage • Flowability • Caking • Thermostability	• Solubility index • Scorched particles • Free fat • White flecks and specks • Dustiness	• Geometric - Perimeter - Area - Shape factor - Fractal dimension - Feret diameter - Compactness • Texture - Fractal texture - Entropy - Contrast - Lacunarity

2.2 Particle size

Particle mean size of a spray dried milk powder can be in a range of 30-80 □m, while the agglomerates are over 100 μm (up to a few millimeters) [5]. The size of a powder or particulate material is often used to classify, categorise or characterise them, while its size distribution is a common method used to relate the material heterogeneity with the product physical properties such as apparent density [7]. The particle size is also considered as an important property that influences powder functionality [4].

Different types of instruments and methods for the measurement of particle sizes or their distribution has been applied: such as: sieving, microscope counting (optical microscopic), laser diffraction (such as the Malvern particle size), ultrasonic, sedimentation, or stream scanning techniques. In most of these techniques, the Sauter mean diameter (volume-surface ratio) to express the mean particle size of the powder has been used [4-5][8-12].

2.3 Particle shape

All geometrical features of individual food powder particles or agglomerates can be related to their structures and individual shapes [4]. The shape of particles can be spherical, shriveled or fragmented depending on the type of the material and the process parameters used, mainly the temperature used to obtain them. The sphericity, also refers as circularity, is a parameter commonly applied to describe the shape of particles and agglomerates; when the sphericity parameter shows a value of 1.0, it makes reference to a perfect circle, while when values of 0.7-0.8 are observed, they indicate irregular particle shape.

Particle shape influences functional properties of food powders such as mixing, flowability and bulk density. Normally, a low solid concentration feed during spray drying result in more spherical particles, whereas a high solid concentration feed or a poor atomization procedure generates irregular shapes (sometimes filament-like particles). Particle shapes can be observed in detail by stereo, optical, electronic or confocal scanning microscopy [4][5][7].

2.4 Bulk density and packed bulk density

The density of a powder is defined as its total weigh divided by its total volume and normally is expressed as g/mL or kg/L. Density is considered quite relevant for determining other particle properties such as bulk powder structure and particle size [5][7][11].

Bulk density, also named apparent density, is the weight of powder per unit volume and is normally expressed in g/mL. It is dependent on the degree of interparticulate space or porosity of the bulk volume. Bulk density of powder is influenced by particle density, size distribution, shape, electrostatic effect and moisture content. This property is important in packaging, good reconstitution and retail use.

Packed bulk density, also named compact or tapped density, differs from bulk density in the way they are measured. The packed bulk density is obtained by tapping the powder by a standard mechanical or dropping procedure, where a cylinder containing the powder is dropped straight onto a pad for a given number of times (in general 10 times to 100) from a certain height (10cm). It is much better to use a mechanical tapping device so that the conditions of sample preparation can be more reproducible [4][5]. Packed bulk density of powders can vary from 0.4-0.8g/mL, but it can be increased by the addition of binding agents to the feed, which improves the particle strength, prevents particle ballooning and allows to operate at higher solids concentration feed during spray drying [5][13].

3.0 Rehydration properties

Food powder products, as obtained by spray drying or grinding, are difficult to rehydrate [7] and several factors have been related to this effect such as the size, shape, surface properties, density, uniformity, air content, composition and the presence of additives among others [1]. The rehydration capacity of food powders is generally evaluated by measuring four properties: wettability, sinkability, dispersability and solubility [1][4-5][7][12][14][15].

a) *Wettability.* This property describes the capacity or ability of particles or bulk powder to absorb water on their surface, being the wetting time the most important variable when considering instantiation [7][15]. The wettability property depends largely on the size and on the shape of particles; small particles (less than 100 □m) tend to clump together, by increasing its surface:mass ratio and reducing the rate at which water penetrates. Therefore, increasing particle size (> 100 μm) can decrease the incidence of clumping, by allowing particles or agglomerates to interact with water as it enters through the empty spaces between particles, separating them [1].

b) *Sinkability*. It is the ability of powders to sink in water when they are moistened [4] and it is evaluated by measuring the time they required to sink. This property depends on the particle density, shape and size, where larger and denser particles sink faster as compared to smaller and lighter ones. Particles with a higher content of occluded air exhibit poor sinkability as a result of their low density, regardless of how large they are. Agglomerated powders usually did not sink in water [1].

c) *Dispersibility*. It is described as the ability of powers to be distributed throughout the water, assisted or not by a low energy stirring. This property can be measured as a percentage of dissolved powder after stirring the powder for 20 s and filtering the reconstituted liquid through a 150 μm sieve. It can also be quantified by the rate of increase of opacity or optical density of the solution. It's also important that the particles settle slowly enough or remain suspended so they do not form sediments within a certain period of time.

d) *Solubility.* It refers to the rate and extent at which the components of the powder particles dissolve in water. After reconstituting the powder, the solution is centrifuged and the undissolved particles that settle on the bottom of the centrifuge tube are measured directly by volume (solubility index) or heated to dryness (percentage of soluble solids).

Different techniques have been applied to evaluate food powder instant properties (Barbosa-Cánovas and Juliano, 2005) such as the penetration speed test, the standard dynamic wetting test and dynamic wetting test (Schubert 1980; Pietsch, 1999). However some of them do not consider some

factors such as the solvent temperature, the liquid surface area, the amount of material to be dissolved, or the method used for depositing the powders on the liquid surface [15] regardless they play an important role during the rehydration process.

4.0 Microstructure of food powders

Nowadays, the study of food powder microstructure is very important; however it was ignored by food engineers for a long time. In the past decades, the emphasis of the food industry development was given on designing safe and reliable processes, while innovation and quality were not major driving forces in the food market and the knowledge about the underlying sciences linking food structure to product properties was just initiating. Moreover, the techniques aiding in the study of microstructure were not fully developed to provide useful data (e.g. quantitative information) to engineers [3][16].

Currently, the study of food structure has grown in parallel with the development of better microscopy, visualization, and image processing/analysis techniques (Figure 1), including noninvasive and real-time methods, many of them taken from biology and material sciences. In the next pages, some of the available microscopy and image analysis techniques are explained.

4.1 Microscopy technique

Microscopy methods, as used in the food industry, are frequently a combination of those employed in biological and materials sciences [17]. These techniques, when applied in conjunction with image processing and micro analytical methods are useful to observe food structures as well as to provide the needed data to derive realistic physical or mathematical models of foods. Furthermore, advanced microprobe techniques, that combine microscopy and spectroscopy, have made possible the evaluation of sample's composition as well as the state of the individual phases of the sample in a particular area in the field of view [16][18][19][20].

Examining food microstructure is always a difficult task because of the complexity of the materials involved. One useful approach to differentiate structural features from artifacts is correlative microscopy, defined as the practice of using a combination of microscopic techniques in order to distinguish real images from false responses during image interpretation. Some of the available methods to fulfill these purpose are light microscopy (LM), environmental, scanning electron microscopy (ESEM), and confocal laser scanning microscopy (CLSM), among others, that constitute a battery of powerful techniques matchless in flexibility, intrusion or simplicity of sample preparation, covering the whole dimensional scale from the molecular to the macrostructural level [21-24]. The generated microstructural information can be used to understand different process and to assess the functionality of finished products (so-called structure-function relationships). Efforts has been made to derive the appropriate scaling laws from the results obtained at the

microstructural level and to convert them into a nanoestructural one. Figure 2 shows some of the different microscopes used in food science.

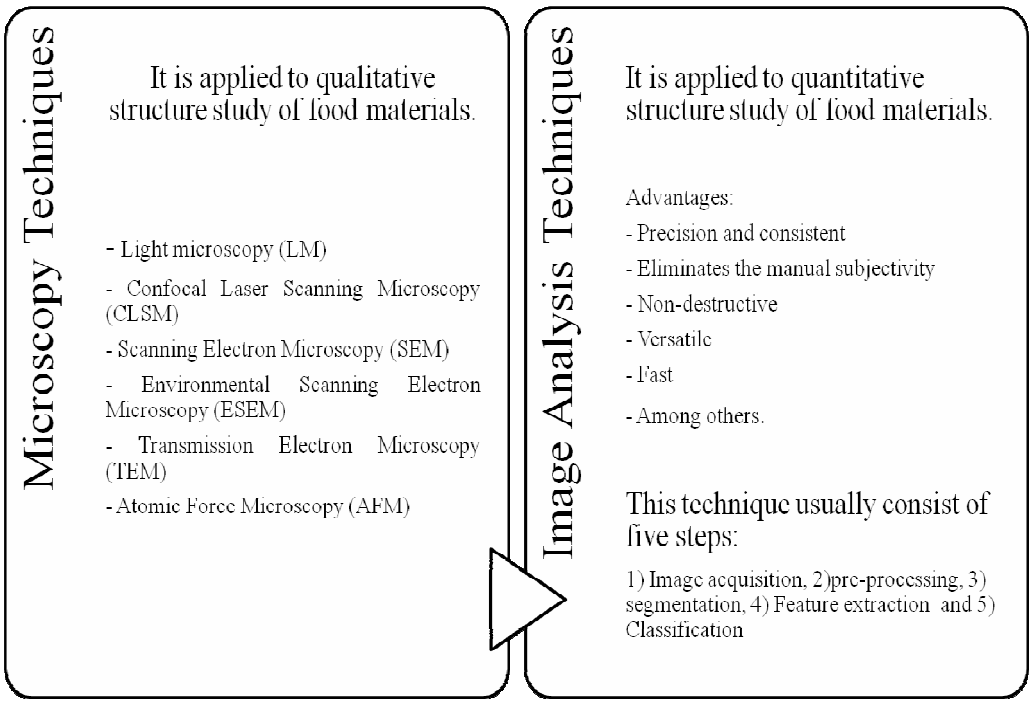

Figure 1 Microscopy and image analysis techniques applied in the study of biomaterial's microstructure.

4.2 Light microscopy and stereo light microscopy

The light microscope is an instrument for visualizing fine detail of an object by creating a magnified image through the use of a series of glass lenses, which first focus a beam of light onto or through an object, and convex objective lenses to enlarge the image formed [17], in other words light microscopy involves passing visible light transmitted through or reflected from the sample through a single or multiple lenses to allow a magnified view of the sample [25]. This technique has a resolution about 10^3 times smaller than the human's vision [26]. The magnification range extends from X10 to X1000, with a resolving power of the order of 0.2 μm, depending on the type and numerical aperture (area available for passage of light) of the objective lenses [17]; in conventional LM, using blue light of wavelength of 470 nm and having an oil immersion objective lens with a numerical aperture equal to 1.40, the resolution would be limited to about 200 nm. However the magnification of light microscopy is modest as compared to electron microscopy and atomic force microscopy [27][28].

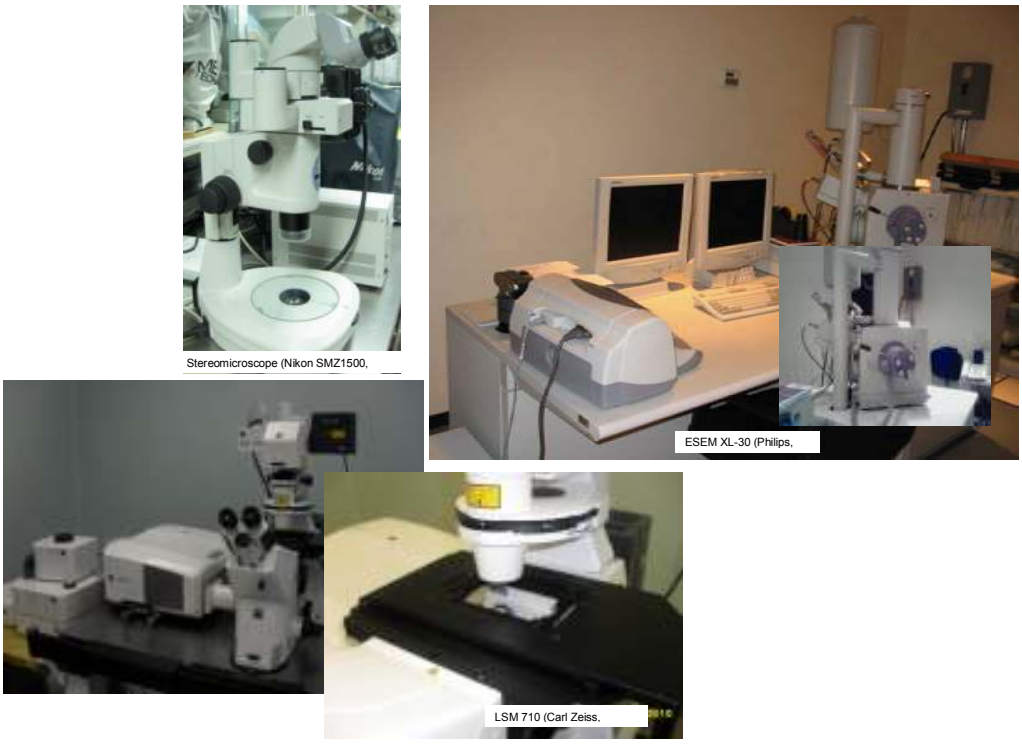

Figure 2 *Different kinds of microscopes applied in the study of food microstructure. A) Stereomicroscope, B) Environmental Scanning Electron Microscope, C) Confocal Laser Scanning Microscope.*

Sample preparation for LM is less complex than others microscopic techniques. Food materials can be examined as a whole, but usually studies of cellular structure require the cutting of sections. Microtomes allow cutting sections of uniform thickness, in order to maintain structural integrity; tissues are often embedded with materials such as paraffin wax, plastics, or resins; alternatively, sectioning can be performed on frozen material. In LM is common to apply a specific stain or dye in order to improve contrast or differentiate tissues. Finally, the specimen is placed on a glass microscope slide, a suitable mounting media is applied, and a cover glass is added.

In LM, the microstructural details become visible due to the absorption of a portion of the light. Incident light is mainly used for the examination of solid or opaque objects, although, new forms of light microscopes has been developed based on fluorescent materials' properties, where the source of light is often a single or multicolor tungsten or quartz halogen lamps, but xenon arc or mercury lamps provide more intense beams, as required for fluorescence microscopy [17].

The Stereo Light Microscope (SLM) is an invaluable tool for scientists in observing the structures of biological materials, where a full view of a specimen is obtained by using a convergent optical system [28]. It is used primarily to assist the quantitative analysis of size, shape and overall morphology of both static and alive specimens. Quantitative SLM techniques are rarely found, even with the recent extensive usage of image processing and analysis hardware and software tools. Moreover, in most cases, the

measurements performed are essentially 2D, such as the perimeter or area of the biomaterials shape [28][29].

4.3 Confocal laser scanning microscopy

Confocal laser scanning microscopy is a rather new technique for structural analysis of biological and food materials. In contrast to conventional light microscopy, the light source is replaced by laser beam, a scanning unit and a pinhole in the back focal plane, which improves the limited depth of focus [30]. The newly developed CLSM is particularly suitable for acquiring high-quality 3D microscopic images of quasi-static specimens, as a serial scanning is done at different focal planes, prohibiting the study of rapid, live 3D motion specimens [29-31]. Advanced computer imaging technologies, fluorescent probe developments, and computer designed optics have all been integrated to improve analytical light microscopes. This combination has produced a microscope with the capacity to obtain higher resolution volumetric images [23].

The primary value of the CLSM is its ability to produce a three-dimension (3-D) image of thick samples by scanning the specimen at different focal planes. Therefore, by moving the focal plane of the instrument by steps of defined distance (□m-range) through the depth of the specimen, a stack of optical sections can be recorded. This property of the CLSM is fundamental for solving 3-D problems where information as obtained from regions distant from the plane of focus can blur the image of such objects; in other words, in the confocal principle, a light source (typically a laser) is focused to a diffraction-limited spot (airy disk) at the specimen by the objective lens. Reflected light or emitted fluorescence is focused by the same lens to a spot at the detector. At this point a pinhole is placed, so that only the in-focus beams will pass through out the pinhole to the detector, while the other will be blocked. By scanning successive planes, a three-dimensional image of the sample can be created. CLSM also offer a modest increase in resolution, since the detected signal is the square of the point spread function of the objective lens [23][30-35]. Since the resolution achieved by a conventional widefield light microscope (0.2 μm theoretical), is not larger than the one obtained from a transmission electron microscope (0.1 nm), the gap between these two commonly used techniques has been bridged [32].

The application of CLSM to food materials has been particularly fruitful in the area of lipid components or fat crystal networks, because optical sectioning overcomes the tendency of fats to smear and migrate and lipids are amenable to fluorescent staining [16]. The possibility to combine CLSM with rheological measurements, light scattering and other physical analytical techniques in the same experiments with specially designed stages offers the possibility to obtain detailed structural information of complex food systems [30]. Also, it is an important tool, when applied in a epi-reflection mode, to study the dynamics of living cells, 3D reconstruction of biomaterials, evaluation of topography and surfaces of samples and the study of the microstructure of aqueous phase separated protein-polysaccharide mixtures, among others [30][32].

4.4 Conventional and environmental SEM

In electron microscopy, a beam of electrons, rather than light, is used to form a magnified image of specimens and where the electrons provide as much as thousand fold increments in resolving power. As an electron beam interacts on the sample, a variety of signals that can be captured to obtain images are generated. The two basic types of electron microscopes are the transmission electron microscope (TEM), in which transmitted electrons are captured, and the scanning electron microscope (SEM), in which secondary electrons are captured. Nowadays, electron microscopy technique has been a useful tool for investigating the microstructures of cereal grains, dough, beef, ken and others [20][35][36].

One of the latest developments in electron microscopy is the environmental scanning electron microscope (ESEM), which enables to be viewed soft, moist and/or electrically insulating materials without pre-treatment, unlike conventional scanning electron microscopy (SEM), in which specimens must be solid, dry and usually electrically conductive [37]. With ESEM wet, fully hydrated or high vapor samples can be analyzed in their native state, which makes possible to obtain better information about food structure [22].

The development of the ESEM technique has have significant implications on the study of the native surfaces of specimens, including rocks and minerals, polymers, biological tissue and cells, food and pharmaceutical products, precious artifacts, forensic material, and nowadays, this technique is highly demanded for obtaining three-dimensional (3D) images of food structures [20][28][35-37]. Therefore, the study of food properties for various applications requires a better understanding of the relationships between the food microstructure and macroscopic properties, showing the importance to know the different techniques available for qualitative and quantitative studies of biomaterials structure.

4.5 Image analysis

Image analysis techniques have been applied increasingly for food quality evaluation and also to provide valuable qualitative and quantitative insights into the microstructural dimensional change behavior during processing of food materials. Increased demands for objectivity, consistency and efficiency have required the introduction of computer-based image processing techniques. Recently, computer vision systems employing image analysis techniques have been developed to quantitatively characterize complex size, shape, color and texture properties of foods. Image analysis techniques usually consist of five steps (Figure 3) [3][38-41].

1. Image acquisition. Several sensors and microscope systems such as charge coupled device (CCD) camera, ultrasound, magnetic resonance imaging (MRI), computed tomography (CT), electrical tomography (ET), TEM, SEM, ESEM, CLSM among others (Figure 3) are used widely to obtain

images of food products. When acquiring images, it is also important to consider the effect of illumination intensity and the specimen's orientation relative to the illumination source because the gray level of the pixels is determined not only by the physical features of the surface but also by these two parameters.

2. Pre-processing. The digital images must be preprocessed to improve the image data, which suppresses unwilling distortions or enhances some image features that are important for further processing and creates a more suitable image than the original for a specific application. Using digital filtering, the noise of the image, which may degrade the quality of an image and subsequently image processing, can be removed and the contrast can be enhanced. In addition, in this step the color image is converted to a grayscale image, called the intensity image.

3. Segmentation. The techniques of image segmentation developed for food quality evaluation can be divided into four different philosophical approaches (thresholding-based, region-based, gradient-based, and classification-based segmentation). Intensity image is used to identify disjoint regions of the image with the purpose of separating the part of interest from the background. The region of interest within the image corresponds to the area where the "studied material "is located. This segmented image (S) is a binary image consisting only of black and white pixels, where "0" (black) and "1" (white) means background and object, respectively.

4. Feature extraction. During this process the segmented image is measured by evaluating geometric properties (perimeter, form factors, Fourier descriptors, invariant moments, and so forth), color characteristics (mean value, gradient, 2nd derivative and so forth) and textural parameters (fractal texture and GLCM texture analysis) (Table 2). The geometric features are computed from the segmented image, while the intensity features are extracted from the intensity image and the color features from the RGB images. Through GLCM texture analysis is possible to obtain different parameters such as angular second moment, contrasts entropy, among others. The texture of an image is characterized by the spatial distribution of grey levels in a neighborhood [42]. Image texture (IT) is defined as repeating patterns of local variations in image intensity that are too fine to be distinguished as separate objects at the observed resolution, that is, the local variation of brightness from 1 pixel to the next (or within a small region). It can be used to describe such image properties as smoothness, coarseness, and regularity. The IT of some food surfaces has been described quantitatively by fractal methods. Besides fractal properties other important characteristics could be obtained from the information of an image such as statistical, geometrical, and signal-processing properties, among others. It is important to know which features will provide relevant information for the classification process. For this reason, a feature selection must be performed in a training phase.

5. Classification. A classifier is designed by following a supervised training, and simple classifiers may be implemented by comparing measured features with threshold values. Nonetheless, it is also possible to use more sophisticated classification techniques such as statistical, fuzzy logic, and

neutral networks that have as a common objective to simulate a human decision-maker´s behavior, and have the advantage of consistency and, to a variable extent, explicitness. The extracted features of each region are analyzed and assigned to one of the defined classes, which represent all possible types of regions expected in the image.

Table 2 Parameters obtained from digital images

Feature extraction		
Geometric parameters	**Color parameter**	**Textural parameters**
Size	RGB	Fractal texture (FDt) Fractional Brownian motion
Area	CIE L*a*b*	
Perimeter	XYZ	GLCM (Grey Level Co-occurrence matrix) texture analysis:
Shape factor	Luv	
Compactness	YCbCr	Entropy
Fractal dimensions (FD)	Intensity	Angular Second moment
Mean particle size	Among others.	
Circularity		Contrast
Feret diameter		Correlation
Eccentricity		Inverse Difference Moment
Among others.		
		Among others.

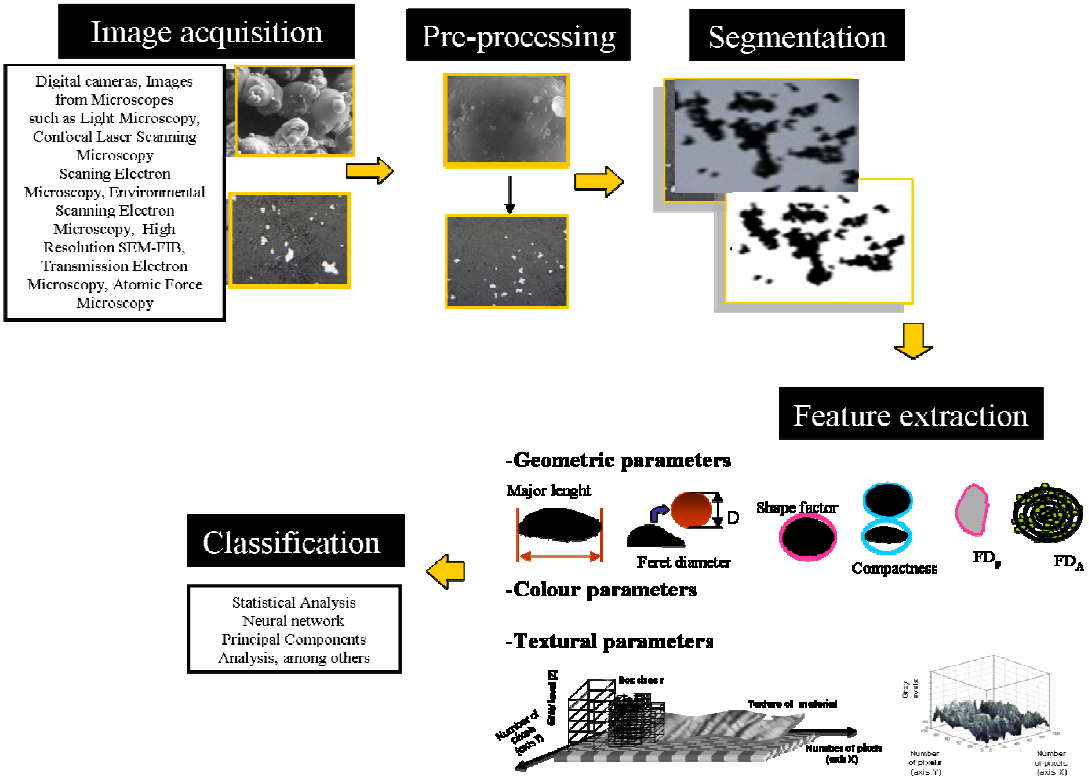

Figure 3 Image analysis methodology

5.0 Case study: milk powder

The relationship between the microstructure of food powders and their rehydration properties can be illustrated by the application of microscopy techniques and image analysis processing on different milk powders samples.

5.1 Materials and methods

Five different commercial milk powder samples were acquired from local retail markets in Mexico City. The bulk and packed bulk density of milk powders were determinate as reported by Shittu and Lawal [12] and Niro's analytical methodology [11], respectively, while moisture was evaluated following the 32.1.02 AOAC method [43].

Milk powder rehydration capability was quantified by evaluating the samples wettability, dispersibility and solubility. Wettability or wetting time was measured as described by Niro Company [11]. The wetting time is defined as the time (in seconds) required to a 10g sample become wetted. Solubility index was evaluated as described by Niro [11] and Shittu and Lawal [12], where the sample (10g) was dispersed in 100 mL of distilled water (24ºC); this suspension was stirred at 400 rpm for 90 seconds and allowed to rest for 15 min, afterward, 50mL of this suspension was centrifuged at 10000 rpm for 5 min. Finally, the precipitate was re-suspended in 50 mL of distilled water and centrifuged at 10000 rpm for 5 min. Precipitate volume was measured directly from centrifuge tubes. Dispersibility was determined by stirring 25 g of the sample with 250 mL of distilled water (25°C) for 20 s at 100 rpm. This suspension was filtered through a membrane of 100 microns; the residue was weighted and the weight difference gives the amount of dust that is dispersed in the liquid [11].

Milk powder agglomerates images were obtained using both, a light stereo-microscope (LSM) (Nikon SMZ1500, Japan) and an Environmental Scanning Electron Microscope (ESEM, XL30 Philips, USA). The images of agglomerates were obtained by LSM fitted with a CCD camera (Nikon Digital Sight DS-2Mv, TV Lens 0.55X DS, Japan) and connected to a PC by means of NIS-Elements F 2.30 Software. RGB images (800x600 square pixels) were captured and converted to 8-bit images. The samples were gently deposited on a glass slide and for each sample, at least 600 particles were characterized to ensure stabilization of the average value and stand error of descriptors. These images were analyzed to obtained morphological parameters such as particle size, shape factor, compactness and fractal dimension of contour (FDc) as described [45].

Fractal dimension of texture (FDt) was extracted from ESEM images [44]. Image analysis was performed using the public domain program NIH ImageJ 1.34s (National Institute of Health, USA, available from: http://rsb.infor.nhi.gov/ij/) combined with other commercial software, such as Sigma ScanPro 5. All morphological and FDt were extracted from images by applying the ImageJ software. FDt of images was evaluated by power-law scaling, using the Shifting Differential Box Counting method as proposed by

Wen-Shiung et al.[44]. FDt was calculated by means of the Mapfractalcount plug-in (v 1.0, available on line). FDt was estimated from the slope in the log (box count) *vs.* log (box size) plot. All analyses were done in triplicate.

5.2 Results and discussion

Table 3, presents the rehydration properties and FDt results of milk powder agglomerates. These data showed that the sample A presents significant difference as compared to the other samples, with the largest values of wettability and insolubility index. It is possible that these differences among samples could be generated by their different composition (sample 2 is whole milk powder added with nutritional components, while sample B, C and D are skim milk powders). Sample B showed the smallest volume of sediments and the lowest value in wettability as compare to others samples. These differences might be due to size and morphology of agglomerates, and image analysis results provide more information about the relationship between rehydration capability and microstructure. When the values of particle size and FDt were large a better rehydration capability (lower values of wettability and insolubility index) was observed as is shown in the Figure 4. These results presented a similar tendency as those reported [4][14].

Table 3 Rehydration properties and FDt values of powder milk samples

Simples of milk powder	***Wettability (seg)***	***Dispersibility (%)***	***Insolubility index (mL)***	**FDt**
A	8019 ± 641.4^{b}	97.577 ± 0.058	2.16 ± 0.19	2.6315 ± 0.0083^{a}
B	6.68 ± 0.16^{a}	99.402 ± 0.009^{a}	0.34 ± 0.02^{a}	2.6479 ± 0.0076^{ab}
C	13.74 ± 0.42^{ac}	99.358 ± 0.036^{a}	0.66 ± 0.08^{ab}	2.6811 ± 0.0187^{ab}
D	140.77 ± 28.00^{bc}	98.409 ± 0.024	0.98 ± 0.08^{b}	2.6987 ± 0.0085^{b}

*Values followed by the simple letter in the same column are not significantly different (Tukey test, $p<0.05$) n=5.

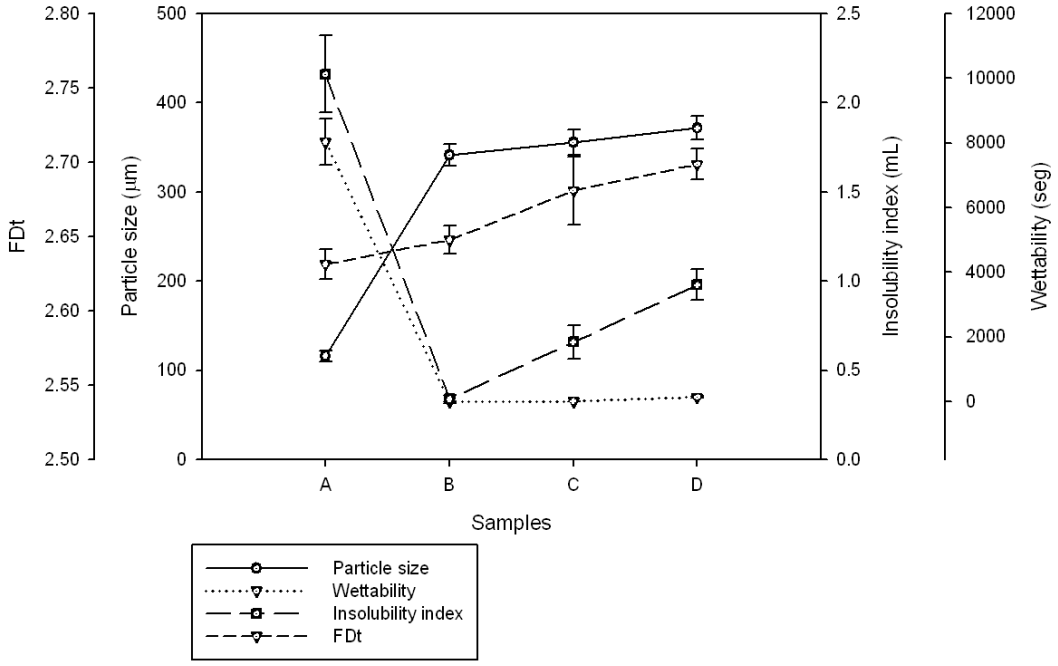

Figure 4 *Relationship between rehydration capability (wettability and insolubility index) and Particle size and FDt values.*

Physical properties of powder milk agglomerates are presented in the Table 4, where the largest bulk density (sample A, Table 4), corresponds to the particle of smallest size (Figure 4), in other words, sample A showed the least capability to particle agglomeration and therefore this sample could be considered to have almost a spherical shape. In contrast, the others samples (see Samples B, C and D, in Table 4) were not significantly different. Samples' moisture content varied from 3 to 4 % and these values were similar to those reported on commercial milk powders.

Table 4 Physical properties of powder milk samples.

Samples of milk powder	***Bulk density (g/mL)***	***Packed bulk density (g/mL)***	***Moisture (%)***
A	0.47	0.61	4
B	0.38	0.56	3.4
C	0.37	0.57	4
D	0.38	0.57	3.8

Morphological parameters of powder milk agglomerates (shape factor, compactness, FDc and particle size) are presented in the Table 5. ANOVA tests showed that these parameters did not present significant differences, with the exception of sample A. Image analysis results showed that samples presented a wide range of particles sizes, varying from 110 to 380 □m, where the lowest sizes could be associated with the minor rehydration capability (see sample A in Table 3). Shape factor and compactness are a measure of the circularity, while FDc is a measure of tortuosity of agglomerates, thus the highest values of shape factor and the lowest values of compactness and FDc were associated with spherical agglomerates and the least rehydration capability (see sample A in Table 3) probably as a result of a smoother surfaces of the surfaces of milk powder agglomerates (see sample A in the Figure 7). The morphological parameters values for different milk samples are shown in Figure 5; these results showed that the largest values of particle sizes can be associated with a major irregularity of agglomerates (larger values of shape factor and FDc). When comparing Figures 4 and 5, the largest sizes of the particles and the irregularity of agglomerates could be related to a better rehydration capability.

Table 5 Morphological parameters of powder milk samples.

Samples of milk powder	***Shape factor***	***Compactness***	**FDc**	***Particle size (□m)***
A	0.641 ± 0.009	24.392 ± 0.729	1.1289 ± 0.0025	116.368 ± 5.808
B	0.469 ± 0.009[a]	37.360 ± 1.126[a]	1.1370 ± 0.0024[a]	341.737 ± 12.392[a]
C	0.435 ± 0.009[a]	43.190 ± 1.533[a]	1.1465 ± 0.0025[b]	355.844 ± 13.975[a]
D	0.441 ± 0.009[a]	40.224 ± 1.273[a]	1.1465 ± 0.0031[ab]	371.626 ± 13.166[a]

*Values followed by the simple letter in the same column are not significantly different (Tukey test, $p<0.05$) n=600.

ESEM and LSM images of the four samples are shown in Figure 6, 7, 8 and 9, where sample A shows a spherical shape (major circularity) and a smoother surface as compared to the others samples. However, the lowest values of DFt (Table 3) were associated to surfaces with smaller roughness in the ESEM images and the least rehydration capability of agglomerates. In contrast, the agglomerates with the highest values of DFt indicate a major roughness of agglomerate surfaces and it can be associated with a more agglomeration level and a larger rehydration capability.

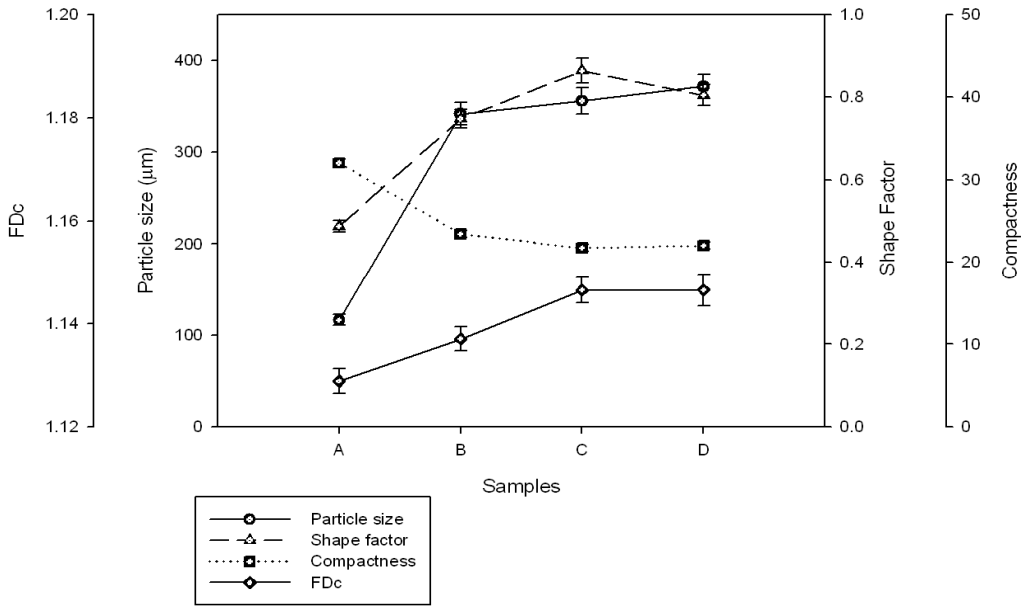

Figure 5 *Relationship between morphological parameters and particle size*

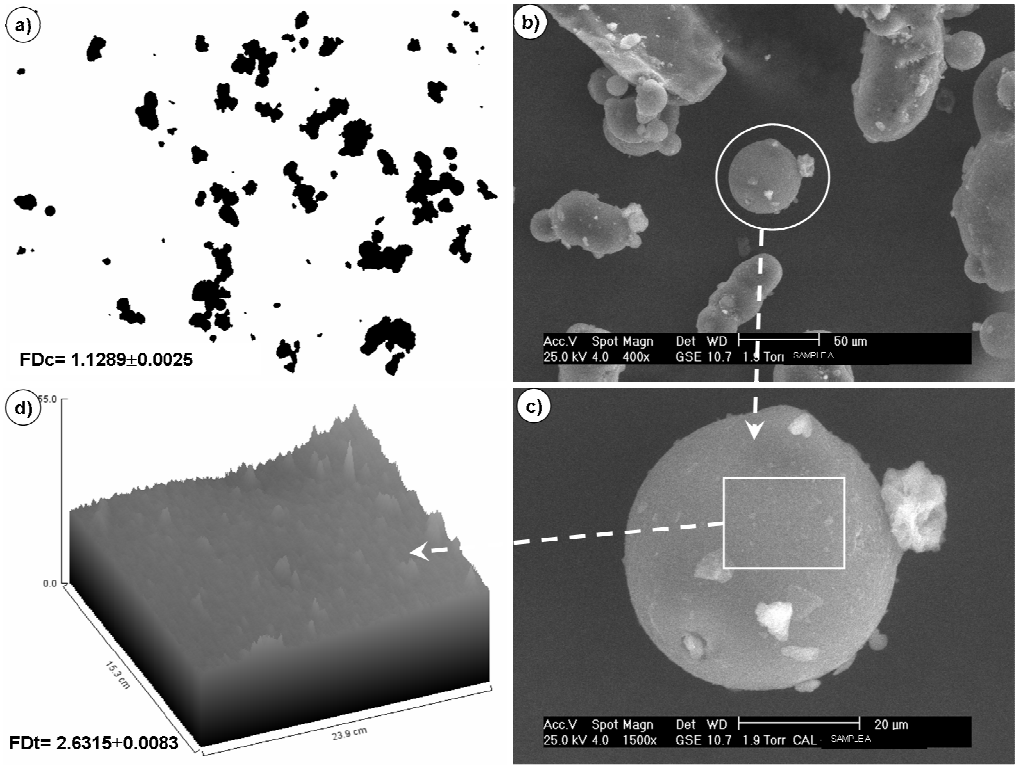

Figure 6 *Sample A of powder milk. a) Agglomerated image of powder milk obtained by means light stereo-microscope at 60X, b) and c) Environmental Scanning Electron Micrographs of particles with an agglomerated structure at 400X and 1500X respectively; and d) Gray level surface plot obtained by ESEM images.*

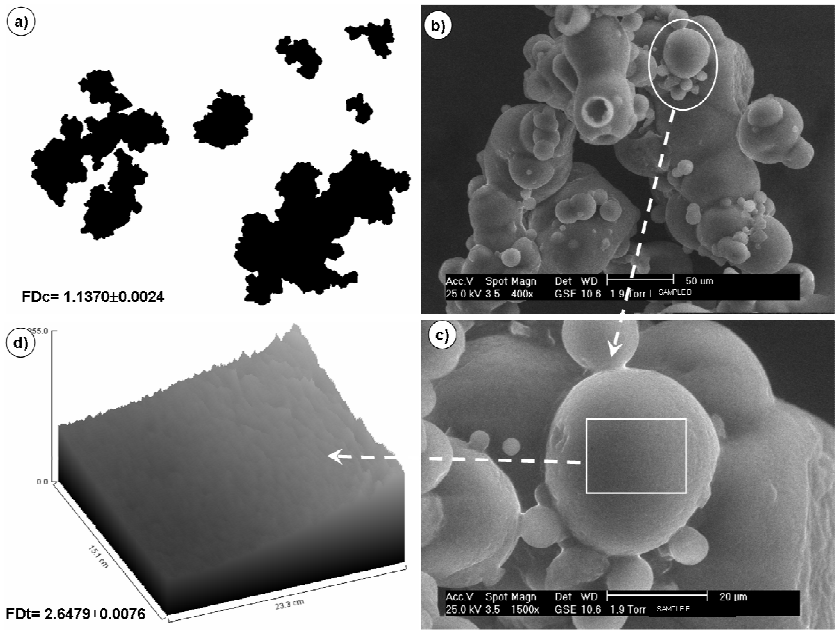

Figure 7 Sample B of powder milk. a) Agglomerated image of powder milk obtained by means light stereo-microscope at 60X, b) and c) Environmental Scanning Electron Micrographs of particles with an agglomerated structure at 400X and 1500X respectively; d) Gray level surface plot obtained by ESEM images.

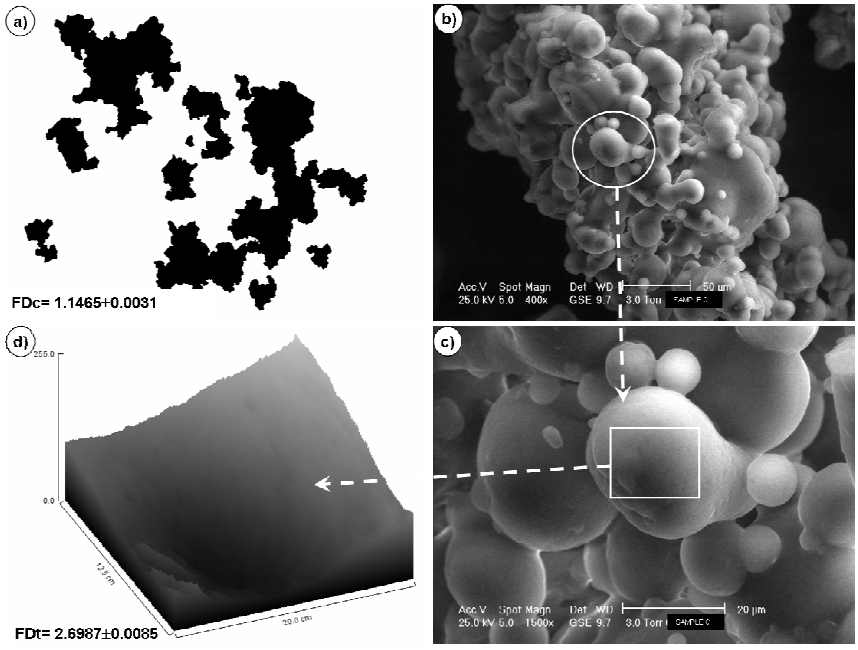

Figure 8. Sample C of powder milk. a) Agglomerated image of powder milk obtained by means light stereo-microscope at 60X; b) and c) Environmental Scanning Electron Micrographs of particles with an agglomerated structure at 400X and 1500X respectively; and d) Gray level surface plot obtained by ESEM images.

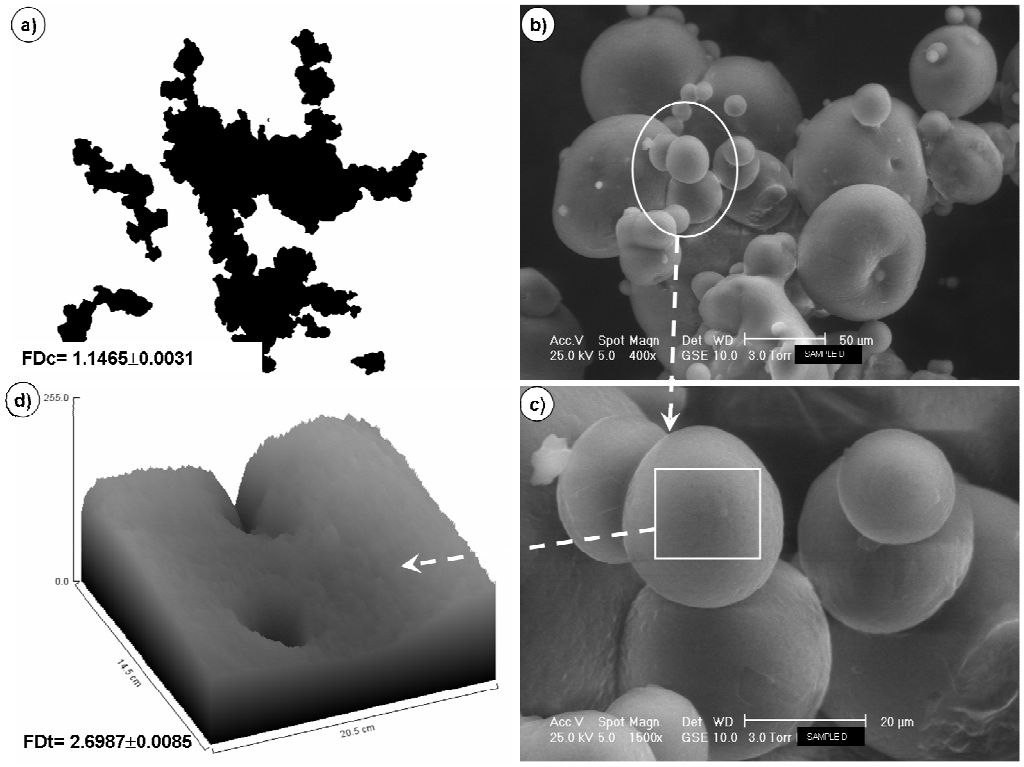

Figure 9. Sample D of powder milk. a) and b) Environmental Scanning Electron Micrographs of particles with an agglomerated structure at 400X and 1500X respectively. c) Agglomerated image of powder milk obtained by means light stereo-microscope at 60X and d) Gray level surface plot obtained by ESEM images.

6.0 Conclusion

The present contribution is a brief description of the application of microscopy techniques and images analysis for morphology and microstructure characterization of food powders and their relationship with rehydration and physical properties. The given example shows simple correlations between microstructure of milk powders, as obtained by image analysis techniques, and their physical and rehydration properties. The more relevant results were the correspondence of higher values of particle size, shape factor, FDc and FDt with a better rehydration capability of samples. The methodology used in this work could be useful to evaluate other powders of importance for food and pharmaceutical industry.

7.0 Acknowledgement

This work has been supported by the Instituto Politénico Nacional (IPN) of México; Secretaría de Investigación y Posgrado (SIP: 20100771) del IPN research projects and Consejo Nacional de Ciencia y Tecnologia (CONACYT: 59730).

8.0 References

1. Hogekamp, S.; Schubert, H. Rehydration of Food Powders. Food Science and Technology International **2003**, *98(3)*, 223-235.
2. Aguilera, J.M. Microstructure and Food Product Engineering. Food Technology **2007,** *54(11)*, 56-65.
3. Chanona-Pérez, J.; Quevedo, R.; Jimenez-Aparicio, A.R.; Gumeta-Chávez, C.; Mendoza-Pérez, J.A.; Calderón-Domínguez, G.; Alamilla-Beltrán, L.; Gutierrez-López, G.F. Chapter 16: Image processing methods and fractal analysis for quantitative evaluation of size, shape, structure and microstructure in food materials. Food Engineering Integrated Approaches. Food Engineering Series **2008**. Edited by Gustavo F. Gutierrez-López, Gustavo V. Barbosa-Cánovas, Jorge Welti-Chanes, Efrén Parada-Arias. Springer. Pp. 277-285.
4. Ortega-Rivas, E. Bulk properties of food particle materials: an appraisal of their characterisation and relevance in processing. Food Bioprocess Technology **2009**, *2*, 28-44.
5. Bhandari, B. Chapter 9: Spray Drying and Powder properties in Food Drying Science and Technology **2008**. Edited by Hui, Y.H., Clary, C., Farid, M.M., Fasina, O.O., Noomhorm, A., Welti-Chanes, J. DEStech Publications, Inc. 215-248.
6. Reh, C.; Bhat, S.N.; Berrut, S. Determination of water content in powdered milk. Analytical, Nutritional and Clinical Methods. Food Chemistry **2004**, *86(3)*, 457-464.
7. Barbosa-Cánovas, G. V.; Ortega-Rivas, E.; Juliano, P.; Yan, H. Food Powders: physical properties, processing, and functionality. Food Engineering Series **2005**.
8. Alvarado, J. de D.; Aguilera, J.M. ”Métodos para medir propiedades físicas en industrias de alimentos: tamaño y forma de partículas, Propiedades físicas de los alimentos en polvo”. Zaragoza, España. **2001**, P.p. 29-47, 135-147.
9. Barbosa-Cánovas, G.V.;Juliano, P. Physical and chemical properties of food powders in Encapsulated and powdered foods **2005**. Edited by C. Onwulata. CRC Taylor and Francis. 39-71.
10. Nijdam, J.J.; Langrish, T.A.G. An investigation of milk powders produced by a Laboratory –scale spray dryer. Drying Technology **2005**. *23*, 1043-1056.
11. Niro, **2005**. Method No. A2a, A2b, A3a, A5a, A7a y A6a. Niro Analytical Methods. [En Línea] Disponible:
12. Shittu, T.A.; Lawal, M.O. Factors affecting instant properties of powdered cocoa beverages. Elsevier Food Chemistry **2007**, *100*, 91-98.
13. Turchiuli, C.; Eloualia, Z.; El Mansouri, N.; Dumoulin, E. Fluidised bed agglomeration: Agglomerates shape and end-use properties. Powder Technology **2005**, *157*, 168-175.
14. Kyaw Hla, P.; Hogekamp, S. Wetting behaviour of instantinez cocoa beverage powders. International Journal of Food Science and Technology **1999**, *34*, 335-342.
15. Pietsch, W. Readily engineer agglomerates with special properties from micro- and nanosized particles. Chemical Engineering Progress **1999**, *8*, 67–81.

16. Aguilera, J.M.; Stanley, D.W.; Baker, K.W. New dimensions in microstructure of food products.Trends in Food Science and Technology **2000**, *11*, 3-9.
17. Holgate, J.H.; Webb, J. Microscopy: Light Microscopy and Histochemical Methods. Encyclopedia of Food Sciences and Nutrition **2003**, Ten-Volume Set. ACADEMIC PRESS. ISBN 13: 978-0-12-227055-0. Pp. 3917-3922.
18. Aguilera, J.M.; Chiralt, A.; Fito, P. Food dehydration and product structure.Trends in Food Science and Technology **2003**.*14*, 432-437.
19. Schoonman, A.; Mayor, G.; Dillmann, M.L.; Bisperink, C.; Ubbink, J. The microstructure of foamed maltodextrin/sodium caseinate powders: a comparative study by microscopy and physical techniques, Food Research International **2001**, *34(1)*, 913-929.
20. Witek, M.; Weglarz, W.P.; De Jong, L.; van Dalen, G.; Blonk, J.C.G.; Heussen, P.; Van Velzen, E.; Van As, H.; van Duynhoven, J. The structural and hydration properties of heat-treated rice studied at multiple length scales. Food Chemistry **2010**, *120*, 1031-1040.
21. James, B.J.; Smith, B.G. Surface structure and composition of fresh and bllmed chocolate analysed using X-ray photoelectron spectroscopy, cryo-scanning electron microscopy and environmental scanning electron microscopy. LWT-Food Science and Technology **2009**, *42*, 929-937.
22. James, B. Advances in “wet” electron microscopy techniques and their application to the study of food structure. Trends in Food Science and Technology **2009**, *20*, 114-124.
23. Amos, W.B.; White, J.G. How the Confocal Laser Scannig Microscope entered Biological Research. Biology of the Cell **2003**, *95*, 335-342.
24. Wirth, R. Focused Ion Beam (FIB) combined with SEM and TEM: Advanced analytical tools for studies of chemical composition, microstructure and crystal structure in geomaterials on a nanometre scale. Chemical Geology **2009**, *261(3-4)*, 217-229.
25. Abramowitz, M.; Davidson, M. W. “Introduction to Microscopy".Molecular Expressions. Retrieved. **2007,** Pp. 08-22.
26. Aguilera, J.M.; Stanley, D.W. Chapter 1: Examining Food Microstructure. In Microstructural Principles of Food Processing and Engineering **1999**. 2a. Edition. An ASPEN Publication.pp. 1-70.
27. Autio, K.; Salmenkallio-Marttila, M. Light microscopic investigations of cereal grains dough’s and breads. LWT **2001**, *34*, 18-22.
28. Schreier, H.W.; Garcia, D.; Sutton, M.A. Advances in Light Microscope Stereo Vision. Experimental Mechanics **2004**, *44(3)*, 278-288.
29. Liao, W.-H.; Aggarwal, S.J.; Aggarwal, J.K. The reconstruction of dynamic 3D structure of biological objects using stereo microscope images. Machine Vision and Applications **1997**, *9*, 166-178.
30. Dürrenberger, M.B.; Handschin, S.; Conde-Petit, B.; Escher, F. Visualization of Food Structure by Confocal Laser Scanning Microscopy (CLSM). LWT **2001**, *34*, 11-17.
31. Cox, G. Biological confocal microscopy. Materials today **2002**. 34-41.
32. Paddock, S.W. Principles and practices of Laser Scanning Confocal Microscopy. Molecular Biotechnology **2000**, *16*, 127-149.
33. Aguilera, J.M.; Stanley, D.W. Chapter 10: The microstructural approach. In Microstructural Principles of Food Processing and Engineering **1999**. 2a. Edition. An ASPEN Publication.pp. 413-423.
34. Blonk, J.C.G.; van Aalst, H. Confocal scanning light microscopy in food research. Food Research International **1993**, *26*, 297-311.

35. Peighambardoust, S.H.; Dadpour, M.R.; Dokouhaki, M. Application of epifluorescence light microscopy (EFLM) to study the microstructure of wheat dough: a comparison with confocal scanning laser microscopy (CSLM) technique. Journal of Cereal Science **2010**, *51*, 21-27.
36. Aguilera, J.M.; Stanley, D.W. Chapter 9: The microstructural approach. In Microstructural Principles of Food Processing and Engineering **1999**. 2a. Edition. An ASPEN Publication.pp. 373-397.
37. Stokes, D.J. Recent advances in electron imaging, image interpretation and applications: environmental scanning electron microscopy. Philosophical Transactions of The Royal Society Londre A. **2003**, *361*, 2771-2787.
38. Pedreschi, F.; Mery, D.; Aguilera, J. M. Classification of Potato Chips Using Pattern Recognition.Journal of Food Science **2004**, *69*, E264-E270.
39. Castelman K. **1996**. Digital image processing. Englewood Cliffs, N. J.: Prentice Hall. p.667.
40. Du, C.; Sun, D. Recent developments in the applications of image processing techniques for food quality evaluation, Trends in Food Science and Technology **2004**, *15(1)*, 230–249.
41. Pérez-Nieto Antonio.; Chanona-Pérez Jorge.; Farrera-Rebollo Reynold.; Gutiérrez-López Gustavo.; Calderón-Domínguez Georgina. Image analysis of structural changes in dough during baking. LWT - Food Science and Technology **2010**, *43*, 535–543.
42. Haralick, R.; Shanmugam, K.; Dinstein, I. Textural Features for Image Classification. IEEE Transactions on Systems, Man, and Cybernetics **1973**, *3*, No.6.
43. AOAC. Official Methods of Analysis. 16th Edn. Arlington Virginia: Association of Official Analytical Chemists International **1995**, 32.1.02.
44. Chen, W.S.; Yuan, S.Y.; Hsieh, C.M. Two algorithms to estimate fractal. Optical engineering **2003**, 42, 2452-2464.
45. Olsen, E.R.; Ramsey, R.D.; Winn, D.S. A modified fractal dimension as a measure of landscape diversity. Photogrammetric engineering and remote sensing **1993**, *59*, 1517-1520.

Index

V

W

Y

Spray drying is a ubiquitous industrial operation found in numerous industries. It is employed to produce engineered powders from liquid feedstocks in a single step. This book compiles the latest development in the spray drying area. In this first edition, two aspects of Computational Fluid Dynamic (CFD) modeling of spray dryers were covered. The chapters include an overview in undertaking such an analysis while a latter chapter focuses on the particle behaviour modelIng in CFD. Apart from modeling, several chapters are included in this first edition focusing on the manipulation of particle properties. Discussion is given on suitable approaches in controlling the physical properties of particles. In particular a chapter was devoted introducing the concept of in-situ particle crystallization control in spray dryers. In the application of the spray drying process, chapters were included discussing on the control of encapsulation in the spray drying of herbal extracts and in the extension of the process to spray-freeze-drying which offers a great potential for product quality manipulation.

Meng Wai Woo

Meng Wai Woo is currently a Research Fellow and a half-time Lecturer of Chemical Engineering in Monash University, Clayton. His research interest is in spray drying and the fouling phenomenon. Within the area of spray drying, he is looking at droplet evaporation, particle formation or interaction phenomena and the functionality of particles. Apart from that, he also has experience in Computational Fluid Dynamics analysis of the spray drying process.

Arun Sadashiv Mujumdar

Dr. Mujumdar, the world-renowned “Drying Guru”, is Professor of Mechanical Engineering at National University of Singapore. Winner of numerous prestigious awards and honors, Prof. Mujumdar has published over 400 refereed papers and over 100 book chapters in heat-mass transfer and drying. Founder of the International Drying Symposium (IDS) series, he is Editor-in-Chief of the archival journal Drying Technology (Taylor & Francis) since 1988 and is also the Editor of over 60 books including the widely acclaimed Handbook of Industrial Drying (CRC Press) now in third edition.

Wan Ramli Wan Daud

Wan Ramli Wan Daud is a Professor of Chemical Engineering at the Department of Chemical & Process Engineering, National University of Malaysia. His research interest is in the area of spray drying, food drying and particulate drying with fluidized beds. Recently, he was awarded the prestigious Outstanding Contribution to the Drying Community 2009 Award at the 6th Asia-Pacific Drying Conference, 19-21 October 2009 in Bangkok. Wan Ramli is also a specialist in the area of Fuel Cell Technology. He is the Founding Director of The Fuel Cell Institute, National University of Malaysia.

ISBN: 978-981-08-6270-1